Coordinated Path Following

of

Multiple Autonomous Vehicles

By

Reza Ghabcheloo

SUBMITTED IN PARTIAL FULFILLMENT OF THE
REQUIREMENTS FOR THE DEGREE OF
DOCTOR OF PHILOSOPHY
AT
INSTITUTO SUPERIOR TÉCNICO
TECHNICAL UNIVERSITY OF LISBON
MAY 29, 2007

“If you can’t explain it simply, you
don’t understand it well enough.”
Albert Einstein

ABSTRACT

The thesis addresses the problem of steering a group of autonomous vehicles along given spatial paths while holding a desired inter-vehicle formation pattern. In short, the problem of Coordinated Path-Following (CPF). The solution proposed unfolds in two basic steps. First, a path-following control law is derived that drives each vehicle to its assigned path no matter what the speed profile of the vehicle is. In the methodology adopted for path-following, to each vehicle there corresponds a virtual reference target that moves along the path. A conveniently defined error vector that captures the "generalized" distance between the vehicle and the target is then driven asymptotically to zero. In the second step, the speeds of all vehicles are adjusted so as to synchronize the positions of the corresponding virtual targets (also called coordination states), thus achieving coordination along the paths. In the problem formulation, it is explicitly assumed that each vehicle transmits its coordination state to a subset of the other vehicles only, as determined by the communications topology adopted. This allows for explicit consideration of stringent communication constraints.

The thesis is organized as follows. Chapter 1 is the Introduction: it contains motivating examples and a summary of the contributions of the thesis. Chapter 2 offers a local solution to the CPF problem using a simple algorithm that builds on linearization techniques and gain scheduling control theory. In Chapter 3, Lyapunov-based techniques and graph theory are brought together to yield a global nonlinear decentralized control structure for CPF. Both bi-directional and uni-directional communication topologies are studied. Chapter 4 addresses important stability and performance issues that arise from the consideration of complex underactuated vehicle dynamics as well as inter-vehicle communication losses and time delays. Finally, Chapter 5 contains the conclusions and discusses challenging issues that warrant further research.

Key words: Coordinated path-following, Coordination control, Path-following, Communication constraints, Switching communication topologies, Time delays, Wheeled robots, Underactuated vehicles, Marine vehicles.

RESUMO

Esta tese aborda o problema do seguimento coordenado de caminhos de múltiplos veículos autónomos. Na sua essência, o problema consiste em coordenar um conjunto de veículos de modo a que sigam caminhos estabelecidos, ao mesmo tempo que mantêm um padrão geométrico desejado. A solução proposta desenrola-se em dois passos. Primeiro, constrói-se uma lei de controlo que obriga cada veículo a convergir para o caminho que lhe está atribuído, qualquer que seja o seu perfil de velocidade. A estratégia adoptada requer a construção de um veículo-referência virtual que se movimenta ao longo do caminho. Define-se um vector de erro que capta a distância "generalizada" entre o veículo real e o virtual, e conduz-se esse erro assimptoticamente para zero. No segundo passo, as velocidades são ajustadas de modo a sincronizar as posições espaciais (também denominadas estados da coordenação) dos veículos virtuais e atingir o padrão gométrico desejado. Na formulação do problema, assume-se explicitamente que existem restrições fortes aos tipos de comunicações que se podem estabelecer entre os veículos. Em particular, assume-se que cada veículo só pode comunicar com um subconjunto de veículos na sua vizinhança.

A tese está organizada em cinco capítulos. O Capítlo 1 introduz o problema a estudar através de exemplos e apresenta as contribuições principais da tese. No Capítulo 2 apresenta-se uma solução - denominada local - para o problema do seguimento coordenado de caminhos recorrendo a técnicas de linearização e comutação de ganhos. No Capítulo 3 levantam-se as restrições mencionadas e consideram-se formações arbitrárias de veículos. Recorrendo a técnicas de Lyapunov e teoria dos Grafos, derivam-se leis descentralizadas e globais para o controlo coordenado de múltiplos veículos. O Capitúlo 4 analisa o impacte de falhas temporárias e atrasos nas comunicações na estabilidade e desempenho de uma formação de veículos. Finalmente, o Capitúlo 5 contém as conclusões e discute problemas para investigação futura.

Palavras-Chave: Seguimento coordenado de caminhos, Controlo cooperativo, Seguimento de caminhos, Redes de Comunicações e Controlo, Sistemas com atrasos, Sistemas com falhas, Veículos sub-actuados, Veículos Terrestres, Veículos Marinhos.

ACKNOWLEDGEMENTS

I would like to start by saying that the last few years have been the most “colorful and spicy” of my life because I truly had the opportunity to meet and get to know people from different countries, with different customs and a wide range of cultural backgrounds. In the process, I learned how boring life would be without these differences and contrasts. I am pleased that I became part of a community where I could appreciate how each individual brings to a common environments his or her unique intrinsic beauty, strength, and values. I am also deeply grateful to all the teachers that opened my eyes and guided my steps in the long and winding (and yet truly challenging and exciting) road to the fantastic world of research.

First and foremost, I thank my thesis advisor, Professor António Pascoal, who was not only scientifically but also socially my teacher and guide. I am grateful to his continuous stream of ideas and insightful comments, excellent guidance and patience, and availability to listen to my concerns and hardships, thus absorbing some of the pressure that I experienced at times. Undoubtedly, he was the most influential person during my PhD studies and I can only wish that the link that we established will continue in the years to come. He is truly a good friend. My special thanks go to my thesis co-advisor, Professor Carlos Silvestre, for his encouraging and useful comments and for always being helpful and giving good insight into the problems. I thank both of them for giving me support and offering me countless opportunities.

Professor Pedro Aguiar came to ISR in the middle of my PhD research. However, he was extremely influential in shaping its final stage. I was lucky to have him as my next door neighbor, always available for discussions and solid advice on theoretical issues. He truly helped me open new horizons and develop new concepts that materialized in the form of joint publications. I am indebted to his guidance and thought provoking discussions. I am also indebted to Professor Isaac Kaminer for his helpful comments, exciting discussions and tremendous insight on the practical implications of the theoretical results derived. I thank him for giving me the opportunity to visit the NPS and hosting me in Monterey, California as a good friend. I am also obliged to Professor Kristing Petterson for being kind enough to invite me to spend three months at the NTNU and for creating a pleasant and challenging research atmosphere that I truly appreciated. My special gratitude goes also to Professor Michael Athans for his cheerful disposition and encouragement and for giving

me great insight into control and estimation theory. I would also like to thank Professor João Hespanha for his insight advice and helpful comments on some of the work that we did jointly.

To Professor Isabel Ribeiro, the Director of ISR, go my special thanks for her determination in pursuing the policy of attracting and encouraging foreign PhD students to come and stay in Portugal and for making the atmosphere of ISR a friendly and motivating one.

I would like to thank all the institutions that supported this work, and in special the FCT (Fundação para a Ciência e a Tecnologia) for providing me with a PhD grant[1].

I also thank Professor João Lemos and Professor José Sá da Costa for having kindly agreed to participate in my thesis research and final PhD committees, and for giving me solid advice on how to shape the thesis. My appreciation goes also to Professor Jorge Martins de Carvalho for his participation in my PhD committee.

I wish to thank my father, mother, brother and sister, although far, for giving me courage and strength through their understanding and moral support. My deepest thanks go to Niina for giving me continuous hope and courage, specially through final stages of my PhD research. I also express my gratitude to the Pestana's family, Eduarda and Rui, who played the role of my family and friends in Portugal. In this regard, I can never forget my Brazilian friends Rodrigo, Ana, and Danilo.

Finally, I wish to thank Rita, Sandra, Karim, Alex, Francisco, Nuno, Guilherme, Luis, Rufino, and Sajjad for their friendship and a pleasant working atmosphere.

Lisbon, Portugal — Reza Ghabcheloo
December 28, 2006

[1]This work was supported by the Portuguese FCT POSI program under framework QCA III. It was also partly supported by MAYA-Sub of the AdI, project GREX / CEC-IST (Contract No. 035223), and the FCT-ISR/IST plurianual funding program (through the POS-Conhecimento Program initiative in cooperation with FEDER).

Table of Contents

List of Figures

CHAPTER 1

INTRODUCTION

This thesis addresses the problem of *coordinated path-following* (CPF) whereby *multiple vehicles are required to follow pre-specified spatial paths while keeping a desired inter-vehicle formation pattern in time*. This problem is strongly motivated by mission scenarios that occur naturally in marine robotics (Pascoal et al. 2000). Namely, in the operation of multiple autonomous vehicles for fast acoustic coverage of the seabed. In this important case, two or more vehicles are required to fly above the seabed at the same or different depths, along geometrically similar spatial paths, and map the seabed using copies of the same suite of acoustic sensors. By requesting that the vehicles traverse identical paths so as to make the acoustic beam coverage overlap along the seabed, large areas can be covered in a short time. This imposes constraints on the inter-vehicle formation pattern. Similar scenarios can of course be envisioned for land and air vehicles.

The problem of coordinated path-following has only recently come to the forum. However, some of the key concepts involved can be in part traced back to the ASIMOV project of the CEC coordinated by IST, that aimed at the coordinated control of marine robots. See for example the following statement in (Pascoal et al. 2000).

> "Three major stumbling blocks have thus far prevented demonstrating the potential applications of Autonomous Underwater Vehicle (AUVs) to demanding industrial and scientific missions. Namely, i) the lack of reliable navigation systems, ii) the impossibility of transmitting data at high rates between

> the AUV and a support ship at slant range, and iii) the unavailability of advanced mission control systems offer effectively affording end-users the tools to seamlessly plan, program, and run scientific / industrial missions at sea, while having access to ocean data in almost real-time so as to re-direct the AUV mission, if required. As a contribution toward solving some of the above-mentioned problems, the ASIMOV project puts forward the key concept of an Autonomous Surface Vehicle (ASV) that will operate in close cooperation with an AUV, as a mobile relay for fast communications. In the scenarios considered, the ASV will be equipped with a differential GPS receiver, an ultra short baseline unit (USBL), a radio link, and a high data rate communication link with the AUV that will be optimized for the vertical channel. By properly maneuvering the ASV to *always remain in the vicinity of a vertical line with the AUV*, a fast communication link can be established to transmit navigational data from the DGPS and USBL units to the AUV and ocean data from the AUV to the ASV, and subsequently to an end-user located on board a support ship or on shore via an aerial link."

The above concept is illustrated in Figure 1.1. Other scenarios can be envisioned, of which the following are representative examples. See (Fossen 2002) and (Pascoal et al. 2006) and the references therein.

- *Image acquisition*- Combined autonomous underwater vehicle control. This scenario occurs when an underwater vehicle carries a strong light source and illuminates the scenery around a second underwater vehicle that must follow a pre-determined path and acquire images for scientific purposes.

- *Fast acoustic coverage of the seabed* - Combined autonomous underwater vehicle control. In this important case, two vehicles are required to maneuver above the seabed at identical or different depths, along parallel paths, and map the sea bottom using two copies of the same suite of acoustic sensors (e.g. sidescan, mechanically scanned pencil beam, and sub-bottom profiler). By requesting the vehicles to traverse identical paths so as to make the acoustic beam coverage overlap on the seabed, large

areas can be covered quickly. One can also envision a scenario where the vehicles use a set of vision sensors to inspect the same scenery from two different viewpoints to try and acquire three-dimensional images of the seabed.

- *Underway replenishment*, or *replenishment at sea*- a challenging mission scenario. "An underway replenishment operation is an operation where fuel, food, parts or personnel are transferred from one vessel to another while both vessels are moving, and is common in marine operations." (Kyrkjebo 2007). In this situation, there is a need to coordinate the two vessels, the mother vessel playing the role of leader and the ship to be replenished that of follower, the vessels moving in a alongside kind of formation. See Figure 1.2.

The above circle of ideas has spurred great interest and has led to the definition of some challenging problems that are of the root of the key questions addressed in this thesis. From a theoretical viewpoint, the plethora of problems that must be solved to achieve coordination of multiple vehicles spans a vast number of fields that include navigation, guidance, and control. Here, we focus on the problem of coordinated motion control. At first inspection, this problem seems to fall within the domain of decentralized control. However, as clearly pointed out by (Fax & Murray 2002*a*,*b*), it possesses several unique aspects that pose new challenges to system designers. Among these, the following are worth stressing:

i) except for some cases in the area of aircraft control, the motion of one vehicle does not directly affect the motion of the other vehicles, that is, the vehicles are dynamically decoupled; the only coupling arises naturally out of the specification of the tasks that they are required to accomplish together.

ii) there are strong practical limitations to the flow of information among vehicles, which is severely restricted by the nature of the supporting communications network. In marine robotics, for example, underwater communications (that rely on the propagation of acoustic waves) are plagued with intermittent failures, delays, and multi-path effects. These effects set tight limits on the effective communication bandwidths that can be achieved and introduce latency in the measurements that are exchanged among the vehicles. As a rule, no vehicle will be able to communicate with the entire formation and the vehicles cannot

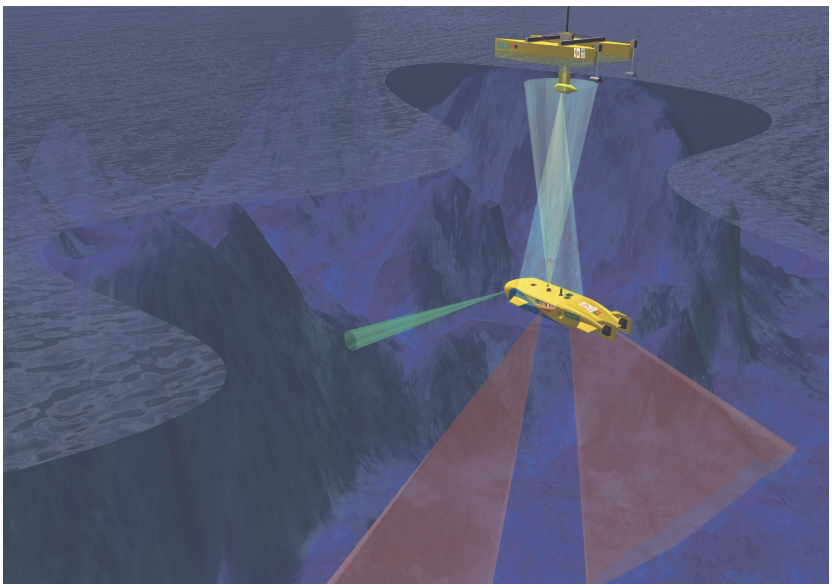

Figure 1.1: ASIMOV project. AUV / ASC coordination

all communicate at the same time. It is therefore imperative to develop coordinated motion control strategies that can yield robust performance in the presence of communication failures and switching communication topologies. New paradigms are required to address these challenges, thus departing from classical centralized control methodologies.

Classical centralized controllers deal with systems in which a single controller possesses all the information needed to achieve desired control objectives, including stability and performance requirements. However, in many applications like the one described before, it is impractical to exchange all the relevant information and convert the problem into a centralized one. Thus the need to study and develop decentralized algorithms where single local controllers act based on partial information to accomplish a common goal. For example, to bring subsets of the states of networked systems to converge to a common value (agreement problem). Over the past few years, there has been a flurry of activity in the area of multi-agent networks with application to engineering and science problems. The thesis exploits some of the ideas proposed in the literature and advances new ones. The main theme of the work revolves around coordinated path-following, as explained below.

Figure 1.2: Underway replenishment. Source: US defence visual information center/public release. ID: DN-SC-05-06680.

1.1 Coordinated path-following

Coordinated Path-Following (CPF) addresses the problem of steering a group of autonomous vehicles along given spatial paths, while holding a desired inter-vehicle formation pattern. The CPF control methodology is a "*Divide to Conquer*" approach. Using this framework, path-following (in space) and inter-vehicle coordination (in time) can be essentially be viewed as decoupled. Path-following for each vehicle amounts to reducing a conveniently defined error variable to zero. Vehicle coordination is typically achieved by adjusting the "speed" of each of the vehicles along its path according to information on the positions of a set of neighboring vehicles, as determined by the topology of the communication network adopted. No other kinematic or dynamic information is exchanged among the vehicles.

1.1.1 Path-following

Consider the autonomous underwater vehicle depicted in Figure 1.3, together a spatial path Γ in the horizontal plane to be followed. It is assumed that the vehicle is equipped with actuators capable of imparting the necessary forces and torques to it. In a great number of cases, the vehicle may be underactuated. The problem of path-following can be briefly stated as follows:

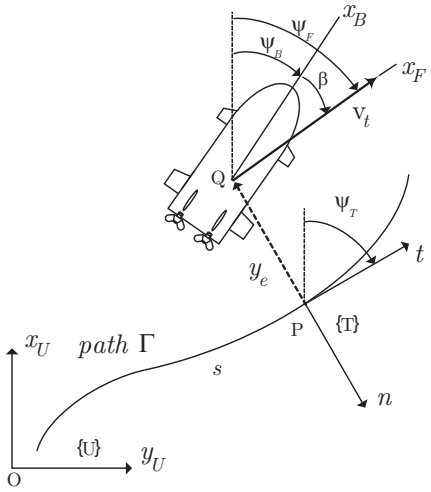

Figure 1.3: Path-following problem

Given a spatial path Γ*, develop a feedback law for the control forces and torques acting on the vehicle so that its centre of mass will converge asymptotically to the path while its total speed tracks a desired temporal profile* $v_d(t)$*,* $t \geq 0$*.*

Consider again Figure 1.3, where P is an arbitrary point on the path and $\mathbf{p}$ denotes its position in the inertial frame $\{\mathrm{U}\}$. Let $\{\mathrm{B}\}\equiv\{x_B, y_B\}$ and $\{\mathrm{F}\}\equiv\{x_F, y_F\}$ denote the body-fixed frame and flow frame, respectively, of the vehicle both with origin at Q, its centre of mass. Recall that the flow frame has its $x-$axis aligned with vehicle's velocity vector. Associated with P, consider the tangent frame $\{\mathrm{T}\}\equiv\{\mathbf{t}, \mathbf{n}\}$, where $\mathbf{t}$ and $\mathbf{n}$ denote the tangent and normal, respectively, to the path. The signed curvilinear abscissa of P along the path is denoted s and is measured from some appropriate origin. With these definitions, the problem of path-following is equivalently defined as that of driving the flow frame $\{\mathrm{F}\}$ to the state-driven (time-varying) tangent frame $\{\mathrm{T}\}=\{\mathrm{T}\}(s)$ while ensuring that $\|\dot{\mathbf{p}}(t)\|$ tracks a desired speed profile. Under these conditions, Q tends to P, x_F aligns itself asymptotically with $x_T \equiv \mathbf{t}$, and $\dot{s} \to v_d$. Several solutions to the problem of path-following of a single vehicle will be presented in this thesis.

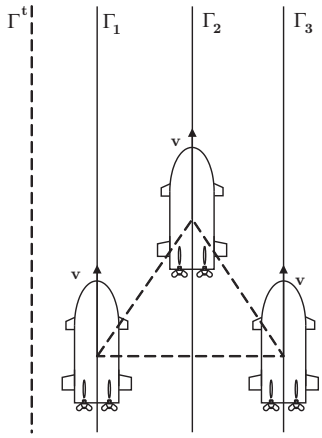

Figure 1.4: Coordination: triangle formation

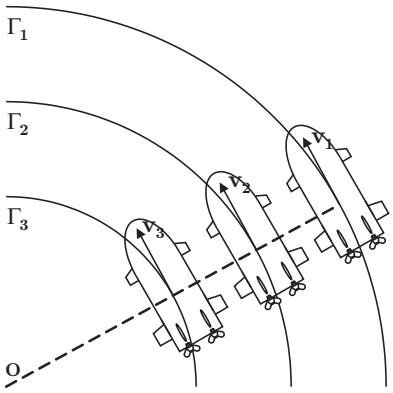

Figure 1.5: Coordination: in-line formation

1.1.2 Coordination

In the most general set-up of the CPF problem, one is given a set of $n \geq 2$ vehicles and a set of n spatial paths Γ_k; $k \in \mathbb{N}_n := \{1,...,n\}$ and require that vehicle k follow path Γ_k. We further require that the vehicles move along the paths in such a way as to maintain a desired formation pattern compatible with the paths. The speeds at which they are required to travel can be imposed in a number of ways; for example, by nominating one of the vehicles as a formation leader, assigning a desired speed to it, and having the other vehicles adjust their speeds accordingly. Figures 1.4 and 1.5 show the simple cases where 3 vehicles are required to follow straight paths and circumferences $\Gamma_i; i = 1,2,3$, respectively, while keeping a desired "triangle" or "in-line" formation pattern.

In the simplest case, the paths Γ_i may be obtained as simple parallel translations of a "template" path Γ^t (Figure 1.4). A set of paths can also be obtained by considering the case of scaled circumferences with a common centre and different radii R_i (Figure 1.5). In the course of this thesis, more general paths and formation patterns will be considered.

Assuming that separate path-following controllers have been implemented for each vehicle, it now remains to coordinate (that is, synchronize) the vehicle motions in time so as to achieve a desired formation pattern. As will become clear throughout the thesis, this will be achieved by adjusting the "speeds" of the vehicles as functions of the "along-path"

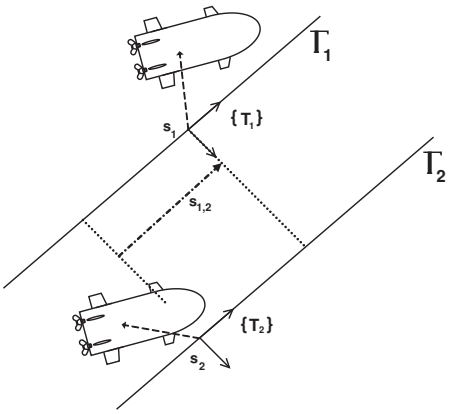

Figure 1.6: Along-path distances: straight lines

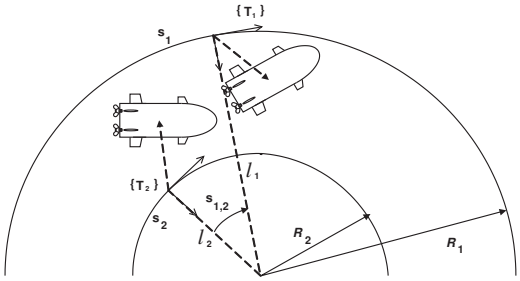

Figure 1.7: Along-path distances: circumferences

distances among them. To better grasp the key ideas involved in the computation of these distances, consider for example the case of in-line formations maneuvering along parallel translations of straight lines. For each vehicle i, let s_i denote the signed curvilinear abscissa of the origin of the corresponding tangent frame $\{\mathrm{T}_i\}$ being tracked, introduced before. Since the flow frame $\{\mathrm{F}_i\}$ tends asymptotically to $\{\mathrm{T}_i\}$, it follows that the vehicles are (asymptotically) coordinated or synchronized if

$$s_{i,j}(t) := s_i(t) - s_j(t) \to 0, t \to \infty; i = 1,..,n; i < j \leq n. \tag{1.1}$$

This shows that in the case of translated straight lines $s_{i,j}$ is a good measure of the along-path distances among the vehicles. Similarly, in the case of scaled circumferences an appropriate measure of the distances among the vehicles is

$$\bar{s}_{i,j} := \bar{s}_i - \bar{s}_j; i = 1,..,n; i < j \leq n \tag{1.2}$$

where $\bar{s}_i = s_i/R_i$. See Figures 1.6 and 1.7.

Notice how the definition of $\bar{s}_{i,j}$ relies on a normalization of the lengths of the circumferences involved and is equivalent to computing the angle between vectors l_i and l_j directed from the centre of the circumferences to origin of the tangent frames $\{\mathrm{T}_i\}$ and $\{\mathrm{T}_j\}$, respectively. In both cases, we say that the vehicles are coordinated if the corresponding along path distance is zero, that is, $s_i - s_j = 0$ or $\bar{s}_i - \bar{s}_j = 0$. The extension of these concepts to a

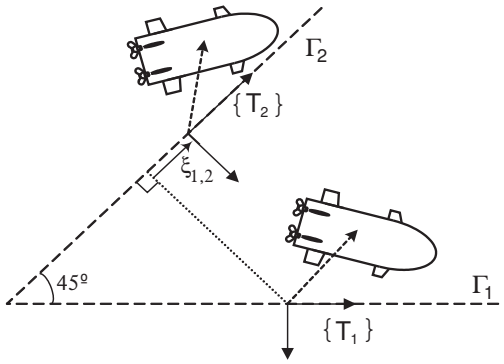

Figure 1.8: A general coordination scheme

more general setting requires that each path Γ_i be parameterized in terms of a parameter ξ_i that is not necessarily the arc length along the path. An adequate choice of the parameterization will allow for the conclusion that the vehicles are synchronized iff $\xi_i = \xi_j$ for all i, j. For example, in the case of two vehicles following two circumferences with radii R_1 and R_2 while keeping an in-line formation pattern, $\xi_i = s_i/R_i; i = 1,2$. This seemingly trivial idea allows for the study of more elaborate formation patterns. As an example, consider the problem depicted in Figure 1.8 where vehicles 1 and 2 must follow paths Γ_1 and Γ_2 while maintaining vehicle 2 "to-the-left-and-behind" vehicle 1, that is, along a straight line that makes an angle of 135 degrees with the positive direction of path Γ_1. Let $\xi_1 = s_1$ and $\xi_2 = s_2\sqrt{2}$. It is clear that the vehicles are synchronized if they are on their assigned paths and $\xi_1 - \xi_2 = 0$. Since the objective of the coordination is to synchronize the ξ_i's, we will refer to them as *coordination states*.

Consider the general problem of synchronizing n coordination states $\xi_i; i \in \mathbb{N}_n$ where ξ_i corresponds to vehicle i and path Γ_i. For simplicity of exposition, assume the vehicles are on their paths, thus avoiding at this introductory stage the problem of path-following/coordination interaction. Let u_i be the control signal of vehicle i available for coordination. The objective is to derive a control law for $u_i; i \in \mathbb{N}_n$, so as to make $\xi_1 = ... = \xi_n$ or, equivalently, $(\xi_i - \xi_j) = 0$ for all $i, j \in \mathbb{N}_n$. It is further required that the fleet of vehicles adopt a desired common speed profile $v_{\mathscr{L}}$, that is, $\dot{\xi}_i = v_{\mathscr{L}}\ \forall i \in \mathbb{N}_n$. This issue requires clarification. Notice that the desired speed assignment is given in terms of the time derivatives of the coordination states ξ_i, not in terms of the actual inertial speeds of the vehicles

undergoing synchronization. Assuming the vehicles have reached their paths, their speeds degenerate into $\frac{ds_i}{dt}; i \in \mathbb{N}_n$ and because $\frac{d\xi_i}{dt} = \frac{d\xi_i}{ds_i}\frac{ds_i}{dt} = v_{\mathscr{L}}$, it follows that $\frac{ds_i}{dt} = v_{\mathscr{L}}/\frac{d\xi_i}{ds_i}$. This yields $\frac{ds_i}{dt} = R_i v_{\mathscr{L}}$ for the example of the circumferences given above. With this speed assignment, one does not have to specify the actual inertial speeds of the vehicles, but rather those of their coordination states which are all equal to $v_{\mathscr{L}}$. In the most general setting $v_{\mathscr{L}}$ may be time-varying. For example, $v_{\mathscr{L}}$ can be taken as an explicit function of time t or of one of the coordination states ξ_i. At this point, two extremely important control design constraints must be taken into consideration. The first type of constraint is imposed by the topology of the inter-vehicle communications network, that is, by the types of links available for communications. The second type of constraint arises from the need to drastically reduce the amount of information that is exchanged over the communications network. In a typical case, it is assumed that the vehicles only exchange information on their "positions" along the paths (the coordination states). As a consequence the coordination laws are necessarily of the form

$$u_i = u_i(\xi_i, \xi_j : j \in N_i) \tag{1.3}$$

where $N_i \subset \mathbb{N}_n$ is the neighboring set, an index set that determines what coordination states $\xi_j;\ j \in N_i$ are transmitted to vehicle i. With this control law, each vehicle i requires only access to its own coordination state and to some or all of the coordination states of the remaining vehicles, as defined by the index set N_i. Throughout the thesis, two types of communication links are considered: i) *bi-directional communication links*, that is, if vehicle i sends information to j, then j also sends information to i; formally, $i \in N_j \Leftrightarrow j \in N_i$; ii) *uni-directional communication links*, where $i \in N_j$ does not necessarily imply that $j \in N_i$. Clearly, the index sets capture the type of communication structure that is available for vehicle coordination. This suggests that the vehicles and the data links among them should be viewed as a *graph* where the vehicles and the data links play the role of vertices of the graph and edges connecting those vertices, respectively. It is thus natural that the machinery of graph theory be brought to bear on the definition of the problem under study.

To better grasp the circle of ideas exposed, a very simple example of a CPF control algorithm for two unicycle type robots is given next. The treatment is rather cursory and most of the details are omitted. This subject will be fully studied in the main body of the

thesis which will address the problem of CPF for multiple underactuated vehicles, general types of paths and formation patterns, and switching communication networks.

1.2 Coordinated path-following: a simple example

Consider the problem of coordinated path-following control for two wheeled vehicles of the unicycle type in the $x-y$ plain. Each vehicle is required to follow a horizontal straight line along the $x-$axis while keeping an in-line formation pattern along the $y-$axis, that is, the vehicles are required to reach agreement on the $x-$coordinate. Let the equations of motion of each vehicle be described by

$$\dot{x} = v\cos\psi$$
$$\dot{y} = v\sin\psi$$

where the forward speed v and the heading angle ψ are taken as the control signals. We will refer to the vehicles as V_1 and V_2 and use subscripts 1 and 2 to distinguish between their states. We further denote by $\Gamma_i; i = 1,2$ the paths to be followed by the vehicles, where Γ_1 and Γ_2 are obtained by shifting the $x-$axis along the vertical coordinate y by Δ_s^1 and Δ_s^2, respectively. Vehicle $i; i = 1,2$ can be driven to the desired path Γ_i using the heading control

$$\psi_i = -\text{sign}(v_i)\sin^{-1}[\frac{2}{\pi}\tan^{-1}\frac{y-\Delta_s^i}{\Delta}], \tag{1.4}$$

where sign$(.)$ is the sign function and $\Delta > 0$ is a tuning variable that is commonly referred in the literature as the LOS[1] distance. The resulting closed-loop dynamics in y are given by

$$\dot{y}_i = -\frac{2|v_i|}{\pi}\tan^{-1}\frac{y_i-\Delta_s^i}{\Delta},$$

thus guaranteeing that $y_i \to \Delta_s^i$ and $\psi_i \to 0$ as $t \to \infty$, if $v_i \nrightarrow 0$.

For each vehicle, its dynamics along the $x-$coordinate can be written as

$$\dot{x}_i = v_i + d_i$$

[1] Line Of Sight

where $d_i = v_i(\cos\psi_i - 1)$ and d_i vanishes as $t \to \infty$, since so does ψ_i. In what follows, we assume that $d_i = 0; i = 1,2$ to simplify the presentation of the key ideas involved in synchronization. Later throughout the thesis, we will consider the case when $d_i \neq 0$.

Consider a coordination problem in which the vehicles are required to agree on the coordination state x_i and follow a common speed profile $v_{\mathscr{L}}(t)$. Assume that the vehicles exchange information on their $x-$coordinate positions only. Coordination can be achieved using the control law

$$\begin{aligned} \dot{x}_1 &= v_1 = -a_1(x_1 - x_2) + v_{\mathscr{L}} \\ \dot{x}_2 &= v_2 = -a_2(x_2 - x_1) + v_{\mathscr{L}} \end{aligned} \tag{1.5}$$

for some $a_i > 0$. To prove agreement between x_1 and x_2, let $e = x_1 - x_2$. This yields $\dot{e} = -(a_1 + a_2)e$ and e converges exponentially to zero. Therefore, $\dot{x}_1$ and $\dot{x}_2$ tend to $v_{\mathscr{L}}$ as $t \to \infty$. Implementing the control signal (1.5) requires that both vehicles know the speed profile $v_{\mathscr{L}}(t)$ in advance. While this is a plausible assumption, it can be alleviated when $v_{\mathscr{L}}$ is constant, as follows. Let V_1 play the role of a leader that sets the formation speed $v_{\mathscr{L}}$, and let V_2 be required to learn it. Set a new coordination control law as

$$\dot{x}_1 = -a_1(x_1 - x_2) + v_{\mathscr{L}}$$

for V_1 and

$$\begin{aligned} \dot{x}_2 &= -a_2(x_2 - x_1) + b_2 e_I \\ \dot{e}_I &= x_1 - x_2 \end{aligned}$$

for V_2, where $b_2 > 0$ and e_I is an auxiliary "integral" state. Let $e := x_1 - x_2$ and $x_c := (e, e_I)^T$. Then, $\dot{x}_c = Ax_c + (v_{\mathscr{L}}, 0)^T$ where

$$A = \begin{pmatrix} -(a_1 + a_2) & -b_2 \\ 1 & 0 \end{pmatrix}.$$

Clearly, A is Hurwitz. In the special case where $b_2 = a_1 a_2$, A has two eigenvalues at $-a_1$ and $-a_2$. Therefore $\dot{x}_c \to 0$ exponentially if $v_{\mathscr{L}}$ is constant. As a consequence, $e \to 0$ as $t \to \infty$, and $\dot{x}_1, \dot{x}_2$ tend to $v_{\mathscr{L}}$. If $v_{\mathscr{L}}$ has a bounded time derivative, $\dot{x}_i - v_{\mathscr{L}}$ will be bounded.

Simulations were performed to visualize the time trajectories of the states in the above-mentioned example. Figure 1.9 illustrates the simulations for the case where $v_{\mathscr{L}} = 0.5[\mathrm{s}^{-1}]$,

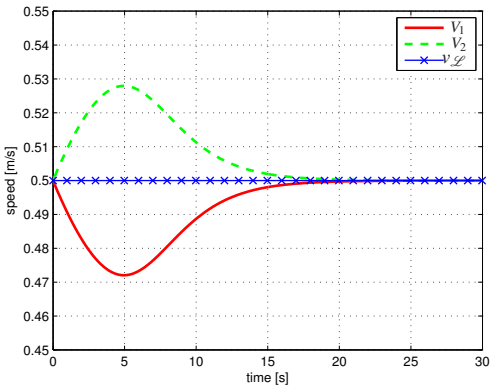

(a) Vehicle speeds

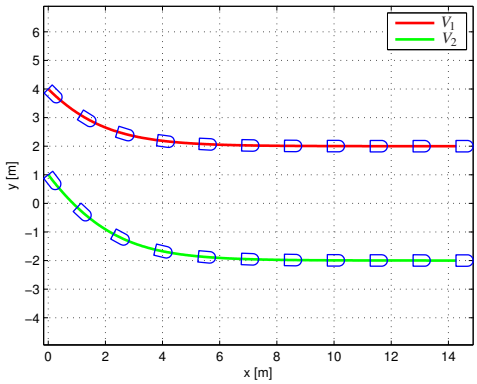

(b) Vehicle trajectories

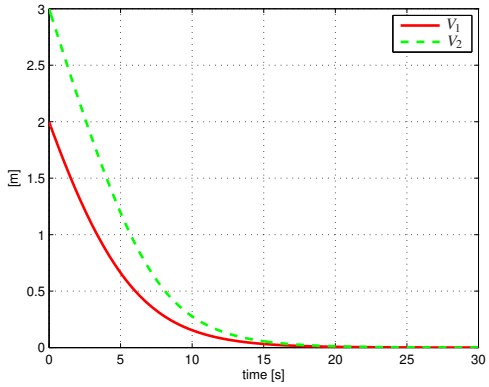

(c) $y_1 - \Delta_s^1$ and $y_2 - \Delta_s^2$

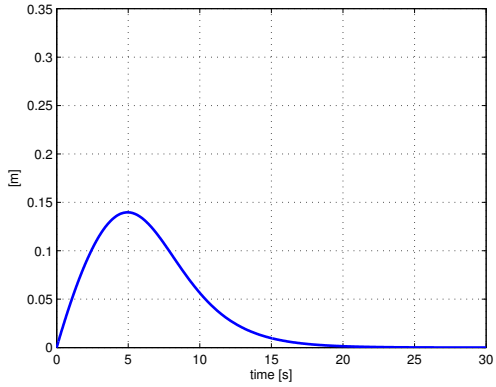

(d) $x_1 - x_2$

Figure 1.9: Simple example: coordination of 2 vehicles along straight lines: fixed communication topology

$\Delta = 1[\text{m}]$, $a_1 = a_2 = 0.2[\text{s}^{-1}]$ and the vehicles were requested to follow Γ_1 and Γ_2 with $\Delta_s^1 = 2[\text{m}]$ and $\Delta_s^2 = -2[\text{m}]$.

Notice how the speeds converge to the desired speed[2] (Figure 1.9(a)), the vehicles converge to their assigned paths (Figure 1.9(b)), the off-path distances go to zero (Figure 1.9(c)), and the coordination error vanishes (Figure 1.9(d)).

We now give some insight into the coordination problem in the presence of communication losses. Consider the previous coordination problem with the following switching

[2] In this case, since the coordination states ξ_i are taken to be the $x-$coordinates of the robots, the desired inertial speeds equal $v_{\mathscr{L}}$ in value.

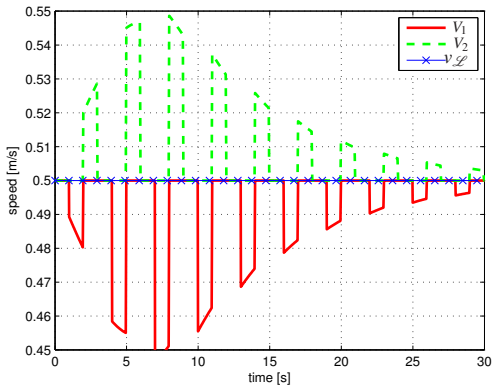

(a) Vehicle speeds

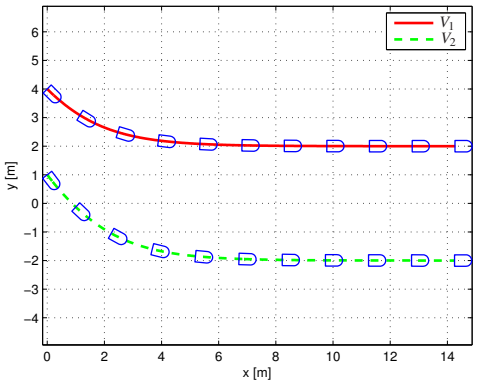

(b) Vehicle trajectories

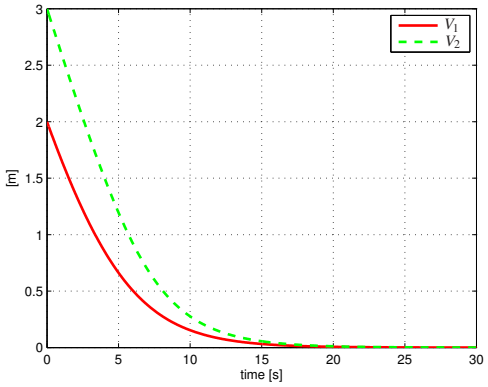

(c) $y_1 - \Delta_s^1$ and $y_2 - \Delta_s^2$

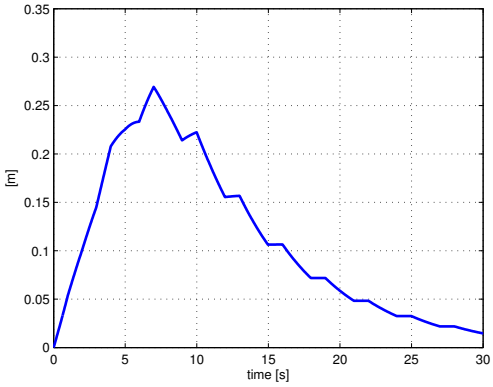

(d) $x_1 - x_2$

Figure 1.10: Simple example: coordination of 2 vehicles along straight lines, with communication losses; $T_0 = T_1 = T_2 = 1$[s]

communication scenarios.

Switching network: There exist $T_M > 0$ and $0 < T_m < T_M$ such that over any interval of length T_M, vehicles V_1 and V_2 exchange information about their states during a total time interval of duration greater than T_m. The communications may occur simultaneously, or each vehicle may only communicate when the other one is not transmitting. For example, vehicle V_2 sends measurements of x_2 to V_1 during T_1 seconds, vehicle V_1 sends measurements of x_1 to V_2 during T_2 seconds non-overlapping with T_1 and $T_1 + T_2 \geq T_m$. In this scenario, during an interval of length T_m the vehicles remain silent during T_0 seconds, where $T_0 \leq T_M - T_m$.

In what follows, we only address the coordination dynamics with the control law of (1.5) and the switching communication topology described above. We will show that coordination is achieved under the above communication scenario. Before proceeding, we need the following Lemma. A proof is given in the Appendix.

Lemma 1.1

Let $p(t)$ be a binary function that takes values in the set $\{0,1\}$ and let

$$\int_{t_1}^{t_2} p(t)dt \leq \alpha(t_2 - t_1), \forall\, t_2 - t_1 \geq T \tag{1.6}$$

for some $0 \leq \alpha < 1$ and $T > 0$. Then, the origin of the scalar switching ODE

$$\dot{x} = -a(1 - p(t))x \tag{1.7}$$

is stable and $x \to 0$ exponentially with rate $(1-\alpha)a$, for any $a > 0$.

In (1.6), α is a measure of the percentage of time that $p(t) = 1$ during any time interval $[t_1, t_2]$ of length at least T, or equivalently, the percentage of time that the dynamics (1.7) take the "unstable" form $\dot{x} = 0$. Equivalently, $(1-\alpha)$ is percentage of time that the dynamics (1.7) take the stable form $\dot{x} = -ax$, over any interval $[t_1, t_2]$ of length at least T. Coming back to the main problem (coordination under communication losses), let $a_i(t) = a$ when V_i receives information from the companion vehicle, and $a_i(t) = 0$ otherwise. Now, recall the dynamics of the coordination error $e = x_1 - x_2$, that is, $\dot{e} = -(a_1(t) + a_2(t))e$. Therefore, if the communication network admits the switching scenarios described above, over any interval of length T_M, $\dot{e} = -ae$ during at least T_m seconds and $\dot{e} = 0$ in the remaining instants. Thus, Lemma 1.1 applies with $1 - \alpha = T_m/T_M$ and $T = T_M$. As a consequence, $e \to 0$ exponentially and coordination is achieved.

This example gives a glimpse of the type of problems that may arise because of temporary communication losses. Namely, the degradation in performance that may occur as the percentage of time that communications are lost increases; in the example above, the degradation of performance translates into a slower rate of decay of the coordination error. One of the key objectives of the thesis is to extend the analysis above to a more general set-up.

1.3 Literature review

Increasingly challenging mission scenarios and the advent of powerful embedded systems and communication networks have spawned widespread interest in the problem of coordinated motion control of multiple autonomous vehicles. The types of applications envisioned are numerous and include aircraft and spacecraft formation flying control (Beard et al. 2001), (Giuletti et al. 2000), (Pratcher et al. 2001), coordinated control of land robots (Ghabcheloo et al. 2007), (Ogren et al. 2002), control of multiple surface and underwater vehicles (Encarnação & Pascoal 2001), (Lapierre et al. 2003), (Skjetne et al. 2002), and networked robots (Cortes & Bullo 2005).

To meet the requirements imposed by these applications, a new control paradigm is needed that departs considerably from classical centralized control strategies. In fact, because of the highly distributed nature of the vehicles' sensing and actuation modules, and due to the very nature of the inter-vehicle communications network, it becomes impossible to tackle the new problems at hand in the framework of centralized control theory. For these reasons, there has been over the past few years widespread interest in the area of multi-agent networks with application to engineering and science problems. Namely, in such topics as parallel computing (Tsitsiklis & Athans 1984), synchronization of oscillators (Papachritodoulou & Jadbabaie 2005), (Sepulchre et al. 2003), collective behavior and flocking (Jadbabaie et al. 2003), consensus (Lin et al. 2005*b*), multi-vehicle formation control (Egerstedt & Hu 2001), asynchronous protocols (Fang et al. 2005), graph theory and graph connectivity (Kim & Mesbahi 2006), and Voronoi tessellations (Bullo & Cortes 2005).

In what follows, for the sake of completeness, we provide a brief summary of two broad classes of research topics that bear close affinity to those addressed in this thesis. Namely, coordinated path-following and applications of graph theory to the study of the limitations introduced by inter-vehicle communication constraints.

1.3.1 Coordinated path-following

The problem of Coordinated Path-Following has only recently been addressed in the literature. Previous work in the area has essentially been restricted to marine robots. See (Fossen 2002), (Encarnação & Pascoal 2001), (Lapierre et al. 2003), (Skjetne et al. 2002), (Skjetne et al. 2003), and (Ghabcheloo, Pascoal & Silvestre 2005*b*) and the references therein for an introduction to and a historical perspective of this vibrant topic of research. See also (Kyrkjebo & Pettersen 2003) and (Kyrkjebo et al. 2004) for a very interesting type of cooperative motion control problems with applications in ship rendezvous maneuvers. The reader will also find in (Pascoal et al. 2006) a fast paced presentation of the problem and a description of some of the techniques developed to solve it.

The problem of coordinated path-following is implicit in the early work of (Encarnação & Pascoal 2001) for coordinated path-following control of an autonomous surface craft (ASC) and an autonomous underwater vehicle (AUV). However, the strategy adopted is not easily generalized to more than two vehicles and requires that a large amount of information be exchanged between them. The latter problem was alleviated in the work of (Lapierre et al. 2003) on coordinated path-following of two underwater vehicles by resorting to a technique that "almost decouples" the spatial and temporal assignments referred to above: both the leader and follower execute path-following algorithms, the leader traveling along its path at the desired speed profile. It is the task of the follower to adjust its total speed based on the measurement of a generalized "along-path distance" between the two vehicles. Intuitively, the follower speeds up or slows down in reaction to the distance between two "virtual target vehicles" involved in the path-following algorithms. This strategy drastically reduces the amount of information that must be exchanged between the two vehicles. Controller design builds on Lyapunov theory and backstepping techniques. The resulting nonlinear feedback control law yields convergence of the two vehicles to the respective paths and forces the follower to accurately track the leader asymptotically. Thus, the mathematical machinery supports the intuition behind the spatial/temporal almost decoupling assumption. Interestingly enough, a solution to the problem of coordinated path-following that relies on the computation of the distance between "virtual target vehicles" was advanced at practically the same time by (Skjetne et al. 2003). However, in

these early approaches to coordinated path-following the communication constraints were never addressed explicitly and new techniques were required to make progress in this yet uncharted territory. It was against this backdrop of ideas that the work of (Ghabcheloo, Aguiar, Pascoal, Silvestre, Kaminer & Hespanha 2006) exploited the use of graph and networked control theory to yield new solutions to the problem of coordinated path-following control in the presence of communications with failures. Currently, research continues on how to better cope with communication failures and/or time-varying communication topologies by incorporating distributed observers. There is also great interest in addressing the problems that arise due to latency in the measurements and in the transmission of information. The problem of coordinated path-following is receiving increased attention and has led to a body of literature that exploits the use of complementary techniques for its solution. A representative example is the PhD thesis (Ihle 2006) recently concluded at the Norwegian University of Science and Technology in Norway, where the author uses the term "synchronized path-following" instead of coordinated path-following. The main body of his work considers fully actuated marine vessels and employs passivity theorems. However, communication constraints are not addressed explicitly.

Recently, we became aware of the work of (Egerstedt & Hu 2001) that addresses a problem akin to that of CPF. The solution adopted builds also on the decoupling of path tracking and coordination. A virtual path with a reference point moving on the latter is considered. The formation is defined by the global minimum of a "rigid body constraint function"; for example, for 3 vehicles the function $f(r) = (\|r_1 - r_2\| - 1)^2 + (\|r_2 - r_3\| - 1)^2 + (\|r_3 - r_1\| - 1)^2$, where r_i denotes the position of vehicle i in the inertial frame, "corresponds" to an equilateral triangle where all sides have length equal to 1. Using this function, a desired trajectory is defined for each robot by a steepest descent method. The authors show that if the robots track their respective reference points perfectly, or if the tracking errors are bounded, the formation error is stabilized about zero. It is interesting to point out that no communication constraints are explicitly considered; however, close analysis of the framework adopted suggests that communication constraints maybe cast in the form of rigid body links.

1.3.2 Communication topologies and graph theory

This section gives a survey of important references on the application of graph theory to the modeling of communication constraints that arise in coordinated control. For the sake of clarity and briefness we keep the technical details to a minimum.

A rigorous methodology to deal with some of the issues that arise in coordinated motion control has emerged from the work reported by (Fax & Murray 2002*a*,*b*) that addresses explicitly and simultaneously the topics of information flow and cooperation control of vehicle formations. The methodology proposed builds on an elegant framework that involves the concept of Graph Laplacian (a matrix representation of the graph associated with a given communication network[3]). In particular, the results in (Fax & Murray 2002*b*) show clearly how the Graph Laplacian associated with a given inter-vehicle communication network plays a key role in assessing stability of the behavior of the vehicles in a formation. It is however important to point out in that work the following: i) the dynamics of the vehicles are assumed to be linear and time-invariant and ii) the information exchanged among vehicles is restricted to linear combinations of the vehicles' state variables. With the set-up adopted in (Fax & Murray 2002*b*), the stability of the formation dynamics can be examined by using a simple Nyquist-like criterion. The key result involves the Laplacian L of the graph associated with the communication topology of a fleet of vehicles and its associated eigenvalues λ_i, together with the loop transfer function $K(s)G(s)$ for each local vehicle control system. It is proved that if *the net encirclement of* λ_i^{-1} *by the Nyquist plot of* $K(s)G(s)$ *is zero (for all* $\lambda_i \neq 0$*), then the formation is stable*. This result shows clearly how the eigenvalues of the graph Laplacian L impact directly on the stability of the formation dynamics. The authors use the fact that for strongly connected graphs, L has a single eigenvalue at zero and the remaining eigenvalues have positive real part. Interestingly enough, the periodicity of a graph places the inverse of the eigenvalues of its Laplacian closer to the imaginary axis. This in turn implies that the stability margin of the resulting coordinated system is degraded. In other words, *aperiodicity is a desirable property of the formation interconnection topologies*. In fact, it can be shown that for directed

[3]The term sensor graph is used instead of communication graph, if the source of the information in the interconnection network is sensory.

graphs, adding communication links to an existing communication graph may destabilize the formation dynamics.

In (Olfati Saber & Murray 2003*a*) the agreement and average-consensus problems for a network of integrators $\dot{x} = u$ with directed information flow (communication links) are studied in detail. We recall that the agreement problem consists of stabilizing all the states of a number of interconnected systems to a common value while in the average-consensus problem this common value is the average of the initial states. It is shown that the control law $u = -Lx$, where L is the graph Laplacian, solves the agreement problem if the graph is strongly connected. It is important to stress, based on the results of (Lin et al. 2005*a*), that strong connectedness of a graph is not a necessary condition to achieve agreement. Olfati Saber & Murray (2003*a*) further show, for a strongly connected graph, that the control law $u = -Lx$ solves the average-consensus problem if and only if the graph is balanced, that is, if the total number of edges entering a vertex and leaving the same vertex are equal for all vertices. It is also shown that the rate of convergence to consensus is related to the smallest nonzero eigenvalue of $(L+L^T)/2$, known as the Fiedler eigenvalue (Fiedler 1973). In (Olfati Saber & Murray 2003*b*), some of these results are extended to include time delays and nonlinear protocols such as saturations in the control actuation.

(Mesbahi 2002) introduced state-dependent graphs, motivated by the earlier observation in (Mesbahi & Hadaegh 2001) that the interaction between the elements of a multibody system is generally dynamic, and consequently the corresponding topology is *time and state dependent*. Following (Mesbahi & Hadaegh 2001), let the dynamics of n interacting elements be $x(k+1) = f(x(k), u(k))$, with the communication (and/or sensor) graph denoted by $\mathcal{G}(x(k))$ to highlight the dependency of the topology on the current state of the system. A state-driven dynamic graph can then be defined as a mapping from the space of configuration state to the set of all labeled graphs defined on n vertices. We say $x_i \sim x_j$ (equivalent relation), if $\mathcal{G}(x_i) = \mathcal{G}(x_j)$. Now, define the *graph G of graphs* $\mathcal{G}_i$ as all possible graphs defined on n vertices as the vertices of G. Vertices (Graphs) $\mathcal{G}_i$ and $\mathcal{G}_j$ are neighbors in G if there is a sequence of control inputs driving the system from the equivalent class x_i to the equivalent class x_j, without passing through other equivalent classes. With this setup, (Mesbahi 2002) relates some dynamic system properties, e.g. controlability, to graph properties such as connectedness.

In the present thesis, inspired by the work in (Lin et al. 2005*a*), we avail ourselves of some important results on directed graphs (digraphs). Consider a system of n integrators written in vector form as $\dot{x} = u$. Assume the communication topology is modeled by a digraph $\mathscr{G}$ defined on n vertices. Following common nomenclature, a vertex i is said to be reachable from vertex j if there is a path (of arcs) from j to i. A globally reachable vertex is one that is reachable from every other vertex in the graph. The main lemma of (Lin et al. 2005*a*) states that *if a graph has a globally reachable vertex, then zero is a single eigenvalue of the graph Laplacian L and all the other eigenvalues have positive real part*. From this lemma, it follows that the control law $u = -Lx$ solves the agreement problem, that is $x_i = x_j; \forall i, j$ at steady-state. Another important property of L, also shown in (Lin et al. 2005*a*), is that if the graph has a globally reachable vertex, for any positive definite diagonal matrix R matrix $-RL$ has a single eigenvalue at zero and the rest are stable (the same stability properties as $-L$). By exploiting this circle of ideas for n unicycle type vehicles, the authors derive a decentralized control law that drives the vehicles to any geometrical 2D pattern (point stabilization) when the communication graph has a globally reachable vertex. Some particular cases are also studied when the globally reachability condition is violated.

The problem of decentralized stabilization of vehicle formations using techniques from graph theory is also studied in (Caughman et al. 2005). Each vehicle (in simplified form) can be seen as a second order linear dynamics with acceleration as the input variable. The formation is defined as converging to a predefined fixed pattern for positions, and agreement in velocities. A static state feedback is derived and stability conditions are presented. The condition under which the controller is designed is similar to the one posed for the communication graph in (Lin et al. 2005*a*) with different graph theory tools. More precisely, in (Caughman et al. 2005) the graph should have *a rooted directed spanning tree* which is equivalent to the condition of having a globally reachable vertex as introduced in (Lin et al. 2005*a*). With this condition, as stated before, the graph Laplacian matrix has a single eigenvalue at zero.

In all the agreement problems posed in the literature, one common property is observed: the formation closed-loop dynamics exhibit a simple zero eigenvalue. This is a natural consequence of the fact that in these problems only the relative motions are of interest

and not the absolute motion. In (Fax & Murray 2002*a*), the zero eigenvalue is interpreted as "the unobservable absolute motion of the formation in the measurements". Logically, the remaining modes of the closed-loop system must be stable. To study the behavior of relative motions, different approaches have been taken in the literature. In (Lin et al. 2005*a*) a similarity transformation is used to "separate" the zero eigenvalue from the remaining ones while in (Olfati Saber & Murray 2003*a*) stability and convergence of an error vector (defined with respect to the average point of the formation) are analyzed, the marginally unstable zero eigenvalue being associated with the evolution of the average formation point. In (Caughman et al. 2005), stability and convergence of the formation dynamics are studied in the quotient space $\mathbb{R}^n/\text{span}\{\mathbf{1}\}$, where $\mathbf{1}$ is the vector with all entries equal to one. In this thesis, this issue is dealt with by introducing adequate error vectors (depending on the problem addressed) using linear transformations that map the error space of interest into a lower dimensional space, the origin of which becomes the equilibrium of the closed-loop system being studied.

(Vicsek et al. 1995) propose a simple discrete-time model of n agents moving in the plane with the same speed and different headings. Each agent's heading is updated using a local rule based on the average of its own heading and the heading of the neighbors (those placed at a certain distance from it). They show that despite a central coordination system, and despite the fact that the neighboring sets change with time, all the agents eventually move in the same direction. The system, in a non-switching case, can be modeled by difference equations of the form $x(t+1) = -Fx(t)$, where F is a stochastic matrix, that is, a nonnegative matrix whose rows sum to one. The work in (Jadbabaie et al. 2003) gives a theoretical explanation for this agreement behavior. Different models which show similar behaviors are also proposed and studied. The novel theorem exploited in this work is *Wolfowitz theorem*, which states that *the multiplication of a sequence of infinite ergodic matrices which selects its elements from a bounded set of ergodic matrices, converge to* $\mathbf{1}c^T$*, where c is a constant vector.* Here, an ergodic matrix is defined as any stochastic matrix for which $\lim_{i\to\infty} M^i$ is a matrix of rank one.

Recent work reported in (Moreau 2005) reveals some interesting results for time-dependent communication topologies. A discrete model similar to one used by (Jadbabaie et al. 2003)

is studied. Let $\mathcal{G}(t)$ denote the active communication graph at time index t. The connectedness across an interval of time is defined as connectedness of the union graph of graphs $\mathcal{G}(t)$ denoted $\bigcup\mathcal{G}$. When the graphs are directed, it is shown that if there is a $T \geq 0$ such that for all t_0, there is a globally reachable vertex in $\bigcup\mathcal{G}$ during the time interval $[t_0, t_0+T]$, then the coordination states converge to the same value. For the case of bi-directional communication (undirected graphs), the condition is relaxed to nonuniform time intervals, that is, the above result holds if the graph $\bigcup\mathcal{G}$ is connected on $[t_0, \infty]$ for any t_0. With a counterexample, the author shows that the condition of uniformity on time intervals for directed graphs is essential. (Moreau 2005) further shows that the propositions mentioned above are extended to more general (nonlinear) discrete-time systems that preserve some convexity properties. It is shown as well that the proposed model covers many other models considered in the literature. The proofs of these results rely heavily on set-valued Lyapunov theory.

Interesting results on time-varying communication topologies are given in (Tanner et al. 2004), where control laws are proposed to solve a flocking problem for n agents consisting of fully actuated double integrators. The control laws result in i) heading alignment, ii) convergence to a common velocity, iii) collision avoidance. The communication network is considered to be bi-directional. The stability of the resulting discontinuous dynamics are analyzed using differential inclusions and nonsmooth analysis. Collision avoidance is achieved by considering an appropriately defined potential function in the stability Lyapunov function. It is also proved that the agents converge to some local minimum defined by potential functions.

It is important to point out that some of the above results can be traced back to the work of Tsitsiklis and Athans in a stochastic framework; see for example (Tsitsiklis & Athans 1984) for a description of their original work and (Blondel et al. 2005) for a new and more recent outlook on this circle of ideas. See also (Bertsekas & Tsitsiklis 1989) and the references therein. For interesting and very recent results on the consensus problem and related problems, the reader is advised to consult (Lin et al. 2004, 2006), and (Cao et al. 2006*a*,*b*).

1.4 Publications and thesis contributions

Inspired by the developments in the field, this thesis tackles a multiple vehicle coordination control problem that departs slightly from mainstream work reported in the literature. Specifically, we consider the problem of steering multiple vehicles to pre-specified spatial paths while holding an inter-vehicle formation pattern in time. We study coordination control problems related to autonomous vehicles in general by dividing the CPF system into two subsystems: path-following and coordination control. At the lower (or inner-loop) level the path-following problem is solved for individual vehicles, each having access to local measurements. Coordination is then achieved by synchronizing the so-called coordination states in the outer loop. Finally, the stability of the resulting interconnected system is proven. Some of the issues related to communication losses are also addressed.

The results obtained in the scope of this thesis have naturally led to a number of publications: two journal articles (Ghabcheloo et al. 2007, Ghabcheloo, Pascoal, Silvestre & Kaminer 2006*a*), one book chapter (Ghabcheloo, Pascoal, Silvestre & Kaminer 2006*b*), and several conference papers (Ghabcheloo, Aguiar, Pascoal, Silvestre, Kaminer & Hespanha 2006) – (Ghabcheloo, Pascoal, Silvestre & Kaminer 2004). There are also two non-refereed reports (Ghabcheloo, Pascoal & Silvestre 2005*a*, 2004). Recently, a paper summarizing key theoretical results on coordination control in the presence of communication losses was submitted for publication. See (Ghabcheloo, Aguiar, Pascoal, Silvestre, Hespanha & Kaminer 2006).

Coordinated path-following mission scenarios occur naturally in underwater robotics as explained in the previous section. This is the area that motivated most of the problems addressed in the thesis. At an early stage of the research, however, we started by addressing similar problems for wheeled robots in the hope that the solutions derived for this simpler case would shed some light into the problem of coordinated path-following for the more complex case of air and marine robots. Preliminary steps in this direction were taken in (Ghabcheloo, Pascoal, Silvestre & Kaminer 2006*a*), (Ghabcheloo, Pascoal, Silvestre & Kaminer 2004) and (Ghabcheloo, Pascoal & Silvestre 2004), where the problem of coordinated path-following of multiple wheeled robots was solved by resorting to linearization and gain scheduling techniques. The solutions obtained are conceptually simple

and embody in themselves a straightforward mechanism that allows for the decoupling of path path-following (in space) and vehicle synchronization (in time). The price paid for the simplicity of the solutions is the lack of global results, that is, attractivity to so-called trimming paths and to a desired formation pattern can only be guaranteed locally, when the initial vehicle formation is sufficiently close to the desired one. This research is summarized in (Ghabcheloo, Pascoal, Silvestre & Kaminer 2006*a*), which is the journal version of (Ghabcheloo, Pascoal, Silvestre & Kaminer 2004).

Later, the above linearization approach was refined and extended to a nonlinear setting in (Ghabcheloo et al. 2007), (Ghabcheloo, Pascoal, Silvestre & Kaminer 2006*b*), and (Ghabcheloo, Pascoal & Silvestre 2005*a*). The new methodologies developed overcome the limitations of linear techniques and yield global results that allow for the consideration of arbitrary paths, formation patterns, and initial conditions. The solutions adopted build on Lyapunov based techniques and address explicitly the constraints imposed by the topology of the inter-vehicle communications network. Once again, using the set-up adopted, path-following (in space) and inter-vehicle coordination (in time) are essentially decoupled.

In coordinated path-following control, the coordination level is supported by a communication network through which the required information are exchanged among the different vehicles. Because of practical considerations, no vehicle will be able to communicate with the entire formation. That is, all-to-all communication is in general impossible and each vehicle is bound to exchange information with its immediate neighbors only. To deal explicitly with this issue, the communication constraints are modeled in terms of graphs, whereby the nodes and edges of a graph represent the vehicles and the communication links among them, respectively. In this set-up, *graph theory* plays a key role in modeling the collective system under study and in deriving formal proofs of coordinated behavior properties. It therefore comes as no surprise that graph theory has steadily become the tool par excellence to formally study the coordinated control of multiple vehicles subject to possibly stringent communication requirements. Depending on the communication network, the resulting graphs are either undirected graphs or directed graphs (digraphs). Although similar, different types of properties are obtained for the two types of graphs. The main difference arises from the fact that the matrices that represent the graphs, namely the graph Laplacian matrix, are symmetric for undirected graphs, but not necessarily so for digraphs

in general. In the course of this PhD research, different control laws were proposed and the stability of the corresponding closed-loop coordination dynamics was studied. For example, (Ghabcheloo, Pascoal & Silvestre 2005*b*) deals with fixed and symmetric communication topologies. However, in real scenarios the communication network is subjected to change because of failures/creations of links. Therefore, the graphs become state dependent or even time-dependent. These problems are addressed in (Ghabcheloo, Aguiar, Pascoal, Silvestre, Kaminer & Hespanha 2006). Latency in the exchange of the information is also addressed in (Ghabcheloo, Aguiar, Pascoal & Silvestre 2006).

The work in (Ghabcheloo, Pascoal & Silvestre 2005*b*) addresses the CPF problem of steering a fleet of wheeled robots along a set of straight lines and circumferences. The communication network is fixed (with respect to time) and bi-directional. (Ghabcheloo, Pascoal, Silvestre & Kaminer 2005) is an extension of (Ghabcheloo, Pascoal & Silvestre 2005*b*) to uni-directional communication networks and (Ghabcheloo, Carvalho, Pascoal & Silvestre 2005) is an extension of (Ghabcheloo, Pascoal, Silvestre & Kaminer 2005) to fully actuated marine vehicles. In the latter case, the added difficulty comes from the fact that marine vehicles show side-slip in their motions which is not the case for wheeled robots. (Ghabcheloo et al. 2007) is a journal version of (Ghabcheloo, Pascoal & Silvestre 2005*b*) and extends the results of the latter to address the problem of CPF for a general class of paths. In this case, the coordination dynamics become time-varying (state-driven) and the proofs become more involved. (Ghabcheloo et al. 2007) examines also the convergence properties of the solutions of the combined path-following and coordination algorithms. (Ghabcheloo, Pascoal, Silvestre & Kaminer 2006*b*) is a collective paper combining (Ghabcheloo et al. 2007) and (Ghabcheloo, Pascoal & Silvestre 2005*b*) in a book chapter.

The techniques used in the aforementioned papers ((Ghabcheloo et al. 2007), (Ghabcheloo, Carvalho, Pascoal & Silvestre 2005), (Ghabcheloo, Pascoal, Silvestre & Kaminer 2005), and (Ghabcheloo, Pascoal & Silvestre 2005*b*)) share a common strategy. More recent publications ((Ghabcheloo, Aguiar, Pascoal, Silvestre, Kaminer & Hespanha 2006), (Ghabcheloo, Aguiar, Pascoal & Silvestre 2006), (Aguiar et al. 2006)) use a different approach to the problem of CPF, leading to a new set-up in which the analysis of the combined path-following and coordination systems is easier to do, even in the presence of time-varying communication networks (failures / creation of links). In the first approach

to solve the CPF problem, the total speeds of the vehicles act as control signals at the coordination level; for the case where the paths are not straight lines or circumferences, the relationship between the total speeds and the coordination states in the coordination dynamics, becomes a function of the positions of the vehicles along the paths or, equivalently, a function of the states of the system. In the new approach, the coordination control signal for each vehicle is the evolution of a free point on the corresponding path. Interestingly enough, with this change of focus, the coordination dynamics take the form of a single integrator and the change of "curvature" along the desired paths is taken care of naturally at the path-following level. This simplifies considerably the proofs of convergence. The results in (Ghabcheloo, Aguiar, Pascoal, Silvestre, Kaminer & Hespanha 2006), (Ghabcheloo, Aguiar, Pascoal & Silvestre 2006), and (Aguiar et al. 2006) extend also previous results in order to deal with a general class of under-actuated autonomous vehicles, as explained below.

Aguiar et al. (2006) address the CPF problem for a group of under-actuated autonomous vehicles. For a general class of vehicles moving in either two or three dimensional space, it is shown how Lyapunov-based techniques and graph theory can be brought together to yield a decentralized control structure. Path-following for each vehicle amounts to reducing the geometric error to a small neighborhood of the origin. The desired spatial paths do not need to be of a particular type (e.g., trimming trajectories) and can be any sufficiently smooth curves. Vehicle coordination is achieved by adjusting the evolution of the coordination state of each vehicle along its path according to information on the positions of a subset of the other vehicles, as determined by the communications topology adopted. (Ghabcheloo, Aguiar, Pascoal & Silvestre 2006) extends the results of (Aguiar et al. 2006) and solves the problem of CPF subjected to switching communication networks and time delays by exploiting interesting results from graph theory. (Ghabcheloo, Aguiar, Pascoal, Silvestre, Kaminer & Hespanha 2006) solves the problem of CPF for a general class of under-actuated autonomous vehicles with temporary communication losses by extending previous results available for systems with "brief instabilities".

The work reported in (Ghabcheloo, Aguiar, Pascoal, Silvestre, Hespanha & Kaminer 2006) is a journal version of (Ghabcheloo, Aguiar, Pascoal, Silvestre, Kaminer & Hespanha 2006), (Ghabcheloo, Aguiar, Pascoal & Silvestre 2006): it provides the proofs of

the results in the latter two conference publications and addresses some issues related to communication losses and time delays.

Part of my research work was done in cooperation with the team of Prof. Isaac Kaminer at the NPS, Monterey, CA. The results of joint work done during my visit to NPS are detailed in (Dobrokhodov et al. 2006) and (Yakimenko et al. 2006).

Finally, (Børhaug et al. 2006) presents the results of my cooperation with the team of Prof. Kristin Pettersen from NTNU, Norway, during the spring of 2006. It proposes a nonlinear coordination control scheme for formation control of a group of underactuated marine vehicles with communication topology constraints (both bi-directional and uni-directional communication links). Its key contribution, when compared with (Aguiar et al. 2006), is the use of a saturation function at the coordination control law to keep the vehicle speeds positive and bounded above.

1.5 Structure of the thesis

The thesis address the problem of coordinated path-following for autonomous vehicles. Different aspects of the problem are explored and several solutions are proposed. The efficacy of the algorithms developed is supported by numerical simulations. The thesis is organized in three main chapters that are easily distinguished by the increasing complexity of the problems addressed and the techniques adopted for their solution.

Chapter 2 This chapter reflects the early stage of research on CPF. The methodology adopted for CPF builds on linearization techniques and draws heavily on previous work on the design and implementation of gain-scheduled controllers for time-varying plants. Using this set-up, path-following and inter-vehicle coordination are essentially decoupled. Vehicle coordination is achieved by adjusting the speed of each of the vehicles along its path, according to information on the position of the remaining vehicles only. The resulting control system is simple to implement and avoids feedforwarding the desired speed of all the vehicles. We consider different vehicle configurations and address some of the problems that arise when the vehicles fail to reach some desired speed. In particular, it is shown how the remaining vehicles

adjust their speeds to try and maintain formation.

Chapter 3 In this chapter, most of the results of Chapter 2 are extended to a more general framework by resorting to nonlinear techniques. The CPF problem is solved for a fleet of wheeled robots and fully actuated marine vehicles. The solution adopted for CPF builds on Lyapunov based techniques and addresses explicitly the constraints imposed by the topology of the inter-vehicle communications network. To achieve coordination, the vehicles adjust their speeds based on information received from the other vehicles, as determined by the communications topology adopted. Tools borrowed from Graph theory play an instrumental role in modeling the constraints imposed by the underlying communication network and allow for the study of the impact that the network has on the behavior of the resulting CPF control system, both in terms of stability and performance. In this chapter, the communication graphs are assumed to be fixed with respect to time, that is, the topology of the communication network is fixed.

Chapter 4 This chapter addresses the CPF problem for a very general class of autonomous, possibly underactuated vehicles. This is in striking contrast with the classes of vehicles considered in Chapter 3, that were either fully actuated or, if underactuated, had the simple dynamics of a wheeled robot. First, a path-following control law is used that drives each vehicle to its assigned path regardless of the temporal speed profile adopted. This is done by making each vehicle approach a conveniently defined virtual target that moves along the path. In the second step, the speeds of the virtual targets are adjusted so as to synchronize their positions, thus achieving coordination of the vehicles along the paths, since each vehicle will tend to its corresponding virtual target on the path. It is shown that the system that is obtained by putting together the path-following and coordination strategies can be naturally viewed as a feedback interconnected system. Using this result and recent results from nonlinear system and graph theory, conditions are derived under which the path-following and the coordination errors are driven to a neighborhood of zero in the presence of communication losses and time delays. Two different situations are considered. The first captures the case where the communication graph is alternately connected and

disconnected (brief connectivity losses). The second reflects an operating scenario where the union of the communication graphs over uniform intervals of time remains connected (uniformly connected in mean), even though the frozen-time graph may never be connected.

CHAPTER 2

LINEARIZATION TECHNIQUES: WHEELED ROBOTS

This chapter addresses the CPF problem for a fleet of wheeled robots along a set of given spatial paths. The paths considered are the concatenation of so-called trimming paths which are straight lines and circumferences for wheeled robots. We solve this and other related problems using a simple algorithm that builds on linearization techniques and gain scheduling control theory. Using this set-up, path-following (in space) and inter-vehicle coordination (in time) are almost decoupled. Path-following for each vehicle amounts to reducing a conveniently defined generalized error vector to zero. It is shown that the linearization of the equations of motion about the trimming paths yields a linear time-invariant (LTI) system. Thus, at this level any LTI control system design strategy can be used for path following control. Vehicle coordination is achieved by adjusting the speed of each of the vehicles along its path, according to information on the position of all or some of the other vehicles. No other information is exchanged among the robots. The set-up adopted allows for a simple analysis of the resulting coordinated path-following control system. We describe the structure of the coordination system proposed and address challenging problems of robustness with respect to certain types of vehicle failures.

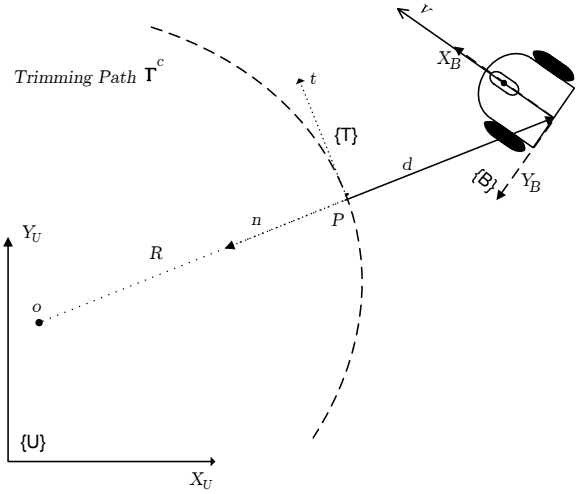

Figure 2.1: Frames and error variables

2.1 Path-following: single vehicle

This section introduces some basic notation and offers two solutions to the problem of path-following for a single wheeled robot.

Consider the wheeled robot of the unicycle type shown in Figure 2.1, together with a spatial path to be followed. The vehicle has two identical parallel, nondeformable rear wheels. It is assumed that the plane of each wheel is perpendicular to the ground and that the contact between the wheels and the ground is pure rolling and nonslipping, that is, the velocity of the center of mass of the robot is orthogonal to the rear wheels axis. Each rear wheel is powered by a motor which generates a control torque. This will in turn generate a control force and torque applied to the vehicle.

The following notation will be used in the sequel. The symbol $\{\mathrm{A}\}:=\{x_A, y_A, z_A\}$ denotes a reference frame with origin at O_A and unit vectors x_A, y_A, z_A. Often, for simplicity of presentation, we omit writing explicitly the third component of the reference frames, because the wheeled robot is restricted to move in the horizontal plane. Let $\{\mathrm{U}\}$ and $\{\mathrm{B}\}$ be inertial and body-fixed reference frames, respectively and assume that the origin O_B of $\{\mathrm{B}\}$ is coincident with the center of mass of the vehicle. Further let $[x,y]^T$ denote the position of O_B in $\{\mathrm{U}\}$ and ψ the parameter that describes the orientation of $\{\mathrm{B}\}$ with respect to $\{\mathrm{U}\}$ (i.e., the robot's orientation with respect to the inertial x-axis). Define v and

r as the linear and rotational velocities of $\{\mathrm{B}\}$ with respect to $\{\mathrm{U}\}$, respectively expressed in $\{\mathrm{B}\}$. With the above notation, the simplified kinematic and dynamic equations of the wheeled robot can be written as

$$\text{Dynamics} \begin{cases} \dot{v} = F/m \\ \dot{r} = N/I \end{cases} \tag{2.1}$$

$$\text{Kinematics} \begin{cases} \dot{\psi} &= r \\ \dot{x} &= v\cos(\psi) \\ \dot{y} &= v\sin(\psi) \end{cases} \tag{2.2}$$

where m denotes the mass of the robot, I is the moment of inertia about its vertical body-axis, and F and N denote the total force and torque respectively, applied to the vehicle. Define

$$x_1 = [v,r]^T; x_2 = [\psi,x,y]^T; u = [F,N]^T \tag{2.3}$$

and assume that $m = I = 1$ in the appropriate units. Equations (2.1) and (2.2) can obviously be cast in the general state space form

$$\begin{aligned} \dot{x}_1 &= f_1(x_1,u) \\ \dot{x}_2 &= f_2(x_1,x_2), \end{aligned} \tag{2.4}$$

where f_1, f_2 are nonlinear functions of their arguments and x_1 and x_2 represent the dynamic and kinematic states, respectively. Even though the simple dynamical model of the wheeled robot does not require that f_1 be a function of x_1, it is convenient to adopt the general state space form because it allows for the inclusion of dissipative (velocity dependent) terms if needed. Notice that the evolution of x_1 does not depend on x_2.

Following (Sivestre 2000), (Silvestre & Pascoal 2002) a trimming trajectory of the wheeled robot is a set

$$\Upsilon^c := \{(x_1^c, x_2^c(.), u^c) : f_1(x_1^c, u^c) = 0\} \tag{2.5}$$

parameterized by the 2-tuple of vectors x_1^c, u^c that make $f_1(x_1,u) = 0$. The notation $x_2^c(.)$ represents the corresponding time-history of state variable x_2 at trimming. Stated in simple terms, along a trimming (also called equilibrium) trajectory, the input u is held fixed,

and the dynamic variables remain constant ($\dot{x}_1 = 0$). Notice, however that the kinematic variables x_2 are allowed to be functions of time.

In the case of the wheeled robot, it is trivial to show that the only possible trimming trajectories correspond to circumferences and straight lines. In other words, with u set to a constant value u^c, v and r assume constant values v^c and r^c respectively, and the $x_2^c(.)$ component of Υ^c is such that $\psi^c(t) = r^c t + \psi_0$, where ψ_o denotes the heading angle at time $t = 0$. Straightforward computations show that in this case the origin O_B of the wheeled robot is driven along a circumference with radius $R = |v^c/r^c|$, where $|.|$ stands for the absolute value. The circle degenerates into a straight line when $r^c = 0$.

Notice in (2.5) that a trimming trajectory is specified in terms of all state and input variables at trimming. However, given fixed values v^c and r^c, the corresponding input u^c and the state $x_2^c(.)$ are, apart from the initial conditions, uniquely determined. In this sense, v^c and r^c determine uniquely the values of $[x^c, y^c]^T$, and thus of the corresponding path (curve in space) Γ^c traversed by the vehicle. Formally,

$$\Gamma^c := \{\Pi_p x_2^c(.) : (x_1^c, x_2^c(.), u^c) \in \Upsilon^c\} \tag{2.6}$$

where $\Pi_p : \mathbb{R}^3 \to \mathbb{R}^2$ denotes the operator that extracts the last two components of $x_2^c(.)$, that is, x and y coordinates. Clearly, a trimming path is simply obtained from a trimming trajectory by keeping the 2-D vector corresponding to the position of the wheeled robot. From the above discussion, and with a slight abuse of language, it can be stated that $\Gamma^c = \Gamma^c(v^c, r^c)$, that is, a trimming path is uniquely determined by the trimming values v^c and r^c or, equivalently, by v^c and c_c, where c_c denotes the path curvature. In what follows it is assumed that Γ^c can be parameterized in some convenient geometric manner, for example in terms of its curvilinear abscissa s (length along the path).

In the sequel, we consider the case where the wheeled robot is required to follow a general path that consists of the union of trimming paths. The emphasis is therefore placed on the development of controllers for accurate following of trimming paths. Consider now Figure 2.1, and suppose it is required for the wheeled robot to follow the trimming path Γ^c, that is, for O_B to converge to and follow the 2-D curve Γ^c at constant linear and rotational speeds v^c and r^c, respectively. A solution to this problem can be easily obtained by recalling the work of (Micaelli & Samson 1993) on path-following, from which the following

intuitive explanation is obtained: a path-following controller should look at i) the distance from the vehicle to the path and ii) the angle between the vehicle velocity vector and the tangent to the path, and reduce both to zero. This motivates the development of the kinematic model of the vehicle in terms of a Serret-Frenet frame $\{\mathrm{T}\}$ that moves along the path; $\{\mathrm{T}\}$ plays the role of the body axis of a "virtual target vehicle" that should be tracked by the "real vehicle". Using this set-up, the abovementioned distance and angle become part of the coordinates of the error space where the path-following control problem is formulated and solved.

Formally, given O_B assume that the closest point P on the path is well defined and consider the Serret-Frenet frame $\{\mathrm{T}\}:=\{\mathbf{t},\mathbf{n}\}$ with its origin at P. As is well known, $\mathbf{t}$ and $\mathbf{n}$ are the tangent and normal to the curve at P, respectively, where the positive direction of $\mathbf{t}$ is defined by traversing the path along increasing values of its length s. Let d_e be the y-component of vector d from P to O_B, expressed in $\{\mathrm{T}\}$ (the x-component is zero). Clearly, d is co-linear with unit vector $\mathbf{n}$. Further let $\psi_T = \psi^c$ parameterize the rotation matrix from $\{\mathrm{T}\}$ to $\{\mathrm{U}\}$, satisfying the relation

$$\dot{\psi}_T = c_c \dot{s} \tag{2.7}$$

where c_c is the curvature of the path and $\dot{s}$ denotes the time derivative of the curvilinear abscissa s of P. Since there is no slippage, $\{\mathrm{B}\}$=$\{\mathrm{T}\}$ at trimming.

Equipped with this notation, we now derive two algorithms for path-following by resorting to linearization techniques. See (Kaminer et al. 1998), (Sivestre 2000), and (Silvestre & Pascoal 2002) for an introduction to these techniques and for their application to path-following control of air and marine robots. The two algorithms build on two different error coordinates and will henceforth be referred to as the *Decoupling* and the *State Transformation* algorithms.

2.1.1 Decoupling algorithm

Given a trimming path, consider the path-following error coordinates

$$\begin{aligned} v_e &= v - v^c \\ r_e &= r - r^c \\ d_e &= \Pi d \\ \psi_e &= \psi - \psi^c = \psi - \psi_T, \end{aligned} \tag{2.8}$$

where $\Pi = \begin{bmatrix} 0 & 1 \end{bmatrix}$. Convergence of a vehicle to the path is equivalent to driving the above error variables to zero. Notice that with the simplified wheeled robot model, $F^c = N^c = 0$. Following the methodology exposed in (Micaelli & Samson 1993) and using (2.2) and (2.1), straightforward computations show that the error dynamics can be written as

$$\begin{aligned} \dot{v}_e &= F \\ \dot{r}_e &= N \\ \dot{d}_e &= v\sin(\psi_e) \\ \dot{\psi}_e &= r - \frac{c_c v\cos(\psi_e)}{1-d_e c_c}. \end{aligned} \tag{2.9}$$

Furthermore, the evolution of the closest point on the path is easily seen to be given by

$$\dot{s} = \frac{v\cos(\psi_e)}{1-d_e c_c}. \tag{2.10}$$

A formal way to derive (2.10) is presented in Section 3.2 which also helps in deriving (2.9). It is important to point out that equations (2.9) and (2.10) are only valid when $d_e c_c < 1$, that is, when the vehicle is "sufficiently close" to the path.

At this point, it is important to examine the equations above. Notice that the first equation in (2.9) is completely independent of the remaining ones. This means that the forward speed v of the vehicle can be manipulated at will by manipulating F, no matter what the evolution of the variables r_e, d_e, and ψ_e is. In particular, when following a desired trimming path *without any inter-vehicle coordination requirements*, the forward speed is simply set to the trimming value v_c. It is then up to the path-following controller to manipulate the torque N so as to drive r_e, d_e, and ψ_e to zero.

This simple circle of ideas is at the core of the technique of coordinated path-following proposed in this chapter: for each vehicle in the formation, the torque N is computed so

as to achieve path-following objectives for a given set of possible forwards speeds and trimming paths, while F controls the forward speed of the vehicle in order to meet the required inter-vehicle formation requirements.

The first step in the decoupling approach to path-following is to linearize the error dynamics about trimming conditions to obtain

$$\begin{aligned} \delta\dot{v}_e &= \delta F \\ \delta\dot{r}_e &= \delta N \\ \delta\dot{d}_e &= v^c\,\delta\psi_e \\ \delta\dot{\psi}_e &= \delta r_e - c_c^2 v^c\,\delta d_e - c_c\,\delta v_e. \end{aligned} \tag{2.11}$$

The resulting system is time-invariant, as proven in (Sivestre 2000) for a more general class of systems. An important assumption is made at this point: since the variable v_e is controlled independently (to meet the formation requirements), δv_e is simply viewed as a vanishing perturbation and thus ignored in the design of a path-following controller that will drive r_e, d_e, and ψ_e to zero. This assumption will be re-visited and proved rigorously later in Section 2.3. In the case of pure path-following about a trimming path (that is, without any formation requirements), δv_e is naturally set to zero. In what follows, it is assumed that the curvature c_c is upper bounded. Ignoring the first independent equation in (2.11) yields the sub-system

$$\begin{aligned} \delta\dot{r}_e &= \delta N \\ \delta\dot{d}_e &= v^c\,\delta\psi_e \\ \delta\dot{\psi}_e &= \delta r_e - c_c^2 v^c\,\delta d_e, \end{aligned} \tag{2.12}$$

for which a stabilizing controller is sought. Notice in the equations the explicit dependence of the dynamics on the path curvature c_c and trimming forward speed $v^c = r^c/c_c$. It is thus natural that the resulting controllers show dependence, that is, be scheduled on the same variables. As is customary in gain scheduling control, the scheduling is done on the *actual values of the variables*, that is, on $c_c(s)$ and $r/c_c(s)$. In what follows the $\mathscr{D}$-methodology introduced in (Kaminer et al. 1995) for the design and implementation of gain scheduled controllers is adopted. See also (Khalil 2002, Chapter 10). The $\mathscr{D}$-methodology addresses explicitly the problem of controller implementation on the original nonlinear plant and

avoids feedforwarding the values of the relevant variables at trimming. As in (Kaminer et al. 1995), append to the original system (2.12) an extra state z, defined by

$$\dot{z} = \delta d_e, \tag{2.13}$$

aimed at driving the steady state of δd_e to zero (in general, one should include as many integrators as the number of control signals). Since the linearized system with input δN and state $[\delta r_e, \delta d_e, \delta \psi_e, z]^T$ is controllable, arbitrary closed loop eigenvalue placement can be achieved with the state feedback control law

$$\delta N = -k_1 \delta r_e - k_2 \delta d_e - k_3 \delta \psi_e - k_4 z, \tag{2.14}$$

yielding the closed-loop characteristic polynomial

$$\lambda^4 + k_1 \lambda^3 + (k_2 + (c_c v^c)^2)\lambda^2 + v^c(k_2 + k_1 c_c^2 v^c)\lambda + k_4 v^c. \tag{2.15}$$

Without loss of generality, and for simplicity of exposition, select the desired values of the closed loop eigenvalues to be coincident and equal to $-\lambda_p$ [rad s^{-1}]; $\lambda_p > 0$. This can be done with the state feedback gains

$$\begin{aligned} k_1 &= 4\lambda_p \\ k_2 &= 4\lambda_p^3/v^c - 4\lambda_p c_c^2 v^c \\ k_3 &= 6\lambda_p^2 - (c_c v^c)^2 \\ k_4 &= \lambda_p^4/v^c \end{aligned} \tag{2.16}$$

that show clearly the dependence on the trimming values of c_c and v^c. Obviously, the gains can also be defined in terms of c_c and r^c/c_c. For implementation purposes, the actual values of c_c and r/c_c are used. Figure 2.2 shows the final implementation of the gain scheduled controller on the nonlinear plant, using the $\mathscr{D}$-methodology (Kaminer et al. 1995).

Notice how the integrator was moved in front of the plant and derivative operators were introduced at the appropriate variables. As explained in (Kaminer et al. 1995), this procedure does not introduce any unstable pole-zero cancelations. In practice, the derivative operator is approximated by $s/(s\tau + 1)$, with τ sufficiently small. With the implementation proposed, there is no need to introduce trimming values for any of the dynamics variables, namely for the angular velocity r. The importance of this property can hardly be overemphasized. In fact, given a desired path with a known curvature c_c and given an arbitrary

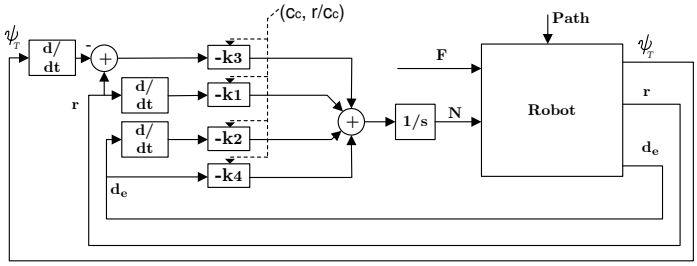

Figure 2.2: Gain Scheduled Controller Implementation using the $\mathscr{D}-$methodology - state feedback

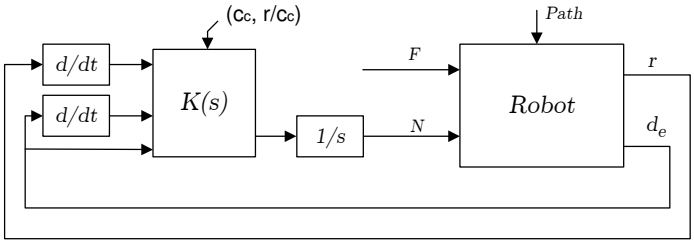

Figure 2.3: Gain Scheduled Controller Implementation using the $\mathscr{D}-$methodology - output feedback case

translational velocity v of the vehicle, the current scheme will make the vehicle converge to the path and acquire the correct rotational speed so as to follow the path with the desired radius. This is done without knowing the translational velocity explicitly. As explained later, this property is extremely important for coordinated path-following because we do not require that all vehicles know the required values of their trimming speeds. The scheme also avoids feedforwarding the trimming value for the input F and can thus cope velocity dependent friction forces not taken into account in the simplified design model introduced above.

A solution to the path-following problem that avoids feeding back all state variables can also be obtained using output feedback. Since the system with input δN and output $[\ \delta r_e,\quad \delta d_e,\quad z\ ]^T$ is controllable and observable, a controller K(s) can be designed (using any of the methods available in the literature) and scheduled on c_c and r/c_c. As an example, an output feedback controller was designed that requires measurements of d_e and r_e only, that is, ψ_e is not measured.

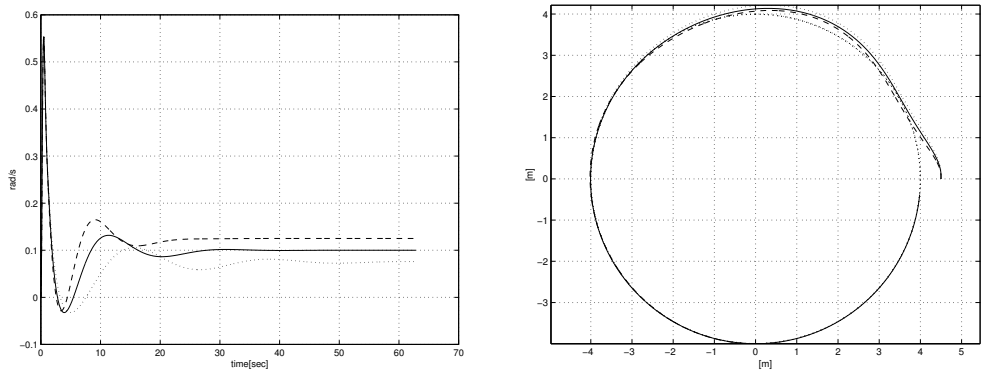

Figure 2.4: Angular speeds and spatial paths of the robot for $v^c = 0.3, 0.4$, and 0.5 [m s^{-1}]

Figure 2.3 shows the final implementation of the gain scheduled controller on the nonlinear plant, using the $\mathscr{D}$-methodology. The figure shows clearly how easy the implementation of the gain scheduled controller is. Figure 2.4 illustrates the behaviour of a wheeled robot following a circular path at velocities 0.3, 0.4, and 0.5 [m s^{-1}], with an output feedback controller designed for $v^c = 0.4$ [m s^{-1}]. As expected, the robot "learns" the required rotational speeds automatically. The controller was designed using H_2 optimization (Zhou et al. 1996) and the performance index was obtained by computing the L_2 norm of

$$e = \begin{pmatrix} 20\delta d_e + 15\delta N \\ 5z + 15\delta N \\ 50\delta r_e + 10\delta \psi_e + 75\delta N \end{pmatrix}.$$

In the design process, we considered an additive disturbance input in the equation for ψ_e in (2.11), thus modeling the disturbance-like term v_e that was eliminated in equations (2.12).

2.1.2 State transformation

The decoupling methodology for path-following is naturally suited to deal with the case where the forward speed of the robot is held constant at a given trimming speed. An alternative scheme that can deal easily with speed variations about a given trimming value requires the introduction of a new variable $\eta = r - c_c v$ that equals zero at trimming, that is,

$\eta_c = 0$. To this effect, define the error variables

$$\begin{aligned} v_e &= v - v^c \\ \eta_e &= \eta - \eta_c = r - c_c v \\ d_e &= \Pi d \\ \psi_e &= \psi - \psi^c = \psi - \psi_T. \end{aligned} \tag{2.17}$$

The new error space differs from the previous one in the equation for η_e only. By defining a new control variable

$$u_e = N - c_c F,$$

the corresponding error dynamics become

$$\begin{aligned} \dot{v}_e &= F \\ \dot{\eta}_e &= u_e \\ \dot{d}_e &= v \sin \psi_e \\ \dot{\psi}_e &= \eta_e + c_c v - \tfrac{c_c v \cos \psi_e}{1 - d_e c_c}. \end{aligned}$$

Linearizing the above equations yields

$$\begin{aligned} \delta \dot{v}_e &= \delta F \\ \delta \dot{\eta}_e &= \delta u_e \\ \delta \dot{d}_e &= v^c \delta \psi_e \\ \delta \dot{\psi}_e &= \delta r_e - c_c^2 v^c \delta d_e. \end{aligned} \tag{2.18}$$

Equation (2.18) shows that the dynamics of δv_e have become uncoupled from those of $\delta \eta_e$, δd_e, and $\delta \psi_e$. This is in contrast with the previous methodology, where δv_e was a coupling variable that was not taken in consideration during the design phase. As will be seen, this uncoupling will render the proof of stability of the overall coordinated path-following system simple.

In what follows, consider equations (2.18) with the dynamics of δv_e deleted. The relevant equations resemble those in (2.12) with δN replaced by δu_e. Notice the important fact that *all relevant state variables and input equal zero at trimming*. At this point, a simple state-feedback or an output-feedback path-following controller can be designed to drive η_e, d_e and ψ_e to zero. The design procedure follows closely that adopted for the decoupling method. For example, appending an integrator to δd_e and choosing the state feedback

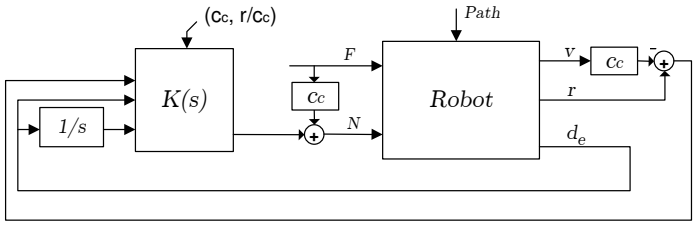

Figure 2.5: Controller implementation, state transformation method

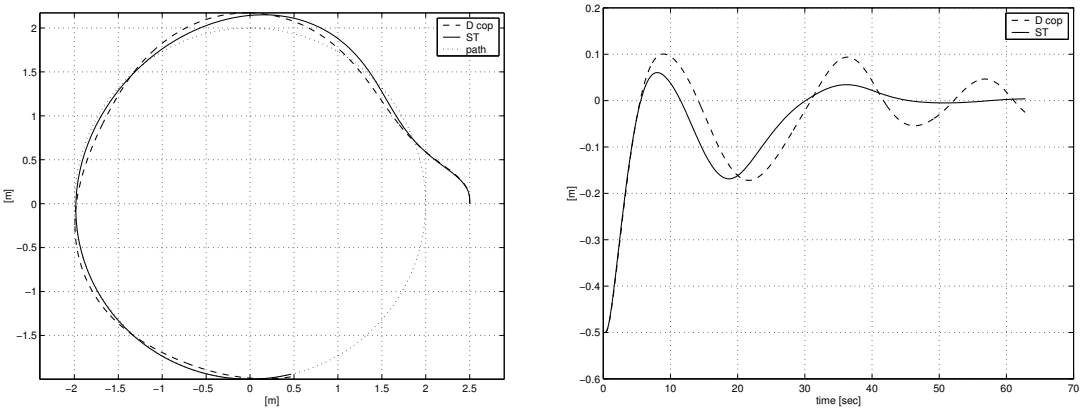

Figure 2.6: Comparison between the decoupling and state transformation methods

control law

$$\delta u_e = -k_1 \delta \eta_e - k_2 \delta d_e - k_3 \delta \psi_e - k_4 z \tag{2.19}$$

with $k_i; i = 1, ..., 4$ scheduled on c_c and r/c_c as in (2.16) places all the the closed loop eigenvalues at $-\lambda_p$ [rad s^{-1}]. An output gain-scheduled feedback control law can also be designed and implemented as shown in Figure 2.5. Notice that the implementation does not require the use of the $\mathscr{D}$-methodology because the trimming values of all relevant state and input variables are zero.

A quick comparison of the two methods shows that the state transformation strategy has the advantage of decoupling the velocity equation from the other variables.

Figure 2.6 shows the results of simulations aimed at illustrating the performance of the two methodologies for path-following. In the simulations, it was required that a wheeled robot follow a circumference with a given radius while the forward speed undergoes variation imposed by a periodic square signal in F. Notice that the state transformation methodology eliminates completely the variations in forward speed. As will be seen later, this

allows for a very simple proof of stability of the complete coordinated path-following system. The downside of the method is that it requires (at a path-following level) knowledge of the forward speed v and force F. This is totally avoided in the decoupling method. The latter seems at first inspection to be far worse than the state transformation method because it cannot, at the path-following level, eliminate the variations in forward speed about a trimming value. However, it will be later proved that the deviation in speed goes to zero at steady state, and this is the reason why the decoupling method works. The advantage of the decoupling method is the fact that no variables related to synchronization must be used. In summary, the state transformation method yields better performance at the price of increased controller complexity. It is up to the designer to decided what method to use depending on practical considerations.

2.2 Vehicle coordination control

We now consider the problem of coordinated path-following control as defined in Section 1.1. Consider a set of $n \geq 2$ wheeled robots and a set of n trimming paths Γ_k; $k = 1,2,...,n$ and require that robot i follow path Γ_i. We further require that the vehicles traverse the paths in such a way as to maintain a desired formation pattern. We assume each path is parameterized in terms of s_i, its curvilinear abscissa, as measured from some adequately chosen point on the path. The paths Γ_i may be obtained as simple translations of a "template" path or as scaled circumferences with a common center and different radii R_i. In this chapter, we restrict ourselves to "in-line" formation patterns.

Assuming that path-following controllers have been implemented separately for each robot, it now remains to synchronize these in time by adjusting the speeds v_i of the robots as a function of the "along-path" distances between them. Formally, we define the distances between vehicles i and j as

$$s_{i,j} = s_i - s_j; i, j = 1,..,n; i \neq j \tag{2.20}$$

in the case of shifted straight lines, and as

$$\bar{s}_{i,j} = \bar{s}_i - \bar{s}_j; i, j = 1,..,n; i \neq j, \tag{2.21}$$

with $\bar{s}_i = s_i/R_i$, in the case of scaled circumferences.

Given the positions $[x_i, y_i]^T$ and $[x_j, y_j]^T$ of robots i and j, respectively it is trivial to compute that

$$s_{i,j} = \begin{cases} \frac{(x_i - x_j) + m(y_i - y_j)}{\sqrt{1+m^2}}; & m < \infty \\ y_i - y_j; & \text{otherwise} \end{cases}$$

in the case of lines,

$$\bar{s}_{i,j} = \text{atan2}(y_i - \bar{y}_0, x_i - \bar{x}_0) - \text{atan2}(y_j - \bar{y}_0, x_j - \bar{x}_0).$$

in the case of circumferences.

To compute the evolution of the along-path distance, use (2.10),(2.21) to obtain

$$\dot{\bar{s}}_{i,j} = \frac{v_i cos(\psi_{e_i})}{R_i(1 - d_{e_i} c_{c_i})} - \frac{v_j cos(\psi_{e_j})}{R_j(1 - d_{e_j} c_{c_j})}, \tag{2.22}$$

which degenerates into

$$\dot{s}_{i,j} = v_i cos(\psi_{e_i}) - v_j cos(\psi_{e_j}) \tag{2.23}$$

for straight lines. In the case of circumferences $c_{c_k} = \pm 1/R_k$, the sign depending on the direction of motion. More details will be presented in Section 2.5.1. Clearly, the objective is to drive $\bar{s}_{ij}$ (or $s_{i,j}$) to zero by manipulating $v_i; i = 1, 2, .., n$ about their trimming values v_i^c. Notice that in the case of "in-line" coordinated path-following the along path distances are zero at trimming, that is, $s_{i,j}^c = \bar{s}_{i,j}^c = 0$.

Adopting a set-up similar to the one used for path-following control, one is naturally led to consider the coordination system that is obtained by linearizing the relevant dynamics equations about trimming, that is,

$$\begin{aligned} \delta \dot{v}_{e_i} &= \delta F_i \\ \delta \dot{s}_{i,j} &= \delta v_{e_i} - \delta v_{e_j} \end{aligned}$$

for straight lines and

$$\begin{aligned} \delta \dot{v}_{e_i} &= \delta F_i \\ \delta \dot{\bar{s}}_{i,j} &= \delta v_{e_i}/R_i - \delta v_{e_j}/R_j + f_i(\delta d_{e_i}) - f_j(\delta d_{e_j}) \end{aligned} \tag{2.24}$$

for circumferences, where

$$f_k(\delta d_{e_k}) = \frac{v_k^c \, \mathrm{sign}(c_{c_k})}{R_k^2} \delta d_{e_k}. \tag{2.25}$$

In the equations above, there are disturbance-like terms $f_k(\delta d_{e_k})$ that come from the path-following system. At this point, it is assumed that these disturbances tend asymptotically to zero. As will be seen later, this fact is trivial to prove in the case of the state-transformation methodology for path-following. A similar conclusion will also be derived for the decoupling strategy. As a consequence of this assumption, the relevant linearized equations for circumferences reduce to

$$\begin{aligned} \delta \dot{v}_{e_i} &= \delta F_i \\ \delta \dot{\bar{s}}_{i,j} &= \delta v_{e_i}/R_i - \delta v_{e_j}/R_j. \end{aligned} \tag{2.26}$$

In the sequel, we analyze the case of *coordinated path-following for circumferences, the results carrying over in an obvious manner to straight lines*.

The final step in the design of a coordination controller for (2.26) is to seek a general control law of the form

$$\delta F_i = g_i(\delta v_{e_i}, \bar{s}_{i,j}; j \in N_i)$$

such that $\bar{s}_{i,j}$ is driven to zero asymptotically. In the above equation, N_i denotes the set of vehicles that vehicle i communicates with. It is then straightforward to implement the controller in a nonlinear setting by once again exploiting the results available in (Kaminer et al. 1995). For practical reasons, we require that the $g_i(.,.)$ depend on δv_{e_i} only, that is, vehicle i does not have access to the speeds of the other vehicles.

At this point, different strategies can be adopted for control, depending on the flow of information among the vehicles. Figure 2.7 shows three representative configurations, illustrated for the case of 3 robots.

Leader-Follower. This configuration captures the case where a vehicle, elected as the "Leader", executes a path-following algorithm at a required forward speed and relays its position to the remaining vehicles. It is up to the "Followers" to keep the formation, based on info received from the Leader.

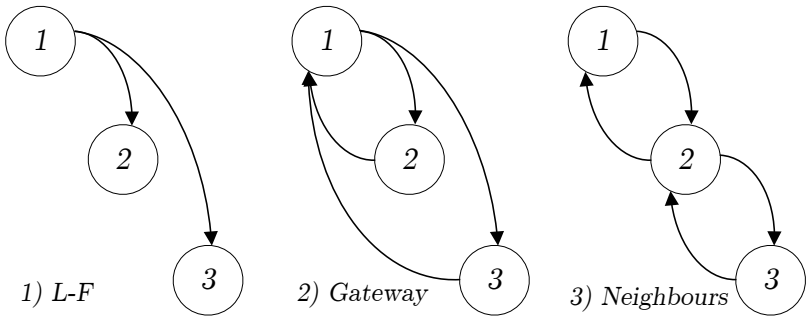

Figure 2.7: Information flow diagram: *1)* Leader-Follower, *2)* Gateway, *3)* Neighbors

Gateway. In this configuration, a vehicle serves as a Gateway (vehicle 1 in Figure 2.7-2). Each of the remaining vehicles sends its position to Gateway and receives the Gateway's position. Coordination is thus achieved through the Gateway vehicle.

Neighbors. In this case, each vehicle communicates with its immediate neighbors. The n vehicles are indexed according to the spatial pattern they are required to achieve, and vehicle $i; i = 2,...,n-1$ communicates with vehicles $i-1$ and $i+1$. Vehicles 1 and n communicate with vehicles 2 and $n-1$, respectively.

Different control laws can now be proposed for the configurations above. In what follows we analyze the Leader-Follower and the Gateway configurations.

2.2.1 Leader-follower

Suppose vehicle 1 is the Leader. A possible coordination control law is

$$\begin{aligned} \delta F_1 &= -a_1 \delta v_{e_1} \\ \delta F_i &= -a_i \delta v_{e_i} + R_i b_i \delta \bar{s}_{1,i}; i = 2,...,n \end{aligned} \tag{2.27}$$

which corresponds to having the leader adjust its own speed independently, while the remaining vehicles control their speeds in response to the along-path distances between them and the leader.

Equations (2.26), together with (2.27), define the coordination system dynamics. Simple computations show that this linear system exhibits one eigenvalue at $-a_1$ [rad s^{-1}], and $n-1$ pairs of eigenvalues at the roots of $\lambda^2 + a_i\lambda + b_i = 0$, i.e. the eigenvalues are

independent of the radii of the circumferences that the vehicles must follow. Clearly, the closed-loop eigenvalues are stable if a_i and b_i are positive. Furthermore, the eigenvalues can be assigned arbitrarily in the left half complex plane by proper choice of parameters a_i and b_i.

Notice, however that the implementation of the coordination system proposed requires that we have access to $\delta v_{e_i}; i = 1,2,...,n$. This is easy to do for vehicle 1, because it acts as a leader and sets the "pace" for the formation by traveling at the desired speed v_1^c, which is set in advance. However, when it comes to the remaining vehicles, it is best not to feedforward the desired speeds $v_i^c; i = 2,..,n$, lest the radii be different from their expected values. In this case, one should require that the vehicles "learn" their speeds $v_i^c; i = 2,..,n$ automatically. This can be done by changing the above control law to include integrators on the states $\delta \bar{s}_{1,i}$ and doing a $\mathscr{D}$-implementation of the resulting control scheme, following the circle of ideas introduced in (Kaminer et al. 1995). Formally, define the new states $\delta e_{1,i}; i = 2,...,n$ through

$$\delta \dot{e}_{1,i} = \delta \bar{s}_{1,i}. \tag{2.28}$$

and modify the control law (2.27) to incorporate extra feedback terms from the new states, yielding

$$\begin{aligned} \delta F_1 &= -a_1 \delta v_{e_1} \\ \delta F_i &= -a_i \delta v_{e_i} + R_i b_i \delta \bar{s}_{1,i} + R_i c_i \delta e_{1,i}. \end{aligned} \tag{2.29}$$

Straightforward computations show that the resulting (coordination) closed loop system exhibits one eigenvalue at $-a_1$ [rad s^{-1}], and $n-1$ triple of eigenvalues at the roots of polynomial $\lambda^3 + a_i\lambda^2 + b_i\lambda + c_i$. Again, the eigenvalues are independent of the radii R_i and can be placed arbitrarily in the left half complex plane. Using the methodology exposed in (Kaminer et al. 1995) it is simple to go from perturbed to global variables and to arrive at the final coordination control law

$$F_1 = -a_1(v_1 - v_1^c) \tag{2.30}$$

$$\begin{aligned} F_i &= -z_i + R_i b_i \bar{s}_{1,i}, \\ \dot{z}_i &= -R_i c_i \bar{s}_{1,i} + a_i \dot{v}_i \end{aligned} \tag{2.31}$$

where the derivative $\dot{v}_i$ can be computed numerically using an approximate differentiation operator.

As in (Kaminer et al. 1995), it can be shown that the linearization of the full nonlinear system (about the trimming conditions corresponding to the situation where the vehicles execute perfect coordinated path-following) has the same set of eigenvalues as those for the linear designs, that is, they are the roots of $\lambda^3 + a_i\lambda^2 + b_i\lambda + c_i$. Thus, from a local point of view, the coordination error converges to zero and the velocities of the robots are synchronized. Notice in the above control law that only the desired velocity v_1^c of the leader must be provided. As for the other velocities, and since they appear only through their derivatives and their steady state values are constant, it is not required to feedforward their trimming values.

2.2.2 Gateway

Inspired by the previous coordination control law, and taking into consideration the communications structure for the *Gateway* configuration (with vehicle 1 as the Gateway vehicle) suggests the control law

$$\begin{aligned} \delta F_1 &= -a_1\delta v_{e_1} - b_0\delta e_v - R_1(b_1\Sigma\delta\bar{s}_{1,i} + c_1\Sigma\delta e_{1,i}) \\ \delta F_i &= -a_i\delta v_{e_i} + R_i(b_i\delta\bar{s}_{1,i} + c_i\delta e_{1,i}) \\ \delta\dot{e}_{1,i} &= \delta\bar{s}_{1,i} \\ \delta\dot{e}_v &= \delta v_{e_1}, \end{aligned} \tag{2.32}$$

where Σ denotes the summation operator over all $i \geq 2$. Define $z_1 = a_1\delta v_{e_1} + b_0\delta e_v - R_1c_1\Sigma\delta e_{1,i}$ and $z_i = a_i\delta v_{e_i} - R_ic_i\delta e_{1,i}; i \geq 2$. A straightforward application of the $\mathscr{D}$-methodology yields the final nonlinear coordination control law

$$\begin{aligned} F_1 &= -z_1 - R_1b_1\Sigma\bar{s}_{1,i} \\ \dot{z}_1 &= a_1\dot{v}_1 + b_0(v_1 - v_1^c) - R_1c_1\Sigma\bar{s}_{1,i} \end{aligned} \tag{2.33}$$

for the Gateway vehicle and

$$\begin{aligned} F_i &= -z_i + R_ib_i\bar{s}_{1,i} \\ \dot{z}_i &= a_i\dot{v}_i - R_ic_i\bar{s}_{1,i}. \end{aligned} \tag{2.34}$$

for the remaining vehicles. The problem of finding a set of gains to obtain a stable system with adequate transient performance is not tackled here. Instead, we simply prove that the above system can always be stabilized in a trivial manner. To simplify the presentation, the analysis is done for the case of three vehicles. Let $a_i = a$, $b_i = b$ and $c_i = c; i = 1,..,3$. The closed loop eigenvalues are easily seen to be the roots of

$$(\lambda^3 + a\lambda^2 + b\lambda + c)\left(\lambda(\lambda + a)(\lambda^3 + a\lambda^2 + 3b\lambda + 3c) + b_0(\lambda^3 + a\lambda^2 + b\lambda + c)\right) = 0. \tag{2.35}$$

The result follows from the fact that if a, b, and c are chosen so as to make $\lambda^3 + a\lambda^2 + b\lambda + c$ a stable polynomial, then so is (2.35) for any positive b_0. This can be easily seen by applying the Routh-Hurwitz criterion.

The stability of the overall coordinated path-following system is explored in the next section.

2.3 Stability of the coordinated path-following control system

In the previous sections, the general problem of coordinated path-following was broken down into two problems: path-following and vehicle coordination (that is, synchronization in time). This procedure, even though not fully justified from a theoretical point of view, allowed for the derivation of simple control laws for the two problems taken separately. In fact, the design of a path-following controller using the decoupling methodology relied on the assumption that the coupling term $-c_c\delta v_e$ in the dynamics (2.11) could indeed be viewed as a vanishing perturbation coming from the coordination level. Conversely, the design of the coordination controller assumed that the perturbation terms δd_{ek} could also be viewed as perturbations being reduced to zero at the path-following level. In view of these yet unjustified assumptions, the control laws derived should, at this stage, be simply viewed as candidates to be brought together to yield a combined coordinated path-following controller, the stability of which must be proven rigorously. This is the objective of this section. A proof of stability is done for the Leader-Follower configuration and for a state feedback control law at the path-following level. Once again, two path-following strategies are considered: decoupling algorithm and state transformation.

2.3.1 Decoupling algorithm

Comparing to state transformation, decoupling strategy is harder to analyze. Consider the Leader-Follower configuration where vehicle 1 is the leader. We only indicate how a set of gains can be found so as to make the linearized coordinated path-following system stable.

From (2.11), (2.14), (2.24), and (2.29), the closed-loop dynamics can be written as

$$\begin{aligned}
\delta\dot{v}_{e_1} &= -a_1\delta v_{e_1} \\
\delta\dot{r}_{e_1} &= -k_1\delta r_{e_1} - k_2\delta d_{e_1} - k_3\delta\psi_{e_1} - k_4 z_1 \\
\delta\dot{d}_{e_1} &= v_1^c\delta\psi_{e_1} \\
\delta\dot{\psi}_{e_1} &= \delta r_{e_1} - c_{c_1}^2 v_1^c\delta d_{e_1} - c_{c_1}\delta v_{e_1} \\
\dot{z}_1 &= \delta d_{e_1} \\
-- &- ---- \\
\delta\dot{v}_{e_i} &= -a_i\delta v_{e_i} + R_i b_i\delta\bar{s}_{1,i} + R_i c_i\delta\bar{e}_{1,i} \\
\delta\dot{r}_{e_i} &= -k_1\delta r_{e_i} - k_2\delta d_{e_i} - k_3\delta\psi_{e_i} - k_4 z_i \\
\delta\dot{d}_{e_i} &= v_i^c\delta\psi_{e_i} \\
\delta\dot{\psi}_{e_i} &= \delta r_{e_i} - c_{c_i}^2 v_i^c\delta d_{e_i} - c_{c_i}\delta v_{e_i} \\
\dot{z}_i &= \delta d_{e_i} \\
\delta\dot{\bar{s}}_{1,i} &= \delta v_{e_1}/R_1 - \delta v_{e_i}/R_i + \frac{v_1^c\,\mathrm{sign}(c_{c_1})}{R_1^2}\delta d_{e_1} - \frac{v_i^c\,\mathrm{sign}(c_{c_i})}{R_i^2}\delta d_{e_i} \\
\delta\dot{e}_{1,i} &= \delta\bar{s}_{1,i};\ \ i = 2,..,n
\end{aligned} \tag{2.36}$$

Without loss of generality, consider the case of two vehicles only. The corresponding closed-loop characteristic polynomial is

$$(\lambda + a_1)(\lambda + \lambda_p)^4\left((\lambda^3 + a_2\lambda^2 + b_2\lambda + c_2)(\lambda + \lambda_p)^4 - (\frac{v_2^c}{R_2})^2\lambda(\lambda + 4\lambda_p)(b_2\lambda + c_2)\right). \tag{2.37}$$

Notice that $(\lambda + a_1)(\lambda + \lambda_p)^4$ can be chosen to be stable by proper design of the path-following controller and thus plays no role in the stability analysis that follows. Choose $a_2 = 3\xi$, $b_2 = 3\xi^2$, and $c_2 = \xi^3$ for some $\xi > 0$, and let $k = \max_{v_2^c, R_2}\{(v_2^c/R_2)^2\}$, that is, let $\sqrt{k}$ be the largest expected trimming value of the rotational speed of the Follower. With the above choices, the relevant part of the characteristic polynomial that depends on k becomes

$$(\lambda + \xi)^3(\lambda + \lambda_p)^4 - 3\xi^2 k\lambda(\lambda + 4\lambda_p)(s + \xi/3) \tag{2.38}$$

Notice that the poles at $-\lambda_p$ come from the path-following, and those at $-\xi$ come from coordination level. Let $\xi = m\lambda_p$, and for a given k choose $\lambda_p = 2mk^{1/2}$. A straightforward but cumbersome application of the Routh-Hurwitz stability criteria reveals that the above system is stable for $m > m_0 = 0.63$. Thus, given any k, λ_p can be chosen large enough

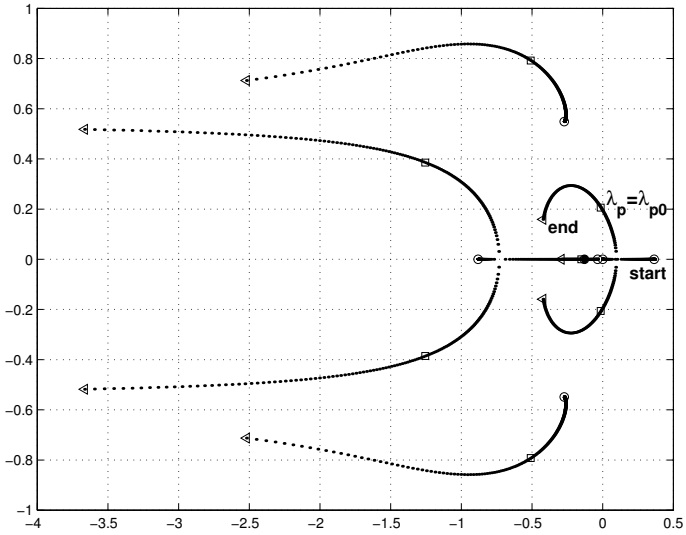

Figure 2.8: Root locus of the coordinated path-following system for varying λ_p

(note that $\lambda_p = 2mk^{1/2}$) to guarantee stability. To better illustrate this result, a numerical example was run with $k = 0.25$ [rad^2 s^{-2}] and $\xi = 2m_0^2 k^{1/2} = 0.4$ [rad s^{-1}]. The critical λ_p was computed as $\lambda_{p_0} = 2m_0 k^{1/2} = 0.63$ [rad s^{-1}]. Figure 2.8 shows the root loci for varying $\lambda_{p_0} - 0.5 < \lambda_p < \lambda_{p_0} + 2$. Clearly, the system is stable for $\lambda_p > \lambda_{p_0}$.

2.3.2 State transformation

The state transformation case is trivial to analyze because there is true decoupling of the path-following and coordination schemes. In fact, close examination of the error dynamics in (2.18) shows that the evolution of the coordination-related variable δv_e is totally independent of the path-following related variables. Furthermore, the latter are driven asymptotically to zero with the control law (2.19) proposed. As a consequence, the variables δde_k that appear at the coordination level in (2.24)-(2.25) vanish asymptotically. The coordination scheme with the control law (2.30) and (2.31) proposed is therefore an asymptotically stable system driven by vanishing external perturbations. As a consequence, all relevant state variables are also driven to zero asymptotically. The same conclusion can be reached by considering the linearized dynamics of the system that arise when a state-feedback /

state-transformation control strategy is used for path-following and a leader-follower configuration is adopted at the coordination level. From (2.18), (2.19), (2.24), and (2.29) the complete dynamics can be written as

$$
\begin{aligned}
\delta\dot{v}_{e_1} &= -a_1\delta v_{e_1} \\
\delta\dot{\eta}_{e_1} &= -k_1\delta\eta_{e_1} - k_2\delta d_{e_1} - k_3\delta\psi_{e_1} - k_4 z_1 \\
\delta\dot{d}_{e_1} &= v_1^c\delta\psi_{e_1} \\
\delta\dot{\psi}_{e_1} &= \delta\eta_{e_1} - c_{c_1}^2 v_1^c\delta d_{e_1} \\
\dot{z}_1 &= \delta d_{e_1} \\
-- &- ----- \\
\delta\dot{v}_{e_i} &= -a_i\delta v_{e_i} + R_i b_i\delta\bar{s}_{1,i} + R_i c_i\delta e_{1,i} \\
\delta\dot{\eta}_{e_i} &= -k_1\delta\eta_{e_i} - k_2\delta d_{e_i} - k_3\delta\psi_{e_i} - k_4 z_i \\
\delta\dot{d}_{e_i} &= v_i^c\delta\psi_{e_i} \\
\delta\dot{\psi}_{e_i} &= \delta\eta_{e_i} - c_{c_i}^2 v_i^c\delta d_{e_i} \\
\dot{z}_i &= \delta d_{e_i} \\
\delta\dot{\bar{s}}_{1,i} &= \delta v_{e_1}/R_1 - \delta v_{e_i}/R_i + \frac{v_1^c\,\mathrm{sign}(c_{c_1})}{R_1^2}\delta d_{e_1} - \frac{v_i^c\,\mathrm{sign}(c_{c_i})}{R_i^2}\delta d_{e_i} \\
\delta\dot{e}_{1,i} &= \delta\bar{s}_{1,i};\ \ i = 2,..,n
\end{aligned}
\tag{2.39}
$$

Using the controller gains in (2.16), the closed loop characteristic polynomial yields $(\lambda+a_1)(\lambda+\lambda_p)^{4n}\Pi_{i=2\ldots n}(\lambda^3+a_i\lambda^2+b_i\lambda+c_i)$. Clearly, the set of eigenvalues of the total linearized path-following control system consists of the union of the two sets of eigenvalues determined for the two systems taken separately. Since the two can be designed to be stable, the stability of the complete coordinated path-following system follows.

2.4 Robustness against vehicle failures

The previous sections described a set of solutions to the problem of coordinated path-following of multiple wheeled robots. However, the important issue of robustness against vehicle failures or loss of inter-vehicle communications was not addressed explicitly. Two possible failure situations are described below as illustrative examples.

Vehicle failures. This situation occurs when one or more of the vehicles cannot achieve their desired formation speeds. For example, in a Leader-Follower configuration one of the vehicles may get "stuck" at some fixed velocity that is different from the assigned one. The need then arises to assess the stability of the resulting formation and, in particular, to find out if the along-path "coordination errors" $\bar{s}_{i,j}$ remain bounded.

Communication failures. In this case, one or more of the inter-vehicle communication links fail temporarily or permanently. For example, the communication link between two vehicles may fail briefly at random instants of time, or one vehicle may only be able to broadcast its position to a subset of the remaining vehicles and receive information from another subset. In both cases, it is crucial to find out if the formation remains stable.

The study of these problems is far from complete and warrants further research efforts. In this chapter, for the sake of completeness, we simply touch upon a number of simple problems in the area of robustness against vehicle failures by examining the coordination dynamics only. Communication failures are addressed in Chapter 4 for general autonomous vehicles in nonlinear framework.

Leader-follower configuration

In the absence of vehicle failures, the coordination dynamics can be written as

$$\begin{aligned} \dot{v}_1 &= -a_1 v_1 + a_1 v_1^c \\ \dot{v}_i &= -z_i + R_i b_i \bar{s}_{1,i} \\ \dot{\bar{s}}_{1,i} &= \tfrac{1}{R_1} v_1 - \tfrac{1}{R_i} v_i \\ \dot{z}_i &= -a_i z_i + R_i (a_i b_i - c_i) \bar{s}_{1,i} \end{aligned} \tag{2.40}$$

Equation (2.40) was derived using (2.30), (2.31) and the vehicle dynamics $\dot{v}_i = F_i$.

Suppose now that due to a failure the speed of the leader is fixed at some positive speed

v_0. The dynamics of the remaining vehicles become

$$\begin{aligned} \dot{v}_i &= -z_i + R_i b_i \bar{s}_{1,i} \\ \dot{\bar{s}}_{1,i} &= \tfrac{1}{R_1} v_0 - \tfrac{1}{R_i} v_i \\ \dot{z}_i &= -a_i z_i + R_i (a_i b_i - c_i) \bar{s}_{1,i}. \end{aligned} \tag{2.41}$$

Clearly, the eigenvalues of (2.41) are those of (2.40) except for the eigenvalue at $-a_1$. Thus, if the dynamics without failures are asymptotically stable, so are the dynamics in the case where the leader fails. As a consequence, $1/R_1 v_0 - 1/R_i v_i$ and $\bar{s}_{1,j}; i = 2, ..n$ are driven to zero. Stated intuitively, all vehicles slow down or speed up in order to adopt the speeds that are required to maintain formation. Should the failure occur in one the followers, say vehicle $i = 2$, it is possible to show that all the remaining vehicles ($i \geq 3$) will still synchronize with the Leader.

Gateway configuration

In the case of the Gateway configuration, a similar analysis shows that if for some reason the velocity of the Gateway vehicle is fixed at v_0, then (as in the case of the Leader-Follower configuration) the other vehicles will adapt their velocities so as to keep the formation. It is interesting to examine the case where a vehicle other than the Gateway vehicle has a failure and its speed gets fixed at v_0.

Without any loss of generality, assume that the vehicle with a failure is vehicle 2. In this case, straightforward computations show that the coordination dynamics become

$$\begin{aligned} \dot{v}_1 &= -z_1 - R_1 b_1 \textstyle\sum_{i=2}^{n} \bar{s}_{1,i} \\ \dot{v}_i &= -z_i + R_i b_i \bar{s}_{1,i} \\ \dot{\bar{s}}_{1,2} &= \tfrac{1}{R_1} v_1 - \tfrac{1}{R_2} v_0 \\ \dot{\bar{s}}_{1,i} &= \tfrac{1}{R_1} v_1 - \tfrac{1}{R_i} v_i \\ \dot{z}_1 &= -a_1 z_1 + b_0 (v_1 - v_1^c) - R_1 (a_1 b_1 - c_1) \textstyle\sum_{i=2}^{n} \bar{s}_{1,i} \\ \dot{z}_i &= -a_i z_i + R_i (a_i b_i - c_i) \bar{s}_{1,i} \end{aligned} \tag{2.42}$$

for $i \in \{3, ..., n\}$. Equation (2.42) was derived using (2.33) and (2.34) and dynamics $\dot{v}_i = F_i$. If properly designed, the coordination law will ensure that the above system is stable. It

can then be concluded that all vehicles except vehicle 2 will learn their correct speeds and keep the formation. That is,

$$v_i \rightarrow \frac{R_i}{R_1} v_1 = \frac{R_i}{R_2} v_0$$
$$v_1 \rightarrow \frac{R_1}{R_2} v_0.$$

Vehicle 2 , however, will exhibit a finite-state steady state error

$$\bar{s}_{2,1} \rightarrow \frac{b_0}{c_1}(v_0/R_2 - v_1^c/R1), \tag{2.43}$$

and the rest will coordinate, that is, $\bar{s}_{i,1} \rightarrow 0$; $i \in \{3, ..., n\}$. The results above were derived using the fact that the left-hand side of (2.42) is zero at steady-state.

Simulation results are presented and discussed in the next section.

2.5 Simulations

This section contains the results of simulations that illustrate the performance of the coordinated path-following control system developed in this chapter.. The impact of vehicle failures on system performance is also illustrated. In what follows, for the sake of completeness, we show how, in the control laws derived, the signs of the curvature c_c and the feedback signal denoted d_e are computed.

2.5.1 Control of direction of motion

In the proposed path-following control laws, distance d_e to a path can be easily computed for circumferences and straight lines as follows. Let $(\bar{x}_0, \bar{y}_0, R)$ denote a circumference with center $(\bar{x}_0, \bar{y}_0)^T$ and radius R, and let (x_0, y_0, m) be a straight line with slope m, passing through a point with coordinates x_0, y_0. Further let $(x, y)^T$ denote the position of the center of mass of the robot. Then,

$$\text{Line} \quad : \quad d_e \quad = \quad \begin{cases} \pm\frac{y-mx-(y_0-mx_0)}{\sqrt{1+m^2}}; & m < \infty \\ \pm(-x+x_0); & \text{otherwise} \end{cases}$$

$$\text{Circ.} \quad : \quad d_e \quad = \quad \pm(R-\sqrt{(x-\bar{x}_0)^2+(y-\bar{y}_0)^2})$$

Proper care must now be taken to compute the correct sign of d_e. To do effect, start by defining the desired direction of motion along the path, that is, the direction in which the path parameter s increases. At any point on that path, define the $x-$axis of a Serret-Frenet frame (denoted **t**) as colinear with the tangent to the path, directed along the desired direction of motion. Finally, given a left-handed universal reference frame $\{\mathrm{U}\}$, obtain the complete Serret-Frenet frame by rotating $\{\mathrm{U}\}$ so as to align their $x-$axis. This will naturally define the $y-$axis of the Serret-Frenet frame, normally referred to as a normal to the path, denoted **n**. The sign of d_e is now taken as that of its component along **n**, computed for the Serret-Frenet at the point on the trajectory that is closest to the vehicle.

Figures 2.9 and 2.10 show how the tangent frames are chosen for lines and circumferences, respectively. We choose **t** according to the desired direction of motion, and **n** is defined accordingly. Figure 2.11 illustrates the results of a simulation performed for two

different signs of d_e in the feedback loop. As seen, when the initial direction of the vehicle is in the opposite direction of the desired motion, the vehicle is pushed off the path and turns back to the correct direction.

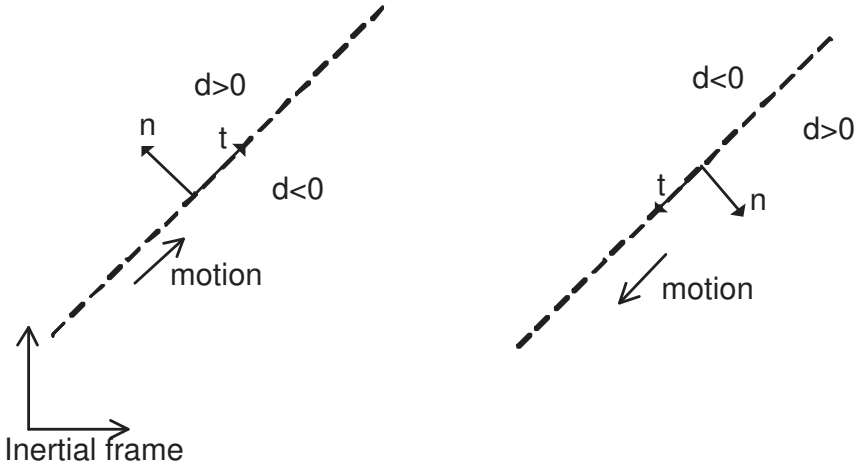

Figure 2.9: Serret-Frenet frame for lines

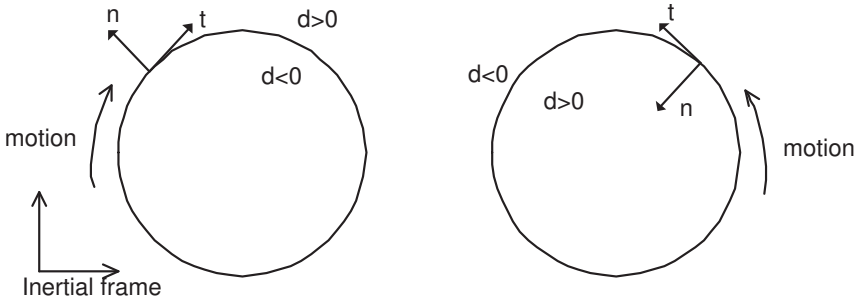

Figure 2.10: Serret-Frenet frame for circumferences

2.5.2 Coordinated path-following

Figures 2.12 and 2.13 correspond to simulations where 4 wheeled robots were required to follow paths that consists of portions of straight lines and nested arcs of circumferences, while holding an in-line formation pattern. In the simulation, the controller gains were scheduled on the path's curvature as well as on the rotation speed of the vehicles, as explained before. The simulation assumed a Gateway configuration, where the Gateway vehicle (vehicle number 1, denoted $V1$) was assigned a piecewise constant speed profile

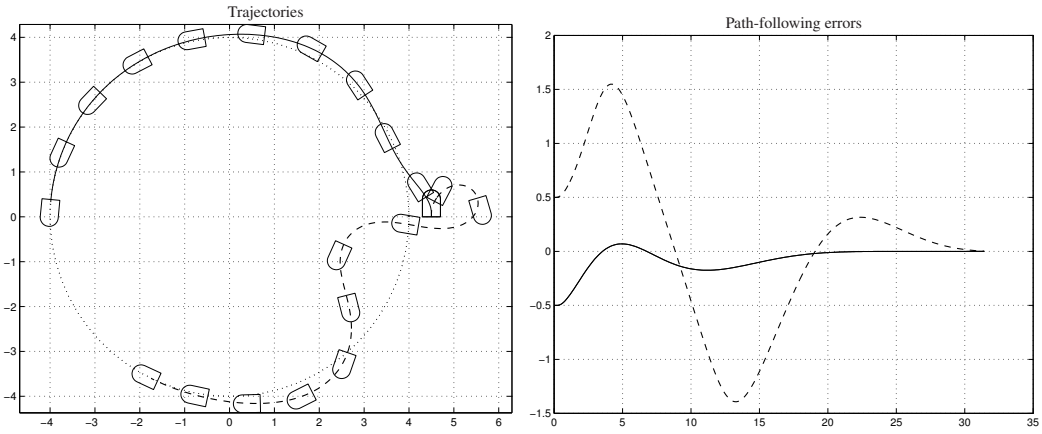

Figure 2.11: The effect of choosing different Serret-Frenet frames for the same geometrical path

that acted as a reference for the actual speed of that vehicle, shown in Figure 2.13. During the first phase of the maneuver, along an arc of a circumference, the desired speed of $V1$ was set to 0.1 [m s^{-1}]. All vehicles started at zero speed, on top of their respective paths. During the successive legs of the mission, the reference speed for vehicle $V1$ was set to 0.2, 0.4, and 0.2 [m s^{-1}]. Notice how the remaining vehicles adjust their speeds to meet the formation requirements. Figure 2.14 shows the coordination errors, as captured by the along-path distances between vehicle 1 and the remaining vehicles. The figures include information on both $s_{i,j}$ and $\bar{s}_{i,j}$. Because the paths to be followed consist of segments of straight lines and semi-circumferences, normalization factors were used to make the above variables non-dimensional.

2.5.3 Coordinated path-following with vehicle failures

Consider CPF of 3 vehicles with Gateway communication topology, with $V1$ as the gateway, required to follow circumferences with radii 2, 3 and 4[m], at desired trimming speed $v_1^c = 0.2[\text{ms}^{-1}]$. Figure 2.15 illustrates a failure scenario in which vehicle 2 fails to reach to desired speed $v_2^c = \frac{3[m]}{2[m]} v_1^c = 0.3[\text{ms}^{-1}]$ and gets stuck at $v_0 = 0.25[\text{ms}^{-1}]$. Consider the control law (2.33) and (2.34) with control gains

$$b_0 = 5,\ a_i = 3\lambda,\ b_i = 3\lambda^2,\ \text{and}\ c_i = \lambda^3$$

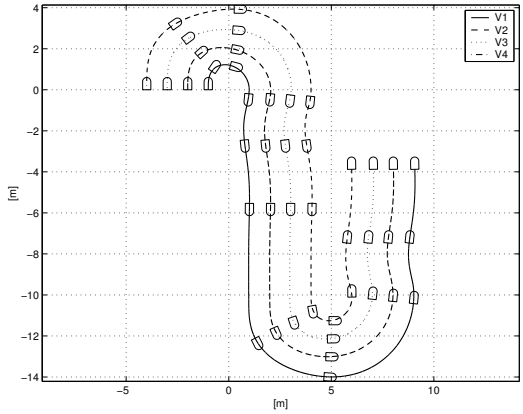

Figure 2.12: Coordinated path-following: Gateway configuration, trajectories

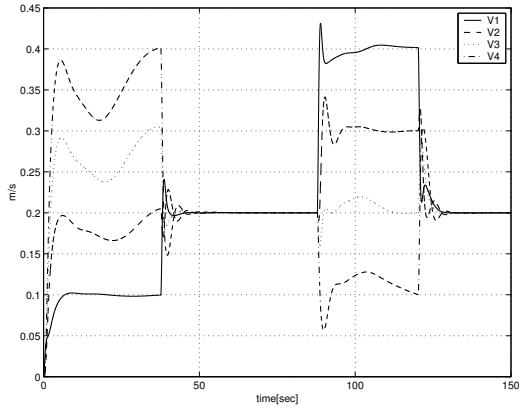

Figure 2.13: Coordinated path following: Gateway configuration, vehicle speeds

where we set $\lambda = 1$. The simulation results are shown in Figure 2.15–(a),(c),(e). Notice how the coordination errors at steady-state tend to 0.083[rad]=4.75[deg] which confirms (2.43). Figure 2.15–(b),(d),(f) show that this steady-state error can be eliminated by adding an extra integrator state to the controller. Consider extra integrator state $\dot{z}_{1,i} = \delta e_{1,i}; i = 2,...,n$ together with dynamical control laws (2.32). Define $z_1 = a_1 \delta v_{e_1} + b_0 \delta e_v - R_1 c_1 \Sigma \delta e_{1,i} - R_1 d_1 \Sigma z_{1,i}$ and $z_i = a_i \delta v_{e_i} - R_i c_i \delta e_{1,i} - R_i d_i z_{1,i}; i \geq 2$, where $d_i > 0; \forall i$. A straightforward application of the $\mathscr{D}$-methodology yields the final nonlinear coordination control law

$$\begin{aligned} F_1 &= -z_1 - R_1 b_1 \Sigma \bar{s}_{1,i} \\ \dot{z}_1 &= a_1 \dot{v}_1 + b_0 (v_1 - v_1^c) - R_1 c_1 \Sigma \bar{s}_{1,i} - R_1 d_1 \Sigma \delta e_{1,i} \end{aligned}$$

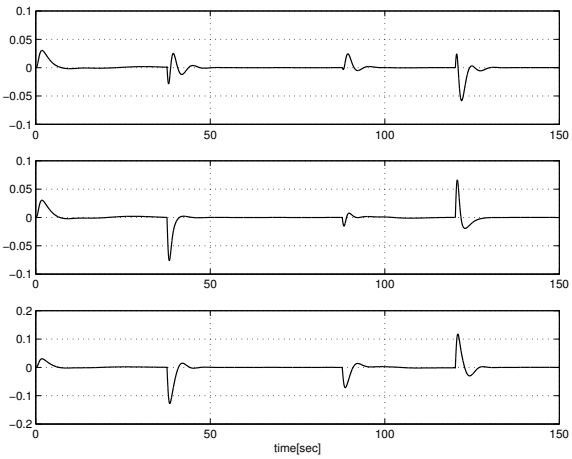

Figure 2.14: Coordinated path-following: Gateway configuration, the coordination errors between vehicle 1 and the remaining vehicles, 2, 3 and 4

for the Gateway vehicle and

$$\begin{aligned} F_i &= -z_i + R_i b_i \bar{s}_{1,i} \\ \dot{z}_i &= a_i \dot{v}_i - R_i c_i \bar{s}_{1,i} - R_i d_i \delta e_{1,i}. \\ \delta \dot{e}_{1,i} &= \bar{s}_{1,i} \end{aligned}$$

for the remaining vehicles. In the simulations, the control gains were set to

$$b_0 = 5,\, a_i = 4\lambda,\, b_i = 6\lambda^2,\, c_i = 4\lambda^3 \,\text{and}\, d_i = \lambda^4,$$

with $\lambda = 1$ that results in a stable system. The stability proof is straightforward and we will not go through the details of the proof for this case. Notice that the Gateway vehicle needs to transmit $\bar{s}_1$ to the other vehicles, and they ($i = 2, \ldots, n$) need to transmit $\bar{s}_i$ as well as $\delta e_{1,i}$ to the Gateway.

2.6 Summary

This chapter offers a solution to coordinated path-following of a fleet of wheeled robots along a set of given spatial paths, the so-called trimming paths. The methodology proposed builds on linearization techniques and draws heavily on previous work on the implementation of gain-scheduled controllers. Using this set-up, path-following and inter-vehicle coordination are essentially decoupled. Path-following for each vehicle amounts to reducing

a conveniently defined error vector to zero. Vehicle coordination is achieved by adjusting the speed of each of the vehicles along its path, according to information on the position of the remaining vehicles only. This allowed for a simple analysis of the resulting coordinated path-following control system. The resulting control system is simple to implement and avoids feedforwarding the desired speed of all the vehicles. In fact, only the velocity of one of the vehicles is required, the other vehicles recruiting their velocities automatically to keep the formation. We consider different vehicle configurations and address some of the problems that arise when a vehicle fails to reach some desired speed. In particular, it is shown how the remaining vehicles adjust their speeds and try to maintain formation. This chapter of the work was a first attempt to derive simple, easy to implement control systems for coordinated path-following. Extending the results to a full nonlinear setting, thus achieving global stability and convergence, is the subject of Chapter 3. The issues related to communication losses and time delays are addressed in Chapter 4.

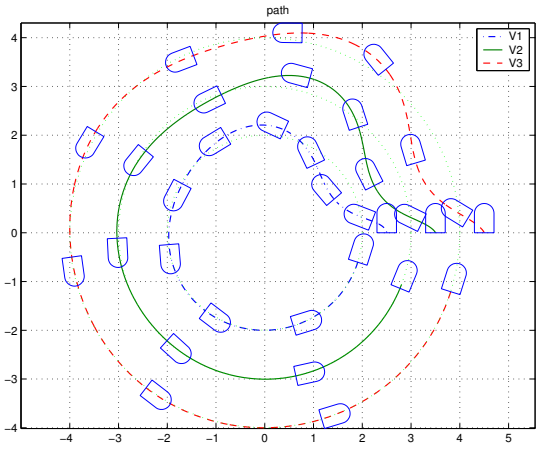

(a) Trajectories

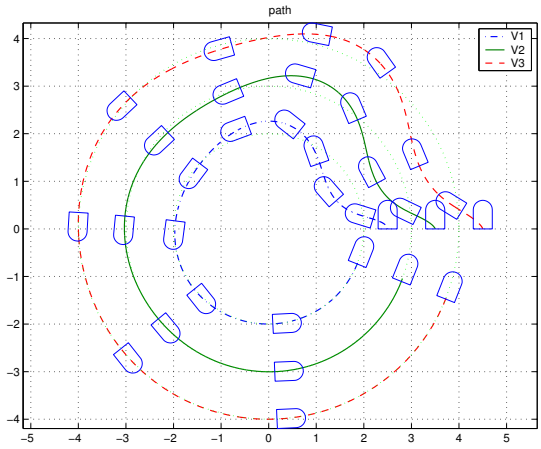

(b) Trajectories, extra integral

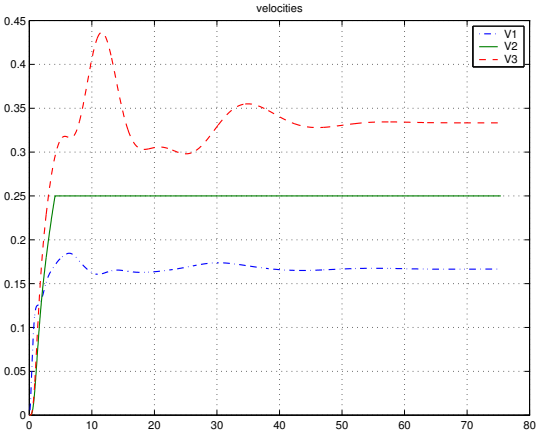

(c) Speeds

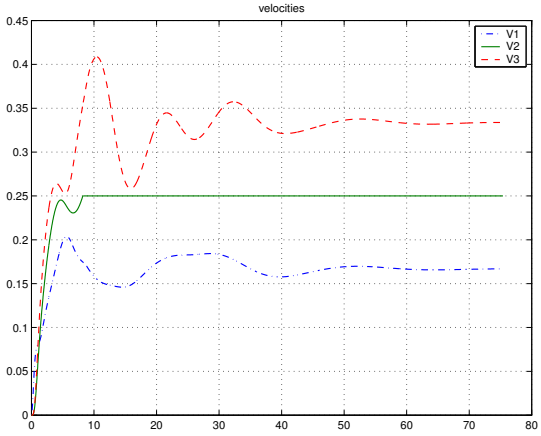

(d) Speeds, extra integral

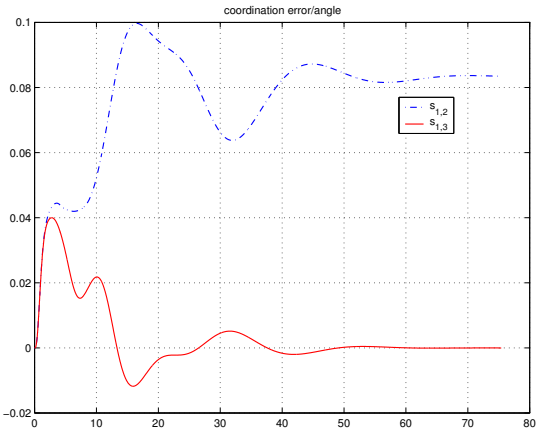

(e) Coordination errors

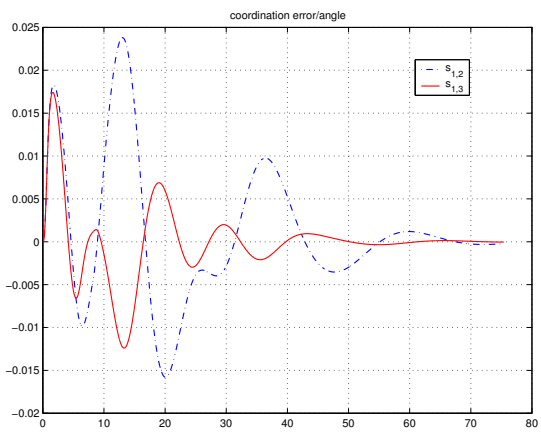

(f) Coordination errors, extra integral

Figure 2.15: Gateway topology. Coordination of 3 vehicles. Failure of vehicle 2

CHAPTER 3

FIXED COMMUNICATION TOPOLOGIES: WHEELED ROBOTS, FULLY ACTUATED MARINE VEHICLES

This chapter offers several solutions to the problem of coordinated path-following of wheeled robots. The results are also extended to cope with fully actuated marine vehicles. The types of communication topologies considered are quite general. Tools from Graph theory are used to deal with communication constraints. Bi-directional (symmetric) and uni-directional (asymmetric) communication networks are addressed separately, and the topologies are assumed to be fixed with respect to time[1]. We start with some preliminaries.

3.1 Mathematical preliminaries

This section summarizes the mathematical machinary required to study the problems of path-following and coordinated path-following. Different notions of stability equilibrium points of ODE and related theorems are described. The section ends with an overview of important concepts in Graph theory.

[1] Switching communication networks are addressed in Chapter 4.

3.1.1 Stability definitions and related theorems

Most of the definitions and theorems in this section borrow from (Khalil 2002), (Rouche et al. 1977) and (Horn & Johnson 1985).

Norms and properties

The symbol $\|.\|_p$ ($p \geq 1$) denotes both the *p-norm* of a vector and the *induced p-norm* of matrix as follows. Given a vector $x = (x_1, ..., x_n)^T \in \mathbb{R}^n$,

$$\|x\|_p = (\sum_{i=1}^{n} |x_i|^p)^{1/p}$$

and $\|x\|_\infty = \max_i |x_i|$. Given a matrix $A : \mathbb{R}^n \to \mathbb{R}^m$,

$$\|A\|_p = \sup_{x \neq 0} \frac{\|Ax\|_p}{\|x\|_p} = \max_{\|x\|_p = 1} \|Ax\|_p.$$

We will drop p from the notation indicating that the norm can be any p-norm. Notice that $\|x\|_2^2 = x^T x$. The vector 2-norm is also called the *Euclidean norm* (or l_2 norm), and the matrix induced 2-norm is called the spectral norm because

$$\|A\|_2 = \max\{\sqrt{\lambda} : \lambda \in \sigma(A^T A)\},$$

where $\sigma(A^T A)$ denotes set of the eigenvalues of $A^T A$, also called the *spectrum* of $A^T A$.

Some useful inequalities related to norms are worth recalling. All vector p-norms in a finite dimensional space are equivalent in the sense that for any $p_1 \neq p_2$, there exist $a, b > 0$ such that

$$a\|x\|_{p_1} \leq \|x\|_{p_2} \leq b\|x\|_{p_1}.$$

Young's inequality

$$|x^T y| \leq a x^T x + b y^T y,\ ab = \frac{1}{4}.$$

Hölder inequality

$$|x^T y| \leq \|x\|_{p_1} \|y\|_{p_2},\ \frac{1}{p_1} + \frac{1}{p_2} = 1.$$

We will use the preceding inequality for $p_1 = p_2 = 2$.

Systems and dynamics

We consider *nonautonomous systems* described by ordinary differential equations of the form

$$\dot{x} = f(t,x) \tag{3.1}$$

where $f : [0,\infty) \times D \to \mathbb{R}^n$ is piecewise continuous in t and locally Lipschitz in x on $[0,\infty) \times D$ with $D \in \mathbb{R}^n$ a domain that contains the origin $x = 0$. The function $f(t,x)$ is said to be *locally Lipschitz* at $(t_0,x_0) \in [0,\infty) \times D$ if there is $L > 0$ such that

$$\|f(t,x) - f(t,y)\| \leq L\|x - y\|$$

for all (t,x) and (t,y) in some neighborhood of (t_0,x_0). The function f is *uniformly continuous* in x on $[0,\infty) \times D$ if $\forall \varepsilon > 0, \exists \delta > 0$ such that $\|f(t,x) - f(t,y)\| < \varepsilon$ for all $x,y \in D$ satisfying $\|x - y\| < \delta$ and $\forall t \geq 0$. Roughly speaking, small changes in x results in small changes in $f(t,x)$ uniformly in t. Notice that the Lipstchitz property of a function is stronger than uniform continuity. That is, if $f(t,x)$ is Lipstchitz in x on $[0,\infty) \times D$, then it is uniformly continuous on $[0,\infty) \times D$, but the converse is not true. The origin is an *equilibrium point* of (3.1) if

$$f(t,0) = 0, \ \forall t \geq 0$$

Theorem 3.1 (Existence and uniqueness)
Let $f(t,x)$ be piecewise continuous in t and locally Lipschitz in x for all $t \geq t_0$ and all x in the domain D. Let W be a compact set of D, and $x_0 \in W$, and suppose it is known that every solution of

$$\dot{x} = f(t,x), \ x(t_0) = x_0$$

lies entirely in W. Then there is a unique solution that is defined for all $t \geq t_0$.

Class $\mathscr{K}$ and $\mathscr{K}\mathscr{L}$ functions

- Class $\mathscr{K}$: a continuous, strictly increasing function $\alpha : [0,a) \to [0,\infty)$ such that $\alpha(0) = 0$. For example, $\alpha(r) = r^c, c \in \mathbb{R}^+$.

- Class $\mathscr{K}_\infty$: a class $\mathscr{K}$ for which $a = \infty$, $\alpha(r) \to \infty$ as $r \to \infty$.

- Class $\mathscr{KL}$: a continuous function $\beta : [0,a) \times [0,\infty) \rightarrow [0,\infty)$, such that for each fixed s the mapping $\beta(r,s) \in \mathscr{K}$ with respect to r, and for each fixed r the mapping $\beta(r,s)$ is decreasing with respect to s and $\beta(r,s) \rightarrow 0$ as $s \rightarrow \infty$. For example, $\beta(r,s) = r^c e^{-s}$

Stability definitions Denote by $x(t); t \geq t_0$ the solution of (3.1) with initial condition $x(t_0)$. The equilibrium $x = 0$ of $\dot{x} = f(t,x)$ is

- *uniformly stable* (US), if there exist a class $\mathscr{K}$ function $\alpha(.)$ and a positive constant c independent of t_0, such that

$$\|x(t)\| \leq \alpha(\|x(t_0)\|), \ \forall t \geq t_0, \forall \|x(t_0)\| < c$$

- *uniformly asymptotically stable* (UAS), if there exist a class $\mathscr{KL}$ function $\beta(.,.)$ and a positive constant c independent of t_0, such that

$$\|x(t)\| \leq \beta(\|x(t_0)\|, t - t_0), \ \forall t \geq t_0, \forall \|x(t_0)\| < c \tag{3.2}$$

- *uniformly globally asymptotically stable* (UGAS), if the previous condition holds for any initial state $x(t_0)$.

- *exponentially stable* (ES), if inequality (3.2) is satisfied with

$$\beta(r,s) = kre^{-\gamma s}, \ k > 0, \gamma > 0.$$

- *equi-asymptotically stable*, if it is asymptotically stable uniformly with respect to the initial conditions. In other words, if we relax uniformity of UAS with respect to t_0, we get equi-asymptotical stability. See (Rouche et al. 1977) for a regorous definition.

Lyapunov stability, non-autonomous system A function $V : [0,\infty) \times D \rightarrow \mathbb{R}$, denoted $V(t,x)$ is positive definite if $V(t,x) \geq \alpha_1(\|x\|)$, for some $\alpha_1(.)$ of class $\mathscr{K}$ and all $t \geq 0$. Identically, a function $V(t,x)$ as defined above is decrescent if $V(t,x) \leq \alpha_2(\|x\|)$, for some $\alpha_2(.)$ of class $\mathscr{K}$ and $t \geq 0$.

Theorem 3.2 (Lyapunov theorem)

Let $V : [0,\infty) \times D \rightarrow \mathbb{R}$ be a $\mathscr{C}^1$ function such that

$$\alpha_1(\|x\|) \leq V(t,x) \leq \alpha_2(\|x\|)$$
$$\dot{V} := \frac{\partial V}{\partial t} + \frac{\partial V}{\partial x} f(t,x) \leq -\alpha_3(\|x\|)$$

$\forall t \geq 0, \forall x \in D$, *where* $\alpha_1(.)$, $\alpha_2(.)$, *and* $\alpha_3(.)$ *are class* $\mathcal{K}$ *functions defined on* $[0,r); r > 0$. *Then* $x = 0$ *is a UAS equilibrium of* (3.1). *If all the assumptions are satisfied globally* $r = +\infty$, *and* $\alpha_1, \alpha_2 \in \mathcal{K}_\infty$, *then* $x = 0$ *is UGAS. If* $\alpha_i(s) = k_i s^2$; $i = 1,2,3$ *for some* $k_i > 0$, *then the origin is UGES. If* $\alpha_3 = 0$, *then the origin is US.*

We now consider the systems that are driven by external inputs.

Input-to-state stability The system $\dot{x} = f(t,x,u)$ is said to be *input-to-state stable* (ISS) with state x and input u if there exist a $\mathcal{KL}$ function β, and a class $\mathcal{K}$ function γ such that for any initial state $x(t_0)$ and any bounded input $u(t)$, the solution $x(t)$ exists $\forall t \geq t_0$ and satisfies

$$\|x(t)\| \leq \beta(\|x(t_0)\|, t - t_0) + \gamma(\sup_{t_0 \leq \tau \leq t} \|u(\tau)\|)$$

It can be shown that if $u(t)$ vanishes as $t \to \infty$, then $\|x(t)\| \to 0$, (Sontag & Wang 1996).

Example 3.1. Consider the linear system with dynamics $\dot{x} = Ax + Bu$ where A is a stability matrix. Using the fact that

$$\|e^{(t-t_0)A}\| \leq k e^{-\lambda(t-t_0)}$$

for some $k, \lambda > 0$, it follows that

$$\|x(t)\| \leq k e^{-\lambda(t-t_0)} \|x_0\| + \frac{k\|B\|}{\lambda} \sup_{t_0 \leq \tau \leq t} \|u(\tau)\|.$$

and the system is ISS with state x and input u.

Lemma 3.1

Suppose that $f(t,x,u)$ *is continuously differentiable and globally Lipschitz in* (x,u), *uniformly in* t. *If the unforced system* $\dot{x} = f(t,x,0)$ *has a UGES equilibrium point at the origin* $x = 0$, *then the system* $\dot{x} = f(t,x,u)$ *is input-to-state stable (ISS).* (Khalil 2002, pp. 174)

Lyapunov functions with negative semi-definite derivative Theorems 3.3 to 3.6 provide

tools to deal with the Lyapunov functions whose time derivatives are not negative definite.

Theorem 3.3 (Barbashin and Krasovskii (Special case of LaSalle's invariance principle)) *Let $x = 0$ be an equilibrium point for the autonomous system $\dot{x} = f(x)$. Let $V : D \to \mathbb{R}$ be a $\mathscr{C}^1$ positive definite function on a neighborhood D of 0, such that $\dot{V} \leq 0$ in D. Let $E = \{x \in D | \dot{V}(x) = 0\}$ and suppose that no solution can stay forever in E, other than the trivial solution. Then the origin is asymptotically stable.*

Theorem 3.4 (Invariance principle-like theorem for non-autonomous systems) *Consider the system (3.1) with domain $D = \{x \in \mathbb{R}^n : \|x\| < r\}$. Let $V : [0,\infty) \times D \to \mathbb{R}$ be a continuously differentiable function such that*

$$\alpha_1(\|x\|) \leq V(t,x) \leq \alpha_2(\|x\|)$$
$$\dot{V}(t,x) \leq -W(x) \leq 0$$

$\forall t \geq 0, \forall x \in D$, where $\alpha_1(.)$ and $\alpha_2(.)$ are class $\mathscr{K}$ functions defined on $[0,r)$ and $W(x)$ is continuous on D. Then, all solutions of $\dot{x} = f(t,x)$ with $\|x(t_0)\| < \alpha_2^{-1}(\alpha_1(r))$ are bounded and satisfy

$$W(x(t)) \to 0 \text{ as } t \to \infty.$$

Moreover, if all the assumptions hold globally and $\alpha_1(.)$ belongs to class $\mathscr{K}_\infty$, the statement is true for all $x(t_0) \in \mathbb{R}^n$.

Theorem 3.5 (Matrosov 1962, non-autonomous systems) *Consider the system (3.1). Let there exist two $\mathscr{C}^1$ functions $V : [0,\infty) \times D \to \mathbb{R}$, $W : [0,\infty) \times D \to \mathbb{R}$, a $\mathscr{C}^0$ function $U : D \to \mathbb{R}$, three functions $\alpha_1, \alpha_2, \alpha_3 \in \mathscr{K}$ and two constant c_1 and c_2, such that for every $(t,x) \in [0,\infty) \times D$*

1. $\alpha_1(\|x\|) \leq V(t,x) \leq \alpha_2(\|x\|)$,
2. $\dot{V}(t,x) \leq U(x) \leq 0$; *Define* $E := \{x \in D : U(x) = 0\}$,
3. $|W(t,x)| < c_1$,
4. $\max(\text{dist}(x,E), |\dot{W}(t,x)|) \geq \alpha_3(\|x\|)$,
5. $\|f(t,x)\| < c_2$.

where $\text{dist}(x,E) = \min_{e\in E} \|x-e\|$. *Then the origin is UAS,* (Rouche et al. 1977, pp. 62).

Theorem 3.6 (Massera, equi-asymptotic stability)

Suppose there exist a $\mathscr{C}^1$ *function* $V : [0,\infty)\times\mathbb{R}^n \to \mathbb{R}$ *and functions* $\alpha_1(.),\alpha_2(.) \in \mathscr{K}$ *such that* $\forall t \geq 0, \forall x \in \mathbb{R}^n$

$$\alpha_1(\|x\|) \leq V(t,x) \leq \alpha_2(\|x\|)$$

Further assume there exist a function $U : [0,\infty)\times\mathbb{R}^n \to \mathbb{R}$ *and a function* $\alpha_3(.) \in \mathscr{K}$ *such that*

$$U(t,x) \geq \alpha_3(\|x\|); U(t,0) = 0,$$

and for any ρ_1 *and* ρ_2 *with* $0 < \rho_1 < \rho_2$, $\lim_{t\to\infty} \dot{V} + U(t,x) = 0$, *uniformly on* $\rho_1 \leq \|x\| \leq \rho_2$. *Then the origin is an equi-asymptotically stable equilibrium of* (3.1), (Massera 1949) and (Rouche et al. 1977, pp. 34).

Lemma 3.2 Barbalat's lemma

Let $\phi : \mathbb{R} \to \mathbb{R}$ *be a uniformly continuous function on* $[0,\infty)$. *Further assume* $\lim_{t\to\infty} \int_0^t \phi(\tau)d\tau$ *exists and is finite. Then* $\phi(t) \to 0$ *as* $t \to \infty$.

Linear systems

Lemma 3.3 ***UGES and ISS.***

Consider the linear time-varying system

$$\dot{x} = A(t)x \tag{3.3}$$

where $A(t)$ *is a piecewise continuous matrix function in* t. *Let* (3.3) *be UGES, and* $B(t)$ *be bounded and tend to zero as* $t \to \infty$. *Then*

1. $\dot{x} = A(t)x + d$ *is ISS with* d *as input,*
2. $\dot{x} = (A(t) + B(t))x$ *is UGES.*
3. $\dot{x} = (A(t) + B(t))x + d$ *is ISS with* d *as input.*

Lemma 3.4

System (3.3) *is UAS if and only if it is UES. Moreover, local stability for* (3.3) *implies global stability.*

Positive definiteness and Schur complements Suppose that a symmetric matrix is partitioned as

$$\begin{pmatrix} A & B \\ B^T & C \end{pmatrix}$$

where A and C are square. This matrix is positive definite iff A and $C - B^T A^{-1} B$ are positive definite.

Properties of max$(.,.)$

- For any $a, b, c \in \mathbb{R}$

$$\max(a,b) \geq 1/2(a+b)$$
$$\max(a,b,c) \geq 1/3(a+b+c).$$

- If $a \geq c$ and $0 < \beta \leq 1$ then

$$\max(a,b) \geq \max(c,b)$$
$$\max(a,b) = \max(a,b,c)$$
$$\max(a,b) \geq \max(a,\beta b)$$

3.1.2 Graph theory

Cooperative control strategies for multiple vehicles are supported by the communications network over which the vehicles exchange motion-related information. Practical constraints related to limited bandwidth, range of communications, energy minimization, and possible interferences dictate that is general no vehicle will be able to communicate with the entire vehicle formation. The topology of the communications network must therefore be addressed explicitly. For our purposes, this will be done by using Graph Theory which is the tool par excellent to describe the type of network available for communications and to study the impact of communication topologies on the performance that can be achieved with different coordination strategies.

The communication links among the vehicles can be bi-directional or uni-directional. In bi-directional networks all data links are bi-directional, that is, if vehicle i sends information to j, then j also sends information to i. In a uni-directional network, there are

vehicles which only send or receive information. In the context of Graph theory *undirected graphs* are specially suited to model bi-directional communication networks. To model uni-directional communications networks *directed graphs* must be used.

This section summarizes some key concepts and results of graph theory that are relevant to the thesis. The definitions and theorems in this section borrow from (Balakrishnan & Ranganathan 2000), (Biggs 1996) and (Godsil & Royle 2001) for undirected graphs, and from (Bang-Jensen & Gutin 2002) and (Godsil & Royle 2001) for directed graphs. For important matrix analysis tools that support the developments in graph theory, reader is referred to (Horn & Johnson 1985). The PhD theses (Fax 2002) and (Lin 2006) offer a good collection of theorems on directed graphs.

Undirected graphs

An *undirected graph* or simply a graph $\mathcal{G}(\mathcal{V},\mathcal{E})$ (abbv. $\mathcal{G}$) consists of a set of *vertices* $V_i \in \mathcal{V}(\mathcal{G})$ and a set of *edges* $\mathcal{E}(\mathcal{G})$, where an edge $\{V_i,V_j\}$ is an unordered pair of distinct vertices V_i and V_j in $\mathcal{V}(\mathcal{G})$. A *simple graph* is a graph with no edges from one vertex to itself. We will only consider simple graphs, and will refer to them simply as graphs. In this thesis, the vertices and the edges of a graph represent the vehicles and the data links among them, respectively. If $\{V_i,V_j\} \in \mathcal{E}(\mathcal{G})$, then we say that V_i and V_j are *adjacent* or *neighbors*. The set of the neighbors of V_i is denoted by N_i. A *path* of length r from V_i to V_j in a graph is a sequence of $r+1$ distinct vertices starting with V_i and ending with V_j, such that two consecutive vertices are adjacent. The graph $\mathcal{G}$ is said to be *connected* if two arbitrary vertices V_i and V_j can be joined by a path of arbitrary length.

The assumption that all communication links are bi-directional seems to imply that no specific orientations should be assigned to the edges of the underlying coordination graph. This is true from a pure communications standpoint. However, the fact that we wish the coordination control law to reflect the topology of the communication network requires that we take a different approach to the problem at hand. To see this, let $\mathcal{G}$ be the undirected graph that captures a given bi-directional communication network. Then, $\mathcal{G}$ has n vertices (as many as the vehicles). Associate to each vertex i the coordination state ξ_i of the corresponding vehicle. As discussed in the Introduction, Section 1.1, it is the objective

of the coordination system to drive the errors $(\xi_i - \xi_j)$ to 0 for all i, j. This must be done by controlling the speed of each vehicle in the formention via a suitably designed coordination control law. Consider vehicle i (represented by vertex i) and its set of neighbors N_i. It is natural that the coordination law for vehicle i include terms of the form $\xi_i - \xi_j; j \in N_i$ or combinations thereof. To make this circle of ideas formal we recall the definition of orientation of a graph and related concepts.

An *orientation* of a graph $\mathscr{G}$ is the assignment of a direction to each edge of that graph. To this effect, select for each edge $\{V_i, V_j\}$ in $\mathscr{E}(\mathscr{G})$ one of the V_i, V_j to be the head of the edge and the other the tail, and view the edge oriented from its tail to its head. After this operation, the elements of $\mathscr{E}(\mathscr{G})$ become ordered pairs (V_i, V_j), henceforth known as *arcs*. See Figure 3.1(a) for the case of an undirected graph with three vertices and the graph with an associated orientation in Figure 3.1(b). Formally, an orientation of $\mathscr{G}$ can be defined as a function σ from the arcs of $\mathscr{G}$ to $\{-1, 1\}$ as follows: $\sigma(V_i, V_j) = 1$ if edge $\{V_i, V_j\}$ is oriented form tail V_i to head V_j; $\sigma(V_i, V_j) = -1$ if edge $\{V_i, V_j\}$ is oriented form tail V_j to head V_i. Notice that $\sigma(V_i, V_j) = -\sigma(V_j, V_i)$. For example, in Figure 3.1(b), $\sigma(V_1, V_2) = +1$ and $\sigma(V_1, V_3) = -1$. An oriented graph is a graph with a particular orientation denoted $\mathscr{G}^\sigma$. The *incidence matrix* M of $\mathscr{G}^\sigma$ is the $\{0, \pm 1\}$-matrix with rows and columns indexed by the vertices and the arcs of $\mathscr{G}^\sigma$, respectively. If $\mathscr{G}^\sigma$ has n vertices and ε arcs, M is of order $n \times \varepsilon$ and its kl-entries are

$$m_{kl} = \begin{cases} +1, & \text{if } V_k \text{ is the head of arc } l \\ -1, & \text{if } V_k \text{ is the tail of arc } l \\ 0, & \text{otherwise} \end{cases}$$

where an arbitrary numbering of the arcs is assumed. Note that each column of M contains only two non-zero entries, $+1$ and -1, representing the head and the tail of the incident arc. The following result plays a key role in the development that follows.

Lemma 3.5 (Godsil & Royle 2001)

Let $\mathscr{G}$ be a graph with ε edges and n vertices. Let M be the incidence matrix of $\mathscr{G}^\sigma$ with an arbitrary orientation σ. If $\mathscr{G}$ is connected, then $\varepsilon \geq n-1$, $\operatorname{Rank} M^T = n-1$, *and* $\operatorname{Kern} M^T = \mathbf{1}$.

Given an undirected graph, its *degree matrix* D is defined as the diagonal matrix of

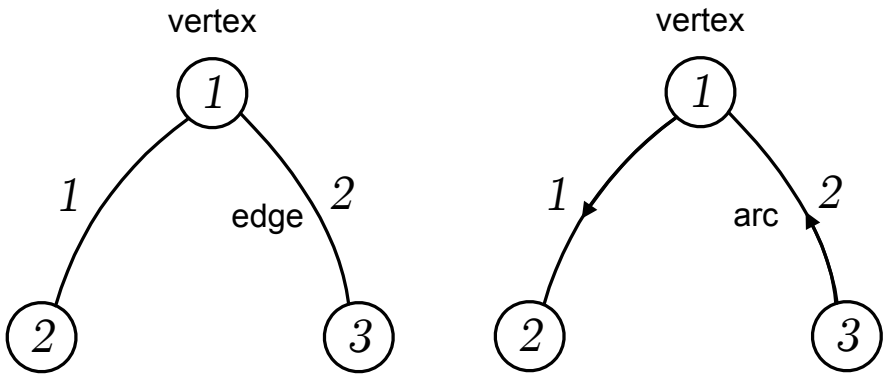

(a) An undirected graph (b) A graph with an associated orientation

Figure 3.1: An undirected graph with an associated orientation

order n with $|N_i|$ (the cardinality of N_i) in the ii-entry[2]. Further, the *adjacency matrix* A is a square matrix with rows and columns indexed by the vertices, such that the ij-entry of A is 1 if $\{V_i, V_j\} \in \mathscr{E}$ and zero otherwise. We continue by introducing the concept of *Laplacian* of an undirected graph (Biggs 1996). Let $\mathscr{G}$ be an undirected graph with n vertices and assign an arbitrary orientation to it. Consider the corresponding incidence matrix M. The Laplacian L of $\mathscr{G}$ is the symmetric, positive semi-definite square matrix $L = MM^T$ of order $n \times n$. This definition of Laplacian is equivalent to the more used one of $L = D - A$, where D and A denote the degree matrix and the adjacency matrix of $\mathscr{G}$, respectively. By construction, L is *independent* of the particular orientation assigned to an undirected graph $\mathscr{G}$. Furthermore, all eigenvalues of L are non-negative, and $L\mathbf{1} = \mathbf{0}$. If $\mathscr{G}$ is connected, $\operatorname{Rank} L = n - 1$ and consequently L has a single eigenvalue at zero with corresponding right eigenvector $\mathbf{1}$. Furthermore, the diagonal elements of the Laplacian matrix of a connected graph are positive and its off diagonals are non-positive. The following statement is taken from (Biggs 1996).

Lemma 3.6

Let D and A be degree matrix and adjacency matrix of an undirected graph $\mathscr{G}$, respectively. If σ is an arbitrary orientation of $\mathscr{G}$ and M is the incidence matrix of $\mathscr{G}^\sigma$, then $MM^T = D - A$.

[2] $|N_i|$ is also called the valency of vertex V_i.

Let $\mathscr{G}$ be an undirected graph defined by n vertices and ε edges numbered $1,...,\varepsilon$ with incidence matrix $M \in \mathbb{R}^{n\times\varepsilon}$. Further, let $W = [w_k]_{\varepsilon\times\varepsilon}$, where $w_k > 0$ is a weight associated with edge k, be a diagonal matrix and define the *weighted graph Laplacian* $L_w = MWM^T$. If $z = L_w\xi$, then

$$z_i = \sum_{j\in N_i, k=e(i,j)} w_k(\xi_i - \xi_j)$$

where the notation $k = e(i,j)$ means the k-th edge $\{V_i, V_j\}$.

The following example illustrates some of the definitions and properties introduced above.

Example 3.2. Consider the graph $\mathscr{G}$ of Figure 3.1(a) with the orientation inherited from the directions assigned to its edges as in Figure 3.1(b). Clearly, $\mathscr{V} = \{1,2,3\}$, $\mathscr{E} = \{\{1,2\},\{1,3\}\}$, $\sigma(1,2) = 1$, and $\sigma(1,3) = -1$. Then,

$$M = \begin{pmatrix} -1 & 1 \\ 1 & 0 \\ 0 & -1 \end{pmatrix}, L = MM^T = \begin{pmatrix} 2 & -1 & -1 \\ -1 & 1 & 0 \\ -1 & 0 & 1 \end{pmatrix},$$

and

$$D = \begin{pmatrix} 2 & 0 & 0 \\ 0 & 1 & 0 \\ 0 & 0 & 1 \end{pmatrix}, \text{ and } A = \begin{pmatrix} 0 & 1 & 1 \\ 1 & 0 & 0 \\ 1 & 0 & 0 \end{pmatrix}.$$

Notice that for any arbitrary orientation, the graph Laplacian will remain unchanged and $L = MM^T = D - A$.

We now summarize a set of more advanced results in graph theory.

Spanning tree of a graph

A *subgraph* of a graph $\mathscr{G}$ is a graph $\mathscr{G}_1$ such that $\mathscr{V}(\mathscr{G}_1) \subseteq \mathscr{V}(\mathscr{G})$ and $\mathscr{E}(\mathscr{G}_1) \subseteq \mathscr{E}(\mathscr{G})$, that is, the vertices and edges sets of $\mathscr{G}_1$ are subsets of those of $\mathscr{G}$. If $\mathscr{V}(\mathscr{G}_1) = \mathscr{V}(\mathscr{G})$, we call $\mathscr{G}_1$ a *spanning subgraph* of $\mathscr{G}$. A *cycle* is a close path (that is, a path from vertex V_i to itself) in which the intermediate edges are all distinct. A connected graph without cycles is defined as a *tree*. A *spanning tree* of a connected undirected graph $\mathscr{G}$ is a spanning subgraph of $\mathscr{G}$ which is a tree. The following results are worth stressing.

Lemma 3.7 (Balakrishnan & Ranganathan 2000)

The number of edges in a tree with n vertices is $n-1$. Conversely, a connected graph with n vertices and $n-1$ edges is a tree. Moreover, every connected graph contains a spanning tree.

Informally, a spanning tree $\mathscr{T}$ of a connected graph $\mathscr{G}$ is defined as what is left of a graph $\mathscr{G}$ after deleting from it the maximum number of edges while keeping the resulting graph connected. These results are now exploited to give further insight into the structure of a connected graph $\mathscr{G}$ with n vertices and ε edges.

Lemma 3.8 L **decomposition**

If $\mathscr{G}$ is connected, the graph Laplacian L can be written as $L = M_1 Y^2 M_1^T$, where $M_1 \in \mathbb{R}^{n\times n-1}$ is a full rank incidence matrix and $Y > 0$ is an $n \times n$ real matrix.

Proof. Since $\mathscr{G}$ is connected, $\varepsilon \geq n-1$. We analyze the cases $\varepsilon \geq n$ and $\varepsilon = n-1$ separately. Suppose $\varepsilon \geq n$ and choose a spanning tree $\mathscr{T}$ in $\mathscr{G}$, which is known to exist because of Lemma 3.7 and ensures that the spanning tree has $n-1$ edges. Index the edges of $\mathscr{G}$ that are in $\mathscr{T}$ from 1 to $n-1$ and the remaining edges from n to ε. Associate now an arbitrary orientation σ to graph $\mathscr{G}$ and compute the corresponding incidence matrix M of $\mathscr{G}^\sigma$. Partition M as $M = [M_1, M_2]$, where $M_1 \in \mathbb{R}^{n\times n-1}$ becomes the incidence matrix of $\mathscr{T}^\sigma$ with the orientation inherited from $\mathscr{G}^\sigma$.

Since $\mathscr{T}$ is connected, Rank$M_1 = n-1$ and $M_1^T M_1$ is invertible. Let $U = M_2^T M_1 (M_1^T M_1)^{-1}$. Then, M_2 and M_1 are related through the expression $M_2^T = U M_1^T$. Close inspection of U shows that it is a matrix with entries in the set $\{0, \pm 1\}$. This is a simple consequence of the following two facts: i) the columns of M_1 are linearly independent and each column of M_2 is a linear combination of the columns of M_1, and ii) given an arbitrary column of M_2, the coefficients of its expansion in terms of the columns of M_1 are $+1$ or -1. To see this, consider an arbitrary edge $i \geq n$ (corresponding to column $j = i-n+1$ of M_2), joining vertices V_k and V_l. $\mathscr{T}$ is connected, and therefore there exists a path Γ from V_k to V_l entirely contained in $\mathscr{T}$. Because the edges in this path correspond to a subset of the columns $1, \ldots, n-1$ of matrix M_1 and each edge has an assigned orientation, the results follow. As a result, $M = [M_1 \; M_1 U^T] = M_1 [I \; U^T]$ and the Laplacian of $\mathscr{G}$ admits the representation

$$L \;=\; MM^T = M_1 Y^2 M_1^T \tag{3.4}$$

with

$$Y^2 \quad = \quad I + U^T U; Y > 0. \tag{3.5}$$

Consider now the case where $\varepsilon = n$ edges (that is, $\mathscr{G}$ is already a tree). The above equalities apply with $U = 0$ and $Y = I$. Furthermore, M_2 is obviously null. □

Example 3.3. Consider the connected graph $\mathscr{G}$ that is obtained by adding to that of Figure 3.1(a) an extra edge $\{V_2, V_3\}$ with orientation $\sigma(V_2, V_3) = 1$. The resulting graph is not a tree. However, it admits an obvious spanning tree for which

$$M_1 = \begin{pmatrix} -1 & 1 \\ 1 & 0 \\ 0 & -1 \end{pmatrix}, M_2 = \begin{pmatrix} 0 \\ -1 \\ 1 \end{pmatrix}, U^T = \begin{pmatrix} -1 \\ -1 \end{pmatrix}, \text{and } Y^2 = \begin{pmatrix} 2 & 1 \\ 1 & 2 \end{pmatrix}.$$

To do the above computations in a systematic way, start by choosing $n-1 = 2$ independent columns of M to build M_1. Then M_2 is simply the rest of the columns. Compute $U = M_2^T M_1 (M_1^T M_1)^{-1}$ and then Y from (3.5).

Directed graphs

This section deals with directed graphs. A first reading will show obvious connections with the theory of oriented graphs exposed in the previous section. However, there are some subtle differences that will be stressed in the course of the presentation.

A *directed graph* or simply a *digraph* $\mathscr{G} = \mathscr{G}(\mathscr{V}, \mathscr{E})$ consists of a finite set $\mathscr{V}$ of *vertices* or *nodes* $V_i \in \mathscr{V}$ and a finite set $\mathscr{E}$ of ordered pairs $(V_i, V_j) \in \mathscr{E}$, henceforth referred to as *arcs*. Given an arc $(V_i, V_j) \in \mathscr{E}$, its first and second elements are called the tail and head of the arc, respectively. In the present work, the vertices of a graph represent vehicles and the arcs the uni-directional data links among them. We define the flow of information in an arc to be directed from its *head* to its *tail*. The *in-degree* (*out-degree*) of a vertex V_i is the number of arcs with V_i as its head (tail). If $(V_i, V_j) \in \mathscr{E}$, then we say that V_i is *adjacent* to V_j.

At this point, we recall the definition of oriented graph which is an undirected graph with an orientation assigned to each of its edges. A difference between a digraph and an

oriented graph is that if V_i and V_j are vertices, a digraph allows both (V_i, V_j) and (V_j, V_i) as arcs, while only one is permitted in an oriented graph. Furthermore, in a digraph the directions are fixed and imposed by the communication topology under study, but in an oriented graph the underlying graph is fixed, while the orientation may vary.

A *path* of length r from V_i to V_j in a digraph is a sequence of $r+1$ distinct vertices starting with V_i and ending with V_j such that consecutive vertices are adjacent. If there is a path in $\mathscr{G}$ from vertex V_i to vertex V_j, then V_j is said to be *reachable* from V_i. In this case, there is a path of consecutive communication links directed from vehicle j (transmitter) to vehicle i (receiver). Vertex V_i is *globally reachable* if it is reachable from every other vertex in the digraph.

The *adjacency matrix* of a digraph $\mathscr{G}$, denoted A, is a square matrix with rows and columns indexed by the vertices, such that the ij-entry of A is 1 if $(V_i, V_j) \in \mathscr{E}$ and zero otherwise. The *degree matrix* D of a digraph $\mathscr{G}$ is a diagonal matrix where the ii-entry equals the *out-degree* of vertex V_i. The *Laplacian matrix* of a digraph is defined as $L = D - A$. The following Lemma plays a key role in the development that follows.

Lemma 3.9 (Lin et al. 2005*a*)

The Laplacian matrix of a digraph with at least one globally reachable vertex has a simple eigenvalue at 0 *with right eigenvector* $\mathbf{1}$. *All the other eigenvalues have positive real parts.*

The result above can be found in the literature stated in different, yet equivalent manners and using different terminology. In this sense, the statements *i)* the digraph has "a center node", *ii)* the digraph is "quasi-strongly connected", *iii)* the digraph has a "rooted spanning tree" are equivalent. See for example (Lin 2006) and (Caughman et al. 2005) and references therein.

From the above lemma, if L is the Laplacian of a digraph with a globally reachable vertex, then there exists a nonsingular matrix F, partitioned as

$$\begin{aligned} F &= \begin{pmatrix} \mathbf{1} & F_1 \end{pmatrix}, \\ F^{-1} &= \begin{pmatrix} \beta^T \\ F_2 \end{pmatrix}, \end{aligned} \tag{3.6}$$

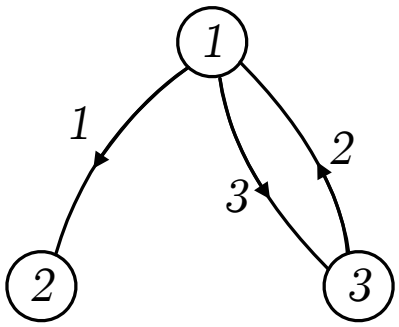

Figure 3.2: A directed graph

such that

$$F^{-1}LF = \begin{pmatrix} 0 & \mathbf{0}^T \\ \mathbf{0} & L_{11} \end{pmatrix}, \tag{3.7}$$

where $\mathbf{0} = [0,...,0]^T$ is a vector of appropriate dimensions, β is a left eigenvector associated with the 0 eigenvalue, and L_{11} is nonsingular and has the property that all its eigenvalues have positive real parts. From the fact that $F^{-1}F = I_n$, it can be easily concluded that

$$\begin{aligned} F_2F_1 &= I_{n-1} \\ F_2\mathbf{1} &= \mathbf{0} \\ \beta^T F_1 &= \mathbf{0}^T \\ L &= F_1L_{11}F_2 \end{aligned} \tag{3.8}$$

Example 3.4. Figure 3.2 shows a digraph with three vertices of which V_2 is the only globally reachable vertex. The degree matrix D, the adjacency matrix A, and the Laplacian of the graph are

$$D = \begin{pmatrix} 2 & 0 & 0 \\ 0 & 0 & 0 \\ 0 & 0 & 1 \end{pmatrix}, A = \begin{pmatrix} 0 & 1 & 1 \\ 0 & 0 & 0 \\ 1 & 0 & 0 \end{pmatrix}, L = \begin{pmatrix} 2 & -1 & -1 \\ 0 & 0 & 0 \\ -1 & 0 & 1 \end{pmatrix}.$$

It is easy to check that L has a single eigenvalue at zero with right and left eigenvector $\mathbf{1}$ and $\beta = [0,1,0]^T$, respectively, and $\{0.38, 2.62\}$ are the two other eigenvalues.

To generate matrices F_1 and F_2 introduced in (3.6), start by choosing F_1 such that $\beta^T F_1 = \mathbf{0}^T$. One simple numerical way to do this is to compute the *svd* [3] of $\beta\beta^T$; this will return a matrix of the form $[\beta\ F_1]$. Afterwards, construct $F = [\mathbf{1}, F_1]$ and extract F_2 from F^{-1}. The result for the Laplacian given above is

$$F_1 = \begin{pmatrix} 1 & 0 \\ 0 & 0 \\ 0 & 1 \end{pmatrix},\ F_2 = \begin{pmatrix} 1 & -1 & 0 \\ 0 & -1 & 1 \end{pmatrix}, L_{11} = F_2 L F_1 = \begin{pmatrix} 2 & -1 \\ -1 & 1 \end{pmatrix}.$$

Let $\xi = (\xi_1, ..., \xi_n)^T \in \mathbb{R}^n$ and define $z = L\xi$ where L is the Laplacian matrix of a graph $\mathscr{G}$. Then, the i'th element z_i of vector z is

$$z_i = \sum_{j \in N_i} (\xi_i - \xi_j) = |N_i|\xi_i - \sum_{j \in N_i} \xi_j, \tag{3.9}$$

that is, z_i is a linear combination of the terms $(\xi_i - \xi_j)$, where j spans over the neighboring set N_i, the index set which defines the vertices adjacent to vertex i in graph $\mathscr{G}$. Formally, $j \in N_i$ iff $(V_i, V_j) \in \mathscr{E}$. For digraphs, N_i defines the set of the vehicles that vehicle i *receives* information from, and for undirected graphs, N_i denotes the set of those that vehicle i *exchanges* information with; this is because of the symmetry property $j \in N_i$ iff $i \in N_j$ that does not hold in general for digraphs. From a control point of view, notice that variables z_i inherit and embody in themselves the communication constraints imposed by sets $N_i; i \in \mathbb{N}_n$. That is, if variables ξ_j: $j \in N_i$ are the only measurements available to vehicle i, a single variable z_i can be used for control purposes. The *decentralization property* (3.9) plays a key role in the computation of a decentralized coordination control law that takes into consideration the a priori existing communication constraints.

Example 3.5. Assume L is the Laplacian matrix of the graph illustrated in Figure 3.2, see Example 3.4. By direct calculation, it is easy to show that

$$L\xi = \begin{pmatrix} (\xi_1 - \xi_2) + (\xi_1 - \xi_3) \\ 0 \\ \xi_3 - \xi_1 \end{pmatrix}$$

which verifies the decentralization property (3.9) with $N_1 = \{2, 3\}$, $N_2 = \emptyset$, and $N_3 = \{1\}$.

[3] Singular Value Decomposition

3.2 Path-following: single vehicle

The following section describes two novel solutions to the problem of path-following (PF) in 2D for a single wheeled robot. In Section 3.2.2, after some adaptation, the solutions are extended to address the PF problem of fully actuated marine vehicles. The solutions build on and simplify the nonlinear control law first proposed in (Soetanto et al. 2003).

3.2.1 Wheeled robots

Consider a wheeled robot of the unicycle type depicted in Figure 3.3, together a spatial path Γ in horizontal plane to be followed. The vehicle is motorized at rear wheels generating a control force and a control torque. See Section 2.1 for more details about the physical characteristics of the vehicle. Recall the path-following problem briefly stated in Section 1.1,

Given a spatial path Γ*, develop a feedback control law for the force and torque acting on a wheeled robot so that its center of mass converges asymptotically to the path while its total speed tracks a desired temporal profile*.

An elegant solution to this problem was first advanced at a *kinematic* level in (Micaelli & Samson 1993), from which the following intuitive explanation is obtained: a path-following controller should "look" at i) the distance from the vehicle to the path and ii) the angle between the vehicle's velocity vector and the tangent to the path, and reduce both to zero. This suggests that the kinematic model of the vehicle be derived with respect to a Serret-Frenet frame (or tangent frame) $\{\mathrm{T}\}$ that moves along the path, with $\{\mathrm{T}\}$ playing the role of the body-axis of a "virtual target vehicle" that must be tracked by the "real vehicle". Using this set-up, the aforementioned distance and angle become part of the coordinates of the error space where the path-following control problem can be formulated and solved.

Chapter 2 used the ideas of (Micaelli & Samson 1993) in the framework of linear systems. The set-up adopted in (Micaelli & Samson 1993) was later reformulated in (Soetanto et al. 2003), leading to a feedback control law that steers the *dynamic model* of a wheeled robot with parameter uncertainty along a desired path and yields global convergence results. This is in striking contrast with the results described in (Micaelli & Samson 1993),

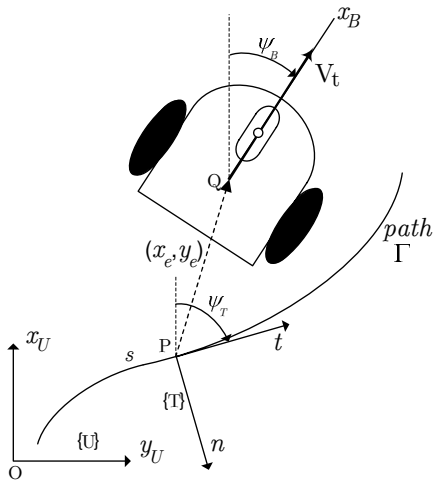

Figure 3.3: Frames and error variables

where only local convergence to the path has been proven. The key enabling idea involved in the derivation of a globally convergent path-following control law is to add another degree of freedom to the rate of progression of a "virtual target" to be tracked along the path, thus bypassing the singularity problems that arise in (Micaelli & Samson 1993) when the position of the virtual target is simply defined by the projection of the actual vehicle on that path. Formally, this is done by making the center of the Serret-Frenet frame $\{\mathrm{T}\}$ that is attached to the path evolve according to an extra "virtual" control law.

To this effect, consider Figure 3.3 where P is an arbitrary point on the path to be followed and Q is the center of the mass of the vehicle. Associated with P, consider the Serret-Frenet $\{\mathrm{T}\}$. The signed curvilinear abscissa of P along the path is denoted by s. Clearly, Q can be expressed either as $\mathbf{q} = (x, y)$ in the inertial reference frame $\{\mathrm{U}\}$, or as (x_e, y_e) in $\{\mathrm{T}\}$. Let $\mathbf{p}$ be the position of P in $\{\mathrm{U}\}$. Further let ${}^U_T R$ and ${}^U_B R$ denote the rotation matrices from $\{\mathrm{T}\}$ to $\{\mathrm{U}\}$ and from $\{\mathrm{B}\}$ to $\{\mathrm{U}\}$ respectively, parameterized by the yaw angles ψ_T and ψ_B. The rotation matrix for a rotation of angle ψ about z axis is defined as

$$R(\psi) = \begin{pmatrix} \cos\psi & -\sin\psi \\ \sin\psi & \cos\psi \end{pmatrix}.$$

Define the variables v and $r = \dot{\psi}_B$ as the linear and angular speed of the robot, respectively, calculated in $\{\mathrm{U}\}$ and expressed in $\{\mathrm{B}\}$. From the figure, it follows that

$$\mathbf{q} = \mathbf{p} + {}^{U}_{T}R \begin{pmatrix} x_e \\ y_e \end{pmatrix}. \tag{3.10}$$

Taking derivatives and expressing the result in frame $\{\mathrm{U}\}$ yields

$${}^{U}_{B}R \begin{pmatrix} v \\ 0 \end{pmatrix} = {}^{U}_{T}R \begin{pmatrix} \dot{s} \\ 0 \end{pmatrix} + {}^{U}_{T}\dot{R} \begin{pmatrix} x_e \\ y_e \end{pmatrix} + {}^{U}_{T}R \begin{pmatrix} \dot{x}_e \\ \dot{y}_e \end{pmatrix}.$$

From the above expression, using

$$\dot{R}(\psi) = \dot{\psi} R(\psi) \begin{pmatrix} 0 & -1 \\ 1 & 0 \end{pmatrix},$$

simple calculations lead to the kinematics of the robot in the (x_e, y_e) coordinates as

$$\text{Kinematics} \begin{cases} \dot{x}_e &= (y_e c_c(s) - 1)\dot{s} + v\cos\psi_e \\ \dot{y}_e &= -x_e c_c(s)\dot{s} + v\sin\psi_e \\ \dot{\psi}_e &= r - c_c(s)\dot{s}. \end{cases} \tag{3.11}$$

where $\psi_e = \psi_B - \psi_T$ and $c_c(s)$ is the path curvature at P determined by s, that is $\dot{\psi}_T = c_c(s)\dot{s}$. Notice how the kinematics are driven by v, r and the term $\dot{s}$ that plays the role of an extra control signal.

Under the usual simplifying assumptions, the dynamics of the wheeled robot can be written as

$$\text{Dynamics} \begin{cases} \dot{v} = F/m \\ \dot{r} = N/I \end{cases} \tag{3.12}$$

where m denotes the mass of the robot, I is the moment of inertia about the vertical body-axis, and F and N denote the total force and torque applied to the vehicle. We assume without loss of generality that $m = I = 1$ in the appropriate units. With this set-up, the problem of path-following can be mathematically formulated as follows:

Definition 3.1 (Path-Following. Wheeled robot)

Let Γ be a spatial path to be followed by a wheeled robot. Further let the kinematic and dynamic equations of motion of the robot be given by (3.11) and (3.12), respectively. Given

the path Γ *and a desired speed path profile* $v_d(t)$ *for the vehicle speed* v*, derive feedback control laws for* F*,* N *and* $\dot{s}$ *to drive* x_e, y_e, ψ_e*, and* $v - v_d$ *asymptotically to* 0.

Remark 3.1. In Figure 3.3, if P is chosen to be the closest point on the path, that is, $x_e \equiv 0$, from (3.11) the evolution of s is driven as

$$\dot{s} = \frac{v \cos \psi_e}{1 - y_e c_c(s)}.$$

This is a formal way to derive the kinematics equations (2.2) in Chapter 2.

Solutions

Driving the speed v to the desired speed is trivial to do with the simple control law $F = \dot{v}_d - k_0(v - v_d)$, which makes the error $v - v_d$ decay exponentially to zero. Controlling v is therefore decoupled from the control of the other variables, and all that remains is to find suitable control laws for N and for $\dot{s}$ to drive x_e, y_e, ψ_e to zero, no matter what the evolution of $v(t)$ is. The only technical assumptions required are that the path be sufficiently smooth and $v(t)$ be *nonzero* for "long enough" time.

Solution 1 The first solution to Problem 3.1 is given below.

Proposition 3.1 (Path-following 1. Wheeled robot)

Consider a wheeled robot with equations of motion given by (3.11) *and* (3.12)*. Define*

$$\begin{aligned} \sigma = \sigma(y_e) &= -\text{sign}(v) \sin^{-1} \tfrac{k_2 y_e}{|y_e| + \varepsilon_0}, \\ \phi &= c_c \dot{s} + \dot{\sigma} - k_1(\psi_e - \sigma) - v y_e \Delta, \end{aligned} \tag{3.13}$$

where $k_1 > 0$*,* $0 < k_2 \leq 1$*,* $\varepsilon_0 > 0$*, and*

$$\Delta(\psi_e, \sigma) = \begin{cases} 1 & \text{if } \psi_e = \sigma \\ \frac{\sin \psi_e - \sin \sigma}{\psi_e - \sigma} & \text{otherwise} \end{cases}$$

Let the control laws for N *and* $\dot{s}$ *be given by*

$$N = \dot{\phi} - k_4(r - \phi) - (\psi_e - \sigma) \tag{3.14}$$

$$\dot{s} = v \cos \psi_e + k_3 x_e \tag{3.15}$$

for some $k_3, k_4 > 0$*. Consider the following conditions.*

i $v(t)$ *is uniformly continuous on* $\mathbb{R}^+ := [0,\infty)$ *and* $\lim_{t\to\infty} v(t) \neq 0$.

ii $\int_{t_0}^{\infty} \min(k, |v(t)|)dt = \infty$ *for some* $k > 0$.

Under condition i *or* ii*, Problem 3.1 is solved and* $(x_e, y_e, \psi_e) = (0,0,0)$ *is a semi-globally asymptotically stable equilibrium point.*

Remark 3.2. Next we show that ii$\not\Rightarrow$i and i$\Rightarrow$ii. However, we will give a separate proof of the above proposition for i and ii, since the proof under condition ii is easier to do and it also simplifies the proof of stability and convergence of the relevant errors of closed-loop combined path-following and coordination control systems.

Denote i_1: $v(t)$ is uniformly continuous on $\mathbb{R}^+ := [0,\infty)$, and i_2: $\lim_{t\to\infty} v(t) \neq 0$, that is, i=$\mathrm{i}_1 \wedge \mathrm{i}_2$. To show that ii$\not\Rightarrow$i, consider the simple counterexample given by $v_1(t) = e^t$, a function that satisfies ii but is not uniformly continuous on $\mathbb{R}^+$, that is, ii$\not\Rightarrow \mathrm{i}_2$. Next we show that even ii$\wedge \mathrm{i}_1 \not\Rightarrow \mathrm{i}_2$. To this effect, let $k \geq 1$ and define $v_2(t)$ as a sequence of triangles centered at $\frac{1}{n}$; $n = 1,2,3,...$ with hight and width $\frac{1}{\sqrt{n}}$. It is easy to check that $v_2(t)$ is uniformly continuous and $\lim_{t\to\infty} v_2(t) = 0$; however, $\int_0^{\infty} \min(k, |v_2(t)|)dt = \sum_{n=1}^{\infty} \frac{1}{n} = \infty$. We now show that i$\Rightarrow$ii. Let $v_3(t)$ be uniformly continuous, that is, i_1 applies, and $\int_0^{\infty} \min(k, |v_3(t)|)dt < \infty$, that is, $\sim$ii. Then from Barbalat's lemma $\lim_{t\to\infty} v_3(t) = 0$, that is, $\sim \mathrm{i}_2$. Formally, $\mathrm{i}_1 \wedge \sim$ii$\Rightarrow \sim \mathrm{i}_2$ and the result follows.

Solution 2 The second solution to Problem 3.1 is stated next.

Proposition 3.2 (Path-following 2. Wheeled robot)
Consider a wheeled robot with equations of motion given by (3.11) and (3.12). Let σ *and* ϕ *be as in (3.13) with* $\Delta \equiv 0$*. Let the control laws for* N *and* $\dot{s}$ *be given by*

$$N = \dot{\phi} - k_4(r - \phi) - (\psi_e - \sigma) \tag{3.16}$$

$$\dot{s} = v\cos\psi_e + k_3 x_e \tag{3.17}$$

for some $k_3, k_4 > 0$*. If* $v(t)$ *is uniformly continuous and* $\lim_{t\to\infty} v(t) \neq 0$*, then* $(x_e, y_e, \psi_e) = (0,0,0)$ *is a semi-globally asymptotically stable equilibrium point and Problem 3.1 is solved.*

Remark 3.3. Notice that the only difference in the control laws given in two the propositions stated above is in the definition of ϕ where in the latter Δ is set to zero.

Remark 3.4. It is easily seen that if time grows unbounded, $\dot{s}$ tends to v, that is, the speed of the virtual target approaches v asymptotically. Furthermore, r approaches $c_c\dot{s} = c_c v$ as t increases.

Remark 3.5. Notice in equations (3.14) and (3.15) that $\dot{v}$ appears explicitly in the control laws derived. In practice, this variable may be estimated explicitly using an approximate derivative operator or computed implicitly using the dynamics (3.12) of the vehicle model. The latter approach needs to be fully justified in the presence of model uncertainties by resorting to analysis tools that are routinely used in adaptive control. The first approach may introduce unacceptable noise levels. These issues are not addressed in detail in the thesis. For implementation purposes, the term $\partial c_c/\partial s$ must also be computed. Theoretically, this can be done for paths with differentiable curvature $c_c(s)$. In practice, however, this condition may be violated at isolated instants of time. See Appendix 6.1 for details on the implementation of the control laws derived.

Proofs

This section contains the proofs of Propositions 3.1 and 3.2. The key ideas in developing the control laws borrow from the work of (Soetanto et al. 2003) and (Kaminer et al. 2005) where Proposition 3.1 was proved under the condition that $v(t) \geq v_m > 0$. Here, we give a rigorous proof under conditions i and ii. Condition ii will be useful for further developments in proving stability and convergence of the interconnected system consisting of the path-following subsystems and the coordination control subsystem.

Proof of Proposition 3.1. By assumption, the speed v of the robot is controlled independently and is viewed as an exogenous variable that satisfies either of the conditions i or ii of the proposition. Consider the Lyapunov function candidate

$$V_p = \frac{1}{2}x_e^2 + \frac{1}{2}y_e^2 + \frac{1}{2}(\psi_e - \sigma)^2 + \frac{1}{2}(r-\phi)^2 \tag{3.18}$$

which is positive definite and radially unbounded. With N and $\dot{s}$ as in (3.14) and (3.15), respectively the time derivative of V_p along the trajectories of the vehicle with kinematics

described in (3.11) and dynamics $\dot{r} = N$ yields

$$\dot{V}_p = -k_3 x_e^2 - k_1(\psi_e - \sigma)^2 - k_2|v(t)|\frac{y_e^2}{|y_e| + \varepsilon_0} - k_4(r-\phi)^2, \tag{3.19}$$

which is negative semidefinite (notice that $v(t)$ can go through 0). Simple computation reveals that $\phi = c_c v$ and $\sigma = 0$ at the equilibrium $x_e = y_e = \psi_e = 0$. Define $X_p = (x_e, y_e, \psi_e, r - c_c v)^T$. Then, $X_p = \mathbf{0}$ is a stable equilibrium point.

Furthermore, for any initial condition there exists a $c > 0$, such that $V_p \leq \frac{1}{2}c^2$ for all $t \geq t_0$, since $\dot{V}_p \leq 0$. Therefore, $|y_e(t)| \leq c \ \forall t \geq t_0$. Then

$$\dot{V}_p \leq -2\min(k_1, k_3, k_4, \frac{k_2}{c + \varepsilon_0}|v(t)|)V_p. \tag{3.20}$$

Hereafter, the proof follows separately under conditions i and ii.

Condition i. Since V_p is positive definite and radially unbounded, and $\dot{V}_p \leq 0$, for any initial condition of the state there is $c_o > 0$ such that $\|X_p(t)\| < c_o$ for all $t \geq t_0$. Therefore, from the fact that the vector field in (3.11) is locally Lipschitz in X_p uniformly in t and $v(t)$ is uniformly continuous, we conclude that $X_p(t)$ is uniformly continuous in t on $[t_0, \infty)$. To conclude asymptotic stability start by noticing that because $V_p(t, X_p(t))$ is nonincreasing and bounded from below by zero, it converges to a limit as $t \to \infty$. From

$$-\int_{t_0}^{t} \dot{V}_p(\tau, X_p(\tau))d\tau = V_p(t_0, X_p(t_0)) - V_p(t, X_p(t)), \tag{3.21}$$

it follows that $\lim_{t\to\infty} \int_{t_0}^{t} \dot{V}_p(\tau, X_p(\tau))d\tau$ exists and is finite. Because $X_p(t)$ and $v(t)$ are uniformly continuous, so is $\dot{V}_p(t, X_p(t))$. A straightforward application of Barbalat's lemma (Khalil 2002) allows for the conclusion that $\lim_{t\to\infty} \dot{V}_p(t, X_p(t)) = 0$. Therefore, from (3.19), x_e, $(\psi_e - \sigma)$, $(r - \phi)$ and $v(t)y_e^2$ vanish as $t \to \infty$. Moreover, since V_p is bounded below by zero and nonincreasing, we can conclude that V_p has a limit so $\lim_{t\to\infty} y_e = y_{e,lim}$. Because $\lim_{t\to\infty} v(t) \neq 0$ and $v(t)y_{e,lim}^2$ vanishes, $y_{e,lim} = 0$. As a consequence, the origin $X_p = \mathbf{0}$ is semi-globally attractive and thus semi-globally asymptotically stable. See the Appendix for an alternative argument under condition i.

Condition ii. Rewrite (3.20) as

$$\dot{V}_p \leq -2\frac{k_2}{c+\varepsilon_0}\min(k,|v(t)|)V_p \tag{3.22}$$

where $k = \frac{c+\varepsilon_0}{k_2}\min(k_1,k_3,k_4)$. Therefore

$$V_p(t) \leq V_p(t_0)e^{-2\frac{k_2}{c+\varepsilon_0}\int_{t_0}^{t}\min(k,|v(\tau)|)d\tau}$$

and since the integral tends to infinity as $t \to \infty$, V_p tends to zero asymptotically. As a consequence, the origin $X_p = \mathbf{0}$ is semi-globally attractive and thus semi-globally asymptotically stable.

□

Remark 3.6. Notice from (3.20) that if $|v(t)|$ has a positive lower bound, that is, $\inf_t |v(t)| = v_m > 0$ for all $t \geq t_0$, then X_p is *exponentially* attractive to zero. The same can be easily concluded if $v(t)$ admits the integral condition

$$\exists T > 0, \lambda > 0 : \forall t > 0, \int_t^{t+T} \min(k,|v(\tau)|)d\tau \geq \lambda T$$

Proof of Proposition 3.2. The first part of the proof unfolds in two basic steps. Step 1 derives a controller at a kinematic level by acting on the angular speed r. Step 2 addresses the vehicle dynamics by using a backstepping approach, leading to a control law for the torque N. These two steps can be tackled simultaneously by considering the candidate Lyapunov function

$$V_1 = \frac{1}{2}(\psi_e - \sigma)^2 + \frac{1}{2}(r-\phi)^2 \tag{3.23}$$

where ϕ plays the role of a virtual control (i.e., the desired behavior for the angular rate r) and the term $(\psi_e - \sigma)^2$ aims to shape the approach angle to the path as function of the "distance" y_e to that path. Simple computations show that $\dot{V}_1 = -k_1(\psi_e - \sigma)^2 - k_2(r-\phi)^2$. Letting $k = \min(k_1,k_2)$ yields $\dot{V}_1 \leq -2kV_1$, thus proving that V_1, and therefore $(\psi_e - \sigma)$ and $(r-\phi)$, converge to zero exponentially.

In the second part of the proof, we first study the case where $|v(t)| \geq \varepsilon > 0$ and restrict ourselves to showing convergence of the solutions of (3.11) to zero. Later, we will lift this limitation. Start with the candidate Lyapunov function

$$V_2(x_e, y_e) = \frac{1}{2}x_e^2 + \frac{1}{2}y_e^2$$

and the auxiliary function

$$U(t, x_e, y_e) = -y_e v(t) \sin\sigma(y_e) + k_3 x_e^2.$$

Under the conditions stated above, it can be shown that $V_2(x_e, y_e)$ and $U(t, x_e, y_e)$ satisfy the conditions of a theorem on (equi-)asymptotic stability due to J. Massera, see Chapter 3.1, page 71. Simple calculations, applying the control law given in Proposition 3.2, yield

$$\begin{aligned} \dot{V}_2 &= v(t) y_e \sin\psi_e - k_3 x_e^2 \\ \dot{V}_2 + U &= v(t) y_e (\sin\psi_e - \sin\sigma). \end{aligned} \tag{3.24}$$

Recall the result in the first part of the proof, that is $(\psi_e - \sigma) \to 0$ which allows for the conclusion that $\dot{V}_2 + U \to 0$ as $t \to \infty$ uniformly on $\rho_1 < x_e^2 + y_e^2 < \rho_2$, for any $0 < \rho_1 < \rho_2$. It follows from Massera's theorem in Section 3.1.1 that $(x_e, y_e) = (0,0)$ is an equi-asymptotically stable equilibrium point and therefore the solutions $x_e(t)$ and $y_e(t)$ tend to zero asymptotically, uniformly with respect to the initial conditions. Moreover, it is now straightforward to re-visit the result in the first part of the proof to show that ψ_e tends to zero and thus completing the proof for the case where $|v(t)| \geq \varepsilon > 0$.

Consider now the situation where the condition $|v(t)| \geq \varepsilon$ for some $\varepsilon > 0$ is violated. Because by assumption $v(t) \to 0$ as $t \to \infty$, the only possibility is for $v(t)$ to take zero values during discrete or over compact interval of time. Consider the latter situation. Interestingly enough, the conclusion on boundedness and convergence of $\psi_e - \sigma(y_e) \to 0$ remain valid. Therefore, at the times for which $v(t) = 0$, $\dot{V}_2 = -k_3 x_e^2 \leq 0$ and therefore, $(x_e, y_e) = (0,0)$ is a stable equilibrium point, x_e and y_e remain bounded, and so does ϕ_e. We conclude that the states decay toward zero when $|v(t)|$ is bounded away from zero, and stay bounded when $|v(t)|$ is zero. Since the period of time that $v(t)$ is bounded away from zero is infinity, the error variables will converge to zero as $t \to \infty$. Even, if $v(t) \to 0$ as $t \to \infty$, the conclusions on boundedness remain valid, and x_e and $\dot{s}$ will tend to zero, but not y_e. □

3.2.2 Fully actuated marine vehicles

Consider a fully actuated autonomous underwater vehicle depicted in Figure 3.4, together a spatial path Γ in $x-y$ plane to be followed. We assume the vehicle is fully actuated and is therefore equipped with enough thrusters capable of generating separate control forces in surge and sway, together with a control torque in yaw (about the z-axis). The problem of path-following can now be briefly stated as follows:

Given a spatial path Γ, develop feedback control laws for the surge and sway forces and (yaw) torque acting on the underwater vehicle so that its center of mass converges asymptotically to the path while its total speed tracks a desired temporal profile and the side-slip angle remains at a given desired value.

The solution to this problem is similar to that given in Section 3.2.1 for wheeled robots, with some extra concerns for marine vehicles due to non-zero side-slip angle. The details are given next.

To this effect, consider Figure 3.4 where P is an arbitrary point on the path to be followed and Q is the center of the mass of the vehicle. Associated with P, consider the Serret-Frenet $\{\mathrm{T}\}$. The signed curvilinear abscissa of P along the path is denoted by s. Clearly, Q can be expressed either as $\overrightarrow{OQ} = (x,y)$ in the inertial reference frame $\{\mathrm{U}\}$, or as (x_e, y_e) in $\{\mathrm{T}\}$. Let $\overrightarrow{OP}$ be the position of P in $\{\mathrm{U}\}$ and define two frames with their origin at the center of mass of the vehicle: i) the *body-fixed frame* denoted $\{\mathrm{B}\}$ with its x-axis along the main axis of the body, and ii) the *flow frame* denoted $\{\mathrm{F}\}$ with its x-axis along the total velocity v_t of the vehicle. Further let ${}^U_T R$, and ${}^U_F R$ denote the rotation matrices from $\{\mathrm{T}\}$ to $\{\mathrm{U}\}$ and from $\{\mathrm{F}\}$ to $\{\mathrm{U}\}$ parameterized by ψ_T and ψ_F, respectively. The yaw angle of the vehicle will be denoted ψ_B. Define the variables u and v as the surge and sway linear speeds, respectively and $r = \dot{\psi}_B$ as the angular speed of the vehicle. We will use the term v_t for the total velocity of the vehicle, that is,

$$\begin{pmatrix} v_t \\ 0 \end{pmatrix} = {}^F_B R \begin{pmatrix} u \\ v \end{pmatrix}. \tag{3.25}$$

which implies $|v_t| = \sqrt{u^2+v^2}$. Simple calculations similar to those in Section 3.2.1 lead to

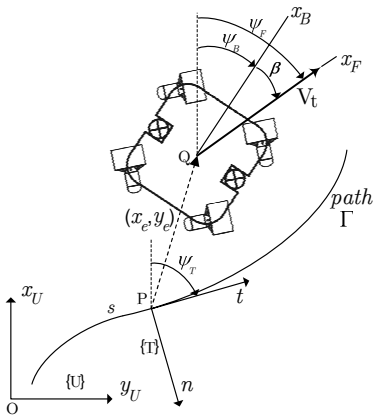

Figure 3.4: Frames and error variables

the kinematics of the vehicle in the (x_e, y_e) coordinates as

$$\text{Kinematics} \begin{cases} \dot{x}_e &= (y_e c_c(s) - 1)\dot{s} + v_t \cos\psi_e \\ \dot{y}_e &= -x_e c_c(s)\dot{s} + v_t \sin\psi_e \\ \dot{\psi}_e &= r - c_c(s)\dot{s} + \dot{\beta} \end{cases} \tag{3.26}$$

where $\psi_e = \psi_F - \psi_T$ is the error angle,

$$\beta = \psi_F - \psi_B \tag{3.27}$$

is the side-slip angle, and $c_c(s)$ is the path's curvature at P determined by s, that is $\dot{\psi}_T = c_c(s)\dot{s}$.

Remark 3.7. For marine vehicles, solving the path-following problem is equivalent to driving the flow-frame {F} to the Serret-Frenet {T} as (3.26) clearly shows. In the case of wheeled robots, the total velocity is aligned with the body axis, therefore the flow frame and body-fixed frame coincide.

Consider now the simplified dynamics of a fully actuated underwater vehicle in body-fixed frame, written as (Aguiar 2002)

$$\text{Dynamics in } \{\text{B}\} \begin{cases} \dot{u} &= \frac{1}{m_u}(\tau_u + m_v v r - d_u u) \\ \dot{v} &= \frac{1}{m_v}(\tau_v - m_u u r - d_v v) \\ \dot{r} &= \frac{1}{m_r}(\tau_r + m_{uv} u v - d_r r) \end{cases} \tag{3.28}$$

where τ_u, τ_v and τ_r denote the surge force, sway force and torque applied to the vehicle, respectively, and m's and d's are vehicle parameters. Using (3.25) and (3.27), the dynamics (3.28) can be rewritten in terms of (v_t, β, r) as

$$\text{Dynamics in } \{\text{F}\} \begin{cases} \dot{v}_t &= f_{v_t}(v_t,\beta,r) + \tau_{v_t}(\tau_u,\tau_v,v_t,\beta) \\ \dot{\beta} &= f_\beta(v_t,\beta,r) + \tau_\beta(\tau_u,\tau_v,v_t,\beta) \\ \dot{r} &= f_r(v_t,\beta,r) + \frac{1}{m_r}\tau_r \end{cases} \tag{3.29}$$

where

$$\begin{aligned} f_{vt} &= (\tfrac{m_v}{m_u} - \tfrac{m_u}{m_v}) v_t r \sin\beta\cos\beta - (\tfrac{d_u}{m_u}\cos^2\beta + \tfrac{d_v}{m_v}\sin^2\beta) v_t \\ f_\beta &= -\tfrac{m_v}{m_u} r + (\tfrac{m_v}{m_u} - \tfrac{m_u}{m_v}) r\cos^2\beta + (\tfrac{d_u}{m_u} - \tfrac{d_v}{m_v})\sin\beta\cos\beta \\ f_r &= -\tfrac{d_r}{m_r} + \tfrac{m_{ur}}{m_r} v_t^2 \sin\beta\cos\beta \\ \tau_{vt} &= \tfrac{\cos\beta}{m_u}\tau_u + \tfrac{\sin\beta}{m_v}\tau_v \\ \tau_\beta &= -\tfrac{\sin\beta}{v_t m_u}\tau_u + \tfrac{\cos\beta}{v_t m_v}\tau_v. \end{aligned} \tag{3.30}$$

Notice that the transformation between (τ_u, τ_v) and (τ_{v_t}, τ_β) is nonsingular; the determinant of the transformation matrix is $m_v m_u v_t$. With this set-up, the equations resemble those of the wheeled robot, and therefore the problems and the solutions are defined in a similar manner. Specifically, the problem of path-following can be mathematically formulated as follows:

Definition 3.2 (Path-following. Fully actuated marine vehicle)

Given a spatial path Γ *and desired time profiles* $v_{t,d}(t)$ *and* $\beta_d(t)$ *for the vehicle total speed* v_t *and side-slip angle* β*, respectively, derive a feedback control law for* τ_{v_t}, τ_β, τ_r *and* $\dot{s}$ *to drive* x_e, y_e, ψ_e, $\beta - \beta_d$ *and* $v_t - v_{t,d}$ *asymptotically to* 0.

Driving the speed v_t and β to their desired values is trivial to do with the simple control laws $\tau_{v_t} = -f_{v_t} + \dot{v}_{t,d} - k_0(v_t - v_{t,d})$ and $\tau_\beta = -f_\beta + \dot{\beta}_d - k_0(\beta - \beta_d)$, which make the errors $v_t - v_{t,d}$ and $\beta - \beta_d$ decay exponentially to zero. Controlling v_t and β is therefore decoupled from the control of the other variables, and all that remains is to find suitable control laws for τ_r and for $\dot{s}$ to drive x_e, y_e, ψ_e to zero, no matter what the evolutions of $v_t(t)$ and $\beta(t)$ are. The solution to Problem 3.2 is stated next.

Proposition 3.3 (Fully actuated marine vehicle)

Consider a fully actuated marine vehicle with the equations of motion governed by (3.26) *and* (3.29)*. Let* ϕ *and* σ *be defined as in* (3.13)*. If the conditions of Proposition* 3.1 *hold, the control laws*

$$\tau_r = m_r\left(-f_r + \dot{\phi} - k_4(r-\phi) - (\psi_e - \sigma)\right) \tag{3.31}$$

$$\dot{s} = v_t \cos\psi_e + k_3 x_e \tag{3.32}$$

make the equilibrium point of (3.26) *and* (3.29) *semi-globally asymptotically stable.*

Proof. The proof follows the sequence of steps taken in the proof of Proposition 3.1. □

The results on multi-vehicle coordinated path-following for fixed communication topologies are presented next.

3.3 Vehicle coordination control. Fixed communication topologies

In this chapter we propose several solutions to the problem of coordinated path-following under the restriction that the underlying communication network be fixed. Conditions are derived under which coordination is achieved. The chapter concludes by addressing some issues that arise in the scope of bi-directional and uni-directional communication topologies.

3.3.1 Coordination error dynamics

Equipped with the results obtained in Chapter 3.2 for the path-following problem of a single vehicle, we now consider the problem of coordinated path-following control. In the most general set-up, one is given a set of $n \geq 2$ wheeled robots (or fully actuated marine vehicle) and a set of n spatial paths Γ_k; $k = 1,2,...,n$ and require that robot k follow path Γ_k. We further require that the vehicles move along the paths in such a way as to maintain a desired formation pattern compatible with those paths. Recall that in the solutions given for the path-following problem, the vehicle is driven to the "virtual target" which is parameterized by s_i, the signed curvilinear abscissa on the path. Assume each vehicle is equipped with a path-following control law, so that the evolution of the corresponding "virtual target" is given by

$$\dot{s}_i = v_i \cos \psi_{ei} + k_{3i} x_{ei} \tag{3.33}$$

as derived in (3.32), where v_i denotes the total speed of the vehicle. It now remains to coordinate (that is, synchronize) the vehicles in time so as to achieve a desired formation pattern. As will become clear shortly, this will be achieved by adjusting the speeds of the vehicles as functions of the "along-path" distances among them.

The dynamics of the total speed of the i'th vehicle, that is, (3.12) for a wheeled robot and (3.29) for a marine vehicle, can be rewritten as

$$\dot{v}_i = \bar{F}_i \tag{3.34}$$

where $\bar{F}_i = F_i/m$ for a wheeled robot, and $\bar{F}_i = \tau_{v_{ti}} + f_{v_{ti}}$ for a marine vehicle.

Now, let each path Γ_i be parameterized in terms of a parameter ξ_i that is not necessarily the arc length along the path. An adequate choice of the parameterization will allow for the conclusion that the vehicles are synchronized iff $\xi_i = \xi_j$ for all i, j. For example, in the case of two vehicles following two circumferences, Figure 1.5, with radii R_1 and R_2 while keeping an in-line formation pattern, $\xi_i = s_i/R_i; i = 1,2$. See Chapter 1 for more details. Denote by $s_i = s_i(\xi_i); i = 1,2,...,n$ the corresponding arc length. We define $R_i(\xi_i) = \partial s_i/\partial \xi_i$ and assume that $R_i(\xi_i)$ is positive and uniformly bounded for all ξ_i. In particular, s_i is a monotonically increasing function of ξ_i. We further assume that all $R_i(\xi_i)$ is bounded away from 0 and that $\partial R_i/\partial \xi_i$ is uniformly bounded. The symbol $R_i(.)$ is motivated by the nomenclature adopted before for the case of paths that are nested arcs of circumferences. Using equation (3.33) and the fact that $\dot{\xi}_i = R_i \dot{s}_i$, it is straightforward to show that the evolution of ξ_i is given by

$$\dot{\xi}_i = \frac{1}{R_i(\xi_i)}(v_i \cos \psi_{ei} + k_{3i} x_{ei}) \tag{3.35}$$

which can be re-written as

$$\dot{\xi}_i = \frac{1}{R_i(\xi_i)} v_i + d_i \tag{3.36}$$

where

$$d_i = \frac{1}{R_i(\xi_i)}[(\cos \psi_{ei} - 1)v_i + k_{3i} x_{ei}]. \tag{3.37}$$

Notice from Section 3.2 that if vehicle i tends to the assigned path $d_i \to 0$ asymptotically as $t \to \infty$, if v_i is bounded. Later in this chapter, it will be shown that this assumption is met. Suppose one vehicle, henceforth referred to as vehicle $\mathscr{L}$, is elected as a "leader" and let the corresponding path $\Gamma_{\mathscr{L}}$ be parameterized by its length, that is, $\xi_{\mathscr{L}} = s_{\mathscr{L}}$. In this case, $R_{\mathscr{L}}(\xi_{\mathscr{L}}) = 1$. It is important to point out that $\mathscr{L}$ can always be taken as a "virtual" vehicle that is added to the set of "real" vehicles as an expedient to simplify the coordination strategy. Let $v_{\mathscr{L}} = v_{\mathscr{L}}(t)$ be a desired speed profile assigned to the leader in advance, that is $\dot{\xi}_{\mathscr{L}} = v_{\mathscr{L}}$, and known to all the other vehicles. Notice now that in the ideal steady situation where the vehicles move along their respective paths while keeping the desired formation, we have $\xi_i - \xi_{\mathscr{L}} = 0$ and therefore $\dot{\xi}_i = v_{\mathscr{L}}$ for all $i = 1,..,n$. Thus,

$v_{\mathscr{L}}$ becomes the desired speed of each of the vehicles, expressed in ξ_i coordinates. As such, *one can proceed without having to resort to the concept of an actual or virtual leader vehicle, thus making the coordination scheme truly distributed.*

From (3.36), making $d_i = 0$, it follows that the desired *inertial* velocities of vehicles $1 \leq i \leq n$ equal $R_i(\xi_i)v_{\mathscr{L}}(t)$. This suggests the introduction of the speed-tracking error vector

$$\eta_i = v_i - R_i(\xi_i)v_{\mathscr{L}},\ 1 \leq i \leq n. \tag{3.38}$$

Taking into account the vehicle dynamics, (3.38) yields

$$\dot{\eta}_i = u_i = \bar{F}_i - \frac{d}{dt}\left(R_i(\xi_i)v_{\mathscr{L}}\right). \tag{3.39}$$

Using (3.36), it is also easy to compute the dynamics of the origin of each Serret-Ferret frame $\{\mathrm{T}_i\}$ as

$$\dot{\xi}_i = \tfrac{1}{R_i}\eta_i + v_{\mathscr{L}} + d_i. \tag{3.40}$$

To write the above dynamic equations in vector form, define $\eta = [\eta_i]_{n\times 1}$, $\xi = [\xi_i]_{n\times 1}$, $u = [u_i]_{n\times 1}$, $d = [d_i]_{n\times 1}$ and $C = C(\xi) = \mathrm{diag}[1/R_i(\xi_i)]_{n\times n}$ to obtain

$$\begin{aligned} \dot{\eta} &= u \\ \dot{\xi} &= C\eta + v_{\mathscr{L}}\mathbf{1} + d \end{aligned} \tag{3.41}$$

where $\mathbf{1} = [1]_{n\times 1}$. In the above, matrix C is positive definite and bounded, that is,

$$0 < c_1 I \leq C(\xi(t)) \leq c_2 I \tag{3.42}$$

for all t, where c_1 and c_2 are positive scalars and I the identity matrix. Notice that C is allowed to be (state-driven) time-varying, thus allowing for more complex formation patterns than those in the motivating examples of Chapter 1. We will present an example for coordinated path-following with varying C, later in Section 3.4.

The objective is to derive a control strategy for u to make $\xi_1 = \ldots = \xi_n$ or, equivalently, $(\xi_i - \xi_j) = 0$ for all i, j. The first type of constraints is imposed by the types of links available for communication. The second type of constraints arises from the need to drastically reduce the amount of information that is exchanged over the communications

network. It will be assumed that the vehicles only exchange information on their positions and speeds. We will derive several solutions to the problem of the vehicles coordination with bi-directional and uni-directional communication.

Remark 3.8. Since the coordination states are non-dimensional variables, one can always normalize them, that is, make $\xi_i' = k\xi_i$ for some $k > 0$. Consequently, $R_i' = \partial s_i/\partial \xi_i' = \partial s_i/(k\partial \xi_i) = R_i/k$ and $C' = kC$. This is particularly helpful when the paths are concatenation of sub-paths of different types (straight lines, nested arcs, etc.). Using different normalization gains for each part, it is possible to bring all the parametrization variables to the same range.

3.3.2 Bi-directional communications

We now comment on the type of communication constraints contemplated in this section. It is assumed that i) the *communications are bi-directional*, that is, if vehicle i sends information to j, then j also sends information to i. Formally that is $j \in N_i$ iff $i \in N_j$, and ii) the *communications graph is connected*. Notice that if assumption (ii) is not verified, then there are two or more clusters of vehicles and no information is exchanged among the clusters. Clearly, in this situation no coordination is possible.

Definition 3.3 (Coordination control)

Consider the vehicle coordination system with dynamics (3.41) where C satisfies the bounds in (3.42), $v_{\mathscr{L}}$ is the desired formation speed, and d tends asymptotically to zero. Further assume that each of the n vehicles has access to its own state and exchanges information on its path parameter (coordination state) ξ_i and speed tracking error η_i with some or all of the other vehicles defined by neighboring sets N_i. Determine a feedback control law for u such that $\lim_{t\to\infty} \eta_i = 0$ and $\lim_{t\to\infty}(\xi_i - \xi_j) = 0$ for all $i, j = 1, .., n$.

In the sequel, three solutions are presented for coordination control problem above: *i)* Proposition 3.4 offers two solutions with linear control laws, and *ii)* Proposition 3.5 gives a version of one of the solutions in *i* with a nonlinear control law which employs a saturation function.

Coordination problem solutions

The next proposition offers two solutions to coordination problem Definition 3.3, under the basic assumption that the communications graph $\mathcal{G}$ is bi-directional and connected.

Proposition 3.4 (Solution I & II. Linear control laws)
Consider the coordination problem defined in 3.3 with $d = \mathbf{0}$ and assume that the underlying communications graph $\mathcal{G}$ (defined by sets N_i) is connected. Let L be the Laplacian of $\mathcal{G}$, and $A = \text{diag}[a_i]_{n\times n}$ and $B = \text{diag}[b_i]_{n\times n}$ be arbitrary positive definite diagonal matrices. Then, the control laws

Solution I

$$u = -(LC + C + A)\eta - AL\xi \tag{3.43}$$

Solution II

$$u = -A\eta - BCL\xi, \tag{3.44}$$

solve the coordination problem. Namely, the control laws meet the communication constraints and the origin is a uniformly globally exponentially stable (UGES) equilibrium point of the coordination closed-loop subsystem.

Proof. The proof is given later in this section. □

When using the term *stability of the equilibrium of the coordination system*, we refer to the stability of $\eta_i = 0, \xi_i - \xi_j = 0; \forall i, j = 1, ..., n$. The following proposition offers another solution to the coordination problem in Definition 3.3. The control law is a version of (3.43) with a saturation function that adds an extra option for the designer to keep the speeds of the vehicles in a bounded region. Recall that the disturbance-like term d tends to zero if $v(t)$ is bounded. Thus, boundedness of $v(t)$ simplifies the proof of stability of the system resulting from putting together the path-following and the coordination subsystems.

Proposition 3.5 (Solution III. With saturation function)
Consider the coordination problem described in Definition 3.3 and assume that the communications graph $\mathcal{G}$ is connected and $d = \mathbf{0}$. Let L be the Laplacian of $\mathcal{G}$, and $A = \text{diag}[a_i]_{n\times n}$ and $B = \text{diag}[b_i]_{n\times n}$ be arbitrary positive definite diagonal matrices. Then, the

control law

$$u = -(A^{-1}L + A)C\eta - B\,\mathrm{sat}(\eta + A^{-1}L\xi), \tag{3.45}$$

where sat *is the saturation function*

$$\mathrm{sat}(x) = \begin{cases} x_m & x > x_m \\ x & |x| \leq x_m \\ -x_m & x < -x_m \end{cases} \tag{3.46}$$

with $x_m > 0$ arbitrary, solves the coordination problem. Namely, the control law meets the communication constraints and the origin is a uniformly globally asymptotically stable (UGAS) equilibrium point of the coordination closed-loop subsystem.

Proof. The proof is given later in this section. □

Remark 3.9. The assumption that d tends asymptotically to 0 as $t \to \infty$ will be justified later in this chapter, which contains the analysis of the dynamic behavior of the combined path-following and coordination systems.

Proofs

We start by modeling the communication network as an undirected graph $\mathscr{G}$ which we assume is connected. Choose a spanning tree $\mathscr{T}$ of the connected graph $\mathscr{G}$ and associate to $\mathscr{G}$ an arbitrary orientation σ. Partition the incidence matrix M of $\mathscr{G}^\sigma$ as $M = [M_1, M_2]$, where M_1 is the incidence matrix of $\mathscr{T}^\sigma$. As explained in Section 3.1.2, the graph Laplacian can be written as $L = M_1 Y^2 M_1^T$ for some $Y > 0$, where M_1 is of order $n \times n-1$, $\mathrm{Rank} M_1 = n-1$, $M_1^T M_1$ is invertible, and $M_1 \mathbf{1} = \mathbf{0}$. Introduce formally the *graph-induced coordination error* as

$$\theta := Y M_1^T \xi. \tag{3.47}$$

Notice that $\theta \in \mathbb{R}^{n-1}$. From the above relation, $\theta = \mathbf{0}$ is equivalent to $\xi_i = \xi_j, \forall i, j$. Consequently, if θ is driven to zero asymptotically, so are the coordination errors $\xi_i - \xi_j$ and the problem of coordinated path-following (Definition 3.3) is solved. This justifies the choice of the error vector (3.47).

Proposition 3.4

Proof of Solution I. Consider the coordination dynamics (3.41) with the control law (3.43). The closed-loop dynamics in terms of $(\eta,\theta)\in\mathbb{R}^n\times\mathbb{R}^{n-1}$ can be represented as

$$\begin{aligned}\dot{\eta} &= -(M_1Y^2M_1C+C+A)\eta - AM_1Y\theta\\ \dot{\theta} &= YM_1^TC\eta + YM_1^Td.\end{aligned} \tag{3.48}$$

Let

$$z=\eta+M_1Y\theta$$

and consider the candidate Lyapunov function

$$V=\frac{1}{2}\theta^T\theta+\frac{1}{2}z^Tz.$$

Clearly, V is positive definite and radially unbounded on (η,θ). Computing the derivative of V along the solutions of (3.48) with $d=\mathbf{0}$ yields

$$\dot{V}=-\eta^TC\eta-z^TAz$$

which is negative and is zero only at equilibrium point, since M_1 is full rank and $Y>0$. Therefore, $\dot{V}$ is negative definite and resorting the Lyapunov stability theorem $(\eta,\theta)=(\mathbf{0},\mathbf{0})$ is a uniformly globally exponentially stable (UGES) equilibrium point.

We now examine the form of the control law (3.43), which can be written as

$$u_i=-(a_i+\frac{1}{R_i})\eta_i-\sum_{j\in N_i}(a_i\xi_i+\frac{1}{R_i}\eta_i-a_i\xi_j-\frac{1}{R_j}\eta_j).$$

Notice how the control input of vehicle i is a function of its own speed-tracking error and coordination state as well as of the coordination states and speed-tracking errors of the other vehicles included in the index set N_i. Clearly, the control law is decentralized and meets the constraints imposed by the communications network, as required. □

Proof of Solution II. Consider the coordination dynamics (3.41) with the control law (3.44). The closed-loop dynamics in terms of (η,θ) can be written as

$$\begin{aligned}\dot{\eta} &= -A\eta - BCM_1Y\theta\\ \dot{\theta} &= YM_1^TC\eta + YM_1^Td.\end{aligned} \tag{3.49}$$

In what follows, we show that for $d = \mathbf{0}$ the functions V and W defined as

$$\begin{aligned} V &= \tfrac{1}{2}\eta^T B^{-1}\eta + \tfrac{1}{2}\theta^T\theta \\ W &= \eta^T M_1 Y \theta. \end{aligned} \tag{3.50}$$

satisfy the conditions of Matrosov theorem (see page 70), thus proving that the origin is a UGES equilibrium point for the dynamic equations (3.49).

Let $x := (\eta^T, \theta^T)^T$ and define $\Omega := \{x \in \mathbb{R}^n \times \mathbb{R}^{n-1} : \|x\| \leq \alpha\}$. It is easy to see that conditions 1, 3, and 5 of Matrosov's theorem (on page 70) are indeed satisfied for any $(\eta, \theta) \in \Omega$ and for some $c_1, c_2 > 0$ and $\alpha_1, \alpha_2 \in class\mathcal{K}$. Computing the derivative of V along the solutions of (3.49) yields $\dot{V} = -\eta^T B^{-1} A \eta$, which fulfills condition 2. It remains to show that condition 4 is satisfied for some $\alpha_3 \in class\mathcal{K}$. To this effect, start by defining $E = \{x \in \Omega : \dot{V} = 0\} = \{(\mathbf{0}^T, \theta^T)^T \in \Omega\}$ and compute the distance of point x to E as

$$\text{dist}(x, E) = \|\eta\| = \sqrt{\eta^T \eta}. \tag{3.51}$$

Compute also the derivative of W to obtain

$$\begin{aligned} \dot{W} &= -\eta^T A M_1 Y \theta - \theta^T Y M_1^T C B M_1 Y \theta + \eta^T M_1 Y^2 M_1^T C \eta \\ &= -x^T Q x + \eta^T (P + M_1 Y^2 M_1^T C)\eta \end{aligned} \tag{3.52}$$

where

$$Q = \begin{pmatrix} P & \frac{1}{2} A M_1 Y \\ \frac{1}{2} Y M_1^T A & Y M_1^T C B M_1 Y \end{pmatrix} \tag{3.53}$$

with an arbitrary P. Now, to make $Q > 0$, let $P = \frac{\rho}{4c_1} B^{-1} A^2$ for some $\rho > 1$, where c_1 is the uniform lower bound of $C(t)$ in (3.42). This can be shown by taking Schur complements as follows. Since $P > 0$, then $Q > 0$ if

$$\begin{aligned} Y M_1^T C B M_1 Y - \tfrac{1}{4} Y M_1^T A P^{-1} A M_1 Y &= Y M_1^T (CB - \tfrac{1}{4} A^2 P^{-1}) M_1 Y \\ &= Y M_1^T B (C - \tfrac{c_1}{\rho} I) M_1 Y > 0 \end{aligned}$$

where we used the fact that $C - \frac{c_1}{\rho} I > 0$. Define $P_1 = P + \frac{1}{2}(LC + CL)$, and rewrite (3.52) as

$$\dot{W} = -x^T Q x + \eta^T P_1 \eta. \tag{3.54}$$

It can be shown that $P_1 > 0$ for large enough ρ. The proof is identical to that of Lemma 6.1, since P and C are positive definite diagonal matrices. Then, we have

$$\begin{aligned} p_1\eta^T\eta \leq \eta^T P_1\eta \leq p_2\eta^T\eta \\ q_1x^Tx \leq x^TQx \leq q_2x^Tx \end{aligned} \tag{3.55}$$

for some positive scalars p_1, p_2, q_1, q_2. Since $\|x\| = (\eta^T\eta + \theta^T\theta)^{1/2} < \alpha$ for all $x \in \Omega$, then

$$\frac{1}{\alpha}\eta^T\eta \leq \sqrt{\eta^T\eta} \leq \alpha \tag{3.56}$$

and finally

$$\max(\sqrt{\eta^T\eta}, |\dot{W}|) \geq \max(\frac{1}{\alpha}\eta^T\eta, |\dot{W}|). \tag{3.57}$$

Therefore, to prove that condition 4 of the Matrosov theorem is satisfied, it is sufficient to show that $\max(\frac{1}{\alpha}\eta^T\eta, |\dot{W}|) \geq \alpha_3(||x||)$ for some $\alpha_3(.) \in class\mathscr{K}$. This is done next.

Choose β such that $0 < \beta < \min(1, \alpha p_2)$. Obviously, $\beta < 1$ and $\beta/(\alpha p_2) < 1$. We consider two different possibilities: i) $\dot{W} \geq 0$ and ii) $\dot{W} < 0$.

i) Suppose $\dot{W} \geq 0$. From (3.54), $\eta^T P_1\eta \geq x^TQx$ and therefore

$$x^TQx \leq p_2\eta^T\eta \Rightarrow \frac{1}{\alpha p_2}x^TQx \leq \frac{1}{\alpha}\eta^T\eta. \tag{3.58}$$

Simple algebra shows that

$$\begin{aligned} \max(\text{dist}(x,E), \dot{W}) &\geq \max\left(\tfrac{1}{\alpha}\eta^T\eta, \eta^TP_1\eta - x^TQx\right) \\ &= \max\left(\tfrac{1}{\alpha}\eta^T\eta, \tfrac{1}{\alpha p_2}x^TQx, \eta^TP_1\eta - x^TQx\right) \\ &\geq \max\left(\tfrac{1}{\alpha}\eta^T\eta, \tfrac{1}{\alpha p_2}x^TQx, \tfrac{\beta}{\alpha p_2}(\eta^TP_1\eta - x^TQx)\right) \\ &\geq \tfrac{1}{3}\left(\tfrac{1}{\alpha}\eta^T\eta + \tfrac{1}{\alpha p_2}x^TQx + \tfrac{\beta}{\alpha p_2}(\eta^TP_1\eta - x^TQx)\right) \\ &\geq \tfrac{1}{3}\left((\tfrac{1}{\alpha} + \tfrac{\beta p_1}{\alpha p_2})\eta^T\eta + \tfrac{(1-\beta)q_1}{\alpha p_2}x^Tx\right) \\ &\geq \lambda_1 x^Tx \end{aligned} \tag{3.59}$$

where $\lambda_1 = \frac{(1-\beta)q_1}{3\alpha p_2}$ and we used the properties of $\max(.,.)$ listed in Section 3.1.1.

ii) Suppose $\dot{W} \leq 0$. From (3.54), $\eta^T P_1 \eta \leq x^T Q x$, and therefore

$$\begin{aligned} \max(\text{dist}(x,E), -\dot{W}) &\geq \max\left(\tfrac{1}{\alpha}\eta^T\eta, x^TQx - \eta^TP_1\eta\right) \\ &\geq \max\left(\tfrac{1}{\alpha}\eta^T\eta, \tfrac{\beta}{\alpha p_2}(x^TQx - \eta^TP_1\eta)\right) \\ &\geq \tfrac{1}{2}\left(\tfrac{1}{\alpha}\eta^T\eta + \tfrac{\beta}{\alpha p_2}(x^TQx - \eta^TP_1\eta)\right) \\ &\geq \tfrac{1}{2}\left(\tfrac{1-\beta}{\alpha}\eta^T\eta + \tfrac{\beta q_1}{\alpha p_2}x^Tx\right) \\ &\geq \lambda_2 x^T x \end{aligned} \tag{3.60}$$

where $\lambda_2 = \frac{\beta q_1}{2\alpha p_2}$.

Let $\lambda = \min(\lambda_1, \lambda_2)$ and define $\alpha_3(\|x\|) = \lambda x^T x$, which is of *class* $\mathscr{K}$. Results i) and ii) above show that $\max(\text{dist}(x,E), |\dot{W}|) \geq \alpha_3(||x||)$, thus showing that the origin is a UGAS, therefore UGES equilibrium point, since the dynamics are linear. □

Remark 3.10. Consider the coordination dynamics (3.41) with the linear control law

$$u = -A\eta - BCMWM^T$$

where $A = \text{diag}[a_i]$, $B = \text{diag}[b_i]$ and $W = \text{diag}[w_i]$ are positive diagonal matrices, and M is the incidence matric of the communication graph, that is, the graph Laplacian $L = MM^T$. We further assume that matrix $C = C(\xi)$ is constant. While restrictive, this still allows one to consider paths that consist of translations of straight lines, nested circumferences, and parallel translations of one arbitrary path. Define the graph-induced coordination error $\theta = M^T\xi$ and compute the closed-loop dynamics in terms of η and θ as

$$\begin{aligned} \dot{\eta} &= -A\eta - BCM\theta \\ \dot{\theta} &= M^TC\eta \end{aligned}$$

for $d = \mathbf{0}$. Let

$$V = \frac{1}{2}\eta^T B^{-1}\eta + \frac{1}{2}\theta^T W\theta \tag{3.61}$$

be the candidate Lyapunov function whose time derivative along the solutions of the closed-loop dynamics is $\dot{V} = -\eta^T B^{-1} A\eta$, which is negative semi-definite. Note that $\dot{V} = 0 \Rightarrow \eta = \mathbf{0}$ which in turn implies that $M\theta = \mathbf{0}$. Moreover, $M\theta = \mathbf{0} \Rightarrow L\xi = \mathbf{0} \Rightarrow \xi \in \text{span}\{\mathbf{1}\} \Rightarrow \theta = M^T\xi = \mathbf{0}$. Since the system is time-invariant and V is radially unbounded, a straightforward

application of LaSalle's invariance principle shows that the origin is UGES. Let $k = e(i,j)$ mean that edge $\{V_i, V_j\}$ is the $k-th$ element in the ordered list of edges. Close examination of the control law reveals that it can be written in a decentralized form as

$$u_i = -a_i\eta_i - \frac{b_i}{R_i(\xi_i)} \sum_{\substack{j \in N_i \\ k = e(i,j)}} w_k(\xi_i - \xi_j) \tag{3.62}$$

Notice that vehicle i only has access to its speed and the coordination state, and to the coordination states ξ_j of its neighbors. Making W identity, the abovementioned control law degenerates to (3.44).

Proposition 3.5

Proof of the coordination control law with sat(.) With the control law (3.45), the dynamics of the coordination system (3.41) can be written in terms of η and θ as

$$\begin{aligned} \dot{\eta} &= -(A^{-1}M_1Y^2M_1^T + A)C\eta - B\,\mathrm{sat}(\eta + A^{-1}M_1Y\theta), \\ \dot{\theta} &= YM_1^TC\eta + YM_1^Td, \end{aligned} \tag{3.63}$$

where we used the fact that $M_1^T v_{\mathscr{L}} \mathbf{1} = \mathbf{0}$. Let

$$z = \eta + A^{-1}M_1Y\theta$$

and consider the candidate Lyapunov function

$$V = \frac{1}{2}\theta^T\theta + \frac{1}{2}z^Tz.$$

Clearly, V is positive definite and radially unbounded on (η, θ). Computing the derivative of V along the solutions of (3.63) with $d = \mathbf{0}$ yields

$$\dot{V} = -\eta^TAC\eta - z^TB\mathrm{sat}(z).$$

which is negative definite with respect to $(\eta^T, z^T)^T = \mathbf{0}$, or equivalently with respect to $(\eta^T, \theta^T)^T = \mathbf{0}$, since M_1 is full rank and $Y > 0$. Therefore the origin is a UGAS equilibrium point of (3.63). The control law (3.45) in a decentralized form can be written as

$$u_i = -\frac{a_i}{R_i}\eta_i - \frac{1}{a_i}\sum_{j\in N_i}\left(\frac{1}{R_i}\eta_i - \frac{1}{R_j}\eta_j\right) - b_i\,\mathrm{sat}\left(\eta_i + \frac{1}{a_i}\sum_{j\in N_i}(\xi_i - \xi_j)\right). \tag{3.64}$$

Notice that the control signal of vehicle i is a function of its own speed and coordination state as well as of the coordination states and speeds of the other vehicles defined by N_i. Clearly, the control law is decentralized and meets the constraints imposed by the communications network, as required. □

3.3.3 Time-varying pattern tracking

In Chapter 1, with the help of simple motivating examples, we showed how the problem of coordinated path-following can be essentially reduced to that of "aligning" the coordination states ξ_i asymptotically, that is, making $\xi_i - \xi_j \to 0$ for all i and j as $t \to \infty$. Further, it was also shown how the coordination ξ_i state of each vehicle yields a re-parametrization of its assigned path as a function of path length s_i, that is, $\xi_i = \xi_i(s_i)$. Using this set-up, formation patterns (compatible with the paths being followed) are obtained by proper choice of the parametrization functions $\xi_i(s)$, which must be computed in advance. In the case of complex but fixed formation patterns that are path-dependent, the re-parametrization can be done but may assume a complicated form. This problem is further aggravated in the case of desired formation patterns that are explicit functions of time, because in this case the above re-parametrization is simply non-existent. This section offers a methodology for time-varying pattern tracking that is simple to implement and overcomes the above problems. The rationale behind the methodology can be explained by referring to the simple case of a number of vehicles doing coordinated path-following along parallel straight lines. With $\xi_i = s_i$ and the methods proposed so far, coordination is achieved when the vehicles assume an in-line formation pattern, which will henceforth be called the *baseline pattern* or configuration. Now, it is easy to go from the baseline configuration to a more complex, possibly time-varying formation, by introducing appropriate offsets in the desired positions of the vehicles with respect to the position of a fictitious Leader or with respect to the average point of the formation. We take the latter approach and formalize it as follows. Recall the coordination dynamics

$$\begin{aligned} \dot{\eta} &= u \\ \dot{\xi} &= C\eta + v_{\mathscr{L}}\mathbf{1} + d \end{aligned} \tag{3.65}$$

and assume as before, at this stage, that $d = \mathbf{0}$. Define α (the *average point of the formation*) and δ (the offset of the vehicles with respect to α) as

$$\alpha := \frac{1}{n}\mathbf{1}^T\xi \tag{3.66}$$

and

$$\delta := \xi - \alpha\mathbf{1}, \tag{3.67}$$

respectively and notice that $\mathbf{1}^T\delta = 0$. Define now the (pattern-induced) reference vector $h(t)$ with respect to α, which satisfies necessarily the relation $\mathbf{1}^T h(t) = 0$. Then, the problem of time-varying pattern tracking is reduced to that of making $(\delta - h) \to \mathbf{0}$ as $t \to \infty$.

With the change of variables

$$\begin{aligned} \mu &= \eta - C^{-1}\dot{h} \\ \theta &= YM_1^T(\xi - h) \\ u_0 &= \tfrac{d}{dt}(C^{-1}\dot{h}), \end{aligned} \tag{3.68}$$

the dynamics of (μ, θ) are given by

$$\begin{aligned} \dot{\mu} &= u - u_0 \\ \dot{\theta} &= YM_1^T C\mu \end{aligned} \tag{3.69}$$

The methodology used in the last section can now be exploited to show that the coordination control law $u = u_0 - (A^{-1}M_1Y^2M_1^T + A)C\mu - B\text{sat}(\mu + A^{-1}M_1Y\theta)$ or, equivalently (in the original state-space) the control law

$$u = \frac{d}{dt}(C^{-1}\dot{h}) - (A^{-1}L + A)(C\eta - \dot{h}) - B\text{sat}(\eta - C^{-1}\dot{h} + A^{-1}L(\xi - h)) \tag{3.70}$$

renders the origin of the closed-loop system uniformly globally asymptotically stable (UGAS). As a consequence, as $t \to \infty$, $\theta \to \mathbf{0}$. Therefore, using the fact that $M_1^T\mathbf{1} = \mathbf{0}$, $M_1^T(\xi - h) \to \mathbf{0}$ implies that $M_1^T(\delta - h) \to \mathbf{0}$. Because $\mathbf{1}^T\delta = 0$ and $\mathbf{1}^T h = 0$, that is, $\delta - h$ is normal to the null space of M_1^T, we conclude that $(\delta - h) \to \mathbf{0}$ as required. In the exposition above, it was implicitly assumed that the reference $h(t)$ is sufficiently smooth in order for its derivatives to exist.

The above control law can be written in decentralized form as

$$u_i = \frac{d}{dt}(R_i\dot{h}_i) - a_i(\frac{1}{R_i}\eta_i - \dot{h}_i) - \frac{1}{a_i}\sum_{j\in N_i}(\frac{1}{R_i}\eta_i - \dot{h}_i - \frac{1}{R_j}\eta_j + \dot{h}_j)$$

$$-b_i\,\mathrm{sat}(\eta_i - R_i\dot{h}_i + \frac{1}{a_i}\sum_{j\in N_i}(\xi_i - h_i - \xi_j + h_j)).$$

Notice that vehicle i needs to know the difference $\xi_j - h_j$ between the coordination variable ξ_j and reference h_j of vehicle j (but not the coordination state ξ_j itself) together with $\frac{1}{R_j}\eta_j - \dot{h}_j$.

Remark 3.11. The offset $h(t)$ can always be given with respect to any convenient reference point. It is a simple matter to compute the average of h and subtract the average from h to make the condition $\mathbf{1}^T h = 0$ hold. That is, the new h is computed as $h - (\frac{\mathbf{1}^T h}{n})\mathbf{1} = (I - \frac{1}{n}\mathbf{1}\mathbf{1}^T)h$.

3.3.4 Uni-directional communications

In this section, we study the stability of the coordination dynamics under the assumption that the communications among the vehicles are uni-directional. Moreover, we will assume that the coordination dynamics (3.41) are time-invariant, that is, the matrix $C(\xi)$ is constant. While restrictive, this assumption still allows one to consider paths that consist of straight lines, nested circumferences, and parallel translations of one arbitrary path.

Let $\mathscr{G}$ denote the graph that represents the communication network among the vehicles and L the associated Laplacian matrix. Moreover, assume that $\mathscr{G}$ has a globally reachable vertex. In this case, L can be decomposed as in (3.6), that is, $L = F_1 L_{11} F_2$. Define $\theta = F_2\xi \in \mathbb{R}^{n-1}$. The coordination dynamics (3.41) can be written in terms of η and θ as

$$\begin{aligned} \dot{\eta} &= u \\ \dot{\theta} &= F_2 C\eta + F_2 d, \end{aligned} \tag{3.71}$$

using the fact that $F_2\mathbf{1} = \mathbf{0}$. Moreover, since $\mathrm{Rank}F_2 = n-1$, then $\theta = \mathbf{0} \Leftrightarrow \xi_i = \xi_j$ for all i, j. Consequently, if θ is driven to zero asymptotically, so are the coordination errors $\xi_i - \xi_j$ and the problem of coordinated path-following is solved. This *key observation* sets the stage for the mathematical formulation of the coordinated control problem that follows.

In this section, we will give solutions to the vehicle coordination problem as stated in Definition 3.3 with constant matrix C and uni-directional communication topologies.

Coordination control solution

The main result of this section is stated below.

Proposition 3.6 (Coordination, Directed graph)
Consider the coordination dynamics (3.41) with constant matrix C. The control law

$$u = -A\eta - BC^{-1}L\xi, \tag{3.72}$$

solves the coordination problem for positive definite scalar matrices $A = aI$ and $B = bI$ if the graph $\mathcal{G}(L)$ has at least one globally reachable vertex and

$$\frac{a^2}{b} > \max_{\mu \in \sigma(L)-\{0\}} \frac{\mathrm{Im}(\mu)^2}{\mathrm{Re}(\mu)} \tag{3.73}$$

where $\sigma(.)$ stands for the spectrum of a matrix and $\mathrm{Im}(.)$ and $\mathrm{Re}(.)$ denote the imaginary and real part of a complex number. Furthermore, the control law (3.72) can be written in decentralized form as

$$u_i = -a\,\eta_i - bR_i(\xi_i)\sum_{j\in N_i}(\xi_i - \xi_j) \tag{3.74}$$

Proof. Consider for the time being the case where $d = \mathbf{0}$ (this assumption will be lifted later). The unforced closed-loop coordination system consisting of equations (3.71)-(3.72) can be written as

$$\begin{array}{rcl} \dot{\eta} & = & -A\eta - BC^{-1}F_1L_{11}\theta \\ \dot{\theta} & = & F_2C\eta \end{array} \tag{3.75}$$

We now show that the closed-loop matrix

$$A_{cl} = \begin{pmatrix} -A & -BC^{-1}F_1L_{11} \\ F_2C & 0 \end{pmatrix}$$

is a stability (Hurwitz) matrix, thus proving that the linear system (3.75) is uniformly globally exponentially stable (UGES). To this effect, we start by computing the eigenvalues of

A_{cl} as functions of the eigenvalues of L_{11}. Simple computations show that

$$\begin{aligned}\sigma(A_{cl}) &= \sigma(\begin{pmatrix} F^{-1}B^{-1}C & 0 \\ 0 & I \end{pmatrix} A_{cl} \begin{pmatrix} C^{-1}BF & 0 \\ 0 & I \end{pmatrix}) \\ &= \sigma(\begin{pmatrix} -aI_n & -\begin{pmatrix} \beta^T \\ F_2 \end{pmatrix} F_1 L_{11} \\ bF_2 \begin{pmatrix} \mathbf{1} & F_1 \end{pmatrix} & 0 \end{pmatrix}) \\ &= \sigma(\begin{pmatrix} -aI_n & -\begin{pmatrix} \mathbf{0}^T \\ I_{n-1} \end{pmatrix} L_{11} \\ b\begin{pmatrix} \mathbf{0} & I_{n-1} \end{pmatrix} & 0 \end{pmatrix}),\end{aligned} \tag{3.76}$$

and therefore $\sigma(A_{cl}) = \sigma(A_{cl_1})$, where

$$A_{cl_1} = \begin{pmatrix} -a & \mathbf{0}^T & \mathbf{0}^T \\ \mathbf{0} & -aI_{n-1} & -L_{11} \\ \mathbf{0} & bI_{n-1} & 0 \end{pmatrix} \tag{3.77}$$

where 0 denotes a square matrix of zeros. It is easily seen that $\lambda = -a$ is an eigenvalue of A_{cl_1} and thus of A_{cl}. The rest of the eigenvalues are given by the roots of

$$\det(\begin{pmatrix} (\lambda+a)I_{n-1} & +L_{11} \\ -bI_{n-1} & \lambda I_{n-1} \end{pmatrix}) = 0. \tag{3.78}$$

At this point, use the Lemma that for any matrices A, B, C and D with proper dimensions

$$\det(\begin{pmatrix} A & B \\ C & D \end{pmatrix}) = \det(AD - BC),$$

if $CD = DC$. Applying the Lemma, (3.78) can be simplified to

$$\det(\lambda(\lambda+a)I + bL_{11}) = 0. \tag{3.79}$$

Let $\mu \in \sigma(L_{11})$ be an arbitrary eigenvalue of L_{11}, recall that $\mathrm{Re}(\mu) > 0$. From (3.79), it follows that

$$\mu = -\frac{\lambda(\lambda+a)}{b}. \tag{3.80}$$

Clearly, to every μ there correspond two possible values for λ given by

$$\lambda_{1,2}(\mu) = -\sqrt{b}(c \pm \sqrt{c^2 - \mu}) \tag{3.81}$$

where $c = 0.5a/\sqrt{b}$. Let $\mu = \mu_r + \mu_i\sqrt{-1}$ with $\mu_r > 0$. Then, the real parts of the corresponding eigenvalues $\lambda_{1,2}(\mu)$ are negative if

$$\frac{a^2}{b} > \max_{\mu \in \sigma(L_{11})} \frac{\mu_i^2}{\mu_r}. \tag{3.82}$$

The technical condition (3.73) in the statement of the theorem follows immediately from the fact that $\sigma(L) = \sigma(L_{11}) \cup \{0\}$. □

Remark 3.12. Notice that the eigenvalues of the closed-loop coordination system given in (3.81) are independent of the matrix C. A similar result was derived in Chapter 2 for communication links with a simple structure, using linearization techniques. This result is therefore a non-trivial extension of the results in Chapter 2 to a nonlinear setting and to more realistic communication structures.

Remark 3.13. Notice that the coordination control law

$$u = -A\eta - BCL\xi. \tag{3.83}$$

is the same as (3.44) derived for the case of undirected graphs but differs from

$$u = -A\eta - BC^{-1}L\xi \tag{3.84}$$

derived for the case of directed graphs in (3.72). The stability condition for the closed-loop system resulting from (3.65) with control (3.83) changes to

$$\frac{a^2}{b} > \max_{0 \neq \mu \in \sigma(L)} \frac{\mathrm{Im}(\mu)^2}{\mathrm{Re}(\mu)} c^2, \tag{3.85}$$

where $C = cI$. Notice that the stability condition is no longer independent of matrix C.

Remark 3.14. The stability condition (3.85) does not contradict Proposition 3.4 where we have shown that the closed-loop coordination dynamics are stable for any diagonal matrix A and B. The argument is as follows. The eigenvalues of the graph Laplacian L are

all real numbers if the graph is symmetric, for example in the case of undirected graphs. Considering the fact that the condition (3.85) is always true for any positive a and b, if all the eigenvalues of L are real, the statement of the proposition is verified.

Remark 3.15. The pattern tracking algorithm derived in Section 3.3.3 can be extended to the case of uni-directional communications. However, the results can only be guaranteed for time-invariant systems and therefore apply to fixed formation patterns. Let the constant vector h be the desired reference pattern defined with respect to the middle point of the formation, that is, $\mathbf{1}^T h = \mathbf{0}$. Using arguments similar to those in Section 3.3.3, it can be shown that the control law

$$u = -A\eta - BC^{-1}L(\xi - h) \tag{3.86}$$

solves the coordination problem and that the vehicles exponentially converge to the desired pattern defined by h, that is, $\lim_{t\to\infty}(\xi_i - h_i) - (\xi_j - h_j) = 0; \forall i, j$.

3.3.5 Truly decentralized vehicle coordination

In all the solutions derived so far to the coordinated path-following control problem, we assumed that a predefined velocity profile $v_{\mathscr{L}}$ is known to all vehicles. This is apparent in the coordination dynamics of (3.41), where the speed error is defined as $\eta_i = v_i - R_i v_{\mathscr{L}}$. In many situations, however it is natural to assume that the "pace of the fleet" is set during the mission by one of the members, namely the Leader.

In order to make the coordination algorithms truly decentralized, this section derives a strategy that keeps the amount of required information flow as low as before, while $v_{\mathscr{L}}$ is known only to one of the vehicles. With the structure proposed, the only vehicle who knows the value of $v_{\mathscr{L}}$ (actually the one that sets its value) is a globally reachable vertex in the underlying communication graph. We further assume that $v_{\mathscr{L}}$ is constant and present the solution for general digraphs. An undirected graph will be modeled by its equivalent symmetric digraph, that is, a digraph with two arcs in opposite directions for each edge of the undirected graph.

Consider the coordination problem of n vehicles supported by a communication network. Let the underlying graph $\mathscr{G}_n$ have at least one globally reachable vertex which will

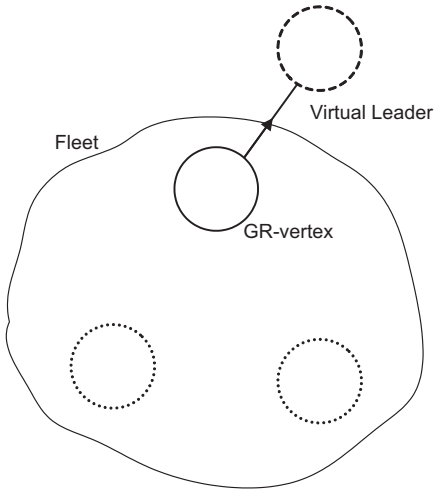

Figure 3.5: Augmented graph. $v_{\mathscr{L}}$ known only to the virtual leader

be called GR-vertex. Number the vertices of $\mathscr{G}_n$ in increasing order as $\{2,...,n+1\}$ and assume without loss of generality that V_2 is a GR-vertex. Add a vertex numbered 1 to $\mathscr{V}(\mathscr{G}_n)$, where V_1 is a virtual vehicle moving at constant speed $v_{\mathscr{L}}$. Construct the graph $\mathscr{G}_{n+1}$ by adding an arc namely arc (V_2,V_1), that captures the transmission of information from V_1 (virtual leader) to V_2 (GR-vertex), see Figure 3.5. Notice that vertex V_1 in $\mathscr{G}_{n+1}$ is the only GR-vertex: it is globally reachable because it is reachable from V_2 while V_2 is reachable from every other node but V_1, and it is unique since none of the other vertices can be reached from V_1. Therefore, $\mathscr{G}_{n+1}$ has a GR-vertex. The Laplacian matrix of $\mathscr{G}_{n+1}$ has the structure

$$L = \begin{pmatrix} 0 & \mathbf{0}^T \\ -e_1 & L_n \end{pmatrix} \tag{3.87}$$

where $e_1 = [1,0,...,0]^T$ and L_n is a $n \times n$ matrix. That is, the first row of L that corresponds to the "virtual leader" is zero.

Let D and A be the out-degree and adjacency matrices of graph $\mathscr{G}_{n+1}$, respectively, modified as follows: set the $11-$entries of D and A to 1. With this modification, the new D is invertible [4] and $L = D - A$ does not change. Define a normalized version of the graph

[4] Every other vertex has at least out-degree equal 1, since V_1 is the only globally reachable vertex.

Laplacian as $\tilde{L} = D^{-1}L = I - D^{-1}A$. Further define

$$\bar{\xi} = D^{-1}A\xi \Leftrightarrow \bar{\xi}_i = \begin{cases} \frac{1}{|N_i|}\sum_{j\in N_i}\xi_j, & |N_i| \neq 0 \\ \xi_i, & |N_i| = 0 \end{cases}, \tag{3.88}$$

where ξ is the vector of coordination states of graph $\mathcal{G}_{n+1}$. Notice that since $|N_i|$ is the number of the neighbors of V_i, then $\bar{\xi}_i$ is the average of the coordination states of its neighbors.

We now rewrite a version of the coordination closed-loop dynamics with system dynamics (3.34), (3.36) and the control law (3.72), for constant $v_{\mathcal{L}}$ and a constant matrix C, in terms of the states v and ξ, as follows

$$\begin{aligned} \dot{v} &= F \\ \dot{\xi} &= Cv + d \end{aligned} \tag{3.89}$$

with the control law

$$F = -a(v - C^{-1}v_{\mathcal{L}}\mathbf{1}) - bC^{-1}L\xi,$$

where $a, b > 0$ satisfy condition (3.73), and L is the graph Laplacian of $\mathcal{G}_{n+1}$. The arguments of Proposition 3.6 apply to (3.89). Thus, for $d = \mathbf{0}$, at steady-state $v_i = R_i v_{\mathcal{L}}$ and $\dot{\xi}_i = v_{\mathcal{L}}$ and therefore the average of the derivative of any subset of the coordination states, namely N_i, is $v_{\mathcal{L}}$, that is, $\dot{\bar{\xi}}_i = v_{\mathcal{L}}; \forall i$. This suggests to feedback $\dot{\bar{\xi}}_i$ (or any estimate of it) instead of $v_{\mathcal{L}}$, that is, to apply the control law

$$F = -a(v - C^{-1}\dot{\bar{\xi}}) - bC^{-1}\tilde{L}\xi. \tag{3.90}$$

Notice that L and $\tilde{L}$ coincide at the nonzero entries, therefore using $\tilde{L}$ instead of L only changes the gains and not the communication constraints (the details will be shown later). Simple manipulations yield the dynamics

$$\dot{\bar{\xi}} = D^{-1}A\dot{\xi} = D^{-1}ACv.$$

Therefore, F derived in (3.90) can be written in terms of the states (ξ, v) as $F = -aC^{-1}\tilde{L}Cv - bC^{-1}\tilde{L}\xi$. This justifies the choice of control law that will be given next.

Notice that all the vectors in (3.89) have dimension $n+1$ with compatible matrices, where the first rows belong to the "virtual leader", that is

$$\begin{aligned} v_1 &= v_{\mathscr{L}} \\ \xi_1 &= \xi_{\mathscr{L}} \\ f_1 &= 0 \\ R_1 &= 1, (11\text{-entry of } C) \\ d_1 &= 0. \end{aligned} \tag{3.91}$$

The above introduction motivates the following proposition.

Proposition 3.7 (Truly decentralized coordination control)
The control law

$$F = -aC^{-1}LCv - bC^{-1}L\xi, \tag{3.92}$$

where L is the (normalized) graph Laplacian of $\mathscr{G}_{n+1}$, stabilizes the coordination dynamics (3.89) for constant $v_{\mathscr{L}}$ and constant C if

$$\frac{a^2}{b} > \max_{\mu\in\sigma(L)-\{0\}} \frac{\mu_i^2}{\mu_r(\mu_r^2+\mu_i^2)}, \tag{3.93}$$

where $\mu_r = \mathrm{Re}(\mu)$ and $\mu_i = \mathrm{Im}(\mu)$ and at steady-state $v_i = R_i v_{\mathscr{L}}$ and $\xi_i = \xi_j \forall i,j = 1,\ldots,n+1$. Furthermore, (3.92) meets the communication constraints.

Proof. Since L has a globally reachable vertex, it can be decomposed as in (3.6) where $L = F_1 L_{11} F_2$. Define the error vector $\theta = F_2\xi$. Since $\mathrm{Rank}F_2 = n$, $\theta = \mathbf{0} \Leftrightarrow \xi_i = \xi_j \forall i,j$. The closed-loop dynamics in terms of v and θ, for $d = \mathbf{0}$, are given by

$$\begin{aligned} \dot{v} &= -aC^{-1}F_1L_{11}F_2Cv - bC^{-1}F_1L_{11}\theta \\ \dot{\theta} &= F_2Cv. \end{aligned} \tag{3.94}$$

We proceed in three steps to verify that *i*) $\theta = \mathbf{0}$ and $v_i = R_i v_{\mathscr{L}}; \forall i$ is an equilibrium point of the closed-loop coordination system, *ii*) the control laws are in decentralized form, and *iii*) the control laws render the closed-loop system asymptotically stable, that is, stability and convergence of the solutions to the equilibrium are observed.

i) *Equilibrium point.* From the first row of (3.94) or (3.92) we have that $\dot{v}_1 = 0$. Thus, it is enough to choose the initial condition $v_1(0) = v_{\mathscr{L}}$ to guarantee that $v_1(t) = v_{\mathscr{L}}$. At

equilibrium $\dot{\theta}_{eq} = \mathbf{0}$ and therefore $F_2 C v_{eq} = \mathbf{0}$ or equivalently $C v_{eq} = v_o \mathbf{1}$ for some $v_o \in \mathbb{R}$; the first row of these equations shows that $v_o = v_{\mathscr{L}}$. Substituting $v_{eq} = C^{-1} v_{\mathscr{L}} \mathbf{1}$ in the first equation of (3.94) results in $C^{-1} F_1 L_{11} \theta_{eq} = \mathbf{0}$. Then, multiplying on the left by $L_{11}^{-1} F_2 C$ yields $\theta_{eq} = \mathbf{0}$.

ii) *Decentralized control law.* The control law given in (3.92) in a decentralized form can be written as

$$\begin{aligned} F_i &= -aR_i \textstyle\sum_{j\in N_i} (\frac{1}{R_i} v_i - \frac{1}{R_j} v_j) - bR_i \sum_{j\in N_i} (\xi_i - \xi_j) \\ &= -a|N_i| v_i - b|N_i| R_i \xi_i + R_i \textstyle\sum_{j\in N_i} a \frac{v_j}{R_j} + b\xi_j, \end{aligned}$$

for vehicle i. If we substitute L by $\tilde{L} = I - D^{-1}A$ in the control law, then the control signal becomes

$$\tilde{F}_i = -av_i - bR_i \xi_i + \frac{R_i}{|N_i|} \sum_{j\in N_i} a \frac{v_j}{R_j} + b\xi_j.$$

Notice that $F_i = |N_i| \tilde{F}_i$.

iii) *Stability and convergence.* We now show that under condition (3.93), the eigenvalues of the closed-loop matrix

$$A_{cl} = \begin{pmatrix} -aC^{-1} F_1 L_{11} F_2 C & -bC^{-1} F_1 L_{11} \\ F_2 C & 0 \end{pmatrix}$$

are on the left-half-plane, except one eigenvalue at zero which corresponds to $\dot{v}_1 = 0$, thus proving that equilibrium $\theta_{eq} = \mathbf{0}$ and $v_{eq} - C^{-1} v_{\mathscr{L}} \mathbf{1} = \mathbf{0}$ of the linear system (3.94) is UGES. We start by computing the eigenvalues of A_{cl} as functions of the eigenvalues of L_{11}. Simple computations show that

$$\begin{aligned} \sigma(A_{cl}) &= \sigma\left(\begin{pmatrix} F^{-1}C & 0 \\ 0 & I \end{pmatrix} A_{cl} \begin{pmatrix} C^{-1}F & 0 \\ 0 & I \end{pmatrix} \right) \\ &= \sigma\left(\begin{pmatrix} -a \begin{pmatrix} 0 & \mathbf{0}^T \\ \mathbf{0} & L_{11} \end{pmatrix} & -b \begin{pmatrix} \beta^T \\ F_2 \end{pmatrix} F_1 L_{11} \\ F_2 \begin{pmatrix} \mathbf{1} & F_1 \end{pmatrix} & 0 \end{pmatrix} \right), \end{aligned}$$

and therefore $\sigma(A_{cl}) = \sigma(A_{cl_1})$, where

$$A_{cl_1} = \begin{pmatrix} 0 & \mathbf{0}^T & \mathbf{0}^T \\ \mathbf{0} & -aL_{11} & -bL_{11} \\ \mathbf{0} & I_n & 0 \end{pmatrix} \tag{3.95}$$

Clearly, A_{cl_1} has one eigenvalue at 0 which corresponds to $\dot{v}_1 = 0$, the virtual leader's dynamic. The rest of the eigenvalues are the roots of

$$\det(\begin{pmatrix} \lambda I_n + aL_{11} & bL_{11} \\ -I_n & \lambda I_n \end{pmatrix}) = 0.$$

At this point, use the Lemma that for any square matrices A, B, C and D

$$\det(\begin{pmatrix} A & B \\ C & D \end{pmatrix}) = \det(AD - BC),$$

if $CD = DC$. Applying the Lemma, the characteristics polynomial of A_{cl} is simplified to $\det(\lambda^2 I_n + (a\lambda + b)L_{11})$. Therefore if $\mu \in \sigma(L_{11})$, then

$$\mu = \frac{-\lambda^2}{a\lambda + b}.$$

Knowing that $\mathrm{Re}(\mu) > 0$, after some algebra, it can be shown that the roots of $\lambda^2 + a\mu\lambda + b\mu = 0$ have negative real part if

$$\frac{a^2}{b} > \max_{\mu \in \sigma(L_{11})} \frac{\mu_i^2}{\mu_r(\mu_i^2 + \mu_r^2)}. \tag{3.96}$$

and the results follow. □

Remark 3.16. Notice that because of the way the graph $\mathcal{G}_{n+1}$ was constructed, L is not symmetric. Thus, L_{11} has some non-real eigenvalues, that is, $\exists \mu \in \sigma(L_{11}) : \mu_i \neq 0$. On the other hand, since $\mu_r > 0$, the right-hand side of (3.96) cannot be zero or infinity. That is, the inequality has always a positive bounded right-hand side.

3.3.6 Path-following and coordination control interconnection

This section examines the behavior of the *coordinated path-following system* that results from putting together the path-following control and the coordination control systems presented in the previous sections. In particular, we show that the trajectories of *the relevant state variables tend asymptotically to* 0.

Recall how the two subsystems are connected via d and v in the equations of motions (3.11) and (3.41). Proposition 3.1 showed that the origin is a globally asymptotically stable equilibrium of path-following subsystem, under some mild technical assumptions. In particular, either of the following conditions was required

C.1 the speed $v_i(t)$ is uniformly continuous and $\lim_{t\to 0} v_i(t) \neq 0$, or

C.2 $\int_{t_0}^{\infty} \min(k, |v_i(t)|)dt = \infty$.

Under these conditions, the disturbance-like term d_i that appears at the coordination level was shown to vanish asymptotically to zero *if*

C.3 the speed v_i is bounded,

thus making the states of the coordination system tend asymptotically to zero. It follows from these considerations that $X_p := [X_{pi}]_{n\times 1}$ (X_{pi} is the state of path-following subsystem i) and X_c (the states of the coordination control subsystem) in Figure 3.6 tend asymptotically to zero if the speed v satisfies C.1 $\wedge$ C.3 or C.2 $\wedge$ C.3. These results are formally applied in the proofs of the propositions that contained in the present section.

We proposed three different solutions in Section 3.2 to the problem of path-following for wheeled robots (Propositions 3.1 and 3.2) and fully actuated marine vehicles (Proposition 3.3). Moreover, in the previous chapters, several coordination control strategies were derived. Thus, different combinations of path-following and coordination control strategies are possible. We will group these combinations into two categories, based on the proof of convergence of the resulting coordinated path-following system, and present key results in Propositions 3.8 and 3.9. This approach is summarized in Table 3.1 that shows how the coordination control strategies are classified in two general control laws: *i*) Linear and *ii*) with a sat(.) function.

In Proposition 3.8, it is more natural to address the problem using C.1, while the proof of Proposition 3.9 is easier referring to C.2, as will become clear shortly. Since the proofs are identical in every combination in each group, we will present statements of only representative members.

Proposition 3.8 (Coordinated path-following I)

Consider a fleet of n wheeled robots, each equipped with the path-following control law of Proposition 3.1. Let the corresponding coordination system be based on a bi-directional communication network and use the control law (3.45). Let $X_{pi} = (x_{ei}, y_{ei}, \psi_{ei})^T$ *denote the state of the path-following subsystem of vehicle i;* $1 \leq i \leq n$ *. Further let* $X_c = (\eta^T, \theta^T)^T$ *be*

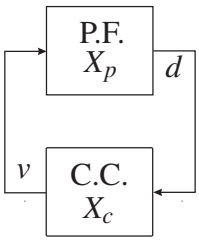

Figure 3.6: Closed-loop system consisting of the path-following and coordination control subsystems

		Path-following		
		Prop. 3.1	Prop. 3.2	Prop. 3.3
Coordination control	Linear	Prop. 3.9	Prop. 3.9	×
	Sat(.)	Prop. 3.8	Prop. 3.8	Prop. 3.8

Table 3.1: Path-following and coordination: a summary of results

the relevant state of the coordination subsystem. Suppose matrix $A > 0$ *in the coordination control law (3.45) satisfies the constraint*

$$a_1^2 > \frac{1}{2}\left(\frac{c_2}{c_1} - \frac{a_1}{a_2}\right) \max_i |N_i| \tag{3.97}$$

where $a_1 I \leq A \leq a_2 I$*, and* c_1 *and* c_2 *are as defined in (3.42). Then, given any initial state* $X_{pi}(0)$*;* $1 \leq i \leq n$ *and* $X_c(0)$*, the resulting trajectories* $X_{pi}(t)$ *and* $X_c(t)$ *are driven asymptotically to* 0*.*

Proof. The closed-loop system consisting of the Path-Following (PF) and Coordination Control (CC) subsystems of Proposition 3.1 and control law (3.45), respectively are depicted in Figure 3.6.

Define $V_\eta = \eta^T \eta$ and compute its derivative along the solutions of the coordination subsystem (3.63) to obtain

$$\dot{V}_\eta \quad = -\eta^T CQC\eta - 2\eta^T B \,\mathrm{sat}(\eta + A^{-1} M_1 Y \theta)$$

where $Q = C^{-1}A^{-1}L + LC^{-1}A^{-1} + 2C^{-1}A$. From Lemma 6.1, and because $C(t)$ is diagonal and has a positive uniform lower bound c_1, it follows from condition (3.97) that there exists

$\bar{\gamma} = \gamma c_1^2 > 0$ such that $\eta^T CQC\eta \geq \bar{\gamma}\|\eta\|^2$ and therefore

$$\dot{V}_\eta \leq -\bar{\gamma}\|\eta\|^2 + 2b_2 x_m \sqrt{n}\|\eta\|,$$

where $b_2 I \geq B$, and x_m is the limit of sat(.). Clearly, $\dot{V}_\eta$ is negative if $\|\eta\| > 2b_2 x_m \sqrt{n}/\bar{\gamma}$. Therefore, η is uniformly ultimately bounded and so is $v(t) = \eta + v_{\mathscr{L}} C^{-1}\mathbf{1}$. See Khalil (2002) for the definition of ultimate boundedness, together with related results of interest. From the form of the closed-loop dynamics (3.63) it follows that $\dot{\eta}$ is bounded and therefore $\dot{v}$ is also bounded. As a consequence, $v(t)$ is uniformly continuous.

It is now necessary to show that $\lim_{t\to\infty} v_i(t) \neq 0$ for all i. Assume by contradiction that $\exists j$ such that $v_j(t) = 0$ for all $t > t_0 \geq 0$ and $\lim_{t\to\infty} v_i(t) \neq 0\ \forall i \neq j$ (the analysis for the case where v_j tends to 0 but is not identically 0 after a certain finite time can be done identically). Recall from the proof of Proposition 3.2 that all x_{ei}'s converge to zero as $t \to \infty$ *even if* $v_i(t)$ tends to 0. Thus, $d_j = \frac{1}{R_j}[(\cos\psi_{ej} - 1)v_j + k_3 x_{ej}]_{|v_j=0}$ is also bounded and tends to zero. Furthermore, according to Proposition 3.1, the states $X_{pi}\ \forall i \neq j$ are bounded and converge to zero and so do the $d_i; \forall i \neq j$. Since η and d are bounded, so is $\dot{\theta}$. Therefore θ is bounded in any bounded interval of time. It is easy to check that (3.63) is small-signal L_∞ stable with d as an input, that is, $\exists r > 0$ such that if $\|d\| < r$ the states remain bounded. Because $\|d\| \to 0$, as $t \to \infty$, then $\exists T > 0 : \forall t > T, \|d(t)\| < r$. Therefore the states remain bounded and decay to zero as $d \to 0$, namely the coordination states X_c vanish asymptotically. Thus, $\eta = v - v_{\mathscr{L}} C^{-1}\mathbf{1}$ and in particular $\eta_j = v_j - R_j v_{\mathscr{L}}$ converge to 0, which contradicts the assumption that $v_j = 0$ because $v_{\mathscr{L}} \neq 0$ and R_j is strictly positive. □

Proposition 3.9 (Coordinated path-following II)

Consider a fleet of n wheeled robots each equipped with the path-following control law of Proposition 3.1. Let the corresponding coordination system be based on a bi-directional (or uni-directional) communication network and uses control law (3.44). Let $X_{pi} = (x_{ei}, y_{ei}, \psi_{ei})^T$; $1 \leq i \leq n$ *denote the state of the path-following subsystem of each vehicle. Further let* $X_c = (\eta^T, \theta^T)^T$ *be the relevant state of the coordination subsystem. Then, given any initial state* $X_{pi}(0)$; $1 \leq i \leq n$ *and* $X_c(0)$, *the resulting trajectories* $X_{pi}(t)$ *and* $X_c(t)$ *are driven asymptotically to* 0.

Proof. Recall the coordination subdynamics with either of the control laws (3.43), (3.44) or (3.72) derived in the previous sections as follows

$$\begin{aligned}\dot{\eta} &= u(\eta,\theta)\\ \dot{\theta} &= YM_1^T C\eta + YM_1^T d,\end{aligned}$$

where $u(.,.)$ is a linear function of its arguments. It was proved that the origin is a globally exponentially stable equilibrium of the above dynamics with $d = \mathbf{0}$. Therefore the closed-loop dynamics of the coordination control system are linear, and can be represented as $\dot{X}_c = A(t)X_c$ for $d = \mathbf{0}$. Using $\eta_i = v_i - R_i v_{\mathscr{L}}$, rewrite the disturbance-like terms d_i as

$$\begin{aligned}d_i &= \tfrac{1}{R_i}[(\cos\psi_{ei}-1)v_i + k_3 x_{ei}]\\ &= \tfrac{1}{R_i}(\cos\psi_{ei}-1)\eta_i + (\cos\psi_{ei}-1)v_{\mathscr{L}} + \tfrac{k_3}{R_i}x_{ei}.\end{aligned}$$

Now we rewrite the coordination subdynamics as

$$\dot{X}_c = (A(t)+B(t))X_c + \tilde{d}, \tag{3.98}$$

where

$$\begin{aligned}B &= \begin{pmatrix} 0 & 0 \\ 0 & YM_1^T \end{pmatrix}\begin{pmatrix} 0 & 0 \\ \tilde{B} & 0 \end{pmatrix}\\ \tilde{d} &= \begin{pmatrix} 0 & 0 \\ 0 & YM_1^T \end{pmatrix}\begin{pmatrix} \mathbf{0} \\ \tilde{d}_0 \end{pmatrix}\end{aligned} \tag{3.99}$$

with $\tilde{B} = \mathrm{diag}[\frac{1}{R_i}(\cos\psi_{ei}-1)]$ and $\tilde{d}_0 = \mathrm{vect}[(\cos\psi_{ei}-1)v_{\mathscr{L}} + \frac{k_3}{R_i}x_{ei}]$. Moreover, recall the Lyapunov function (3.18)

$$V_{pi} = \frac{1}{2}x_{ei}^2 + \frac{1}{2}y_{ei}^2 + \frac{1}{2}(\psi_{ei}-\sigma_i)^2 + \frac{1}{2}(r_i-\phi_i)^2$$

used in the proof of the stability of the path-following subdynamics and its derivative

$$\dot{V}_{pi} = -k_1 x_{ei}^2 - k_2(\psi_{ei}-\sigma_i)^2 - k_3|v_i|\frac{y_{ei}^2}{|y_{ei}|+\varepsilon} - k_4(r_i-\phi_i)^2.$$

Write the path-following subdynamics (3.11) in the general form

$$\dot{X}_{pi} = f(v_i(t), X_{pi}). \tag{3.100}$$

We first prove that the solution of the differential equations of the closed-loop system exists for all $t \geq 0$. Assume $T > 0$ is the maximum length of time over which the solution exists. Therefore $\forall t \in [0,T)$, $\dot{V}_{pi} \leq 0$ and thus X_{pi} is bounded uniformly with respect to T. That is, the solutions of (3.100) lie in a compact set for $\forall t \in [0,T)$, so the solution exists and is unique, see Lemma 3.1. Therefore, $\|A(t)+B(t)\|$ and $\tilde{d}$ are bounded uniformly with respect to T, so the solution of (3.98) exists and is unique over $0 \leq t < T$. Moreover, $X_c(t)$ may go unbounded only as if $t \to \infty$. Since T is arbitrary, the solution exists and is unique for all $t \geq 0$.

It follows from the above that $\forall t \geq 0$, $\dot{V}_{pi} \leq 0$, and therefore $X_{pi} = \mathbf{0}$ is stable $\forall i$. Thus, for any initial condition, there exists $c > 0$ such that $V_{pi} \leq \frac{1}{2}c^2$ and $y_{ei}(t) \leq c$, $\forall t \geq 0$. As a consequence we have

$$\dot{V}_{pi} \leq -2\min(k_1,k_3,k_4,\frac{k_2}{c+\varepsilon_0}|v_i(t)|)V_{pi} \equiv -\phi_i(t)V_{pi}, \tag{3.101}$$

and therefore

$$V_{pi}(t) \leq V_{pi}(t_0)e^{-\int_{t_0}^{t}\phi_i(\tau)d\tau}. \tag{3.102}$$

Now we show that

$$\lim_{t\to\infty}\int_{t_0}^{t}\phi_i(\tau)d\tau = \infty, \tag{3.103}$$

for all i. By *contradiction* assume that

$$\exists j, \int_{t_0}^{\infty}\min(k,|v_j(\tau)|)d\tau < M$$

for some $k,M > 0$. Notice that boundedness of the above integral as well as the integral in (3.103) are equivalent. To avoid unnecessary indexing, assume the integral (3.103) is unbounded for all the other indices, that is, $\forall i \in \mathbb{N}_n/\{j\}$. Otherwise they can be treated in the same way as j as will become clear shortly.

Recall the coordination subdynamics as $\dot{X}_c = (A+B)X_c + \tilde{d}$ with $\tilde{B}$ and $\tilde{d}_0$ redefined as follows. Let $\tilde{B} = \text{diag}[\tilde{B}_{ii}]$ where $\tilde{B}_{jj} = 0$, and $B_{ii} = \frac{1}{R_i}(\cos\psi_{ei}-1)$; $\forall i \neq j$. Further $\tilde{d}_0 = \tilde{d}_1 + \tilde{d}_2$ where $\tilde{d}_{1j} = k_3 x_{ej}$, $\tilde{d}_{2j} = \frac{1}{R_j}(\cos\psi_{ej}-1)v_j$, $\tilde{d}_{1i} = (\cos\psi_{ei}-1)v_{\mathscr{L}} + k_3 x_{ei}$, and $\tilde{d}_{2i} = 0$, $\forall i \neq j$. Since B vanishes as $t \to \infty$, the linear dynamics $\dot{X}_c = (A+B)X_c$ are

$UGES$ and $\dot{X}_c = (A+B)X_c + \tilde{d}$ is ISS with input $\tilde{d}$. Notice that the disturbance-like term $\tilde{d}_1$ is L_∞ and $\tilde{d}_2$ is L_1. Since $X_c(t)$ is a solution of a linear differential equation driven by inputs of types L_1 and L_∞, $X_c(t)$ is bounded, namely, η_j or v_j is bounded. Consequently, $\tilde{d}$ is bounded, so is $\dot{X}_p$ and $\dot{v}_j$. Therefore v_j is uniformly continuous. Since the integral of its absolute value is bounded, resorting to Barbalat's lemma implies that $\lim_{t\to\infty} v_j(t) = 0$. Further, using the same argument as in Proposition 3.2, $\lim_{t\to\infty} x_{ej}(t) = 0$. Therefore $\tilde{d}$ vanishes as $t \to \infty$ and so does X_c, namely $\eta_j = v_j - R_j v_{\mathscr{L}}$ tends to zero, which contradicts the fact that $R_j v_{\mathscr{L}} \neq 0$. Therefore integral in (3.103) is infinity.

It now follows that $V_{pi}(t); \forall i$ vanishes as $t \to \infty$ and so does X_{pi}. Therefore, $X_{pi} = \mathbf{0}$ is UGAS. Consequently, $B(t)$ and $\tilde{d}$ are bounded and converge to zero and it follows from Lemma 3.3 $\dot{X}_c = (A+B)X_c + \tilde{d}$ is ISS with $\tilde{d}$ as input. That is, $X_c(t)$ tends to zero, since so does $\tilde{d}$. □

3.4 Simulations

3.4.1 Bi-directional communications

This section contains the results of simulations that illustrate the performance obtained with the coordinated path-following control laws developed in this chapter for the case of bi-directional communication networks. Figures 3.7 and 3.8 illustrate the situation where 3 wheeled robots are required to follow paths that consist of parallel straight lines and nested arcs of circumferences, that is, C is piecewise constant and defined as follows:

$$\begin{aligned} C = &\ \text{diag}[\tfrac{1}{2}, \tfrac{1}{3}, \tfrac{1}{4}], && \text{arc I} \\ C = &\ I_3, && \text{line I} \\ C = &\ \text{diag}[\tfrac{1}{4}, \tfrac{1}{3}, \tfrac{1}{2}], && \text{arc II} \\ C = &\ I_3, && \text{line II} \end{aligned}$$

The coordination control laws were computed according to (3.45) with $A = I_3$, $B = 0.25 I_3$, and $x_m = 1$. Figure 3.7 corresponds to the case of an in-line formation pattern. Figure 3.8 shows the case where the vehicles are required to keep a triangular formation pattern with constant pattern $h^T = [-0.25, +0.5, -0.25]$. In both simulations, vehicle 1 is allowed to communicate with vehicles 2 and 3, but the last two do not communicate between themselves directly. The reference speed $v_{\mathscr{L}}$ was set to $v_{\mathscr{L}} = 0.1$ [s^{-1}]. This in turn acted as a reference for the actual speeds of the vehicles which can be computed as $v_r = v_{\mathscr{L}} C^{-1} \mathbf{1}$. Notice how the vehicles adjust their speeds to meet the formation requirements and the path-following errors decay to 0. In the in-line formation case (Figure 3.7), the coordination errors $\xi_{12} = \xi_1 - \xi_2$ and $\xi_{13} = \xi_1 - \xi_3$ converge to zero. In the triangle formation case (Figure 3.8), $\xi_{12} \to -0.75$ and $\xi_{13} \to 0$ as desired.

Figure 3.9 illustrates a different kind of coordinated maneuver in the $x-y$ plane: one robot is required to follow the $x-$axis, while the other must follow a sinusoidal path as the two maintain an in-line formation along the $y-$axis. In this case, C is time varying. Notice in Figure 3.9(b) how vehicle 1 adjusts its speed along the path so as to achieve coordination. As seen in sub-Figures 3.9(c) and 3.9(d), the vehicles converge to the assigned paths and drive the error between their $x-$coordinates to 0. The coordination control signals were calculated using (3.43), with $A = I_2$. The vehicles are coordinated if their $x-$coordinates

are equal, that is, the coordination states are defined as $\xi_i = x_i; i = 1,2$. The paths are defined by $y_1 = 1 + \sin(\frac{2\pi}{\lambda}x_1)$ and $y_2 = -1$ with $\lambda = 1$. The arc-lengths are computed as $s_1 = \int_0^{x_1} \sqrt{1 + (\frac{dy_1}{dx_1}(x))^2}dx$ and $s_2 = x_2$. The C matrix is $C = \text{diag}[1/R_1, 1/R_2]$, where

$$R_1 = \frac{ds_1}{d\xi_1} = \frac{ds_1}{dx_1} = \sqrt{1 + (\tfrac{2\pi}{\lambda})^2 \cos^2(\tfrac{2\pi}{\lambda}x_1)}$$
$$R_2 = 1.$$

Clearly, in this case C is a state-driven, time-varying matrix that must be used to compute the time-varying reference speed for vehicle 1, see Figure 3.9.

3.4.2 Uni-directional communications

The performance obtained with the control laws developed for the directed communication topologies are illustrated in this section. Figure 3.10 corresponds to a simulation where 3 wheeled robots were required to follow 3 circumferences, with radii 2[m], 3[m] and 4[m], while keeping an in-line formation pattern. The Laplacian matrix L (that captures the communication network among the vehicles) and the coordination controller gains are

$$L = \begin{pmatrix} 1 & -1 & 0 \\ 0 & 1 & -1 \\ -1 & 0 & 1 \end{pmatrix} \text{ and } \quad a = 2; b = 1, \tag{3.104}$$

respectively. The eigenvalues of L belong to the set $\{0, 0.86 \pm j0.5\}$, thus verifying condition (3.97). The reference speed $v_{\mathscr{L}}$ was set to $0.1[\text{s}^{-1}]$. Figure 3.10(a) shows the evolution of the vehicles as they start from the same point off the assigned paths and converge to the latter. Figure 3.10(b) is a plot of the vehicle speeds that ensure coordination along the paths. Finally, Figures 3.10(c) and 3.10(d) show the coordination errors $\xi_1 - \xi_2$ and $\xi_1 - \xi_3$ and the path-following errors y_{ei}, respectively, decaying to 0.

3.5 Summary

This chapter presented several solutions to the coordinated path-following problem of a fleet of wheeled robots and fully actuated marine vehicles along a set of general types of paths, under the constraints of symmetric and asymmetric communication networks. The

solutions adopted build on Lyapunov based techniques and addresses explicitly the constraints imposed by the topology of the inter-vehicle communications network. With this set-up, path-following (in space) and inter-vehicle coordination (in time) are essentially designed decoupled. Further, it was shown that the relevant error variables converge to zero when putting together the path-following and coordination subsystems. Path-following for each vehicle amounts to reducing a conveniently defined error vector to zero. Vehicle coordination is achieved by adjusting the speed of each of the vehicles along its path, according to information on the position of the other vehicles. The methodology proposed led to a decentralized control law whereby the exchange of data among the vehicles is kept at a minimum. Some other particular issues were also addressed: time-varying pattern tracking and truly decentralized coordination strategies where only one of the vehicles decides the value of the reference speed $v_{\mathscr{L}}$.

The problem of robustness against temporary communication losses is the subject of the next chapter.

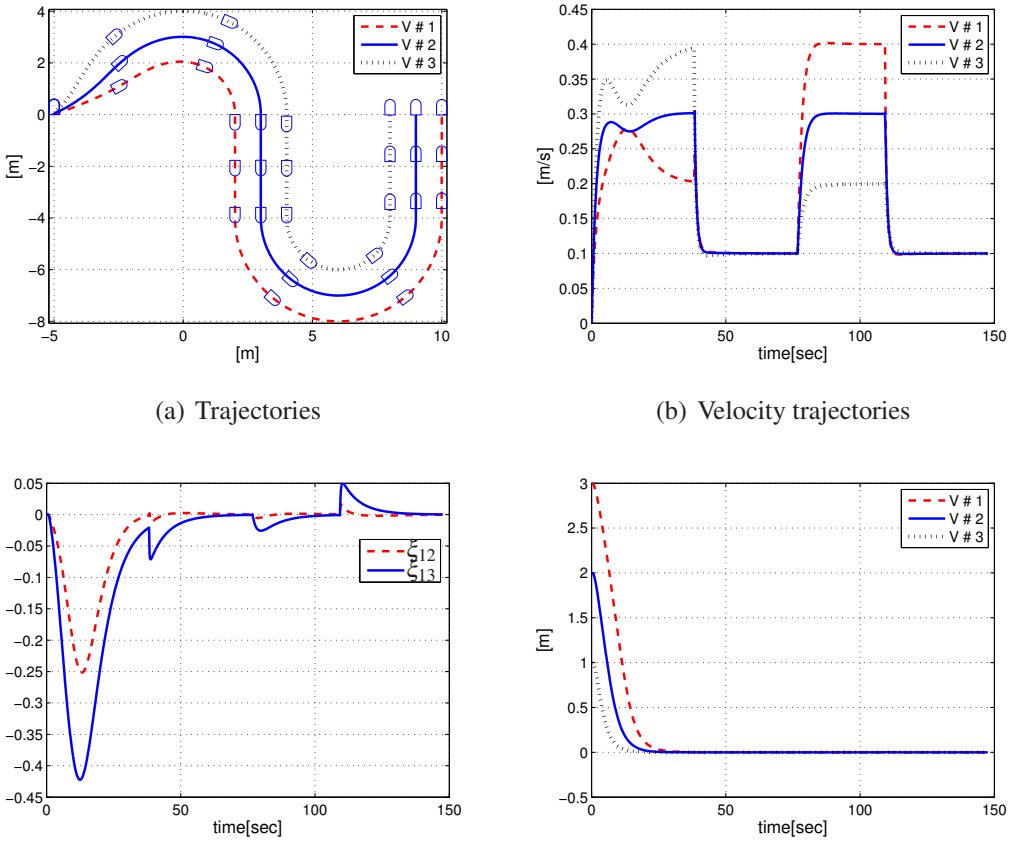

(a) Trajectories

(b) Velocity trajectories

(c) Coordination errors

(d) Path-following errors (y_e)

Figure 3.7: In-line formation, piecewise constant C, bi-directional communications

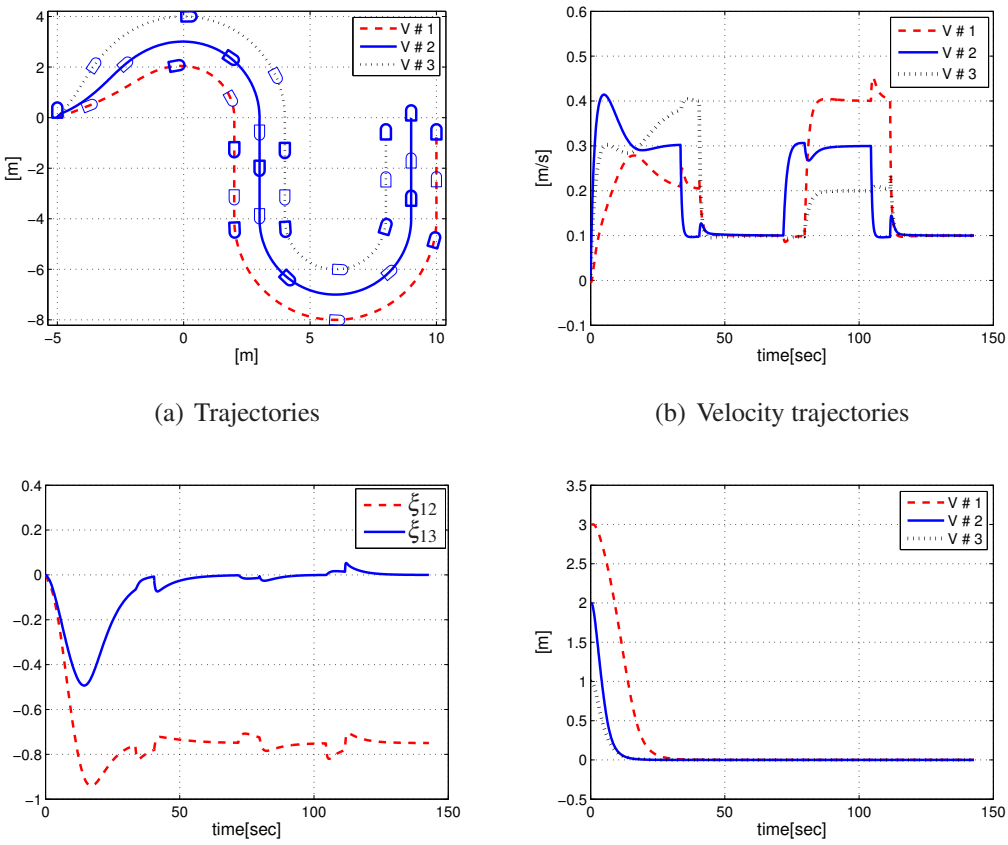

(a) Trajectories

(b) Velocity trajectories

(c) Coordination errors

(d) Path-following errors (y_e)

Figure 3.8: Triangular formation, piecewise constant C, bi-directional communications

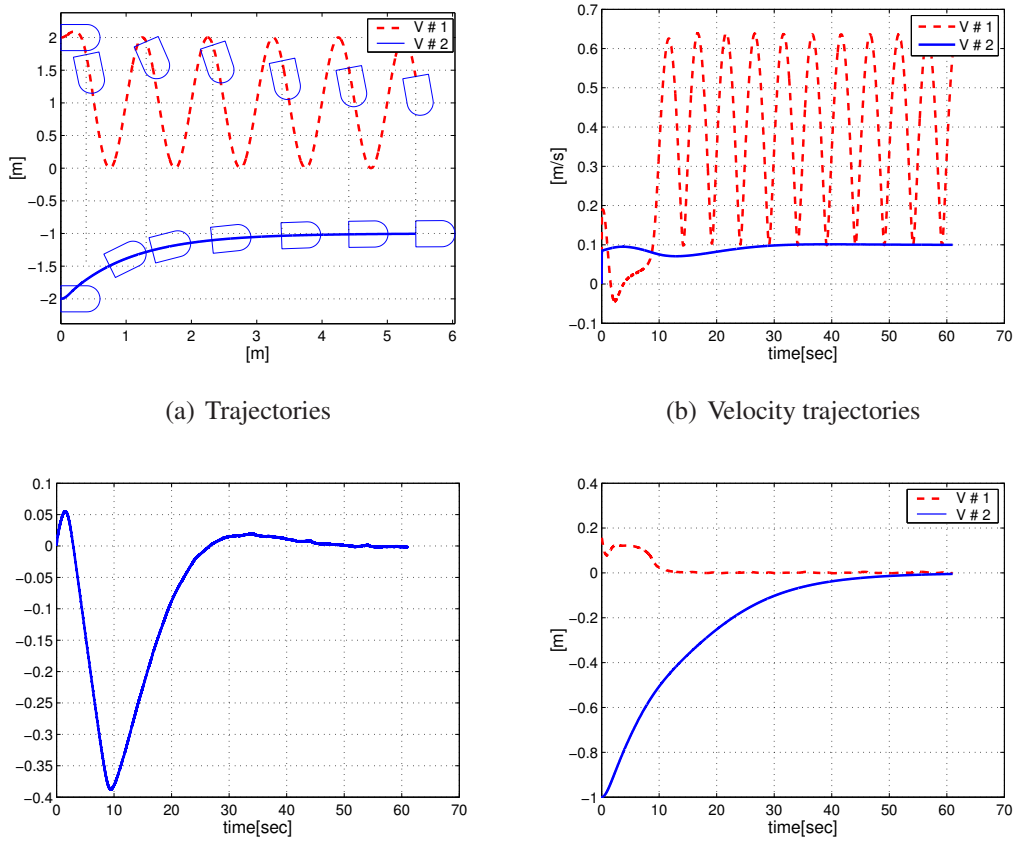

(a) Trajectories

(b) Velocity trajectories

(c) Coordination error

(d) Path-following errors (y_e)

Figure 3.9: Coordination of 2 vehicles, varying C, bi-directional communications

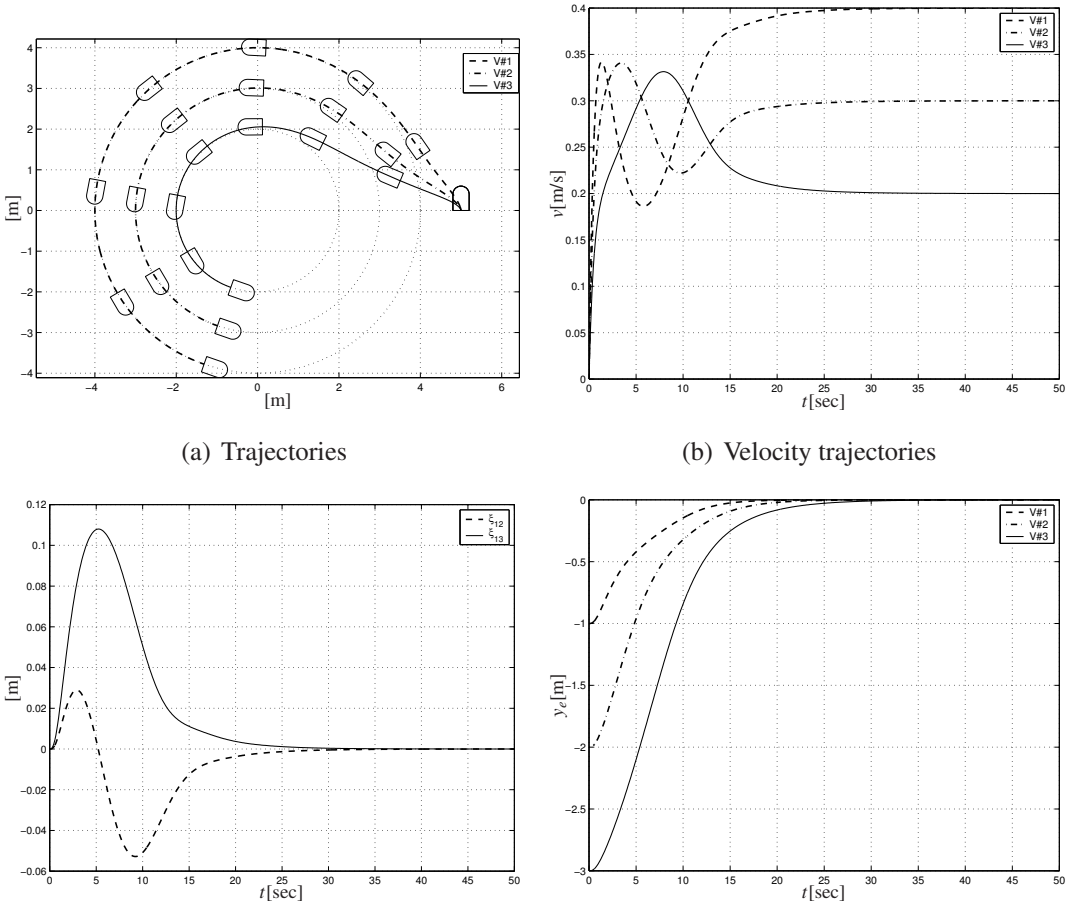

(a) Trajectories

(b) Velocity trajectories

(c) Coordination error

(d) Path-following errors (y_e)

Figure 3.10: Coordination of 3 vehicles, uni-directional communications

CHAPTER 4

SWITCHING COMMUNICATION TOPOLOGIES: GENERAL AUTONOMOUS VEHICLES

This chapter addresses the problem of coordinated path-following control of a group vehicles in the presence of varying communication topologies and fixed time-delays. Its key contributions are twofold: *i*) the class of vehicle considered is very general and includes underactuated vehicles, and *ii*) problems that arise due to temporary communication losses and fixed time delay are dealt with in a rigorous mathematical framework. The chapter concludes with a study on the coordinated path-following problem for underactuated autonomous underwater vehicles.

4.1 Problem statement

Consider a group of n vehicles numbered $1,..,n$. We let the dynamics of vehicle i be modeled by a general system of the form

$$\begin{aligned} \dot{x}_i &= f_i(x_i, u_i, w_i) \\ y_i &= h_i(x_i, v_i) \end{aligned} \tag{4.1}$$

where $x_i \in \mathbb{R}^n$ is the state, $u_i \in \mathbb{R}^m$ is the control signal, and $y_i \in \mathbb{R}^q$ is the output that we require to reach and follow a path $y_{d_i}(\gamma_i) : \mathbb{R} \to \mathbb{R}^q$ parameterized by $\gamma_i \in \mathbb{R}$. Signals w_i and v_i denote the disturbance inputs and measurement noises, respectively. Later in Section 4.5, an example will be given where the dynamics of (4.1) are those of a very general class of

autonomous underwater vehicles. In this case, the output y_i corresponds to the position of the vehicle with respect to a inertial coordinate frame.

For any timing law $\gamma_i(t)$, the path-following and speed tracking error variables are defined as

$$e_i(t) := y_i(t) - y_{d_i}(\gamma_i(t)) \tag{4.2}$$

and

$$\eta_i(t) := \dot{\gamma}_i(t) - v_{r_i}(t), \tag{4.3}$$

respectively, where $v_{r_i}(t) \in \mathbb{R}$ denotes a desired temporal speed profile. *Notice that this notation is slightly different from the one in the previous chapters. This is done in order to keep close to the notation used in (Aguiar & Hespanha 2006) that inspired the development in this chapter.*

In preparation for the development that follows we set $v_{r_i}(t) = v_{\mathscr{L}}(t) + \tilde{v}_{r_i}(t)$, where $v_{\mathscr{L}}(t)$ is a nominal, pre-determined speed profile and $\tilde{v}_{r_i}$ can be seen as the perturbation component of v_{r_i} about $v_{\mathscr{L}}$. As will be seen later, $v_{\mathscr{L}}(t)$ denotes the component of $v_{r_i}(t)$ that is common to all the vehicles and is known in advance and

$$\tilde{v}_{r_i}(t) = v_{r_i}(t) - v_{\mathscr{L}}(t) \tag{4.4}$$

is the remaining component that is not known beforehand. We assume the time-derivative of $v_{\mathscr{L}}(t)$ is known and that $v_{\mathscr{L}}(t)$ and $y_{d_i}(\gamma_i)$ are sufficiently smooth with respect to their arguments.

Inspired by the work in (Aguiar et al. 2005, Ghabcheloo et al. 2007, Skjetne et al. 2004), we start by defining a problem of path-following for each vehicle.

Definition 4.1 (Path-following (PF) problem)
Consider a vehicle with dynamics (4.1) together with a spatial path $y_{d_i}(\gamma_i)$ to be followed and a desired, pre-determined temporal speed profile $v_{r_i}(t)$ to be tracked. Let the path-following error and the speed tracking error be as in (4.2) and (4.3), respectively. Given $\varepsilon > 0$, design a feedback control law for u_i such that all closed-loop signals are bounded and both $\|e_i\|$ and $|\eta_i|$ converge to a neighborhood of the origin of radius ε.

Stated in simple terms, the problem above amounts to requiring that the output y_i of a vehicle converge to and remain inside a tube centered around the desired path y_{d_i}, while ensuring that its rate of progression $\dot{\gamma}_i$ also converge to and remain inside a tube centered around the desired speed profile $v_{r_i}(t)$.

We henceforth assume that the path-following controllers adopted meet a number of technical conditions described next. In Section 4.5, we introduce a path-following control solution for a general underacuated vehicle that does indeed satisfy the required technical conditions.

4.1.1 Path-following control

Consider vehicle i and assume a solution to the path-following problem of Definition 4.1 exists. Let the corresponding closed-loop path-following system be described by

$$\dot{\zeta}_i = f_{c_i}(t, \zeta_i, \tilde{v}_{r_i}, d_i) \tag{4.5}$$

where d_i subsumes all the exogenous inputs (including disturbances and measurement noises), state vector ζ_i includes necessarily e_i but may or may not include η_i, and $\tilde{v}_{r_i}$ is defined in (4.4). Two types of path-following strategies are considered:

Type I- variable η_i plays the role of an auxiliary control for the path-following algorithm in that it defines what the evolution of γ_i should be. In this case η_i is a state of the closed-loop PF system, that is, ζ_i includes η_i.

Type II- $\eta_i = 0$. The dynamics of $\dot{\gamma}_i$ are simply $\dot{\gamma}_i = v_{r_i}$. Clearly in this case, ζ_i does not include η_i.

Recall now the definition of input-to-state stability (ISS). See (Sontag 1998, Sontag & Wang 1996) and (Khalil 2002, pp. 217) for details on ISS and its relation to Lyapunov theory. Let $\zeta_i(t)$ be a solution of (4.5) for a given signal $\tilde{v}_{r_i}(t)$ and $d_i(t)$, and initial condition $\zeta_i(t_0)$. System (4.5) is said to be input-to-state stable (ISS) with ζ_i as state and d_i and $\tilde{v}_{r_i}$ as input if

$$\|\zeta_i(t)\| \leq \beta(\|\zeta_i(t_0)\|, t - t_0) + \rho_1\left(\sup_{t_0 \leq s \leq t} \|\tilde{v}_{r_i}(s)\|\right) + \rho_2\left(\sup_{t_0 \leq s \leq t} \|d_i(s)\|\right), \quad \forall t \geq t_0.$$

where $\beta(.,.)$ is a function of *class*$\mathscr{KL}$ and $\rho_i(.); i = 1,2$ are functions[1] of class $\mathscr{K}$.

Assumption 4.1. *We assume that there exists a Lyapunov function $W_i(t,\zeta_i)$ satisfying*

$$\underline{\alpha}_1\|\zeta_i\|^2 \leq W_i \leq \bar{\alpha}_1\|\zeta_i\|^2 \tag{4.6}$$

$$\dot{W}_i \leq -\lambda_1 W_i + \rho_1|\tilde{v}_{r_i}|^2 + \rho_2 d_i^2, \tag{4.7}$$

where λ_1, ρ_1, ρ_2, $\underline{\alpha}_1$, and $\bar{\alpha}_1$ are positive values, and $\dot{W}_i$ is taken along the solutions of (4.5), that is,

$$\dot{W}_i = \frac{\partial W_i}{\partial t} + \frac{\partial W_i}{\partial \zeta_i} f_{c_i}$$

This assumption implies that the PF system is ISS with input $(d_i, \tilde{v}_{r_i})$ and state ζ_i. To verify this, integrate (4.7) and use (4.6) to obtain

$$\underline{\alpha}_1\|\zeta_i(t)\|^2 \leq \bar{\alpha}_1\|\zeta_i(t_0)\|^2 e^{-\lambda_1(t-t_0)} + \frac{\rho_1}{\lambda_1}\sup|\tilde{v}_{r_i}|^2 + \frac{\rho_2}{\lambda_1}\sup|d_i|^2,$$

and therefore

$$\|\zeta_i(t)\| \leq \alpha\|\zeta_i(t_0)\|e^{-0.5\lambda_1(t-t_0)} + \rho_v\sup|\tilde{v}_{r_i}| + \rho_d\sup|d_i|$$

where $\alpha = \sqrt{\bar{\alpha}_1/\underline{\alpha}_1}$, $\rho_v = \sqrt{\rho_1/(\lambda_1\underline{\alpha}_1)}$, and $\rho_d = \rho_2/(\lambda_1\underline{\alpha}_1)$.

4.1.2 Vehicle coordination

Assuming a path-following controller has been implemented for each vehicle, it now remains to coordinate (that is, synchronize) the entire group of vehicles so as to achieve a desired formation pattern compatible with the paths adopted. Let Γ_i denote the desired path to be followed by vehicle i, and consider the position of the associated virtual target being tracked, $y_{d_i}(\gamma_i)$ along Γ_i. Since each vehicle, $y_i(t)$, tends asymptotically to $y_{d_i}(\gamma_i)$, it follows that an adequate choice of the path parametrizations will allow for the conclusion that the vehicles are coordinated or have reached *agreement*, iff $\gamma_{i,j} = 0; \forall j,i \in \mathbb{N}_n$. As will become clear, coordination is achieved by adjusting the speed of each virtual target $\dot{\gamma}_i; i \in \mathbb{N}_n$ as a function of the along-path distances γ_{ij}; $j \in N_i$, where N_i denotes the set of the

[1] See Section 3.1 for the definition of *class*$\mathscr{K}$ and *class*$\mathscr{KL}$.

neighbors of vehicle i. We will require that the formation as a whole (group of multiple vehicles) travels at an assigned speed profile $v_{\mathscr{L}}(t)$ while coordinated, that is, asymptotically $\dot{\gamma}_i = v_{\mathscr{L}}; \forall i \in \mathbb{N}_n$.

From (4.3), the evolution of coordination state $\gamma_i; i \in \mathbb{N}_n$ is governed by

$$\dot{\gamma}_i(t) = v_{r_i}(t) + \eta_i(t) \tag{4.8}$$

where the speed tracking errors η_i are viewed as disturbance-like input signals and the speed-profiles v_{r_i} are taken as control signals that must be assigned to yield coordination of the states γ_i. To achieve this objective, information is exchanged through an inter-vehicle communication network. In general, $\dot{\gamma}_i$ will be a function of x_i, γ_i and of the coordination states of the neighboring vehicles. For simplicity of presentation, in this chapter, we assume that the communication links are bi-directional[2], that is, $i \in N_j \Leftrightarrow j \in N_i$.

Definition 4.2 (Coordinated Path-Following)

Consider a set of vehicles $V_i; i \in \mathbb{N}_n$ with dynamics (4.1), the corresponding paths $y_{d_i}(\gamma_i)$ parameterized by γ_i, and a formation speed assignment $v_{\mathscr{L}}(t)$. Assume that for each vehicle there is a feedback control law that satisfies Assumption 4.1. Further, assume γ_i and $\gamma_j; j \in N_i$ are available to vehicle $i \in \mathbb{N}_n$. Derive a control law for v_{r_i} (or $\tilde{v}_{r_i} = v_{r_i} - v_{\mathscr{L}}$) such that for a given $\varepsilon > 0$ the coordination errors $\gamma_i - \gamma_j$ and the formation speed tracking errors $\dot{\gamma}_i - v_{\mathscr{L}}; \forall i, j \in \mathbb{N}_n$ converge to a ball of radius ε around zero as $t \to \infty$.

We now recall some key concepts from algebraic graph theory (Godsil & Royle 2001) and agreement algorithms and derive some basic tools that will be used in the sequel. The emphasis is on Graph theoretical results required to tackle problems related to switching communication topologies.

4.2 Preliminaries and basic results

4.2.1 Graph theory

Let $\mathscr{G}(\mathscr{V}, \mathscr{E})$ be the undirected graph induced by the inter-vehicle communication network, with $\mathscr{V}$ denoting the set of n vertices (each corresponding to a vehicle) and $\mathscr{E}$ the set of

[2] See Remark 4.3 for a note on the uni-directional case.

edges (each standing for a data link). See Section 3.1 for details of Graph Theory.

We will be dealing with situations where the communication links are time-varying in the sense that links can appear and disappear (switch) due to intermittent failures and/or communication links scheduling. The mathematical set-up required is described next.

A *complete graph* is a graph with an edge between each pair of vertices. A complete graph with n vertices has $\bar{n} = n(n-1)/2$ edges. Let $\mathscr{G}$ be a complete graph with edges numbered $1,...,\bar{n}$. Consider a communication network among n agents. To model the underlying switching communication graph, let $p = [p_i]_{\bar{n}\times 1}$, where each $p_i(t) : [0,\infty) \to \{0,1\}$ is a piecewise-continuous time-varying binary function which indicates the existence of edge i in the graph $\mathscr{G}$ at time t. Therefore, given a switching signal $p(t)$, the dynamic communication graph $\mathscr{G}_{p(t)}$ is the pair $(\mathscr{V}, \mathscr{E}_{p(t)})$, where, if $i \in \mathscr{E}_{p(t)}$ then $p_i(t) = 1$, otherwise $p_i(t) = 0$. For example, $p(t) = [1,0,...,0]^T$ means that at time t only link number 1 is active. Denote by L_p the explicit dependence of the graph Laplacian on p and likewise for the degree matrix D_p and adjacency matrix A_p. Further let $N_{i,p(t)}$ denote the set of the neighbors of agent i at time t.

We discard infinitely fast switchings. Formally, let S_{dwell} denote the class of piecewise constant switching signals such that any consecutive discontinuities are separated by no less than some fixed positive constant time τ_D, the dwell time. We assume that $p(t) \in S_{dwell}$.

4.2.2 Brief connectivity losses

Consider the situation where the communication network changes in time so as to make the underlying dynamic communication graph $\mathscr{G}_{p(t)}$ alternatively connected and disconnected. To study the impact of temporary connectivity losses on the performance of the coordination algorithms developed, we explore the concept of "brief instabilities" developed in (Hespanha et al. 2004). In particular, this concept will be instrumental in capturing the percentage of time that the communication graph is not connected.

Recall that the binary value of the element p_i in p declares the existence of edge i in Graph $\mathscr{G}_p$. We can thus build $2^{\bar{n}}$ graphs indexed by the different possible occurrence of vector p. Let P denote the set of all possible vectors p and let P_c and P_{dc} denote the partitions of P that give rise to connected graphs and disconnected graphs, respectively.

That is, if $p \in P_c$, then $\mathscr{G}_p$ is connected, otherwise disconnected. Define the characteristic function of the switching signal p as

$$\chi(p) := \begin{cases} 0 & p \in P_c \\ 1 & p \in P_{dc} \end{cases} \tag{4.9}$$

For a given time-varying $p(t) \in S_{dwell}$, the connectivity loss time $T_p(\tau,t)$ over $[\tau,t]$ is defined as

$$T_p(t,\tau) := \int_\tau^t \chi(p(s))ds. \tag{4.10}$$

Definition 4.3 (Brief Connectivity Losses)

The communication network is said to have brief connectivity losses*, BCL for short, if*

$$T_p(t,\tau) \leq \alpha(t-\tau) + (1-\alpha)T_0, \ \forall t \geq \tau \geq 0 \tag{4.11}$$

for some $T_0 > 0$ *and* $0 \leq \alpha \leq 1$.

In (4.11), α *provides an asymptotic upper bound on the ratio* $T_p(\tau,t)/(t-\tau)$*, as* $t-\tau \to \infty$ *and is therefore called the* asymptotic connectivity loss rate*. When* $p \in P_{dc}$ *over an interval* $[\tau,t]$*, we have* $T_p(\tau,t) = t-\tau$ *and the above inequality requires that* $t-\tau \leq T_0$*. This justifies calling* T_0 *the* connectivity loss upper bound*. Notice that* $\alpha = 1$ *means that the communications graph is never connected.*

Before closing this section, we introduce a special coordination error vector and some results that will play an important role later. As will be shown later, this error state is zero iff the coordination states are equal. Stack the coordination states in a vector $\gamma := [\gamma_i]_{n\times 1}$. Given a diagonal matrix $K > 0$, define $\beta := K^{-1}\mathbf{1}$ and the error vector

$$\tilde{\gamma} := \mathscr{L}_\beta \gamma, \tag{4.12}$$

where

$$\mathscr{L}_\beta := I - \frac{1}{\beta^T \mathbf{1}} \mathbf{1}\beta^T \tag{4.13}$$

and I is an identity matrix. The following statements hold.

Lemma 4.1

The error vector $\tilde{\gamma}$, the matrix $\mathscr{L}_\beta$, and the graph Laplacian L_p satisfy the following properties:

1. *$\mathscr{L}_\beta$ has $n-1$ eigenvalues at 1 and a single eigenvalue at zero with right and left eigenvectors $\mathbf{1}$ and β, respectively such that $\mathscr{L}_\beta \mathbf{1} = \mathbf{0}$ and $\beta^T \mathscr{L}_\beta = \mathbf{0}^T$.*

2. *$\mathscr{L}_\beta K L_p = K L_p$ for all $p \in P_c \cup P_{dc}$*

3. *$v \mathscr{L}_\beta^T K^{-1} \mathscr{L}_\beta v \leq v K^{-1} v; \forall v \in \mathbb{R}^n$*

4. *$\tilde{\gamma} = \mathbf{0} \Leftrightarrow \gamma \in \text{span}\{\mathbf{1}\}$*

5. *$\beta^T \tilde{\gamma} = 0$*

6. *$L_p \tilde{\gamma} = L_p \gamma$ for all $p \in P_c \cup P_{dc}$*

7. *if $\|\tilde{\gamma}\| < \varepsilon$, then $|\gamma_i - \gamma_j| < \sqrt{2}\varepsilon$ and $\|K L_p \gamma\| < n\varepsilon \|K\|$*

8. *Let*

$$\lambda_{2,m} := \min_{\substack{p \in P_c \\ \mathbf{1}^T v = 0 \\ v^T v \neq 0}} \frac{v^T L_p v}{v^T v}, \qquad \lambda_m := \min_{\substack{p \in P_c \\ \beta^T v = 0 \\ v^T v \neq 0}} \frac{v^T L_p v}{v^T v}, \qquad \bar{\lambda}_m := \min_{\substack{p \in P_c \cup P_{dc} \\ L_p v \neq 0 \\ v^T v \neq 0}} \frac{v^T L_p v}{v^T v}.$$

   Then, $\lambda_m = \frac{(\beta^T \mathbf{1})^2}{n \beta^T \beta} \lambda_{2,m} > 0$ and $\bar{\lambda}_m > 0$.

9. *If $z = L_{p(t)} \gamma$, then the i'th component of z is $z_i = \sum_{j \in N_{i,p(t)}} \gamma_i - \gamma_j$.*

Proof. See the Appendix. □

Property 4 allows for the conclusion that if $\tilde{\gamma}$ tends to zero, then $|\gamma_i - \gamma_j| \to 0; \forall i, j \in \mathbb{N}_n$ as $t \to \infty$ and coordination is achieved. Property 7 gives a bound on the coordination errors $\gamma_i - \gamma_j$ given a bound on the error vector $\tilde{\gamma}$. In the literature, the connectivity of a graph with Laplacian L is the second smallest eigenvalue λ_2 of L. The term $\lambda_{2,m}$ defined in property 8 is an extension of the concept of the connectivity in a collective sense, that is, the smallest graph connectivity over all connected graphs $\mathscr{G}_p$. Given λ_m, the lower bound estimate $\tilde{\gamma}^T L_p \tilde{\gamma} \geq \lambda_m \tilde{\gamma}^T \tilde{\gamma}$, when $p \in P_c$, applies. An identical interpretation applies to $\bar{\lambda}_m$. Notice

from property 9 that if the control signal of vehicle i is computed as a function of z_i, then the proposed control law meets the communication constraints embodied in the sets N_i.

The following lemma plays a key role in deriving the vehicle coordination dynamics with switching topologies in Section 4.5.

Lemma 4.2

Let $\bar{M} \in \mathbb{R}^{n\times n-1}$ *such that* $\text{Rank}\bar{M}^T = n-1$ *and* $\bar{M}^T\mathbf{1} = \mathbf{0}$, *and* $\bar{M}^T\bar{M} = I_{n-1}$. *Define* $U_p := M_p^T\bar{M}$ *with* $M_p \in \mathbb{R}^{n\times n-1}$ *and* $M_pM_p^T = L_p$, *where the latter is the graph Laplacian. Then*

1. $M_p^T = U_p\bar{M}^T$,
2. $\sigma(U_p^TU_p) = \sigma(L_p)\setminus\{0\}$, *where* $\sigma(.)$ *denotes the spectrum of the matrix in the argument.*

Proof. See the Appendix. □

4.2.3 Connected in mean topology

In the previous situation, we considered the case where the communication graph changes in time, alternating between connected and disconnected graphs. We now address a more general case where the communication graph may even fail to be connected at any instant of time; however, we assume there is a finite time $T > 0$ such that over any interval of length T the union of the different graphs is somehow connected. This statement is made precise in the sequel. We now present some key results for time-varying communication graph that borrow from (Lin 2006, Lin et al. 2005*b*, Moreau 2004).

Let $\mathcal{G}_i$; $i = 1,...,q$ be q graphs defined on n vertices, and denote by L_i their corresponding graph Laplacians. Define *union graph* $\mathcal{G} = \cup_i\mathcal{G}_i$ as the graph whose edges are obtained from the union of the edges $\mathcal{E}_i$ of $\mathcal{G}_i$; $i = 1,...,q$. If $\mathcal{G}$ is connected, $L = \sum_i L_i$ has a single eigenvalue at 0 with eigenvector $\mathbf{1}$. Notice that L is not necessarily the Laplacian of $\mathcal{G}$, because for an edge e if $e \in \mathcal{E}_i$ and $e \in \mathcal{E}_j$, for $i \neq j$, then e is counted twice in L through $L_i + L_j$, while we only consider one link in $\mathcal{G}$ as representative of e. However, L has the same rank properties as the Laplacian of $\mathcal{G}$. Since $p \in S_{dwell}$ (only a finite number of

switchings are allowed over any bounded time interval), the union graph is defined over time intervals in the obvious manner. Formally, given two real numbers $0 \leq t_1 \leq t_2$, the union graph $\mathscr{G}([t_1,t_2))$ is the graph whose edges are obtained from the union of the edges $\mathscr{E}_{p(t)}$ of graph $\mathscr{G}_{p(t)}$ for $t \in [t_1,t_2)$.

Definition 4.4 (Uniformly Connected in Mean)

A switching communication graph $\mathscr{G}_{p(t)}$ is uniformly connected in mean *(UCM), if there exists $T > 0$ such that for every $t \geq 0$ the union graph $\mathscr{G}([t,t+T))$ is connected.*

For a given $t > 0$, let $t_0 := t$ and the sequence $t_i; i = 1,...,q$ be the time instants at which switching happens over interval $[t,t+T)$. If the switching communication graph is UCM, then the union graph $\cup_{i=0}^{q}\mathscr{G}_i$ is connected and $\sum_{i=0}^{q} L_{p(t_i)}$ has a single eigenvalue at origin with eigenvector $\mathbf{1}$.

Consider the linear time-varying system

$$\dot{\gamma} = -KL_p\gamma \tag{4.14}$$

where K is a positive definite diagonal matrix and L_p is the Laplacian matrix of a dynamic graph $\mathscr{G}_p$. It is known, see for example (Lin et al. 2005*b*), that

Theorem 4.2 (Agreement)

Coordination (agreement) among the variables γ_i with dynamics (4.14) is achieved uniformly exponentially if the switching communication graph $\mathscr{G}_{p(t)}$ is UCM. That is, under this connectivity condition all the coordination errors $\gamma_{ij}(t)$ converge to zero and $\dot{\gamma}_i \to 0$ as $t \to \infty$.

We now consider the delayed version of (4.14). Let the coordination states γ_i evolve according to

$$\dot{\gamma}(t) = -KD_{p(t)}\gamma(t) + KA_{p(t)}\gamma(t-\tau) \tag{4.15}$$

where $D_{p(t)}$ and $A_{p(t)}$ are the degree matrix and the adjacency matrix of $\mathscr{G}_{p(t)}$, respectively. The following statement can be derived from (Moreau 2004).

Theorem 4.3 (Agreement-delayed information)

The variables γ_i with dynamics (4.15) agree uniformly exponentially for $\tau \geq 0$ if the switching communication graph $\mathcal{G}_{p(t)}$ is UCM. That is, under this connectivity condition all the coordination states $\gamma_i(t)$ converge to the same value and $\dot{\gamma}_i \to 0$ as $t \to \infty$.

Remark 4.1. A version of Definition 4.4 for directed graphs was introduced in (Lin et al. 2005*b*) where the term "Uniformly Quasi Strongly Connected" was used. Here, we adapt it for undirected graphs, thus the term "Uniformly Connected in Mean" seems to be more adequate. Theorem 3.4 in (Lin 2006) provides some of the results in (Lin et al. 2005*b*) for linear systems. Moreover, using the fact that we assume $p(t) \in S_{dwell}$ with a dwell time $\tau_D > 0$, Theorem 4.2 can be deduced from Theorem 1 in (Moreau 2004) where the concept of $\delta-$digraphs was used. More precisely, the results are the same if we set $K = kI$, and $\delta = k\tau_D$ in (Moreau 2004). Likewise, Theorem 4.3 can be derived from Theorem 2 in (Moreau 2004) where the authors consider the Metzler matrices; matrices with all row-sums equal to zero. It is important to underline that matrix $-KL_p$ is a Metzler matrix.

4.2.4 System interconnections. Systems with brief instabilities

We now present a lemma that will be instrumental in deriving the performance measure (decay rate) associated with the coordination algorithm that will be later derived for multi-vehicle systems communicating over networks with brief connectivity losses (Definition 4.3). Here, we avail ourselves of some important results on brief instabilities[3]. See (Hespanha et al. 2004).

Lemma 4.3 System interconnection and brief instabilities

Consider a coupled system consisting of two subsystems

$$\dot{z}_1 = \phi_1(t, z_1, z_2, u_1),$$
$$\dot{z}_2 = \phi_2(t, z_1, z_2, u_2),$$

where z_1 and z_2 denote the state vectors and u_1 and u_2 the inputs. Assume that Lyapunov

[3]Consider the switching linear system $S : \dot{x} = A_p x + B_p u$, with characteristic function $\chi(p) = 0$ if S is stable, and $\chi(p) = 1$ otherwise. Let the instability time $T_p(t, \tau)$ be defined as in (4.10). Then, S has brief instabilities with instability bound T_0 and asymptotic instability rate α if T_p satisfies (4.11).

functions $V_1(t,z_1)$ and $V_2(t,z_2)$ exist and satisfy

$$\begin{aligned} \underline{\alpha}_1\|z_1\|^2 \le V_1 \le \bar{\alpha}_1\|z_1\|^2 \\ \underline{\alpha}_2\|z_2\|^2 \le V_2 \le \bar{\alpha}_2\|z_2\|^2 \end{aligned} \tag{4.16}$$

and

$$\begin{aligned} \tfrac{\partial V_1}{\partial t} + \tfrac{\partial V_1}{\partial z_1}\phi_1 \le -\lambda_1 V_1 + \rho_1\|z_2\|^2 + u_1^2 \\ \tfrac{\partial V_2}{\partial t} + \tfrac{\partial V_2}{\partial z_2}\phi_2 \le -\lambda_2(t) V_2 + \rho_2\|z_1\|^2 + u_2^2 \end{aligned} \tag{4.17}$$

where $\underline{\alpha}_i$, $\bar{\alpha}_i$, ρ_i; $i = 1,2$, and λ_1 are positive values, and system 2 is subjected to brief instabilities characterized by some function $\chi(p)$ and a switching signal $p(t)$. Suppose the brief instabilities are of the form

$$\lambda_2(p) = \begin{cases} \lambda_2 & \chi(p) = 0 \\ -\tilde{\lambda}_2 & \chi(p) = 1, \end{cases}$$

where $\lambda_2 > 0, \tilde{\lambda}_2 \ge 0$, with asymptotic instability rate α and instability bound T_0. Let

$$\lambda_0 := \frac{1}{2}(\lambda_1+\lambda_2) - \sqrt{\frac{1}{4}(\lambda_1+\lambda_2)^2 - \lambda_1\lambda_2 + \frac{\rho_1\rho_2}{\underline{\alpha}_1\underline{\alpha}_2}} \tag{4.18}$$

which satisfies

$$\min(\lambda_1,\lambda_2) - \sqrt{\frac{\rho_1\rho_2}{\underline{\alpha}_1\underline{\alpha}_2}} \le \lambda_0 \le \max(\lambda_1,\lambda_2) - \sqrt{\frac{\rho_1\rho_2}{\underline{\alpha}_1\underline{\alpha}_2}}.$$

Assume that $\alpha < \lambda_0/(\lambda_2+\tilde{\lambda}_2)$ and

$$\rho_1\rho_2 < \underline{\alpha}_1\underline{\alpha}_2\lambda_1\lambda_2. \tag{4.19}$$

Then

1. *the interconnected system is ISS with respect to state $z = \mathrm{col}(z_1,z_2)$ and input $u = \mathrm{col}(u_1,u_2)$,*

2. *there is a Lyapunov function $V(t,z)$ such that*

$$\begin{aligned} \underline{\alpha}\|z\|^2 \le V \le \bar{\alpha}\|z\|^2 \\ V(t) \le cV(t_0)e^{-\lambda(t-t_0)} + g\sup_{[t_0,t]} u^2 \end{aligned} \tag{4.20}$$

where $c = e^{(\lambda_2+\tilde{\lambda}_2)(1-\alpha)T_0}$, $g = \frac{c}{\lambda}\max(1, \underline{\alpha}_1(\lambda_1-\lambda_0)/\rho_2)$, and the rate of convergence is given by $\lambda = \lambda_0 - \alpha(\lambda_2+\tilde{\lambda}_2)$.

In particular, if $\rho_2 = 0$ *and* $\rho_1 > 0$*, then the interconnected system takes a cascade form and is ISS with input u and state z and exhibits convergence rate* $\lambda = \min(\lambda_1, (1-\alpha)\lambda_2 - \alpha\tilde{\lambda}_2)$*. The conclusions are also valid with* $\alpha = 0$ *for the case where system 2 has no instabilities, that is,* $\lambda_2(t) = \lambda_2$*.*

Proof. See the Appendix. □

The reader is referred to (Ito 2002) for the results in the case where system 2 has no brief instabilities.

Equipped with the results derived so far the main results of this chapter are presented next. The following two sections offer solutions to the coordinated path-following problem formulated in Section 4.1.

4.3 Coordinated path-following: no communication delays

Consider now the coordination control problem introduced in Section 4.1 with a switching communication topology parameterized by $p : [0,\infty) \to \{0,1\}$ and with no communication delays.

Recall that the coordination states γ_i are governed by the work in (4.8). Inspired by (Tsitsiklis & Athans 1984, Jadbabaie et al. 2003), we propose the following decentralized feedback law for the reference speeds v_{r_i} as a function of the information obtained from the neighboring vehicles:

$$v_{r_i} = v_{\mathscr{L}} - k_i \sum_{j \in N_{i,p(t)}} \gamma_i(t) - \gamma_j(t) \tag{4.21}$$

where $v_{\mathscr{L}}(t)$ is the assigned speed to the fleet of mobile agents and $k_i > 0$. Notice that with this choice of control law, the term $\tilde{v}_{r_i} = v_{r_i} - v_{\mathscr{L}}$ (for which the time derivative is not available) is given by

$$\tilde{v}_{r_i} = -k_i \sum_{j \in N_{i,p(t)}} \gamma_i(t) - \gamma_j(t). \tag{4.22}$$

Using (4.8), (4.21), and Lemma 4.1 - property 9, the coordination control closed-loop system can be written in vector form as

$$\dot{\gamma} = -KL_{p(t)}\gamma + v_{\mathscr{L}}\mathbf{1} + g_\eta \eta, \tag{4.23}$$

where K =diag$[k_i]$. The auxiliary term g_η was added for the simplicity of the exposition: $g_\eta = 1$ when the closed-loop PF system is of type I (η is considered a state), and $g_\eta = 0$ when the PF system is of type II ($\eta = \mathbf{0}$), see Assumption 4.1. Using properties 2 and 6 of Lemma 4.1, the coordination dynamics (4.23) take the form

$$\dot{\tilde{\gamma}} = -KL_p\tilde{\gamma} + g_\eta \mathscr{L}_\beta \eta. \tag{4.24}$$

Notice from (4.23) that η can be viewed as a coupling term from the path-following to the coordination dynamics.

We now consider n path-following subsystems, each satisfying Assumption 4.1. Let $\zeta = [\zeta_i]_{n\times 1}$ and $V_1 = \sum_i W_i$. Then

$$\begin{aligned} &\underline{\alpha}_1\|\zeta\|^2 \leq V_1 \leq \bar{\alpha}_1\|\zeta\|^2 \\ &\dot{V}_1 \leq -\lambda_1 V_1 + \rho_1 n^2 k_M^2\|\tilde{\gamma}\|^2 + u_1^2 \end{aligned} \tag{4.25}$$

where

$$u_1^2 := \sum_{i=1}^{n} d_i^2. \tag{4.26}$$

To show this, it is enough to use (4.6), (4.7) and the fact that

$$\sum_{i=1}^{n} |\tilde{v}_{r_i}|^2 = \tilde{\gamma}^T L_p K^2 L_p \tilde{\gamma} \leq n^2 k_M^2 \|\tilde{\gamma}\|^2 \tag{4.27}$$

where $k_M := \max_i k_i$, and $\tilde{v}_{r_i}$ and $\tilde{\gamma}$ are defined in (4.22) and (4.12), respectively. See the Appendix for a complete proof of (4.27).

To derive an ISS inequality for the path-following subsystem (4.5) under Assumption 4.1, we start by integrating (4.25). Straightforward computations show that

$$\|\eta(t)\| \leq \|\zeta(t)\| \leq e^{-\bar{\lambda}_1(t-t_0)}\|\zeta(t_0)\| + \bar{\rho}_1 \sup_{\tau\in[t_0,t)} \|\tilde{\gamma}\| + \bar{\rho}_2\|u_1\| \tag{4.28}$$

where $\bar{\lambda}_1 = \frac{\underline{\alpha}_1}{2\bar{\alpha}_1}\lambda_1$, $\bar{\rho}_1 = \sqrt{\frac{\rho_1 n^2 k_M^2}{\lambda_1 \bar{\alpha}_1}}$, and $\bar{\rho}_2 = \frac{1}{\sqrt{\lambda_1 \bar{\alpha}_1}}$.

To deal with switching communication topologies, two approaches are introduced next: "brief connectivity losses", and "uniform switching topologies" as defined in Section 4.1. We present conditions under which the overall closed-loop system formed by the path-following and the coordination subsystems is stable. We also derive some convergence properties.

4.3.1 Brief connectivity losses

In this approach, we use the concept of brief connectivity losses (BCLs) in which the underlying communication graphs are assumed to be alternatively connected and disconnected.

The following result provides conditions under which the overall closed-loop system formed by the path-following and coordination subsystems is ISS.

Theorem 4.4 (CPF with BCLs)

Consider the interconnected system Σ depicted in Figure 4.1, consisting of n path following subsystems that satisfy Assumption 4.1 and the coordination subsystem (4.23) with a communication network subjected to BCLs characterized by (4.11). Let $k_m := \min_i k_i$ and define $k_g := \frac{\lambda_m^2 k_m^3}{n^2 k_M^3}$ and

$$\lambda_0 = \tilde{\lambda}_0 - \sqrt{\tilde{\lambda}_0^2 - k_m \lambda_m \lambda_1 (1 - \frac{\rho_1}{k_g \underline{\alpha}_1 \lambda_1})}$$

where $\tilde{\lambda}_0 = \frac{1}{2}(\lambda_1 + k_m \lambda_m)$, and λ_m as defined in Lemma 4.1–property 8. Assume the following conditions hold:

a) [PF of type I] *The asymptotic connectivity losses rate α satisfies*

$$\alpha < \frac{\lambda_0}{2 k_m \lambda_m}$$

and

$$\frac{\rho_1}{\underline{\alpha}_1 \lambda_1} < k_g.$$

b) [PF of type II] $\alpha < 1$.

Then, Σ is ISS with respect to the states $\tilde{\gamma}$ and ζ and input u_1 (see (4.47)). Furthermore, the path-following error vectors e_i, the speed tracking errors $|\dot{\gamma}_i - v_{\mathscr{L}}|$, and the coordination errors $|\gamma_i - \gamma_j|, \forall i, j \in \mathbb{N}_n$ converge exponentially fast to some ball around zero (depending on the size of u_1) as $t \to \infty$, with rate at least

$$\lambda = \begin{cases} \lambda_0 - 2\alpha k_m \lambda_m, & \text{PF of type I} \\ \min(\lambda_1, 2(1-\alpha) k_m \lambda_m), & \text{PF of type II.} \end{cases}$$

Proof. Choose the Lyapunov candidate function

$$V_2 := \frac{1}{2} \tilde{\gamma}^T K^{-1} \tilde{\gamma}$$

whose time derivative along the solutions of (4.24) is

$$\begin{aligned} \dot{V}_2 &= -\tilde{\gamma}^T L_p \tilde{\gamma} + g_\eta \tilde{\gamma}^T K^{-1} \mathscr{L}_\beta \eta \\ &\leq -\tilde{\gamma}^T L_p \tilde{\gamma} + g_\eta \|K^{-1/2} \tilde{\gamma}\| . \|K^{-1/2} \mathscr{L}_\beta \eta\| \end{aligned}$$

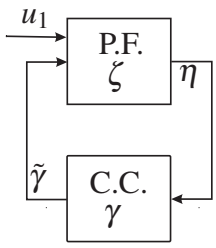

Figure 4.1: Σ: Overall closed-loop system consisting of the path-following and coordination control subsystems

Using properties 3 and 8 of Lemma 4.1 and Young's inequality, we obtain

$$\dot{V}_2 \leq \begin{cases} -\lambda_2 V_2 + \rho_2 \|\eta\|^2 & p \in P_c \\ \tilde{\lambda}_2 V_2 + \rho_2 \|\eta\|^2 & p \in P_{dc} \end{cases} \tag{4.29}$$

where $\lambda_2 = 2(\lambda_m k_m - g_\eta \theta_1)$, $\tilde{\lambda}_2 = 2 g_\eta \theta_1$, $\rho_2 = g_\eta \frac{1}{4 k_m \theta_1}$, and $0 < \theta_1 < \lambda_m k_m$.

Close inspection of (4.29) and (4.25) reveals that the coordination and the path-following subsystems form a feedback interconnected system with η and $\tilde{\gamma}$ as interacting signals, as shown in Figure 4.1. Therefore, according to Lemma 4.3, since system 2 has BCLs as defined in (4.11), the interconnected system is ISS from input d_1 provided that the following conditions are satisfied:

a) [*PF of type I*] For $g_\eta = 1$, from (4.19) we obtain

$$(\rho_1 n^2 k_M^2)(\frac{1}{4 k_m \theta_1}) < (\underline{\alpha}_1)(\frac{1}{2 k_M})(\lambda_1)(2\lambda_m k_m - 2 g_\eta \theta_1)$$

or

$$\frac{\rho_1}{\underline{\alpha}_1 \lambda_1} < \frac{4 k_m}{n^2 k_M^3} \theta_1 (\lambda_m k_m - g_\eta \theta_1)$$

whose right hand side is maximized for $\theta_1 = \frac{1}{2}\lambda_m k_m$. The results follow immediately.

b) [*PF of type II*] For $g_\eta = 0$, (4.29) simplifies to

$$\dot{V}_2 \leq \begin{cases} -\lambda_2 V_2 & p \in P_c \\ 0 & p \in P_{dc} \end{cases}$$

where $\lambda_2 = 2\lambda_m k_m$. Thus, resorting to Lemma 4.3 with $\tilde{\lambda}_2 = 0$ and $\rho_2 = 0$, the results follows. □

Remark 4.2. Consider as an example the coordination path-following problem of 3 agents ($n = 3$). Then $\lambda_m = 1$, and choosing $K = I$ yields $k_m = k_M = 1$. Let $\lambda_1 = 1$, $\underline{\alpha}_1 = \frac{1}{2}$. Thus the interconnected system is ISS from input d_1 if $\rho_1 < 1/18$ and $\alpha < (1 - \sqrt{18\rho_1})/2$ when PF is of type I. Notice that at best α must be smaller than $1/2$. However, Σ is ISS for any $\alpha < 1$ and any ρ_1 when PF is of type II. Taking for example, $\rho_1 = \frac{1}{72}$ and $\alpha = \frac{1}{5}$, the best estimate of the convergence rate is $\lambda = 0.1$ with η as state, while we obtain $\lambda = 1$ with $\eta = 0$.

4.3.2 Uniform switching topology

In this section, we consider the case where the communication network changes but the underlying communication graph is uniformly connected in mean (see Definition 4.4). Recall in this case that there is $T > 0$ such that for any $t \geq 0$, the union graph $\mathscr{G}([t, t+T))$ is connected.

Consider first the unforced coordination closed-loop dynamics, that is,

$$\dot{\tilde{\gamma}} = -KL_p\tilde{\gamma}. \tag{4.30}$$

First, we will show that if the switching communication graph is UCM (with parameter $T > 0$), then $\forall t > 0, \exists \tau \in [t, t+T)$, such that $L_{p(\tau)}\tilde{\gamma}(\tau) \neq 0$.

Let $V = \frac{1}{2}\tilde{\gamma}^T K^{-1}\tilde{\gamma}$ whose time derivative along the solutions of (4.30) is

$$\dot{V} = -\tilde{\gamma}^T L_p \tilde{\gamma}.$$

Notice that $\dot{V}$ is negative semi-definite, the graph being connected or not. Thus $\tilde{\gamma}$ remains bounded.

Consider the sequence $t_i; i = 1, ..., q$ of switching times in the interval $[t, t+T)$, with $t \leq t_1 < t_q < t+T$ and $t_i \leq t_{i+1} - \tau_D; i = 1, ..., q-1$, where τ_D is the dwell time. Let $t_0 := \min(t, t_1 - \tau_D)$ and $T_1 := \max(t_q + \tau_D, t+T) - t_0$. With this construction $T \leq T_1 \leq T + 2\tau_D$, $t_1 - \tau_D \geq t_0$, and $t_q + \tau_D \leq t_0 + T_1$. We now show that $\exists \tau \in \mathbb{T}_1 := [t_0, t_0 + T_1)$ such that [4] $L_{p(\tau)}\tilde{\gamma}(\tau) \neq \mathbf{0}$.

[4] Notice that if $\exists \tau \in \mathbb{T}_1$ such that $L_{p(\tau)}\tilde{\gamma}(\tau) \neq \mathbf{0}$, then $\exists \tau_1 \in [t, t+T)$ such that $L_{p(\tau_1)}\tilde{\gamma}(\tau_1) \neq \mathbf{0}$ since $t_0 \leq t \leq t_0 + \tau_D$ and $t_0 + T_1 - \tau_D \leq t + T \leq t_0 + T_1$.

By contradiction, assume $L_p\tilde{\gamma} = \mathbf{0}\ \forall \tau \in \mathbb{T}_1$ and discard the trivial solution $\tilde{\gamma} = \mathbf{0}$. Then, from (4.30) we have $\dot{\tilde{\gamma}} = \mathbf{0}$, that is, $\tilde{\gamma}$ remains unchanged over $\mathbb{T}_1$. Thus,

$$0 = \sum_{i=0}^{q} L_{p(t_i)}\tilde{\gamma}(t_i) = \left(\sum_{i=0}^{q} L_{p(t_i)}\right)\tilde{\gamma}(t_0).$$

As shown in Section 4.2, since the graph is UCM, the matrix $\sum_{i=0}^{q} L_{p(t_i)}$ has rank $n-1$ and its kernel is span$\{\mathbf{1}\}$. As a consequence, $\tilde{\gamma}(t_0) \in$ span$\{\mathbf{1}\}$, which contradicts the fact that $\beta^T\tilde{\gamma} = 0$.

Therefore, during an interval of length T_1, there is an interval of at least length τ_D such that $L_p\tilde{\gamma} \neq \mathbf{0}$. Without loss of generality assume $L_{p(t_0)}\tilde{\gamma}(t_0) \neq \mathbf{0}$. It follows that

$$\dot{V}(\bar{t}) \leq \begin{cases} -\frac{\bar{\lambda}_m}{k_M}V(\bar{t}) & \bar{t} \in \mathbb{T}_D \\ 0 & \bar{t} \in \mathbb{T}_1 \backslash \mathbb{T}_D \end{cases} \tag{4.31}$$

where $\mathbb{T}_D := [t_0, t_0 + t_D)$ and $\bar{\lambda}_m$ is defined in Lemma 4.1–property 8. We can now conclude that the system (4.30) with UCM switching communication graphs has brief instabilities with asymptotic instability rate $\bar{\alpha} = 1 - \tau_D/T_1 \leq 1 - \tau_D/(T + 2\tau_D)$ and instability upper bound $\bar{T}_0 = T_1 - \tau_D \leq T + \tau_D$. At this point, we can use the results available for switching systems with brief instabilities in (Hespanha et al. 2004) to derive stability conditions and a lower bound on the convergence rate. However, we take an independent approach as follows. If a characteristic function $\bar{\chi}$ is defined as

$$\bar{\chi}(t) = \begin{cases} 0 & t \in \mathbb{T}_D \\ 1 & t \in \mathbb{T}_1 \backslash \mathbb{T}_D, \end{cases}$$

then $\dot{V}(t) \leq -\frac{\bar{\lambda}_m}{k_M}(1 - \bar{\chi}(t))V(t)$. Integrating this differential inequality yields

$$V(t) \leq cV(\tau)e^{-\bar{\lambda}_0(t-\tau)};\ \forall t \geq \tau \geq 0.$$

where $c = e^{\bar{\lambda}_m \bar{T}_0(1-\bar{\alpha})}$, $\bar{\lambda}_0 = (1-\bar{\alpha})\frac{\bar{\lambda}_m}{k_M}$, and where we used the fact that

$$\int_t^\tau \bar{\chi}(s)ds \leq \bar{\alpha}(t-\tau) + (1-\bar{\alpha})\bar{T}_0;\ \forall t \geq \tau \geq 0.$$

Therefore,

$$\|\tilde{\gamma}(t)\| \leq \frac{ck_M}{k_m}e^{-\bar{\lambda}_0(t-\tau)}\|\tilde{\gamma}(\tau)\|$$

and

$$\|\Phi_p(t,\tau)\| \leq \frac{ck_M}{k_m} e^{-\bar{\lambda}_0(t-\tau)}, \tag{4.32}$$

where $\Phi_p(t,\tau)$ denotes the state transition matrix of (4.30). Notice that the above inequality is valid for all $p(t) \in S_{dwell}$ such that the dynamic graph $\mathscr{G}_p$ is UCM. For a given switching signal $p(t)$, input $\eta(t)$, and initial state $\tilde{\gamma}(t_0)$, by the variation of constants formula the solution of (4.24) is given by

$$\tilde{\gamma}(t) = \Phi_{p(t)}(t,t_0)\tilde{\gamma}(t_0) + g_\eta \int_{t_0}^{t} \Phi_{p(t)}(t,\tau)\mathscr{L}_\beta \eta(\tau) d\tau;\ \forall t \geq t_0$$

which implies, using (4.32), that

$$\|\tilde{\gamma}(t)\| \leq \frac{ck_M}{k_m} e^{-\bar{\lambda}_0(t-t_0)}\|\tilde{\gamma}(t_0)\| + g_\eta \frac{ck_M}{\lambda_0 k_m} \sup_{\tau\in[t_0,t)} \eta(\tau). \tag{4.33}$$

Equipped with the technical machinery derived so far, the main results of this section are stated next.

Theorem 4.5 (CPF with UCM)

Consider the interconnected system Σ *depicted in Figure 4.1, consisting of n path-following subsystems that satisfy Assumption 4.1 and the coordination subsystem (4.23) with a communication network uniformly connected in mean with parameter* T*. Then,* Σ *is ISS with respect to the states* $\tilde{\gamma}$ *and* ζ *and input* u_1*, if*

$$\begin{cases} \sqrt{\frac{\rho_1 n^2 k_M^2}{\lambda_1 \bar{\alpha}_1}} \frac{ck_M}{\bar{\lambda}_0 k_m} < 1 & \text{PF of type I} \\ always & \text{PF of type II.} \end{cases}$$

Furthermore, the path-following error vectors e_i*, the speed tracking errors* $|\dot{\gamma}_i - v_{\mathscr{L}}|$*, and the coordination errors* $|\gamma_i - \gamma_j|, \forall i,j \in \mathbb{N}_n$ *converge exponentially fast to some ball around zero (depending on the size of* u_1*) as* $t \to \infty$*, with rate at least* $\min(\bar{\lambda}_0, \bar{\lambda}_1)$*.*

Proof. The result follows by applying the ISS version of the small gain theorem to the interconnection of systems (4.33) and (4.28). □

4.4 Coordinated path-following: delayed information

In this section, we study the coordinated path-following system when the communication channels have the same delay $\tau > 0$. We further assume that the path-following closed-loop subsystems are of type II, that is, $\eta = \mathbf{0}$.

In this case, the control law for the reference speed becomes a function of delayed information, that is

$$v_{r_i} = v_{\mathscr{L}} - k_i \sum_{j \in N_{i,p(t)}} \gamma_i(t) - \gamma_j(t-\tau). \tag{4.34}$$

Using (4.8) and (4.34), the closed-loop coordination subsystem can be written as

$$\dot{\gamma}(t) = v_{\mathscr{L}}\mathbf{1} - KD_{p(t)}\gamma(t) + KA_{p(t)}\gamma(t-\tau) \tag{4.35}$$

where D_p and A_p are the degree matrix and the adjacency matrix of the communication graph, respectively. We are now interested in determining conditions under which coordination is achieved, that is, finding conditions for the existence of a time signal $\gamma_0(t) \in \mathbb{R}$ such that $\gamma = \gamma_0(t)\mathbf{1}$ is a solution of (4.35). If this is the case, then by substituting this solution in (4.35) and using the fact that $A_p = D_p - L_p$, we obtain

$$\dot{\gamma}_0\mathbf{1} = v_{\mathscr{L}}\mathbf{1} - KD_p\gamma_0(t)\mathbf{1} + K(D_p - L_p)\gamma_0(t-\tau)\mathbf{1}$$

which simplifies to

$$\dot{\gamma}_0\mathbf{1} - v_{\mathscr{L}}\mathbf{1} = -(\gamma_0(t) - \gamma_0(t-\tau))KD_p\mathbf{1}. \tag{4.36}$$

This equality is possible iff all the rows of the right-hand side are equal for all time. Two cases are possible.

p1 $\gamma_0(t)$ is either a constant or a periodic signal with period τ: In this case $\gamma_0(t) - \gamma_0(t-\tau) = 0$ and the right-hand side of (4.36) equals zero. Thus (4.36) holds with $\dot{\gamma}_0 = v_{\mathscr{L}}$ where the formation speed $v_{\mathscr{L}}$ must be set to either zero or a periodic signal with period τ. These cases are not interesting from a practical stand point.

p2 $\forall t, KD_{p(t)} = kI$ for some $k > 0$. This requires that the degrees of the nodes of the switching communication graph $\mathscr{G}_p$ never vanish, that is, $|N_{i,p}| \neq 0$, $\forall t$, so that the

degree matrix is always nonsingular and we can set the control gains to $K = kD_p^{-1}$. Therefore, the control gains become piecewise constant as functions of p.

Next, we will address case **p2** and state the first result of the section. To lift the constraint $|N_{i,p}| \neq 0$ and have the coordinated path-following algorithm applicable to more general types of switching topologies, we will later modify control law (4.34).

Lemma 4.4

Consider the coordination system dynamics (4.8) with control law (4.34). Assume that $|N_{i,p(t)}| \neq 0$ for all time, and let the control gains be $k_i(t) = k/|N_{i,p(t)}|$. Then, the states γ_i uniformly exponentially agree if the underlying communication graph $\mathcal{G}_p$ is UCM. In other words, $|\gamma_i - \gamma_j| \to 0$ and $\dot{\gamma}_i \to \dot{\gamma}_0$ as $t \to \infty$, where γ_0 is a solution of the delay differential equation

$$\dot{\gamma}_0 = -k(\gamma_0(t) - \gamma_0(t-\tau)) + v_{\mathcal{L}}. \tag{4.37}$$

Proof. As explained above, with the control law (4.34), the coordination system takes the form (4.35). Let

$$\gamma(t) = \gamma_0(t)\mathbf{1} + \tilde{\gamma}(t) \tag{4.38}$$

and substitute γ from (4.38) in (4.35) to get

$$\begin{aligned} \dot{\gamma}_0(t)\mathbf{1} + \dot{\tilde{\gamma}} = \quad & -K(t)D_{p(t)}\tilde{\gamma}(t) + K(t)A_{p(t)}\tilde{\gamma}(t-\tau) + \\ & -K(t)D_{p(t)}\gamma_0(t)\mathbf{1} + K(t)A_{p(t)}\gamma_0(t-\tau)\mathbf{1} + v_{\mathcal{L}}\mathbf{1} \end{aligned} \tag{4.39}$$

which simplifies to

$$\dot{\tilde{\gamma}} = -k\tilde{\gamma}(t) + kD_p^{-1}A_p\tilde{\gamma}(t-\tau) \tag{4.40}$$

if $\gamma_0(t)$ is the solution of (4.37) and $K(t) = kD_p^{-1}$. From Theorem 4.3, states $\tilde{\gamma}_i$ in (4.40) agree uniformly exponentially. In particular, $\tilde{\gamma} \to 0$ as $t \to \infty$. Thus, from (4.38) $\gamma \to \gamma_0\mathbf{1}$ and the results follow. □

In general, if $v_{\mathcal{L}}$ is time-varying, the delayed differential equation (4.37) has no closed form solution. However, for the particular case of $v_{\mathcal{L}}$ constant, one solution is $\gamma_0(t) = v_{\mathcal{L}}^* t$

where $v^*_{\mathscr{L}} = \frac{v_{\mathscr{L}}}{1+k\tau}$. Notice that due to the transmission delay τ, there is a finite error in the speed tracking, that is, $\dot{\gamma}_i$ converges to $v^*_{\mathscr{L}}$ and not to $v_{\mathscr{L}}$.

Consider now the case where there are instants of time t for which $|N_{i,p(t)}| = 0$ for some $i \in \mathbb{N}_n$. We will present this part only for the case that $v_{\mathscr{L}}$ is constant, that is, $\gamma_0(t) = v^*_{\mathscr{L}} t$ and $v^*_{\mathscr{L}} = \frac{v_{\mathscr{L}}}{1+k\tau}$. In this case, (4.35) can be rewritten in terms of $\tilde{\gamma}$ defined in (4.38) as

$$\dot{\tilde{\gamma}} = -K(t)D_{p(t)}\tilde{\gamma}(t) + K(t)A_{p(t)}\tilde{\gamma}(t-\tau) + v^*_{\mathscr{L}}\tau(kI - K(t)D_p)\mathbf{1}. \tag{4.41}$$

Clearly, when $\tau = 0$ the agreement is achieved for any choice of positive definite K, because of Theorem 4.3. However, this is not the case when $\tau \neq 0$. For example, assume that the agreement dynamics (4.41) are at equilibrium, that is, $\dot{\gamma}_i = v^*_{\mathscr{L}}\ \forall i \in \mathbb{N}_n$. Then, at the times when $|N_{i,p(t)}| = 0$ for some i, the dynamics are disturbed by a signal of amplitude $kv^*_{\mathscr{L}}\tau = v_{\mathscr{L}} - v^*_{\mathscr{L}}$ through the row corresponding to the vertex whose valency vanishes. This problem arises from the fact that the formation at equilibrium would travel at speed $v^*_{\mathscr{L}}$, but during the time that $N_{i,p} = \emptyset$ (empty set) the corresponding coordination state is governed by dynamics $\dot{\gamma}_i = v_{\mathscr{L}}$. This can be resolved by applying different desired speeds when the vehicle has no neighbors. The solution is stated next.

Lemma 4.5

Consider the coordination system dynamics with control law

$$v_{r_i} = \begin{cases} v_{\mathscr{L}} + \frac{k}{|N_{i,p}|}\sum_{j\in N_{i,p}} \gamma_i(t) - \gamma_j(t-\tau), & N_{i,p} \neq \emptyset \\ v^*_{\mathscr{L}}, & N_{i,p} = \emptyset \end{cases} \tag{4.42}$$

where $k > 0$. Then the states γ_i uniformly exponentially agree if the underlying communication graph $\mathscr{G}_p$ is UCM. In other words, $|\gamma_i - \gamma_j| \to 0$ and $\dot{\gamma}_i \to v^*_{\mathscr{L}}$ as $t \to \infty$.

Proof. The dynamics of the closed-loop coordination scheme are written in vector form as

$$\dot{\gamma} = -KD_p\gamma(t) + KA_p\gamma(t-\tau) + \frac{v_{\mathscr{L}} - v^*_{\mathscr{L}}}{k}KD_p\mathbf{1} + v^*_{\mathscr{L}}\mathbf{1}.$$

Letting $\gamma(t) = v^*_{\mathscr{L}} t\mathbf{1} + \tilde{\gamma}(t)$ simplifies the closed-loop dynamics to

$$\dot{\tilde{\gamma}} = -KD_p\tilde{\gamma}(t) + KA_p\tilde{\gamma}(t-\tau)$$

whose agreement property is guaranteed according to Theorem 4.3. The results follow immediately. □

Notice that in order to implement the control law (4.42), the different agents need to know the delay τ to compute $v^*_{\mathscr{L}}$. This raises the interesting question whether it is possible or not to estimate $v^*_{\mathscr{L}}$. We will not study this issue here.

Theorem 4.6 (CPF-delay)

Consider system Σ that is obtained by putting together the n path-following subsystem that satisfies Assumption 4.1 and the coordination subsystems studied in Lemma 4.4 / 4.5. Then, Σ is ISS with input d_1. In particular, the path-following errors $\|e_i\|$ tend to some ball around zero, and the coordination errors $|\gamma_i - \gamma_j|$ and the speed tracking errors $|\gamma_i - v^*_{\mathscr{L}}|$ converge to zero exponentially.

Proof. From (4.34) / (4.42), the signal $\tilde{v}_{r_i} = v_{r_i} - v_{\mathscr{L}}$ takes the form

$$\tilde{v}_{r_i} = k_i \sum_{j \in N_{i,p(t)}} \gamma_i(t) - \gamma_j(t-\tau). \tag{4.43}$$

From Lemma 4.4 / 4.5, we conclude that $\tilde{v}_{r_i}$ converges to zero exponentially. Equations (4.7) and (4.43) show that the path-following and coordination control subsystems form an interconnected cascade system where $\tilde{v}_{r_i}$ can be viewed as the output of the CC subsystem and the input of the PF subsystems. Since that latter is ISS from $\tilde{v}_{r_i}$, the results follow. □

Remark 4.3. The results developed in Section 4.4 are valid for communication networks with uni-directional links.

4.5 Underactuated autonomous vehicles

This section gives a solution to the coordinated path-following problem in Definition 4.2 for general underactuated autonomous vehicles for which the path-following closed-loop systems satisfy Assumption 4.1.

4.5.1 Path-following

Consider a general underactuated vehicle (GUV) modeled as a rigid body subject to external forces and torques. Let $\{\mathrm{U}\}$ be an inertial coordinate frame and $\{\mathrm{B}\}$ a body-fixed coordinate frame whose origin is located at the center of mass of the vehicle. The configuration $(R,\mathbf{p})$ of the vehicle is an element of the Special Euclidean group $SE(3) := SO(3)\times\mathbb{R}^3$, where $R \in SO(3) := \{R \in \mathbb{R}^{3\times 3} : RR^T = I_3, \det(R) = +1\}$ is a rotation matrix that describes the orientation of the vehicle and maps body coordinates into inertial coordinates, and $\mathbf{p} \in \mathbb{R}^3$ is the position of the origin of $\{\mathrm{B}\}$ in $\{\mathrm{U}\}$. Denote by $\nu \in \mathbb{R}^3$ and $\omega \in \mathbb{R}^3$ the linear and angular velocities of the vehicle relative to $\{\mathrm{U}\}$ expressed in $\{\mathrm{B}\}$, respectively. The following kinematic relations apply

$$\dot{\mathbf{p}} = R\nu, \tag{4.44a}$$

$$\dot{R} = RS(\omega), \tag{4.44b}$$

where

$$S(x) := \begin{bmatrix} 0 & -x_3 & x_2 \\ x_3 & 0 & -x_1 \\ -x_2 & x_1 & 0 \end{bmatrix}, \quad \forall x := (x_1,x_2,x_3)^T \in \mathbb{R}^3.$$

We consider here underactuated vehicles with dynamic equations of motion of the following form

$$\mathbf{M}\dot{\nu} = -S(\omega)\mathbf{M}\nu + f_\nu(\nu,\mathbf{p},R) + B_1u_1, \tag{4.45a}$$

$$\mathbf{J}\dot{\omega} = f_\omega(\nu,\omega,\mathbf{p},R) + B_2u_2, \tag{4.45b}$$

where $\mathbf{M} \in \mathbb{R}^{3\times 3}$ and $\mathbf{J} \in \mathbb{R}^{3\times 3}$ denote constant symmetric positive definite mass and inertia matrices; $u_1 \in \mathbb{R}$ and $u_2 \in \mathbb{R}^3$ denote the control inputs, which act upon the system through a constant nonzero vector $B_1 \in \mathbb{R}^3$ and a constant nonsingular matrix $B_2 \in \mathbb{R}^{3\times 3}$, respectively; and $f_\nu(\cdot)$, $f_\omega(\cdot)$ represent all the remaining forces and torques acting on the body.

For the special case of an underwater vehicle, $\mathbf{M}$ and $\mathbf{J}$ also include the so-called hydrodynamic added-mass M_A and added-inertia J_A matrices, respectively, i.e., $\mathbf{M} = M_{RB} + M_A$, $\mathbf{J} = J_{RB} + J_A$, where M_{RB} and J_{RB} are the rigid-body mass and inertia matrices, respectively. See (Fossen 1994) for details.

A solution to the path-following problem (Definition 4.1) of an autonomous underactuated vehicle was given in (Aguiar & Hespanha 2004, 2006) where the control laws require that $\dot{\gamma}_i$ and $\ddot{\gamma}_i$ be known. Recall that we decomposed the desired speed profile to two parts as $v_{r_i} = v_{\mathscr{L}} + \tilde{v}_{r_i}$ in which only the derivatives of $v_{\mathscr{L}}$ can be computed accurately. However, it can be shown that in the control laws of (Aguiar & Hespanha 2004, 2006), if the terms $\dot{\gamma}_i$ and $\ddot{\gamma}_i$ are replaced with $v_{\mathscr{L}}$ and $\dot{v}_{\mathscr{L}}$, respectively, the resulting path-following closed-loop system becomes input-to-state stable (ISS) from $\tilde{v}_{r_i}$ as input. This leads to the following result. In this section, for ease of presentation we delete the subscript i from most of the variables.

Theorem 4.7 (PF-GUV)
Consider a GUV with the equations of motion given by (4.44) and (4.45) with a desired path $\mathbf{p}_d(\gamma)$ in 3D-space to follow. There is a control law for u_1 and u_2 as a function of the local states, $\mathbf{p}_d$, $v_{\mathscr{L}}$, and $\dot{v}_{\mathscr{L}}$ that makes the closed-loop system satisfy Assumption 4.1.

Proof. The design methodology is based on Lyapunov-based theory and backstepping techniques.

Step 1. Define the global diffeomorphic coordinate transformation

$$\mathbf{e} := R^T(\mathbf{p} - \mathbf{p}_d(\gamma_i))$$

which expresses the path tracking error $\mathbf{p} - \mathbf{p}_d$ in body-fixed frame. Recall $\eta = \dot{\gamma}_i - v_r$ the speed tracking error, where $v_r = v_{\mathscr{L}} + \tilde{v}_r$ is the reference speed profile. In sequel, for simplicity of the presentation we assume that $v_{\mathscr{L}}$ is constant. The derivative of $\mathbf{e}$ yields

$$\dot{\mathbf{e}} = -S(\omega)\mathbf{e} + \nu - v_{\mathscr{L}} R^T \mathbf{p}_d^{\gamma} - \tilde{\eta} R^T \mathbf{p}_d^{\gamma}$$

where $\tilde{\eta} := \eta + \tilde{v}_r$ and superscript γ stands for the partial derivative $\frac{\partial}{\partial \gamma}$, for example $\mathbf{p}_d^{\gamma} = \frac{\partial \mathbf{p}_d}{\partial \gamma}$ and $\mathbf{p}_d^{\gamma^2} = \frac{\partial^2 \mathbf{p}_d}{\partial \gamma^2}$.

We start by defining the Lyapunov function $W_1 := \frac{1}{2}\mathbf{e}^T\mathbf{e}$ and compute its time derivative to obtain

$$\dot{W}_1 = \mathbf{e}^T(\nu - v_{\mathscr{L}} R^T \mathbf{p}_d^\gamma) - \tilde{\eta}\mathbf{e}^T R^T \mathbf{p}_d^\gamma,$$

and where we used the fact that $\mathbf{e}^T S(\omega)\mathbf{e} = 0 \; \forall \mathbf{e}, \omega \in \mathbb{R}^3$. We regard ν as a virtual control signal and introduce the virtual control tracking error variable

$$z_1 := \nu - v_{\mathscr{L}} R^T \mathbf{p}_d^\gamma + k_e M^{-1}\mathbf{e}.$$

Then $\dot{W}_1$ can be rewritten as

$$\dot{W}_1 = -k_e \mathbf{e}^T M^{-1}\mathbf{e} + \mathbf{e}^T z_1 + \alpha_1 \tilde{\eta},$$

where $\alpha_1 := -\mathbf{e}^T R^T \mathbf{p}_d^\gamma$. Now we would like to drive z_1 to zero aiming at making $\dot{W}_1$ negative.

Step 2. The time derivative of z_1 yields

$$M\dot{z}_1 = v_{\mathscr{L}}\Gamma\omega + S(Mz_1)\omega + B_1 u_1 + \tilde{\eta}h_1 + h_2$$

where

$$\begin{aligned} \Gamma :=& \quad MS(R^T\mathbf{p}_d^\gamma) - S(MR^T\mathbf{p}_d^\gamma) \\ h_1 :=& \quad -v_{\mathscr{L}} MR^T \mathbf{p}_d^{\gamma^2} - k_e R^T \mathbf{p}_d^\gamma \\ h_2 :=& \quad f_\nu + k_e \nu + v_{\mathscr{L}} h_1 \end{aligned}$$

It turns out that due to lack of actuation, it is not always possible to drive z_1 to zero. Instead, we drive z_1 to a constant design vector $\delta \in \mathbb{R}^3$. To this effect, we define a new error vector $\phi := z_1 - \delta$ and the augmented Lyapunov function

$$W_2 := W_1 + \frac{1}{2}\phi^T M^2 \phi$$

whose derivative yields

$$\dot{W}_2 = -k_e \mathbf{e}^T M^{-1}\mathbf{e} + \mathbf{e}^T\delta + \phi^T M(B\zeta + M^{-1}\mathbf{e} + h_2) + \alpha_2\tilde{\eta}$$

where

$$\alpha_2 := \alpha_1 + \phi^T M h_1, \tag{4.46}$$

$$B := \begin{pmatrix} B_1 & S(M\delta) + v_{\mathscr{L}}\Gamma \end{pmatrix}, \text{ and } \zeta := \begin{pmatrix} u_1 \\ \omega \end{pmatrix},$$

where we used the fact that $\phi^T MS(Mz_1)\omega = \phi^T MS(M\delta)\omega$. Matrix B can be always made full rank, see (Aguiar & Hespanha 2006) for details. Let

$$\beta_1 := B^T(BB^T)^{-1}(-h_2 - M^{-1}\mathbf{e} - k_\phi \phi).$$

To accomplish this step, we set u_1 to be the first entry of β_1, that is

$$u_1 = \pi_1 \beta_1, \quad \pi_1 := (1\ 0_{1\times 3}) \tag{4.47}$$

and introduce the error variable

$$z_2 := \omega - \Pi\beta_1, \ \Pi := \begin{pmatrix} 0_{3\times 1} & I_{3\times 3} \end{pmatrix},$$

that we would like to drive to zero. Now, we can rewrite

$$\dot{W}_2 = -k_e \mathbf{e}^T M^{-1}\mathbf{e} + \mathbf{e}^T\delta - k_\phi \phi^T M\phi + \phi^T MB\Pi^T z_2 + \alpha_2\tilde{\eta}.$$

Remark 4.4. Notice that

$$|\alpha_2| \leq k_1\|\mathbf{e}\| + (k_2 + k_3 k_e)\|\phi\| \tag{4.48}$$

for some $k_i > 0$, $i = 1,2,3$, defined by $v_{\mathscr{L}}$, M, $\mathbf{p}_d^\gamma$ and $\mathbf{p}_d^{\gamma^2}$.

Step 3. Define

$$W_3 := W_2 + \frac{1}{2} z_2^T J z_2 \tag{4.49}$$

whose time derivative applying the control law

$$u_2 = B_2^{-1}(-f_\omega + J\Pi\dot{\beta}_1 - \Pi B^T M\phi - k_z z_2) \tag{4.50}$$

yields

$$\dot{W}_3 = -k_e \mathbf{e}^T M^{-1}\mathbf{e} + \mathbf{e}^T\delta - k_\phi \phi^T M\phi - k_z z_2^T z_2 + \alpha_2\tilde{\eta}. \tag{4.51}$$

Now, use (4.48), (4.51) and Young's inequality, to compute

$$\begin{aligned}\dot{W}_3 \leq\ & -(k_e m - \tfrac{1}{4\lambda_1} - \tfrac{k_1}{4\lambda_2})\|\mathbf{e}\|^2 \\ & -(k_\phi - \tfrac{k_3 k_e + k_2}{4\lambda_3})\|\phi\|^2 - k_{z_2}\|z_2\|^2 \\ & +\lambda_1\|\delta\|^2 + ((k_3 k_e + k_2)\lambda_3 + k_1\lambda_2)|\tilde{\eta}|^2\end{aligned}$$

for some $\lambda_1, \lambda_2, \lambda_3 > 0$, where $m = \|\mathbf{M}^{-1}\|$, $k_\phi = \|K_\phi\|$ and $k_{z_2} = \|K_{z_2}\|$. Choose

$$\lambda_1 = \tfrac{\lambda_4}{2k_1^2}, \quad \lambda_2 = \tfrac{\lambda_4}{2k_1}, \quad \lambda_3 = \tfrac{\lambda_4}{2(k_3 k_e + k_2)},$$

$$k_e = \tfrac{2k_1^2}{m\lambda_4}, \qquad\qquad k_\phi = \tfrac{(k_3 k_e + k_2)^2}{\lambda_4}$$

for some $\lambda_4 > 0$ to get

$$\begin{aligned}\dot{W}_3 \leq\ & -\tfrac{1}{2}mk_e\|\mathbf{e}\|^2 - \tfrac{1}{2}k_\phi\|\phi\|^2 - k_{z_2}\|z_2\|^2 \\ & +\lambda_1\|\delta\|^2 + \lambda_4|\tilde{\eta}|^2.\end{aligned} \tag{4.52}$$

Remark 4.5. For simplicity of the presentation, we do not expand $\dot{\beta}_1$, however, it is important to notice that to compute $\dot{\beta}_1$, we need $\tilde{\eta}$ or $\tilde{v}_r$, but not the time derivative of $\tilde{v}_r$.

Step 4. We can stop here and set $\dot{\gamma}_i = v_r$, that is, $\eta = 0$. In this case, $\tilde{\eta} = \tilde{v}_r$ and from (4.52) we have

$$\dot{W}_3 \leq -\lambda W_3 + \lambda_1\|\delta\|^2 + \lambda_4|\tilde{v}_r|,$$

for some $\lambda > 0$. That is the path-following closed-loop system is ISS with δ and $\tilde{v}_r$ as inputs and $\zeta_i = (\mathbf{e}, \phi, z_2)^T$ as state. An alternative solution is to augment the Lyapunov function

$$W_4 := W_3 + \frac{1}{2}\eta^2 = \frac{1}{2}\mathbf{e}^T\mathbf{e} + \frac{1}{2}\phi^T M^2\phi + \frac{1}{2}z_2^T J z_2 + \frac{1}{2}\eta^2.$$

Set the feedback law

$$\dot{\eta} = -\alpha_2 - k_\eta\eta \tag{4.53}$$

to make

$$\dot{W}_4 = -k_e\mathbf{e}^T M^{-1}\mathbf{e} - k_\phi\phi^T M\phi - k_z z_2^T z_2 - k_\eta\eta^2 + \mathbf{e}^T\delta + \alpha_2\tilde{v}_r$$

which can be rewritten as

$$\dot{W}_4 \leq -\lambda W_4 + g_1\|\delta\|^2 + g_2|\tilde{v}_r|, \tag{4.54}$$

for some $\lambda > 0$, $g_1 > 0$ and $g_2 > 0$. Again, this makes the closed-loop system ISS with δ and $\tilde{v}_r$ as inputs and $\zeta_i = (\mathbf{e}, \phi, z_2, \eta)^T$ as state. □

4.5.2 Coordinated path-following

Notice in step 4 in the proof of Theorem 4.7 that the reason why we set $\eta = \mathbf{0}$ (or we let η evolve according to (4.53)) was to eliminate term $\alpha_{2i}\tilde{\eta}_i$ (or $\alpha_{2i}\tilde{v}_{r_i}$) from $\dot{W}_3$ (or $\dot{W}_4$). In what follows we take an alternative route to eliminate those terms by exploiting the specific form of the coordination control Lyapunov function. In this section, we set

$$v_{r_i} = v_{\mathscr{L}};\ i \in \mathbb{N}_n, \tag{4.55}$$

where $v_{\mathscr{L}}$ is a desired speed profile assigned to the formation. Therefore $\tilde{v}_{r_i} = 0$, $\tilde{\eta}_i = \eta_i$ and the coordination dynamics (4.8) is reduced to

$$\dot{\gamma} = v_{\mathscr{L}}\mathbf{1} + \eta, \tag{4.56}$$

where $\gamma := [\gamma_i]_{n\times 1}$ is the vector of coordination states and $\eta = [\eta_i]_{n\times 1}$. Let

$$W := \sum_{i=1}^{n} W_{3i} = \frac{1}{2}\sum_{i=1}^{n}\left(\mathbf{e}_i^T\mathbf{e}_i + \phi_i^T M^2 \phi_i + z_{2i}^T J z_{2i}\right) \tag{4.57}$$

be a global Lyapunov function for n vehicles. Taking the time derivative of W yields

$$\dot{W} = \alpha_2^T\eta - \sum_{i=1}^{n}\left(k_e\mathbf{e}_i^T M^{-1}\mathbf{e}_i + \mathbf{e}_i^T\delta + k_\phi\phi_i^T M\phi_i + k_z z_{2i}^T z_{2i}\right) \tag{4.58}$$

where $\alpha_2 = [\alpha_{2i}]_{n\times 1}$. We start with a fixed communication topology in the next section and later we extend the results to deal with switching communication networks with brief connectivity losses.

Fixed communications network

This section presents a solution to the coordinated path-following problem with a fixed communication topology. We let

$$\eta = z - A_1^{-1}L\gamma - A_1^{-1}\alpha_2, \tag{4.59}$$

where L is the Laplacian matrix of the underlying communication graph and z is an auxiliary state governed by

$$\dot{z} = -(A_1 + A_2)z + L\gamma + \alpha_2, \tag{4.60}$$

where $A_1 = \text{diag}[a_{1_i}]$ and $A_2 = \text{diag}[a_{2_i}]$ are positive definite matrices. The resulting closed-loop coordination system is described by

$$\begin{aligned} \dot{\gamma} &= v_{\mathscr{L}}\mathbf{1} + z - A_1^{-1}L\gamma - A_1^{-1}\alpha_2 \\ \dot{z} &= -(A_1 + A_2)z + L\gamma + \alpha_2 \end{aligned} \tag{4.61}$$

Consider now the composite (coordination + path-following) Lyapunov function

$$V_c := \frac{1}{2}\theta^T\theta + \frac{1}{2}z^T z + W$$

where $\theta = M^T\gamma$ with M the incidence matrix, that is, $L = MM^T$. We assume that the underlying communication graph is connected; as a consequence, the dimension of the kernel of M^T is one and $M^T\mathbf{1} = \mathbf{0}$. Computing the time-derivative of V_c along the solutions of (4.61) yields

$$\dot{V}_c = -\eta^T A_1\eta - z^T A_2 z - \sum_{i=1}^{n}\left[k_e\mathbf{e}_i^T M^{-1}\mathbf{e}_i + \mathbf{e}_i^T\delta - k_\phi\phi_i^T M\phi_i - k_z z_{2i}^T z_{2i}\right].$$

It is now straightforward to prove the following result:

Theorem 4.8 (Fixed communication)

The feedback laws for u_{1_i}, u_{2_i} for each vehicle i given by (4.47) *and* (4.50) *together with* (4.59) *and* (4.60) *solve the coordinated path-following problem if the communication graph defined by the Laplacian L is connected. In particular, the path-following errors $\mathbf{e}_i$, the coordination errors $|\gamma_i - \gamma_j|$, and the speed tracking errors $|\gamma_i - v_{\mathscr{L}}|$ converge exponentially to some ball around 0 as $t \to \infty$. The radius of the ball is defined by δ (the constant vector defined in step 2 in the proof*[5] *of Theorem 4.7).*

The above results are the basis for the next section where the communication graph is allowed to change in such a way as to become alternately connected and disconnected.

[5] *See page 156.*

Switching communications network

Consider the multiple vehicle coordination problem with a switching communication topology parameterized by p as defined in Section 4.1. Define the "graph-induced coordination error" as $\theta := \bar{M}^T \gamma \in \mathbb{R}^{n-1}$, where $\bar{M}$ defined in Lemma 4.2. Because of the properties of $\bar{M}$, $\gamma_i = \gamma_j, \forall i, j$ is equivalent to $\theta = \mathbf{0}$. Consequently, if θ is driven to zero asymptotically, so are the coordination errors $\gamma_i - \gamma_j$ and the problem of coordinated path-following (defined in Section 4.1) is solved.

Define the coordination control law as in (4.59) for η and (4.60) for the auxiliary state z with $\alpha_2 \equiv 0$. Then the closed-loop coordination system is given by

$$\begin{aligned} \dot{\gamma} &= v_{\mathscr{L}} \mathbf{1} + z - A_1^{-1} L_p \gamma \\ \dot{z} &= -(A_1 + A_2) z + L_p \gamma \end{aligned} \tag{4.62}$$

In decentralized form, (4.62) yields

$$\begin{aligned} \dot{\gamma}_i &= v_{\mathscr{L}} + z_i - \tfrac{1}{a_{1_i}} \textstyle\sum_{j \in N_{i,p}} (\gamma_i - \gamma_j) \\ \dot{z}_i &= -(a_{1_i} + a_{2_i}) z_i + \textstyle\sum_{j \in N_{i,p}} (\gamma_i - \gamma_j). \end{aligned}$$

Let $x_c := (\theta, z)$ be the state of the coordination control (CC) subsystem and define

$$\begin{aligned} A_c(p) &:= \begin{pmatrix} -\bar{M}^T A_1^{-1} \bar{M} U_p^T U_p & \bar{M}^T \\ \bar{M} U_p^T U_p & -A_1 - A_2 \end{pmatrix}, \\ C_c(p) &:= \begin{pmatrix} -A_1^{-1} \bar{M} U_p^T U_p & I \end{pmatrix}. \end{aligned} \tag{4.63}$$

With this notation, the dynamics of x_c are governed by the the Linear Parametrically Varying (LPV) system

$$\begin{aligned} \dot{x}_c &= A_c(p) x_c \\ \eta &= C_c(p) x_c. \end{aligned} \tag{4.64}$$

We now present the main result of this section.

Theorem 4.9 (Main results)

For any brief connectivity losses satisfying $\alpha < 1$ and bounded T_0, there exist control gains such that the interconnected system consisting of the n PF subsystems and the CC subsystem is ISS with state (ζ, x_c) and input $\delta = [\delta_i]_{n \times 1}$.

To prove the theorem, we need the following lemmas.

Lemma 4.6

Consider the LPV system (4.64) with $A_1 = a_1 I, A_2 = a_2 I$. Then there exist $X > 0$, $\lambda_c > 0$ and $\lambda_d > 0$ such that

$$\begin{aligned} A_c(p)X + XA_c(p)^T &\leq -\lambda_c X, \quad \forall p \in P_c \\ A_c(p)X + XA_c(p)^T &\leq +\lambda_d X \quad \forall p \in P_{dc}. \end{aligned} \tag{4.65}$$

and λ_d/λ_c can be made arbitrarily small by proper choice of gains a_1 and a_2.

Proof. Let $\lambda_i \in \sigma(U_p^T U_p)$ and define $\bar{\lambda}_c := \max_{p\in P_c} \lambda_i$, and $\underline{\lambda}_c := \min_{p\in P_c} \lambda_i$.

Now, choose $X = \left(\begin{smallmatrix} I & 0 \\ 0 & xI \end{smallmatrix}\right)$ for some $x > 0$. By substituting X in (4.65) and using Schur's decomposition, it is straightforward to check that the inequalities in (4.65) are satisfied for

$$\begin{aligned} \lambda_d &= \sqrt{(a_1+a_2)^2 + x} - (a_1 + a_2) \\ \lambda_c &= \lambda_p(a_1 + 2a_2)/(2a_1a_2) \\ x &= a_1^2 a_2(\bar{\lambda}_c + \underline{\lambda}_c)/[(a_1+2a_2)(2a_1a_2 - \lambda_p)] \end{aligned} \tag{4.66}$$

where $\lambda_p := \bar{\lambda}_c\underline{\lambda}_c/(\bar{\lambda}_c + \underline{\lambda}_c)$. It is clear when $a_2 \to \infty$, then $\lambda_d \to 0$ and $\lambda_c \to \lambda_p/a_1$. □

Remark 4.6. If λ_c and λ_d are computed according (4.66), they are generally conservative. For specific communication graphs, better bounds can be obtained numerically by finding feasible solutions to the LMIs in (4.65).

Lemma 4.7

Consider the coordination control subsystem (4.64) with brief connectivity losses in the communication network, as defined in (4.11). If the asymptotic connectivity loss rate $\alpha < \lambda_c/(\lambda_c + \lambda_d)$, the states x_p and output η remain bounded and tend exponentially to zero.

Proof. Consider the control parameters as defined in Lemma 4.6 and define the Lyapunov function $V := x_c^T X^{-1} x_c$. The derivative of V along the solutions of (4.64) yields

$$\begin{aligned} \dot{V} &\leq -\lambda_c V, \quad p \in P_c \\ \dot{V} &\leq +\lambda_d V, \quad p \in P_{dc}. \end{aligned}$$

Then $\dot{V} \leq [-\lambda_c(1-\chi(p(t))) + \lambda_d \chi(p(t))]V$. By integrating the latter differential inequalities, it is possible to show that

$$V(t) \leq V(\tau) e^{-\lambda_c(t-\tau-T_p(\tau,t))+\lambda_d T_p(\tau,t)}, \quad \forall t \geq \tau \geq 0$$

which yields

$$V(t) \leq e^{-[(1-\alpha)\lambda_c - \alpha\lambda_d](t-t_0)} V(t_0) e^{(1-\alpha)(\lambda_c+\lambda_d)T_0}, \forall t \geq t_0 \geq 0$$

if the system has brief connectivity losses defined in (4.11). From the assumptions, $\lambda := [(1-\alpha)\lambda_c - \alpha\lambda_d] > 0$. Therefore, $V(t)$ remains bounded and tends to zero, so does x_c. Moreover, by choosing $r = \min(x^{-1}, a_1^2/(\bar{\lambda}_c^2 + x a_1^2))$, then $r C_c(p)^T C_c(p) \leq X^{-1}, \quad \forall p$ and $\eta^T(t)\eta(t) \leq \frac{1}{r} V(t)$, thus completing the proof. □

We are now ready to prove Theorem 4.9.

Proof of Theorem 4.9. Using (4.46) and Young's inequality, it follows from (4.58) that

$$\dot{W} \leq -\lambda_p W + g_1 \|\eta\|^2 + g_2 \|\delta\|^2, \tag{4.67}$$

for some $\lambda_p, g_1, g_2 > 0$, that is, the path-following subsystem with inputs η and δ and state ζ is ISS. In Lemma 4.6, we have showed that $\frac{\lambda_d}{\lambda_c}$ can be made arbitrarily small by increasing the gain a_2. As a consequence $\alpha < 1/(1+\frac{\lambda_d}{\lambda_c})$ and therefore, from Lemma 4.7, it follows that the CC subsystem is exponentially stable. Close examination of (4.67) and (4.64) shows that the CC and PF subsystems form an interconnected cascade system. Since the cascade interconnection of two ISS system is ISS, it follows that the resulting cascade system with input δ and states ζ and x_c is ISS. □

Example 4.1. Consider the problem of coordinated CPF of a group of 3 vehicles, that is, $n = 3$. Vehicle 2 is allowed to communicate with vehicles 1 and 3, but the latter two do not communicate between themselves directly. We consider situation where there are communication losses. Specifically, we assume that the failures in both links occur during a maximum of 75% of the time, with the failures occurring periodically with a period of 10[sec], that is, $\alpha = 0.75$ and $T_0 = 7.5$[sec]. The corresponding eigenvalues defined in the proof of Lemma 4.6 are given by $\bar{\lambda}_c = 3$, $\underline{\lambda}_c = 1$ and $\bar{\lambda}_d = 2$. For $a_1 = 1$ and $a_2 = 1.6$, we have $\lambda_c = 0.98$ and $\lambda_d = 0.12$. Increasing a_2 to 5 results in $\lambda_c = 0.85$ and $\lambda_d = 0.01$.

However, for $a_1 = 1$ and $a_2 \leq 1.5$, there are no λ_c and λ_d that satisfy the conditions of Lemma 4.6.

4.6 An illustrative example

This section illustrates the application of the previous results to underwater vehicles moving in three-dimensional space.

Coordinated path-following of autonomous underwater vehicles (AUVs) in 3-D space

Consider an ellipsoidal shaped underactuated AUV not necessarily neutrally buoyant. Let $\{\mathrm{B}\}$ be a body-fixed coordinate frame whose origin is located at the center of mass of the vehicle and suppose that we have available a pure body-fixed control force τ_u in the x_B direction and two independent control torques τ_q and τ_r about the y_B and z_B axes of the vehicle, respectively. The kinematics and dynamics equations of motion of the vehicle can be written as (4.44) and (4.45), where

$$
\begin{aligned}
&\mathbf{M} = \mathrm{diag}\{m_{11}, m_{22}, m_{33}\}, \mathbf{J} = \mathrm{diag}\{J_{11}, J_{22}, J_{33}\},\\
&u_1 = \tau_u, u_2 = (\tau_q, \tau_r)^T, B_1 = \begin{pmatrix} 1 \\ 0 \\ 0 \end{pmatrix}, B_2 = \begin{pmatrix} 0 & 0 \\ 1 & 0 \\ 0 & 1 \end{pmatrix},\\
&f_\nu = -D_\nu(\nu)\nu - \bar{g}_1(R), \quad f_\omega = -D_\omega(\omega)\omega - \bar{g}_2(R) - S(\nu)\mathbf{M}\nu - S(\omega)\mathbf{J}\omega\\
&D_\nu(\nu) = \mathrm{diag}\{X_{\nu_1} + X_{|\nu_1|\nu_1}|\nu_1|, Y_{\nu_2} + Y_{|\nu_2|\nu_2}|\nu_2|,\\
&\qquad Z_{\nu_3} + Z_{|\nu_3|\nu_3}|\nu_3|\},\\
&D_\omega(\omega) = \mathrm{diag}\{K_{\omega_1} + K_{|\omega_1|\omega_1}|\omega_1|, M_{\omega_2} + M_{|\omega_2|\omega_2}|\omega_2|,\\
&\qquad N_{\omega_3} + N_{|\omega_3|\omega_3}|\omega_3|\},\\
&\bar{g}_1(R) = R^T \begin{pmatrix} 0 \\ 0 \\ W-B \end{pmatrix}, \qquad \bar{g}_2(R) = S(r_\mathrm{B}) R^T \begin{pmatrix} 0 \\ 0 \\ B \end{pmatrix},
\end{aligned}
$$

and gravitational and buoyant forces are given by $W = mg$ and $B = \rho g \nabla$, respectively, where m is the mass of the vehicle, ρ is the mass density of the water, and ∇ is the volume of displaced water. In the simulations presented here, the physical parameters match those of the *Sirene* AUV described in (Aguiar & Pascoal 1997, Aguiar 2002).

Consider the CPF control of three underactuated AUVs. Vehicle 2 is allowed to communicate with vehicles 1 and 3, but the latter two do not communicate between themselves directly. To simulate losses in the communications, we considered the situation where both links fail 75% of the time, with the failures occurring periodically with a period of 10[sec]. Moreover, the information transmission delay is 5[sec]. Notice that during failures all the links become deactivated. Since in this scenario, the valencies of the nodes vanish periodically, we apply the results of Lemma 4.5. In the simulations, we used the control law (4.42)

with $k_i = 0.1[\text{sec}^{-1}]$ for $i = 1,2,3$.

Simulation results

In the simulations, the AUVs are required to follow paths of the form

$$\mathbf{p}_{d_i}(\gamma_i) = \left[c_1 \cos(\tfrac{2\pi}{T}\gamma_i + \phi_d), c_1 \sin(\tfrac{2\pi}{T}\gamma_i + \phi_d), c_2\gamma_i + z_{0_i}\right],$$

with $c_1 = 20\,\text{m}$, $c_2 = 0.05\,\text{m}$, $T = 400$, $\phi_d = -\frac{3\pi}{4}$, and $z_{0_1} = -10\,\text{m}, z_{0_2} = -5\,\text{m}, z_{0_3} = 0\,\text{m}$. The initial conditions are $\mathbf{p}_1 = (5\,\text{m}, -10\,\text{m}, -5\,\text{m})$, $\mathbf{p}_2 = (5\,\text{m}, -15\,\text{m}, 0\,\text{m})$, $\mathbf{p}_3 = (5\,\text{m}, -20\,\text{m}, 5\,\text{m})$, $R_1 = R_2 = R_3 = I$, and $\nu_1 = \nu_2 = \nu_3 = \omega_1 = \omega_2 = \omega_3 = \mathbf{0}$. The reference speed $v_{\mathscr{L}}$ was set to $v_{\mathscr{L}} = 0.5[\text{sec}^{-1}]$.

The vehicles are also required to keep a formation pattern that consists of having them aligned along a common vertical line. Figure 4.2 shows the trajectories of the AUVs. Figure 4.3 illustrates the evolution of the coordination and path-following errors while the communication links fail periodically. Clearly, the vehicles adjust their speeds to meet the formation requirements and the coordination errors $\gamma_{12} := \gamma_1 - \gamma_2$ and $\gamma_{13} := \gamma_1 - \gamma_3$ converge to zero.

4.7 Summary

This chapter addressed the problem of coordinated path-following control of a group vehicles in the presence of varying communication topologies and fixed time-delays.

The key contributions of the chapter are twofold: *i*) the class of vehicle considered is very general and encompasses underactuated vehicles, of which autonomous underwater vehicles with less number of actuators than degrees of freedom are an example, and *ii*) problems that arise due to temporary communication losses and fixed time delay are explicitly addressed in a rigorous mathematical framework.

A number of decentralized coordination schemes were developed. Two types of switching topologies were considered: brief connectivity losses and uniformly connected in mean. Stability and convergence issues of the resulting coordinated path-following systems were examined in detail. In the process, important properties of the interconnection of systems with brief instabilities were derived.

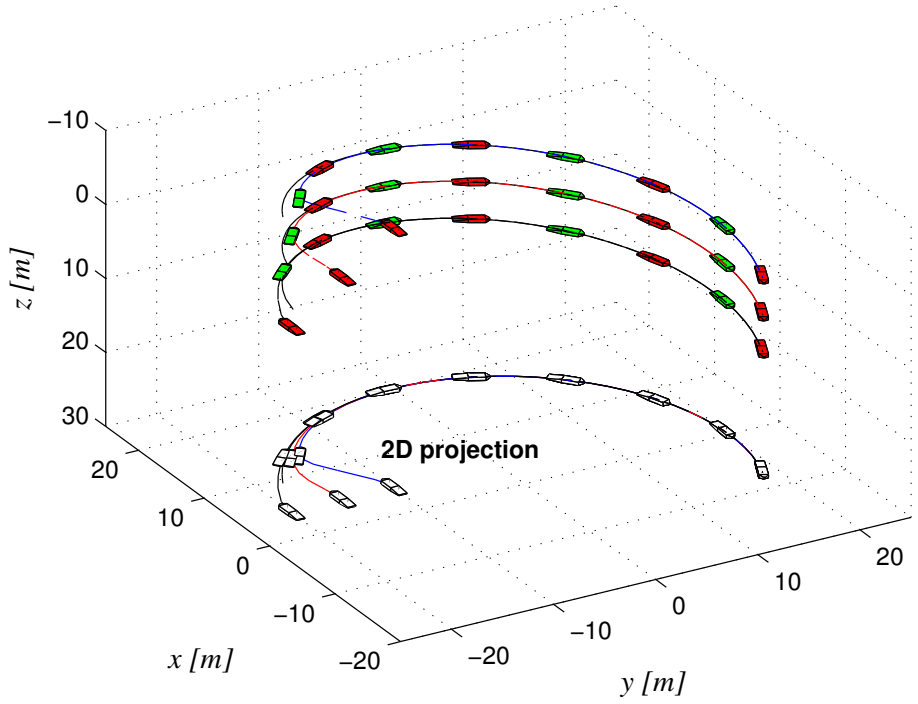

Figure 4.2: CPF of 3 AUVs with communication losses and time delays

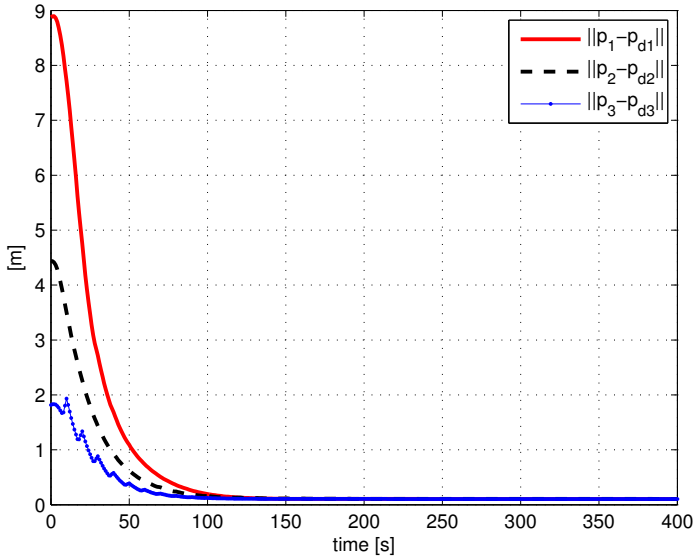

(a) path-following errors

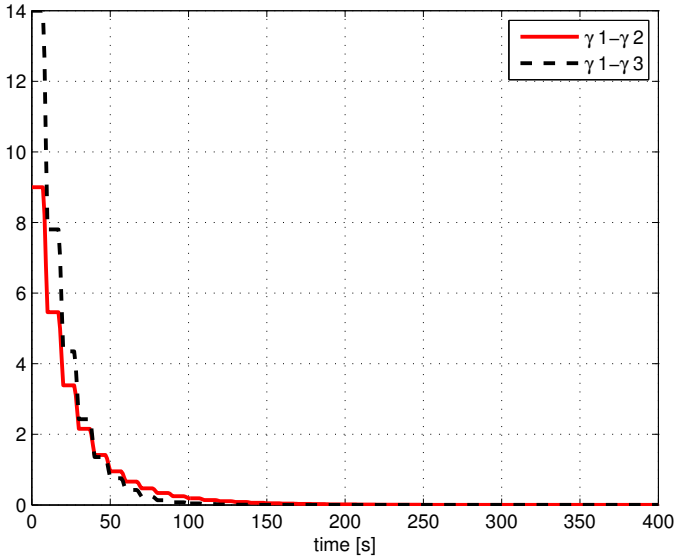

(b) Vehicle coordination errors

Figure 4.3: 75% of temporal communication losses; time delay 5[sec]

CHAPTER 5

CONCLUDING CHAPTER

This thesis addressed the problem of coordinated path-following (CFP) control of multiple vehicles subjected to inter-vehicle communication constraints. The problem is well rooted in challenging mission scenarios and has only recently come to the forum. Solutions were proposed to the CFP problem and their efficacy assessed in simulation.

The strategies adopted have a solid theoretical foundation in Lyapunov-based and Graph theory. The first is naturally suited for nonlinear system design and analysis, whereas the latter is steadily becoming the tool par excellence to capture the topologies of different communication scenarios. In this thesis it was shown how the two methodologies can be brought together to yield tools that effectively allow a system designer to study the stability and performance that can be obtained under different communication scenarios. To the best of our knowledge, this work is the first contribution towards quantifying the performance achievable with coordinated path-following control when the underlying communication network is time-varying and exhibits fixed delays.

The results in this thesis lead naturally to algorithms for CPF control that are applicable to heterogeneous fleets of vehicles evolving in 3D-space. The class of vehicle considered is very general and encompasses underactuated vehicles, of which autonomous underwater vehicles with less number of actuators than degrees of freedom are an example. Furthermore, the thesis addressed in a rigorous mathematical framework the problems that arise due to temporary communication losses and fixed time delays. A number of decentralized coordination schemes were developed and two types of switching topologies were considered: brief connectivity losses and uniformly connected in mean. Stability and convergence

issues of the resulting coordinated path-following systems were examined in detail. In the process, important properties of the interconnection of systems with brief instabilities were derived.

This work is a first step towards the derivation of advanced CPF algorithms for multiple vehicles in the presence of communication constraints and time-delays. Few authors have so far tackled these and related problems in a rigorous mathematical framework. Notable exceptions are the results published in (Fossen 2002), (Skjetne et al. 2002), and in a recent PhD thesis (Ihle 2006). See also (Arrichiello 2006) for a behavioral approach to the coordinated control problem of multiple wheeled robots. This research path is largely unexplored, and much work remains to be done towards the development of algorithms that can withstand the transition from the laboratory to the real world. Especially challenging is the development of new strategies to deal with the fact that communications occur asynchronously at discrete instants of time, and that there are time-varying, distance-dependent delays in the transmission of information among vehicles. Establishing a bridge between the present work and the work that is being carried out in the field of networked control systems is also important. A possible avenue of research is the inclusion of network observers as proposed in (Xu & Hespanha 2006) to facilitate the decision of when to transmit information from one vehicle to its neighbors. The problem of coordinated navigation to dispense with the use of expensive navigation systems installed on-board each vehicle warrants also further research effort. Finally, there is a need to prove the concepts developed in actual trials with multiple vehicles on land, air, and at sea.

CHAPTER 6

APPENDIX

6.1 Path-following control implementation

To implement control laws (3.14), (3.15), (3.16), and (3.17), we need to have access to the following values:

- Position and the orientation of the vehicle in $\{\mathrm{U}\}$-frame, (x, y, ψ_B).
- The path defined in $\{\mathrm{U}\}$-frame and associated with it a curvilinear abscissa s along the path measured from some convenient reference point.
- Curvature $c_c(s)$ of the path as a function of s.
- Vehicle's actual forward and angular velocities, (v, r).
- Estimation (using approximate derivative) of $\dot{v}$. This can be done as well by substituting from the dynamics, knowing that $\dot{v} = F$.

The procedure of calculation of control laws follows

1. Given s the variables ψ_T and $\mathbf{p}$ are known.
2. Compute (x_e, y_e) from (3.10).
3. Compute $\dot{s}$ from (3.15).
4. Compute $\dot{x}_e$, $\dot{y}_e$ and $\dot{\psi}_e$ from (3.11).

5. Integrate $\dot{s}$ to compute s. The values of s used in step 1 come from this step.

6. Do the following computations in order

$$\begin{aligned} \sigma &= -\tfrac{2\psi_a}{\pi}\operatorname{sign}(v)\arctan y_e \\ \tfrac{\partial\sigma}{\partial y_e} &= -\tfrac{2\psi_a}{\pi}\operatorname{sign}(v)\tfrac{1}{1+y_e^2} \\ \tfrac{\partial^2\sigma}{\partial y_e^2} &= \tfrac{2\psi_a}{\pi}\operatorname{sign}(v)\tfrac{2y_e}{(1+y_e^2)^2} \end{aligned}$$

7. $\dot{\sigma} = \frac{\partial\sigma}{\partial y_e}\dot{y}_e$

8. $\ddot{s} = \dot{v}\cos\psi_e - v\sin\psi_e\dot{\psi}_e + k_3\dot{x}_e$

9. $\ddot{y}_e = -\dot{x}_e c_c\dot{s} - x_e\frac{\partial c_c}{\partial s}\dot{s}^2 - x_e c_c\ddot{s} + \dot{v}\sin\psi_e + v\cos\psi_e\dot{\psi}_e$

10. $\ddot{\sigma} = \frac{\partial^2\sigma}{\partial y_e^2}\dot{y}_e^2 + \frac{\partial\sigma}{\partial y_e}\ddot{y}_e$

11. $\phi = c_c\dot{s} + \dot{\sigma} - k_1(\psi_e - \sigma)$

12. and compute N from (3.14) or (3.16).

6.2 Proofs

Proof of Lemma 1.1

Proof. Partition the time interval $[t_0, t]$ along the sequence $t_k = t_0 + kT$ for $k = 0, \ldots, n$ so that $t_n \le t < t_{n+1}$. Then $t_{k+1} - t_k = T$. Integrating (1.7) over $[t_k, t_{k+1}]$ yields

$$x(t_{k+1}) = e^{-a\int_{t_k}^{t_{k+1}}(1-p(t))dt}x(t_k).$$

Therefore,

$$|x(t_{k+1})| \le e^{-a(1-\alpha)T}|x(t_k)| \Rightarrow |x(t_n)| \le e^{-na(1-\alpha)T}|x(t_0)|.$$

Integrating (1.7) over $[t_n, t]$, we have $|x(t)| \le |x(t_n)|$ where we used the fact that $1 - p(t) \ge 0$. By combining the above inequalities and using the fact that $t - t_0 \le (n+1)T$, we get

$$|x(t)| \le be^{-\beta(t-t_0)}|x(t_0)|$$

where $b = e^{a(1-\alpha)T}$ and $\beta = (1-\alpha)a$ and the result follows. □

Proof of Lemma 4.1

1. Since $\text{Rank}(I-\mathscr{L}_\beta)=1$, $\mathscr{L}_\beta$ has $n-1$ eigenvalue at 1. Using the definition of $\mathscr{L}_\beta$, it can be easily verified that $\mathscr{L}_\beta \mathbf{1}=\mathbf{0}$ and $\beta^T\mathscr{L}_\beta=\mathbf{0}^T$, that is zero is an eigenvalue. Therefore, we can conclude that zero is a single eigenvalue.

2. $\mathscr{L}_\beta K L_p=(K-\frac{1}{\beta^T\mathbf{1}}\mathbf{1}\mathbf{1}^T)L_p=KL_p$, since $\mathbf{1}^TL_p=\mathbf{0}^T$.

3. Following some computations we get $\mathscr{L}_\beta^T K^{-1}\mathscr{L}_\beta=K^{-1}-\frac{1}{\beta^T\mathbf{1}}\beta\beta^T$. Then $\nu^T\mathscr{L}_\beta^T K^{-1}\mathscr{L}_\beta\nu=\nu^TK^{-1}\nu-\frac{1}{\beta^T\mathbf{1}}\nu^T\beta\beta^T\nu\leq\nu^TK^{-1}\nu$ for any $\nu\in\mathbb{R}^n$ and equality happens for $\beta^T\nu=0$, thus the result follows.

4. The result follows from the facts that $\tilde{\gamma}=\mathscr{L}_\beta\gamma$, $\mathscr{L}_\beta\mathbf{1}=\mathbf{0}$ and $\text{Rank}\mathscr{L}_\beta=n-1$.

5. Follows from the definition of $\tilde{\gamma}$ in (4.12).

6. Follows from the definition of $\tilde{\gamma}$ and the fact that $L_p\mathbf{1}=\mathbf{0}$.

7. Notice that

$$|\tilde{\gamma}_i-\tilde{\gamma}_j|^2=\tilde{\gamma}_i^2+\tilde{\gamma}_j^2-2\tilde{\gamma}_i\tilde{\gamma}_j\leq 2(\tilde{\gamma}_i^2+\tilde{\gamma}_j^2)\leq 2\|\tilde{\gamma}\|^2<2\varepsilon^2.$$

   but $\tilde{\gamma}_i-\tilde{\gamma}_j=\gamma_i-\gamma_j$, thus $|\gamma_i-\gamma_j|<\sqrt{2}\varepsilon$. For the next part, notice that $KL_p\gamma=KL_p\tilde{\gamma}$, then $\|KL_p\gamma\|\leq\|K\|.\|L_p\|.\|\tilde{\gamma}\|\leq n\varepsilon\|K\|$, where we used the fact that $\|L_p\|\leq n$ and equality happens for a complete graph, that is, $p=[1,...,1]^T$.

8. Recall the fact that if the graph is connected ($p\in P_c$), then L_p has a single eigenvalue at zero associated to the (right and left) eigenvector $\mathbf{1}$, and the rest of the eigenvalues are positive. Let L be a representative graph Laplacian of L_p for $p\in P_c$. Then, there is a unitary matric $U=[u_1,...,u_n]$ where $u_1=\frac{1}{\sqrt{n}}\mathbf{1}$ and a diagonal matrix $\Lambda=\text{diag}[\lambda_1,\lambda_2,...,\lambda_n]$ with $0=\lambda_1<\lambda_2\leq...\leq\lambda_n$, such that $L=U\Lambda U^T$. Then for any $\nu\in\mathbb{R}^n$, we have

$$\begin{aligned}
\nu^TL\nu &= \textstyle\sum_{i=1}^n\lambda_i(u_i^T\nu)^2\\
&= \textstyle\sum_{i=2}^n\lambda_i(u_i^T\nu)^2\\
&\geq \lambda_2\textstyle\sum_{i=2}^n(u_i^T\nu)^2\\
&= \lambda_2\textstyle\sum_{i=1}^n(u_i^T\nu)^2-\lambda_2(u_1^T\nu)^2\\
&= \lambda_2\nu^T\nu-\lambda_2\tfrac{1}{n}(\mathbf{1}^T\nu)^2.
\end{aligned}$$

To compute $\lambda_{2,m}$, simply observe that the second term is zero, therefore $\lambda_{2,m}$ is the minimum λ_2 over $p \in P_c$. Now if $\beta \neq \mathbf{1}$, an standard minimization of vector function $v^T v - \frac{1}{n}(\mathbf{1}^T v)^2$ with constraints $\beta^T v = 0$ and $v^T v = 1$, yields the results. Similarly, it can be shown that $\bar{\lambda}_m > 0$. Numerical computations show that $\lambda_{2,m} = \bar{\lambda}_m$.

9. Recall that the graph Laplacian is $L = D - A$. Using the definitions of degree matrix D and adjacency matrix A, by inspection, it is easy to show the result.

Proof of (4.27)

Denote the i'th column (or row) of L_p by $l_{i,p}$. Then $\tilde{v}_{r_i} = k_i l_{i,p}^T \gamma$. Now

$$\begin{aligned} \sum_i |\tilde{v}_{r_i}|^2 &= \sum_i k_i^2 \gamma^T l_{i,p} l_{i,p}^T \gamma \\ &= \gamma^T \sum_i k_i^2 l_{i,p} l_{i,p}^T \gamma \\ &= \gamma^T L_p K^2 L_p \gamma \\ &= \tilde{\gamma}^T L_p K^2 L_p \tilde{\gamma}. \end{aligned}$$

Therefore since $\max_{p,\|v\|=1} v^T L_p v = n$, the result follows. Notice that in this optimization, the equality happens for a complete graph, and n is the largest eigenvalue for all combinations of p.

Proof of Proposition 4.3 (system interconnection)

Choose $V = V_1 + aV_2$ for some $a > 0$ which is to be chosen later. Clearly, V satisfies the first condition of (4.20) for some $\underline{\alpha} > 0, \bar{\alpha} > 0$. Next, we will show that the second condition is also satisfied. Taking derivative of V yields

$$\dot{V} \leq -(\lambda_1 - \frac{a g_2}{\underline{\alpha}_1}) V_1 - a(\lambda_2 - \frac{g_1}{a \underline{\alpha}_2}) V_2 + g\|d\|^2$$

where $g = \max(1, a)$. At this stage assume g_1 and g_2 are nonzero. Let

$$\lambda_0 = \lambda_1 - \frac{a g_2}{\underline{\alpha}_1} = \lambda_2 - \frac{g_1}{a \underline{\alpha}_2}. \tag{6.1}$$

• $\lambda_2(t) = \lambda_2 > 0$: If there exist positive numbers λ_0 and a satisfying (6.1), then $\dot{V} \leq -\lambda_0 V + g\|d\|^2$ and therefore the interconnected system is ISS from d. The condition of existence of positive solutions is $g_1 g_2 < \underline{\alpha}_1 \underline{\alpha}_2 \lambda_1 \lambda_2$. From there the convergence rate is $\lambda = \lambda_0$.

• $\lambda_2(t)$ has brief instabilities: Using the same Lyapunov function $V = V_1 + aV_2$ and λ_0 as in (6.1), compute the derivative of V to obtian

$$\dot{V} \leq -\lambda_0 V + a(\lambda_2 - \lambda_2(t))V_2 + g\|d\|^2$$

which yields

$$\dot{V} \leq \begin{cases} -\lambda_0 V + g\|d\|^2 & \chi(p) = 0 \\ (\lambda_3 - \lambda_0)V + g\|d\|^2 & \chi(p) = 1, \end{cases}$$

where $\lambda_3 := \lambda_2 + \tilde{\lambda}_2$. Again such λ_0 exists if $g_1 g_2 < \underline{\alpha}_1 \underline{\alpha}_2 \lambda_1 \lambda_2$. Integrating the above differential inequalities and following similar computations as in (Hespanha et al. 2004), it is easy to show that

$$\begin{aligned} V(t) \leq \; & V(t_0) e^{-\lambda_0 (t - t_0 - T_p) + \lambda_4 T_p} + \\ & g \sup_{[t_0,t]} \|d\|^2 \int_{t_0}^{t} e^{-\lambda_0 (t - \tau - T_p) + \lambda_4 T_p} d\tau \end{aligned}$$

where $\lambda_4 := \lambda_3 - \lambda_0$. Notice that $\lambda_4 \geq 0$. This yields

$$V(t) \leq V(t_0) e^{-(\lambda_0 - \alpha\lambda_3)(t - t_0) + \lambda_3 T_\alpha} + \frac{e^{\lambda_3 T_\alpha}}{\lambda_0 - \alpha\lambda_3} g \sup_{[t_0,t]} d^2$$

where $T_\alpha = (1 - \alpha)T_0$, if the system has brief instabilities defined in (4.11). Therefore, the interconnected system is ISS from d as input if $\alpha < \lambda_0 / \lambda_3$.

If $g_2 = 0$ and $g_1 > 0$, the interconnected system takes a cascade configuration and the dynamics of system 2 are reduced to

$$\dot{V}_2 \leq \begin{cases} -\lambda_2 V_2 + d_2^2 & \chi(p) = 0 \\ \tilde{\lambda}_2 V_2 + d_2^2 & \chi(p) = 1, \end{cases}$$

whose solution takes the form

$$V_2(t) \leq V_2(t_0) e^{-(\lambda_2 - \alpha\lambda_3)(t - t_0) + \lambda_3 T_\alpha} + \frac{e^{\lambda_3 T_\alpha}}{\lambda_2 - \alpha\lambda_3} \sup_{[t_0,t]} d_2^2$$

where $\lambda_3 = \lambda_2 + \tilde{\lambda}_2$. Substituting it in the dynamics of system 1 and integration yields

$$V_1(t) \leq a_1 e^{-\lambda_1 t} + a_2 e^{-(\lambda_2 - \alpha\lambda_3)t} + a_3 \sup_{[t_0,t]} \|d\|^2.$$

for some $a_i \in \mathbb{R}$. Therefore, the cascade system is ISS from d as input if $\alpha < \lambda_2 / (\lambda_2 + \tilde{\lambda}_2)$ and the convergence rate will be $\min(\lambda_1, (1 - \alpha)\lambda_2 - \alpha\tilde{\lambda}_2)$.

Proof of Lemma 4.2

Proof. We first show that $\bar{M}\bar{M}^T M_p = M_p$. Since $\bar{M}^T\bar{M} = I$, then $\bar{M}\bar{M}^T$ has $n-1$ eigenvalues at 1 and one eigenvalue at 0. Thus, $\text{Rank}(I - \bar{M}\bar{M}^T) = 1$ and using the fact that $(I - \bar{M}\bar{M}^T)\mathbf{1} = \mathbf{1}$, then $(I - \bar{M}\bar{M}^T)v = \mathbf{0}$ if $v \in \mathbf{1}^\perp$ (the orthogonal space). On the other hand, $M_p^T\mathbf{1} = \mathbf{0}$, that is, M_p has $n-1$ columns orthogonal to $\mathbf{1}$. Therefore $(I - \bar{M}\bar{M}^T)M_p = 0$, or $\bar{M}\bar{M}^T M_p = M_p$. Thus $M_p^T = M_p^T\bar{M}\bar{M}^T = U_p\bar{M}^T$. To prove the second part of the Lemma, notice that

$$\begin{aligned}\sigma(U_p^T U_p) &= \sigma(U_p U_p^T) = \sigma(M_p^T\bar{M}\bar{M}^T M_p)\\ &= \sigma(M_p^T M_p) = \sigma(M_p M_p^T)\setminus\{0\}.\end{aligned}$$

□

Lemma 6.1

Lemma 6.1

Let $\mathcal{G}$ be a connected (undirected) graph with Laplacian L of dimension $n \times n$ and let $C(t) = \text{diag}[c_{ii}]_{n\times n}$ be a diagonal matrix satisfying $c_1 I \le C(t) \le c_2 I$; $c_1 > 0$. Define

$$Q(t) = C^{-1}(t)A^{-1}L + LC^{-1}(t)A^{-1} + 2C(t)^{-1}A,$$

where $A = \text{diag}[a_{ii}]_{n\times n} > 0$ and $a_1 I \le A \le a_2 I$. Suppose

$$a_1^2 > \frac{1}{2}\left(\frac{c_2}{c_1} - \frac{a_1}{a_2}\right)\max_i d_i \tag{6.2}$$

where $d_i = |N_i|$ is the cardinality of N_i, that is, the index set of the neighbors of vertex i in Graph $\mathcal{G}$. Then, there exists $\gamma > 0$ such that $\|Q(t)\| > \gamma$ for all $t \ge 0$.

Proof. L has the property that all its diagonal elements are positive and the off diagonals are non-positive. Because A and C are diagonal, Q inherits that property. This, together with Geršgorin's theorem (Horn & Johnson 1985) imply that if

$$\sum_{j=1}^{n} q_{ij}(t) > \gamma,\ \forall i \tag{6.3}$$

for some $\gamma > 0$, then $\lambda_{min}(Q(t)) > \gamma$ for all t, equivalently $Q\mathbf{1} > \gamma\mathbf{1}$, where the inequality should be interpreted element by element. Because $L\mathbf{1} = \mathbf{0}$, the above condition degenerates

to

$$L\left[\frac{1}{c_{ii}a_{ii}}\right]_{n\times 1}+\left[2\frac{a_{ii}}{c_{ii}}\right]_{n\times 1}>\gamma\mathbf{1}$$

or $2\frac{a_{ii}}{c_{ii}}+\sum_{j\in N_i}(\frac{1}{c_{ii}a_{ii}}-\frac{1}{c_{jj}a_{jj}})>\gamma$ for all i, where we used the properties of L. Therefore, (6.3) is satisfied if

$$2\frac{a_1}{c_2}+d_i(\frac{1}{a_2c_2}-\frac{1}{a_1c_1})>\gamma,\ \forall i$$

which is equivalent to (6.2) because γ can be taken arbitrarily small. □

A proof for Proposition 3.1 under assumption i

Since $v(t)$ is uniformly continuous and $\lim_{t\to\infty}v(t)\neq 0$, we have

$$\exists\varepsilon_1,\varepsilon_2>0,\exists T=T(\varepsilon_1)>0,\{\tau_n^-\},\{\tau_n^+\};n\geq 1,\text{ such that}$$
$$\tau_n^+-\tau_n^-\geq\varepsilon_2,\ \tau_{n+1}^->\tau_n^+,\ \tau_1^->T$$

and $\forall t\in[\tau_n^-,\tau_n^+),|v(t)|>\varepsilon_1$. That is, after some time T, $v(t)$ is larger than some $\varepsilon_1>0$ over an infinite number of finite intervals. Therefore, using (3.20), it is easily seen that for all $t\in[\tau_n^-,\tau_n^+)$ and some $\lambda>0$, $\dot{V}_p\leq-\lambda V_p$ whose integration yields

$$V_p(\tau_n^+)\leq V_p(\tau_n^-)e^{-\lambda\varepsilon_2}. \tag{6.4}$$

Since $\tau_{n+1}^->\tau_n^+$, $\dot{V}\leq 0$ implies that $V_p(\tau_{n+1}^-)\leq V_p(\tau_n^+)$ and using (6.4) we get $V_p(\tau_n^-)\leq V_p(\tau_0^-)e^{-n\lambda\varepsilon_2}$, thus showing that $\lim_{n\to\infty}V_p(\tau_n^-)=0$. That is $V_p(t)$ is a nondecreasing function that tends to zero. This in turn implies that X_p converges asymptotically to 0. Thus $X_p=\mathbf{0}$ is semi-globally asymptotically stable.

BIBLIOGRAPHY

Aguiar, A. P. (2002), Nonlinear Motion Control of Nonholonomic and Underactuated Systems, PhD thesis, Dept. Electrical Engineering, Instituto Superior Técnico, IST, Lisbon, Portugal. 92, 166

Aguiar, A. P., Ghabcheloo, R., Pascoal, A., Silvestre, C., Hespanha, J. & Kaminer, I. (2006), Coordinated path-following of multiple underactuated autonomous vehicles with bi-directional communication constraints, *in* 'International Symposium on Communication, Control and Signal Processing (ISCCSP)', Morocco. 26, 27, 28

Aguiar, A. P. & Hespanha, J. P. (2004), Logic-based switching control for trajectory-tracking and path-following of underactuated autonomous vehicles with parametric modeling uncertainty, *in* 'Proc. of the 2004 Amer. Contr. Conf.', Boston, MA, USA. 156

Aguiar, A. P. & Hespanha, J. P. (2006), 'Trajectory-tracking and path-following of underactuated autonomous vehicles with parametric modeling uncertainty', IEEE Trans. on Automat. Contr. In press. 132, 156, 158

Aguiar, A. P., Hespanha, J. P. & Kokotovic, P. (2005), 'Path-following for non-minimum phase systems removes performance limitations', *IEEE Transactions on Automatic Control* **50**(2), 234–239. 132

Aguiar, A. P. & Pascoal, A. M. (1997), Modeling and control of an autonomous underwater shuttle for the transport of benthic laboratories, *in* 'Proc. of the Oceans'97 Conf.', Halifax, Nova Scotia, Canada. 166

Arrichiello, F. (2006), Coordination Control of Multiple Mobile Robots, Phd thesis, Universitá Degli Studi di Cassino, Cassino, Italy. 172

Balakrishnan, R. & Ranganathan, K. (2000), *A Textbook of Graph Theory*, Springer. 73, 76

Bang-Jensen, J. & Gutin, G. (2002), *Digraph theory, algorithms and applications*, Springer. 73

Beard, R., Lawton, J. & Hadaegh, F. (2001), 'A coordination architecture for spacecraft formation control', *IEEE Trans. on Contr. Systems Tech.* **9**, 777–790. 16

Bertsekas, D. & Tsitsiklis, J. (1989), *Parallel and Distributed Computation: Numerical Methods*, Prentice Hall. 23

Biggs, N. (1996), *Algebraic graph theory*, Second Edition. Cambridge University Press. 73, 75

Blondel, V. D., Hendrickx, J. M., Olshevsky, A. & Tsitsiklis, J. N. (2005), Convergence in multiagent coordination, consensus, and flocking, *in* 'Proc. of the 44th IEEE CDC-ECC', Seville, Spain. 23

Børhaug, E., Pavlov, A., Ghabcheloo, R., Pettersen, K., Pascoal, A. & Silvestre, C. (2006), Formation control of underactuated marine vehicles with communication constraints, *in* 'Proc. of the 7th IFAC Conference on Maneuvering and Control of Marine Craft (MCMC'06)', Lisbon, Portugal. 28

Bullo, F. & Cortes, J. (2005), Adaptive and distributed coordination algorithms for mobile sensing networks, *in* V. Kumar, N. E. Leonard & A. S. Morse, eds, 'Cooperative Control. (Proceedings of the 2003 Block Island Workshop on Cooperative Control)', Vol. 309 of *Lecture Notes in Control and Information Sciences*, Springer Verlag, New York, pp. 43–62. 16

Cao, M., Morse, A. S. & Anderson, B. D. O. (2006*a*), 'Agreeing asynchronously in continuous time', *IEEE Transactions on Automatic Control, submitted* . 23

Cao, M., Morse, A. S. & Anderson, B. D. O. (2006*b*), 'Reaching a consensus in a dynamically changing environment delays and asynchronous events', *SIAM J. on Control and Optimization, submitted* . 23

Caughman, J., Lafferriere, G., Veerman, J. J. P. & Williams, A. (2005), 'Decentralized control of vehicle formation', *Systems and Control Letters* . 21, 22, 79

Cortes, J. & Bullo, F. (2005), 'Coordination and geometric optimization via distributed dynamical systems', *SIAM Journal on Control and Optimization* **44**(5), 1543–1574. 16

Dobrokhodov, V., Kaminer, I., Jones, K. & Ghabcheloo, R. (2006), Vision-based tracking and position estimation for moving targets using small UAVs, *in* 'American Control Conference (ACC)', Minneapolis, Minnesota, USA. 28

Egerstedt, M. & Hu, X. (2001), 'Formation constrained multi-agent control', *IEEE Trans. on Robotics and Automation* **17**(6), 947 – 951. 16, 18

Encarnação, P. & Pascoal, A. (2001), Combined trajectory tracking and path following: an application to the coordinated control of marine craft, *in* 'Proc. of IEEE Conf. Decision and Control (CDC)', Orlando, Florida. 16, 17

Fang, L., Antsaklis, P. J. & Tzimas, A. (2005), Asynchronous consensus protocols: preliminary results, simulations and open questions, *in* 'Proc. of the 44th IEEE CDC-ECC', Seville, Spain, pp. 2194–2199. 16

Fax, A. & Murray, R. (2002*a*), Graph Laplacians and stabilization of vehicle formations, *in* 'Proc. of IFAC World Congress', Barcelona, Spain. 3, 19, 22

Fax, A. & Murray, R. (2002*b*), Information flow and cooperative control of vehicle formations, *in* 'Proc. of IFAC World Congress', Barcelona, Spain. 3, 19

Fax, J. A. (2002), Optimal and Cooperative Control of Vehicle Formations, Phd thesis, California Institute of Technology, Pasadena, California, USA. 73

Fiedler, M. (1973), 'Algebraic connectivity of graphs', *Czechoslavak Mathematical Journal* **23**(98), 298–306. 20

Fossen, T. (1994), *Guidance and Control of Ocean Vehicles*, John Willey & Sons, Inc., New York. 156

Fossen, T. (2002), *Marine Control Systems: Guidance, Navigation and Control of Ships, Rigs and Underwater Vehicles*, Marine Cybernetics AS, ISBN 82-92356-00-2. 2, 17, 172

Ghabcheloo, R., Aguiar, A. P., Pascoal, A., Silvestre, C., Hespanha, J. & Kaminer, I. (2006), 'Coordinated path-following control of multiple vehicles in the presence of communication losses and time delays', *Submitted to SIAM, special issue on Control and Optimization in Cooperative Networks* . 24, 27

Ghabcheloo, R., Aguiar, A., Pascoal, A. & Silvestre, C. (2006), Coordinated path-following control of multiple AUVs in the presence of communication failures and time delays, *in* 'Proc. of the 7th IFAC Conference on Maneuvering and Control of Marine Craft (MCMC'06)', Lisbon, Portugal. 26, 27

Ghabcheloo, R., Aguiar, A., Pascoal, A., Silvestre, C., Kaminer, I. & Hespanha, J. (2006), Coordinated path-following control of multiple underactuated autonomous vehicles in the presence of communication failures, *in* 'Proc. of the 45th IEEE Conference on Decision and Control (CDC'06)', San Diego, California USA. 18, 24, 26, 27

Ghabcheloo, R., Carvalho, D., Pascoal, A. & Silvestre, C. (2005), Coordinated motion control of multiple autonomous underwater vehicles, *in* 'Proc. of International Workshop on Underwater Robotics (IWUR)', Genoa, Italy. 26

Ghabcheloo, R., Pascoal, A. & Silvestre, C. (2004), Coordinated path-following control using linearization techniques, Internal Report CPF01L, Instituto Superior Técnico/Institute for Systems and Robotics. 24

Ghabcheloo, R., Pascoal, A. & Silvestre, C. (2005*a*), Coordinated path-following control using nonlinear techniques, Internal Report CPF02NL, Instituto Superior Técnico/Institute for Systems and Robotics. 24, 25

Ghabcheloo, R., Pascoal, A. & Silvestre, C. (2005*b*), Nonlinear coordinated path-following control of multiple wheeled robots with communication constraints, *in* 'Proc. of International Conference on Advanced Robotics (ICAR)', Seattle, USA. 17, 26

Ghabcheloo, R., Pascoal, A., Silvestre, C. & Kaminer, I. (2004), Coordinated path-following control of multiple wheeled robots, *in* 'Proc. of the 5th IFAC Symposium on Intelligent Autonomous Vehicles', Lisbon, Portugal. 24, 25

Ghabcheloo, R., Pascoal, A., Silvestre, C. & Kaminer, I. (2005), Coordinated path following control of multiple wheeled robots with directed communication links, *in* 'Proc. of the 44th IEEE Conference on Decision and Control and European Control Conference (CDC-ECC)', Seville, Spain. 26

Ghabcheloo, R., Pascoal, A., Silvestre, C. & Kaminer, I. (2006*a*), 'Coordinated path-following control of multiple wheeled robots using linearization techniques', *International Journal of Systems Science* **37**(6), 399–414. 24, 25

Ghabcheloo, R., Pascoal, A., Silvestre, C. & Kaminer, I. (2006*b*), *Group Coordination and Cooperative Control*, Vol. 336 of *ISBN: 3-540-33468-8*, Springer-Verlag, chapter Coordinated Path-Following Control of Multiple Vehicles subject to Bi-directional Communication Constraints, pp. 93–111. 24, 25, 26

Ghabcheloo, R., Pascoal, A., Silvestre, C. & Kaminer, I. (2007), 'Nonlinear coordinated path-following control of multiple wheeled robots with bi-directional communication constraints', *International Journal of Adaptive control and signal Processing* **21**(2-3), 133 – 157. 16, 24, 25, 26, 132

Giuletti, F., Pollini, L. & Innocenti, M. (2000), 'Autonomous formation flight', *IEEE Control Systems Magazine* **20**, 33–34. 16

Godsil, C. & Royle, G. (2001), *Algebraic Graph Theory*, Graduated Texts in Mathematics, Springer-Verlag New York, Inc. 73, 74, 135

Hespanha, J. M., Yakimenko, O. A., Kaminer, I. I. & Pascoal, A. M. (2004), 'Linear parametrically varying systems with brief instabilities: An application to vision/inertial navigation', *IEEE Trans. on Aerospace and Electronics Systems* **40**(3), 889–900. 136, 141, 149, 177

Horn, R. A. & Johnson, C. R. (1985), *Matrix Analysis*, Cambridge Univ. Press. 66, 73, 178

Ihle, I.-A. F. (2006), Coordinated Control of Marine Craft, Phd thesis, Norwegian University of Science and Technology, Trondheim, Norway. 18, 172

Ito, H. (2002), A constructive proof of ISS small-gain theorem usign generalized scaling, *in* 'Proc. of IEEE Conference on Decision and Control'. 143

Jadbabaie, A., Lin, J. & Morse, A. (2003), 'Coordination of groups of mobile autonomous agents using nearest neighbor rules', *IEEE Trans. on Automatic Control* **48**(6). 16, 22, 144

Kaminer, I., Pascoal, A., Hallberg, E. & Silvestre, C. (1998), 'Trajectory tracking for autonomous vehicles: An integrated approach to guidance and control', *Journal Of Guidance, Control, and Dynamics* **21**(1), 29–38. 35

Kaminer, I., Pascoal, A., Khargonekar, P. & Coleman, E. (1995), 'A velocity algorithm for the implementation of gain-scheduled controllers', *Automatica* **31**(1), 1185–1191. 37, 38, 45, 47, 48

Kaminer, I., Pascoal, A. & Yakimenko, O. (2005), Nonlinear path following control of fully actuated marine vehicles with parameter uncertainty, *in* 'Proc. of the 16th IFAC World Congress', Prague, Czech Republic. 87

Khalil, H. K. (2002), *Nonlinear Systems*, Third Edition, Prentice Hall. 37, 66, 69, 88, 120, 133

Kim, Y. & Mesbahi, M. (2006), 'On maximizing the second smallest eigenvalue of state-dependent graph Laplacian', *IEEE Trans. on Automatic Control* **51**(1), 116–120. 16

Kyrkjebo, E. (2007), Motion Coordination of Mechanical Systems: Leader-Follower Synchronization of Euler-Lagrange Systems Using Output Feedback Control, PhD thesis, the Norwegian University of Science and Technology, Trondheim, Norway. 3

Kyrkjebo, E. & Pettersen, K. (2003), Ship replenishment using synchronization control, *in* 'Proc. of the 6th IFAC Conference on Manoeuvering and Control of Marine Craft (MCMC)', Girona, Spain. 17

Kyrkjebo, E., Wondergen, M., Pettersen, K. & Nijmeijer, H. (2004), Experimental results on synchronization control of ship rendezvous operations, *in* 'Proc. of the 6th IFAC Conference on Control Applications in Marine Systems', Ancona,Italy. 17

Lapierre, L., Soentanto, D. & Pascoal, A. (2003), Coordinated motion control of marine robots, *in* 'Proc. of the 6th IFAC Conference on Manoeuvering and Control of Marine Craft (MCMC)', Girona, Spain. 16, 17

Lin, J., Morse, A. S. & Anderson, B. D. O. (2004), 'The multi-agent rendezvous problem - part 2: The asynchronous case', *SIAM J. on Control and Optimization, submitted* . 23

Lin, J., Morse, A. S. & Anderson, B. D. O. (2006), 'The multi-agent rendezvous problem - part 1: The synchronous case', *SIAM J. on Control and Optimization, to appear* . 23

Lin, Z. (2006), Coupled Dynamic Systems: From Structure Towards Stability And Stabilizability, Phd thesis, University of Toronto, Toronto, Canada. 73, 79, 139, 141

Lin, Z., Francis, B. & Maggiore, M. (2005*a*), 'Necessary and sufficient graphical conditions for formation control of unicycles', *IEEE Trans. on Automatic Control* **50**(1), 121–127. 20, 21, 22, 79

Lin, Z., Francis, B. & Maggiore, M. (2005*b*), 'State agreement for coupled nonlinear systems with time-varying interaction', *under revision: SIAM Journal on Control and Optimization* . 16, 139, 140, 141

Massera, J. L. (1949), 'On Liapounoff's conditions of stability', *Annals of Mathematics* **50**(3), 705–721. 71

Mesbahi, M. (2002), On a dynamic extension of the theory of graphs, *in* 'Proc. of the American Control Conference', Anchorange, AL, USA. 20

Mesbahi, M. & Hadaegh, F. (2001), 'Formation flying control of multiple spacecraft via graphs, matrix inequalities, and switching', *Journal of Guidance, Control and Dynamics* **24**(2), 369–377. 20

Micaelli, A. & Samson, C. (1993), Trajectory-tracking for unicycle-type and two-steering-wheels mobile robots, Technical Report 2097, INRIA, Sophia-Antipolis, France. 34, 36, 82, 83

Moreau, L. (2004), Stability of continuous-time distributed consensus algorithm, *in* 'Proc. of the 43rd IEEE Conference on Decision and Control', Atlantis, Paradise Island, Bahamas, pp. 3998 – 4003. 139, 140, 141

Moreau, L. (2005), 'Stability of multiagent systems with time - dependent communication links', *IEEE Trans. on Automatic Control* **50**(2). 22, 23

Ogren, P., Egerstedt, M. & Hu, X. (2002), 'A control Lyapunov function approach to multiagent coordination', *IEEE Trans. on Robotics and Automation* **18**, 847 – 851. 16

Olfati Saber, R. & Murray, R. (2003*a*), Agreement problems in networks with directed graphs and switching topology, *in* 'Proc. of Conference on Decision and Control (CDC)', Hawaii, USA. 20, 22

Olfati Saber, R. & Murray, R. M. (2003*b*), Consensus protocols for networks of dynamic agents, *in* 'American Control Conference', Denver, CO, USA. 20

Papachritodoulou, A. & Jadbabaie, A. (2005), Synchronization in oscilator networks: Switching topologies and non-homogenous delays, *in* 'Proc. of the 44th IEEE Conference on Decision and Control(CDC)', Seville, Spain. 16

Pascoal, A., Silvestre, C. & Oliveira, P. (2006), 'Vehicle and mission control of single and multiple autonomous marine robots', *IEE Control Engineering Series, G. Roberts and R. Sutton (Eds)* pp. 353–386. 2, 17

Pascoal et al., A. (2000), Robotic ocean vehicles for marine science applications: the european ASIMOV project, *in* 'Proc. of OCEANS MTS/IEEE', Rhode Island, Providence, USA. 1

Pratcher, M., D'Azzo, J. & Proud, A. (2001), 'Tight formation control', *Journal of Guidance, Control and Dynamics* **24**(2), 246–254. 16

Rouche, N., Habets, P. & Laloy, M. (1977), *Stability theory by Liapunov's direct method*, Springer-Verlag New York, Inc. 66, 68, 71

Sepulchre, R., Paley, D. & Leonard, N. (2003), Collective motion and oscillator synchronization, *in* 'Proc. of Block Island Workshop on Cooperative Control'. 16

Silvestre, C. & Pascoal, A. (2002), 'On the design of gain-scheduled trajectory tracking controllers', *International Journal of Robust and Nonlinear Control* **12**, 797–839. 33, 35

Sivestre, C. (2000), Multi-Objective Optimization Theory with Applications to the Integrated Design of Controllers Plants for Autonomous Vehicles, Phd thesis (in english), Instituto Superior Técnico, Lisbon, Portugal. 33, 35, 37

Skjetne, R., Flakstad, I. & Fossen, T. (2003), Formation control by synchronizing multiple maneuvering systems, *in* 'Proc. of the 6th IFAC Conference on Manoeuvering and Control of Marine Craft (MCMC)', Girona, Spain. 17

Skjetne, R., Fossen, T. I. & Kokotović, P. K. (2004), 'Robust output maneuvering for a class of nonlinear systems', *Automatica* **40**(3), 373–383. 132

Skjetne, R., Moi, S. & Fossen, T. I. (2002), Nonlinear formation control of marine craft, *in* 'Proc. of the 41st Conf. on Decision and Contr.', Las Vegas, NV. 16, 17, 172

Soetanto, D., Lapierre, L. & Pascoal, A. (2003), Adaptive, non-singular path following, control of dynamic wheeled robots, *in* 'Proc. of ICAR', Coimbra, Portugal. 82, 87

Sontag, E. D. (1998), *Mathematical control theory, deterministic finite dimensional systems*, Texts in Applied Mathematics 6, Second Edition, Springer-Verlag New York, Inc. 133

Sontag, E. D. & Wang, Y. (1996), 'New characterizations of input-to-state stability', *IEEE Trans. on Automatic Control* **41**(9), 1283–1294. 69, 133

Tanner, H., Jadbabaie, A. & Pappas, G. (2004), 'Flocking agents with varying interconnection topology', *submitted to Automatica* . 23

Tsitsiklis, J. N. & Athans, M. (1984), 'Convergence and asymptotic agreement in distributed decision problems', *IEEE Transaction on Automatic Control* . 16, 23, 144

Vicsek, T., Czirok, A., Ben Jacob, E., Cohen, I. & Schochet, O. (1995), 'Novel type of phase transitions in a system of self-driven particles', *Phys. Rev. lett.* **75**, 1226–1229. 22

Xu, Y. & Hespanha, J. (2006), *Communication logic design and analysis for networked control systems*, Current trends in nonlinear systems and control, Boston: Birkhauser. 172

Yakimenko, O., Kaminer, I., Pascoal, A. & Ghabcheloo, R. (2006), Path generation, path following and coordinated control for time-critical missions of multiple UAVs, *in* 'American Control Conference (ACC)', Minneapolis, Minnesota, USA. 28

Zhou, K., Doyle, J. & Glover, K. (1996), *Robust and Optimal Control*, Prentice Hall. 40